

MDC E1003

JSC 09003

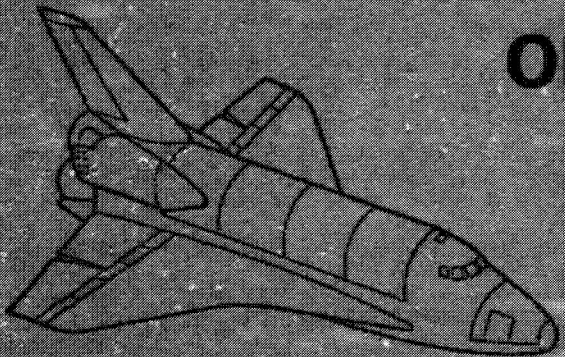
NASA CR-1343+5

(NASA-CR-1343+5) DATA CORRELATION AND
ANALYSIS OF ARC TUNNEL AND WIND TUNNEL
TESTS OF RSI JOINTS AND GAPS. VOLUME
1: (McDonnell-Douglas Astronautics Co.)
230 p HC \$14.50

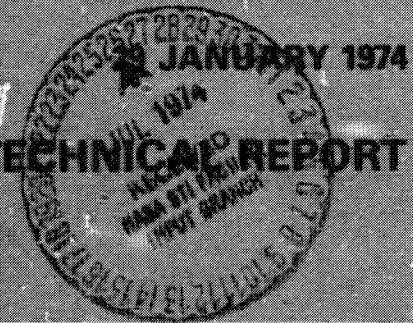
N74-29268

Unclassified
CSCL 22B G3/31 54037

DATA CORRELATION AND ANALYSIS OF ARC TUNNEL AND WIND TUNNEL TESTS OF RSI JOINTS AND GAPS



FINAL REPORT



VOLUME 1 - TECHNICAL REPORT

NASA-CR-
JSC 09003
CR-1343+5

MCDONNELL DOUGLAS ASTRONAUTICS COMPANY - EAST

MCDONNELL DOUGLAS
CORPORATION

COPY NO. 90

SUBMITTED TO NASA/JSC UNDER CONTRACT NAS9-13439
DRL T 918
DRD MA-3847

DATA CORRELATION AND ANALYSIS OF ARC TUNNEL AND WIND TUNNEL TESTS OF RSI JOINTS AND GAPS

FINAL REPORT

29 JANUARY 1974

16 May 1973 to 31 January 1974

MDC E1003
JSC 09003

VOLUME I TECHNICAL REPORT

Prepared by:

H. E. Christensen

H. E. Christensen, Principal Investigator

Prepared by:

H. W. Kipp

H. W. Kipp, Study Manager

Approved by:

J. R. Steele

J. R. Steele, Manager, Thermodynamics

MCDONNELL DOUGLAS ASTRONAUTICS COMPANY - EAST

Saint Louis, Missouri 63166 (314) 232-0232





FINAL REPORT
VOLUME I

REPORT MDC E1003
29 JANUARY 1974

FOREWORD

This report summarizes the work conducted by McDonnell Douglas Astronautics Company-East (MDAC-E) in St. Louis, Missouri for the Structures and Mechanics Division of the NASA Johnson Space Center (NASA-JSC) under Contract NAS9-13439, "Data Correlation and Analysis of Arc Tunnel and Wind Tunnel Test of RSI Joints and Gaps". This final report consists of two volumes: Volume I - Technical Report and Volume II - Data Base. The period of performance was from 16 May 1973 thru 31 January 1974.

Mr. Donald J. Tillian was the NASA Technical Monitor for this study; Messrs. H. E. Christensen and H. W. Kipp were the MDAC Principal Investigator and Study Manager, respectively. Significant contributions to this study were made by Dr. H. J. Brandon, Messrs. L. H. Ebbesmeyer, H. J. Fivel, D. A. Osborne and T. W. Parkinson. The cooperation of numerous NASA Personnel at Ames Research Center, Johnson Space Center and Langley Research Center in providing experimental data, supplemental calculations and valuable counsel was instrumental to the successful completion of this study.

The International System of Units is used as the primary system for all results reported herein. The results are also reported in the British Engineering System of Units which was used as the primary system for calculations made during the course of this study.

PRECEDING PAGE BLANK NOT FILMED



FINAL REPORT
VOLUME I

REPORT MDC E1003
29 JANUARY 1974

TABLE OF CONTENT

<u>SECTION</u>	<u>PAGE</u>
1.0 INTRODUCTION	1
2.0 SUMMARY	3
3.0 TEST PROGRAM AND DATA ASSIMILATION	5
4.0 DATA ANALYSIS.	13
4.1 Heat Protection Ability of Candidate Joints (NASA JSC tests)	13
4.2 Heating Rates in RSI Models of Gaps	35
4.2.1 Comparison of Heating Rate Distributions in RSI Models of Gaps	39
4.3 Analysis of Mach 10 CFHT Tests of Gap Model	57
4.3.1 Analysis of Thin Skin Model.	63
4.3.2 Heating Patterns, Inline versus Staggered Tiles	74
4.3.3 Effect of Gap Width.	74
4.3.4 Effect of Flow Orientation	85
4.3.5 Effect of Steps	89
4.4 Analysis of Mach 8 Variable Density Tunnel Tests.	94
4.4.1 Heating Patterns on Inline Tiles	97
4.4.2 Heating Patterns on Staggered Tiles	97
4.5 Analyses of Ames 3.5 Foot HWT Tests of Gap Models	104
4.5.1 Calibration Plate Heating Pattern	104
4.5.2 Gap Heating Distributions.	104
4.6 Boundary Layer Analyses	116
4.6.1 JSC 10 MW Arc Tunnel Boundary Layer Parameters	116
4.6.2 LaRC Mach 10 CFHT Boundary Layer Parameters.	116
4.6.3 LaRC Mach 8 V.D.T. Boundary Layer Parameters	118
4.6.4 Ames 3.5 Foot HWT, Boundary Layer Parameters	125
4.7 Flow Field Simulation	132
4.8 Comparison of Gap Heating Data from Arc Tunnel and Wind Tunnel Tests	136
4.9 Comparison of Gap Heating Data with Available Theories.	143
5.0 DATA CORRELATION	151
5.1 Data Correlation Procedure	151
5.1.1 Data Ordering and Marriage with Flow Field Parameters . .	151



FINAL REPORT
VOLUME I

REPORT MDC E1003
29 JANUARY 1974

<u>SECTION</u>	<u>PAGE</u>
5.1.2 Data Handling Flow Chart	157
5.1.3 Selecting Data for Correlation	159
5.1.4 Multiple Regression Analysis	159
5.2 Correlation of 10 MW Channel Nozzle Data	163
5.2.1 Transverse Gap Heating Correlation for 10 MW Channel Nozzle Tests	163
5.2.2 In-line Gap Heating Correlation for 10 MW Channel Nozzle Tests	169
5.3 Correlation of Heating in Transverse Gaps	173
5.4 Correlation of CFHT Data, Effects of Flow Angle and Steps	185
5.4.1 Correlation of Maximum and Average Heating, CFHT	185
5.4.2 Correlation of CFHT Gap Heating Distributions with Flow Angle	196
5.5 Correlation Conclusions for Turbulent Boundary Layer Tests	196
6.0 FORMULATION OF GAP HEATING CALCULATION PROCEDURE	205
7.0 INFLUENCE OF GAP HEATING ON TPS REQUIREMENTS	207
8.0 CONCLUSIONS	209
9.0 RECOMMENDATIONS	215
10.0 REFERENCES	217
Appendix A Inverse Solution	A-1
Appendix B Unit Conversions	B-1

List of Pages

Title Page
ii through vii
1 through 218
A1 through A3
B1



FINAL REPORT
VOLUME I

REPORT MDC E1003
29 JANUARY 1974

ABSTRACT

Heat transfer data measured in gaps typical of those under consideration for joints in Space Shuttle RSI thermal protection systems have been assimilated, analyzed and correlated. The data were obtained in four NASA facilities, the JSC 10 MW Arc Jet, the LaRC Mach 10 Continuous Flow Hypersonic Tunnel, the LaRC Mach 8 Variable Density Tunnel and the Ames 3.5' Hypersonic Wind Tunnel. Several types of gaps were investigated with emphasis on simple butt joints. Gap widths ranged from 0.07 to 0.7 cm and depths ranged from 1 to 6 cm. Laminar, transitional and turbulent boundary layer flows over the gap opening were investigated. The angle between gap axis and external flow was varied between 0 and $\pi/2$ radians. The "contoured" cross section gap performed significantly better than all other wide gaps and slightly better than all other narrow gap geometries. Three-dimensional heating variations were observed within gaps in the absence of external flow pressure gradients. Heat transfer correlation equations were obtained for several of the tests. TPS performance with and without gaps was compared for a representative Shuttle entry trajectory. Experimental data employed in the study are summarized in Volume II.



FINAL REPORT
VOLUME I

REPORT MDC E1003
29 JANUARY 1974

1.0 INTRODUCTION

The reusable surface insulation (RSI) thermal protection system (TPS) for Space Shuttle requires gaps at RSI joints to accomodate structural deflection resulting from loads and thermal expansion. In addition, allowance must be made for manufacturing and assembly tolerances. At room temperature, gap widths under current consideration are nominally 0.127 cm (0.050") \pm .038 cm (.015"). In orbital operation, these may shrink to near zero during cold soak or grow by as much as 25%.

The successful application of RSI material for Shuttle thermal protection is significantly affected by entry heating within the RSI gaps. Gap width, depth, crossection geometry, gap orientation, boundary layer state and surface mismatch are all known to affect convective heating within the gap and heat leakage to the protected substructure. For instance, present study results indicate a .127 cm wide flush transverse butt gap increases TPS thickness requirements by approximately 1/2 above the thickness required with no gap.

During 1972 and 1973, extensive tests of various gap configurations were run by NASA to provide a data base for accurate assessment of gap heating. Data were taken in both wind tunnels and in arc tunnels. In the present study, a large segment of the available data (listed in Figure 1) was analyzed and correlated to obtain methods for predicting heating in the RSI gaps on Shuttle.

GAP HEATING DATA SOURCES

INVESTIGATORS	TEST FACILITY AND CONDITIONS	DATA DESCRIPTION
D. J. TILLIAN H. E. CHRISTENSEN (1972-1973)	JSC 10 MW ARC TUNNEL CHANNEL NOZZLE $4.2 < M < 4.7$ $Re \text{ m}^{-1} = 50,000$	LAMINAR B.L.; 60 RUNS; MULLITE RSI MODELS; BUTT, CONTOURED, INCLINED, STEPPED BUTT AND OVERLAPPED BLOCK JOINTS.
D. A. THROCKMORTON H. E. CHRISTENSEN (1973)	LaRC MACH 10 CFHT MODEL TESTED IN TUNNEL WALL $Re \text{ m}^{-1} = 3.3 \times 10^6$	TURBULENT B.L.; 153 RUNS; THIN SKIN MODEL; BUTT JOINTS WITH INLINE AND STAGGERED GAPS; FLOW ORIENTATION, TILE HEIGHT MISMATCH AND GAP WIDTH VARIED.
C. B. JOHNSON (1972)	LaRC MACH 8 VDT, MODEL IN TUNNEL WALL AND FREE STREAM $1.1 \times 10^6 < Re \text{ m}^{-1} < 40 \times 10^6$	LAMINAR AND TURBULENT B.L.; THIN SKIN MODELS; INLINE AND STAGGERED BUTT JOINTS.
W. K. LOCKMAN C. B. BLUMER (1973)	AMES 3.5 FOOT HWT FREE STREAM MODEL $5.0 < M < 5.2$ $1 \times 10^6 < Re \text{ m}^{-1} < 4.6 \times 10^6$	LAMINAR, TRANSITIONAL AND TURBULENT B. L.; 71 RUNS; FLAT PLATE THIN SKIN MODEL; INLINE, TRANSVERSE AND SWEPT BUTT JOINTS.



FINAL REPORT
VOLUME I

REPORT MDC E1003
29 JANUARY 1974

The following major tasks were performed during the study:

- o Assimilation of gap heating data from NASA facilities
- o Analysis of the data to determine heating rates and sensitivities; comparison of the various candidate joints
- o Correlation of the assimilated data and the development of a gap heating procedure which was applied to three Shuttle trajectories.

This volume describes the assimilation, analyses and correlations resulting from the study as well as the conclusions derived therefrom. Volume II of this report presents the basic gap heating data including a description of each test facility, run schedule, test conditions and model descriptive information.



FINAL REPORT
VOLUME I

REPORT MDC E1003
29 JANUARY 1974

2.0 SUMMARY

This study of heat transfer data within gaps representative of those occurring at joints in the Space Shuttle RSI thermal protection system was performed in three tasks, namely, data assimilation, data analysis and correlation of results. Highlights of these tasks are summarized in this section.

The data assimilation task entailed compilation and evaluation of the gap heating data from sources listed in Figure 1. The experimental data were read from magnetic tapes provided by the various test facilities and transcribed into a uniform format in a gap heating data bank. To facilitate data retrieval and analysis, 24 attribute words were assigned to each heating data point. These attribute words consisted of information such as test and geometry identifiers, instrumentation locations, flow orientation, inviscid flow conditions and boundary layer parameters. A computer program, named SELECT, was written to access the data bank to retrieve selected data for further evaluation and analysis. The SELECT program was used for preparing input data for the subsequent multiple regression analysis. The assimilated data are compiled in a test data document which is the second volume of this final report.

The data analysis task consisted of numerous sub tasks which included reduction of temperature histories measured on RSI tiles in the JSC 10 MW channel nozzle to heat flux by means of an inverse solution. These data were subsequently incorporated in the data bank. Additional sub tasks included graphic data presentation, data-theory comparison, sensitivity analysis and boundary layer calculations. End results of the analysis task included the identification of significant phenomena observed in the test program and the preparation of data for correlation. One of the salient results from comparing bondline temperature responses of the various joint configurations tested in the JSC arc jet is the conclusion that whereas gap geometry is relatively unimportant for narrow gaps (0.125 cm - 0.050 in), for larger widths the contoured joint provides significantly better heat protection than any other joint. The significant observation that gap heat transfer distributions in an array of tiles is highly three-dimensional is based on data taken in the CFHT tests. Finally, examination of gap data with laminar external boundary layers indicates that no significant difference exists between normalized heating rate distributions obtained in arc jets and conventional wind tunnels. It remains to be seen if this conclusion holds for turbulent external boundary layers.

Correlating equations for several important classes of gap heating were obtained with the assistance of multiple regression analysis. Correlations were



**RSI GAP HEATING
ANALYSIS**

**FINAL REPORT
VOLUME I**

**REPORT MDC E1003
29 JANUARY 1974**

obtained for transverse gaps and in-line gaps in the presence of a laminar external boundary layer using the data obtained in the JSC 10 MW Channel Nozzle. Two transverse gap correlations for turbulent external boundary layers were obtained for data from the LaRC CFHT and from the Mach 8 VDT. In addition, an equation was obtained from the CFHT data describing the effect of flow angle on gap heating with a turbulent external boundary layer.

An assessment was made of the influence of gap heating on TPS requirements for a laminar external boundary layer using a representative Shuttle entry trajectory. These calculations show an increase in RSI TPS thickness of from 30% to 40% is required to compensate for the adverse effect produced by butt joint gaps 0.075 cm to 0.200 cm (0.030 in to 0.080 in) wide.



FINAL REPORT
VOLUME I

REPORT MDC E1003
29 JANUARY 1974

3.0 TEST PROGRAMS AND DATA ASSIMILATION

The four test programs constituting the principal data base for this study are summarized in Figure 1, Section 1.0. Volume II of this report contains complete summary of the data which were assimilated. The sources of additional data and background information are cited in the relevant portions of the text and listed in the References. Terminology used in this report to describe gap configurations and tile arrangements is depicted in Figure 2.

Gap heating tests performed in the channel nozzle of the JSC 10 mw Arc Tunnel employed arrays of Mullite RSI tile which were heavily instrumented on gap surfaces and in depth at the center of one tile in each array. The tests were designed to provide heating data in the presence of a high enthalpy laminar boundary layer. The gaps between the tiles were adjustable to study the effects of gap width using consistent sets of instrumentation. Four gap settings were employed (0.127, 0.254, 0.381 and 0.762 cm) with tile thickness of 3.175, 5.08 and 6.35 cm. Thirteen models employing a variety of gap and tile configurations were tested. Figure 3 depicts the arc tunnel and shows a 5.08 cm butt joint model. Also shown is a photo of an earlier gap heating test in which the tiles were mounted on a wedge model holder rather than in the wall of the channel nozzle. The matrix of configurations tested in the channel nozzle and in the earlier wedge holder is also shown. Temperature response data from thirty-six gap locations were analyzed to obtain heat flux using the inverse solution technique as described in Section 4.2. Comparisons of the heat protection afforded by the various joint configurations tested appears in Section 4.1. A more complete description of the facility models, test conditions and data appears in Volume II.

The gap heating tests conducted in the LaRC Mach 10 CFHT employed a wall-mounted thin skin "tile" model. These tests provided data in the presence of a relatively thick turbulent boundary layer. The instrumented thin skin tile was surrounded by an array of uninstrumented RSI tiles. The model was mounted on a turntable to permit variation of flow orientation relative to the tile array. Figure 4 shows the instrumented tile, the surrounding matrix of uninstrumented RSI tiles and the installation in the CFHT tunnel wall. A photograph of the installation is shown in Figure 5. A total of 157 runs was made at a unit Reynolds

NOMENCLATURE

SYSTEM INTERNATIONAL UNITS

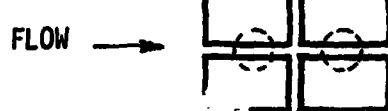
JOINT DESIGN

	BUTT	CONTOURED	INCLINED	OVERLAP BLOCK

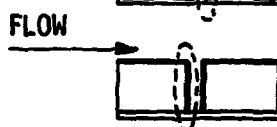
DOWN STREAM SIDE OF GAP



IN-LINE GAP



UPSTREAM SIDE OF GAP



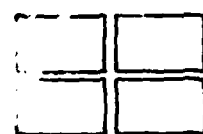
TRANSVERSE GAP



BUTT JOINT FWD STEP



IN-LINE TILES



BUTT JOINT AFT STEP



FLOW

STAGGERED TILES

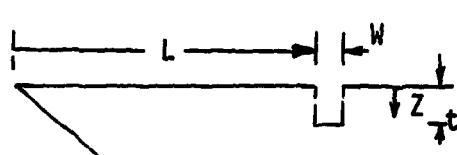
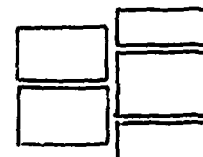
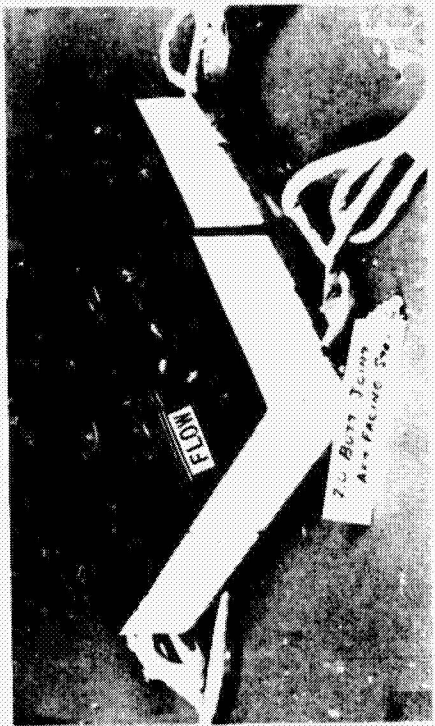
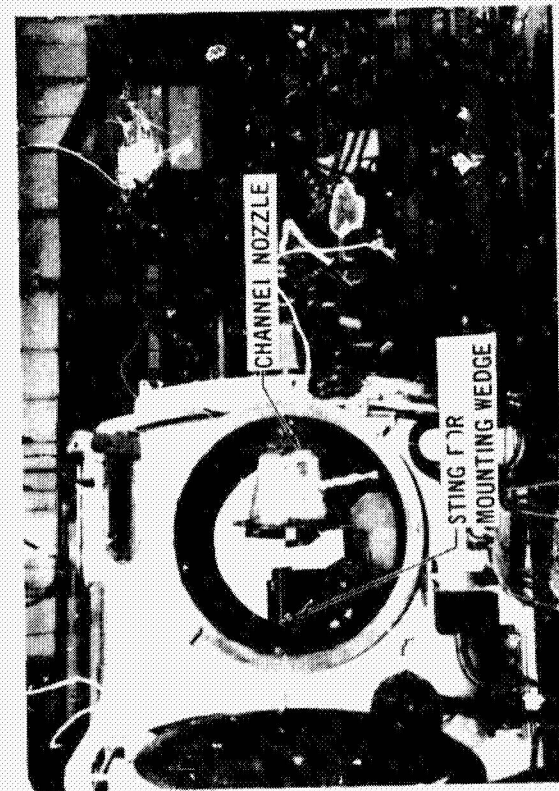
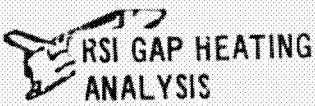


Figure 2

NASA JSC 10 MW, RC TUNNEL TESTS OF GAP HEATING MODELS
(MISSION SIMULATION)



FINAL REPORT
VOLUME I

REPORT MDC E1003
29 JANUARY 1974

5.08 cm BUTT JOINT (0.381 cm AFT FACING STEP)

WEDGE CONFIGURATION	CHANNEL NOZZLE $W = -0.127, 0.124, 0.162$ cm	CHANNEL NOZZLE $W = 0.127, 0.124, 0.161, 0.174$ cm
BUTT	V	V
3.175 cm		
5.08 cm		
6.35 cm		
BUTT STEP	V	V
5.08 cm WITH 0.381 cm FORWARD STEP		
5.08 cm WITH 0.381 cm AFT STEP		
ETACQUED BUTT	V	
5.08 cm		
OVERLAP BLOCK	V	
5.08 cm		
6.35 cm		
CONTINUED	V	
1.175 cm		
5.08 cm		
6.35 cm		
INGENED	V	
5.08 cm		
6.35 cm		

V = GAP WIDENED

TESTING CONTOURED JOINT
(0.762 cm GAP)



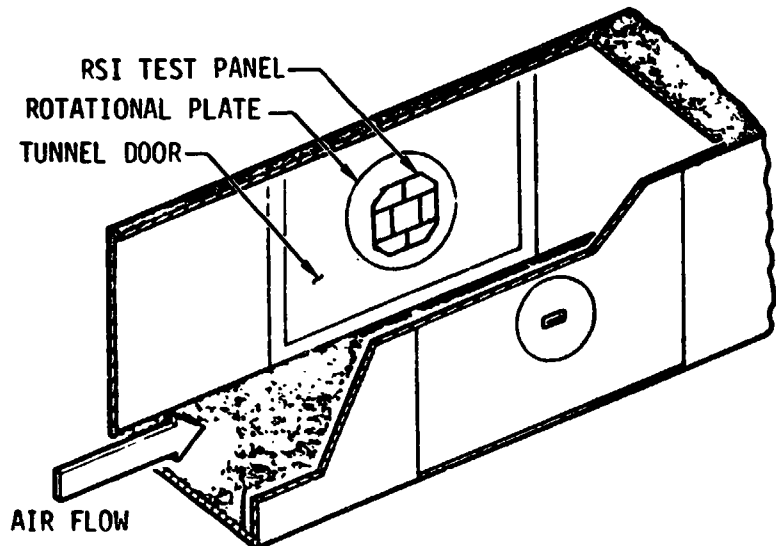
Figure 3



FINAL REPORT
VOLUME I

REPORT MDC E10C3
29 JANUARY 1974

LaRC CFHT GAP HEATING EVALUATION



- o ADJUSTABLE GAP
- o SHIMS FOR STUDYING MISMATCH
- o 0 TO $\pm 90^\circ$ ORIENTATION

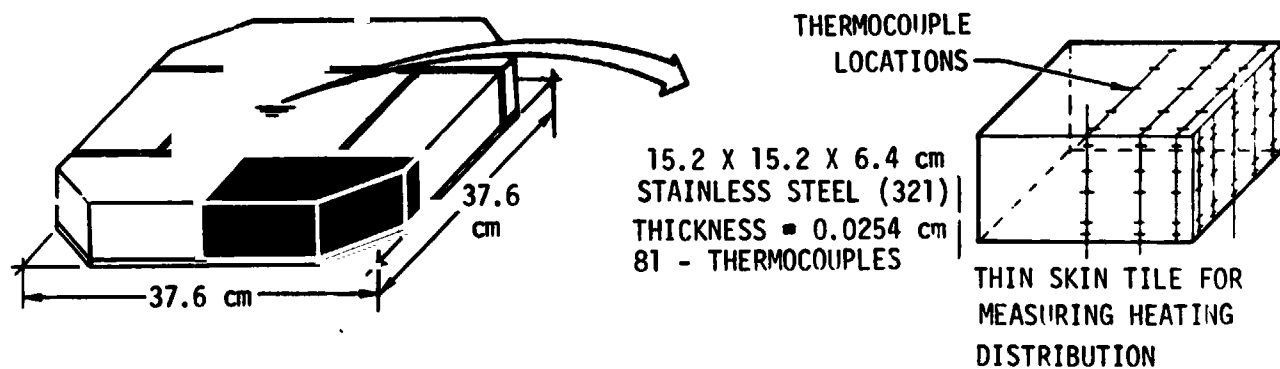
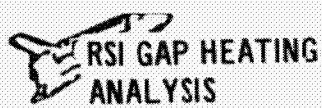


Figure 4



FINAL REPORT
VOLUME I

REPORT MDC E1003
29 JANUARY 1974

LaRC CFHT GAP MODEL

1973

CALIBRATION PLATE

9 FLOW ORIENTATIONS 0 TO $\pi/2$

4 GAP WIDTHS .127, .229, .457, .711 cm

STEPS = 0, + 0.254, - 0.168 cm

MACH = 10.3

$Re_m = 3.28 \times 10^6$

157 TEST RUNS, DATA ASSIMILATED

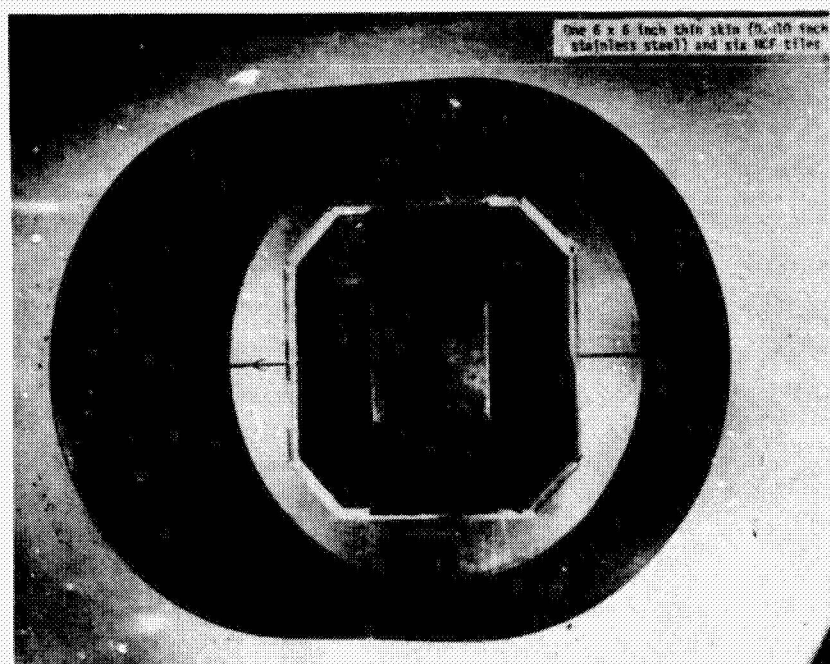


Figure 5



FINAL REPORT
VOLUME I

REPORT MDC E1003
29 JANUARY 1974

number per meter of 3.28×10^6 . The test matrix included nine flow orientations (0 to $\pi/2$ degrees), four gap widths (.127, .229, .457, .711 cm) and three step heights (0, +.254, and -.168 cm). Analysis of the data is documented in Section 4.3 and correlation in Sections 5.3 and 5.4.. The test facility, model description test conditions and data are documented in Volume II. Additional documentation may be found in Reference 1.

Gap heating data were obtained by C. B. Johnson in the LaRC Mach 8 Variable Density Tunnel (VDT) in the presence of laminar and turbulent boundary layers. The models used simulated thin skin tiles which were mounted in a curved plate which was tested both in the free stream and mounted flush to the tunnel wall. In each model position, the test section unit Reynolds number was varied over the range of 1.1×10^6 to 40×10^6 per meter; both in-line and staggered tile configurations were employed. The tile geometry is shown in Figure 6. A total of 22 test runs was assimilated; these results together with a detailed test description are presented in Volume II and Reference 2. Analysis of the VDT data is described in Section 4.4.

Laminar, transitional and turbulent boundary layers were encountered in the gap heating tests conducted by W. K. Lockman and C. B. Blumer in the Ames 3.5 Foot Hypersonic Wind Tunnel (HWT). The model consisted of a 68.6 x 152.4 cm carrier plate into which 68.6 x 106.7 cm instrumented thin skin test articles were inserted. The five insert configurations used in this test program are shown in Figure 7. The configurations include a flat plate used for calibration purposes, a single transverse gap with and without a surface step, multiple transverse gaps, staggered tiles and skewed intersecting gaps. The test program, the models and resulting data are described in detail in Volume II and Reference 3. The analysis of the Ames data is discussed in Section 4.5.



FINAL REPORT
VOLUME I

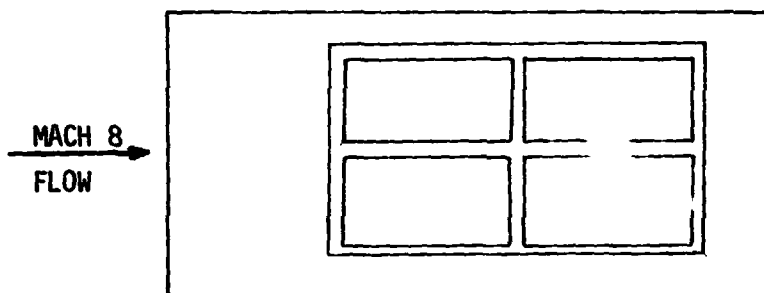
REPORT MDC E1003
29 JANUARY 1974

LaRC MACH 8 V.D.T. GAP HEATING TESTS

- o FREE STREAM AND TUNNEL WALL TESTS
- o GAP WIDTH = 0.159, 0.317 and 0.476 cm
- o $Re_{\text{meter}} = 1.1 \times 10^6$ TO 21.8×10^6

2.54 X 20.32 X 10.16 cm TILES

IN-LINE TILES



STAGGERED TILES

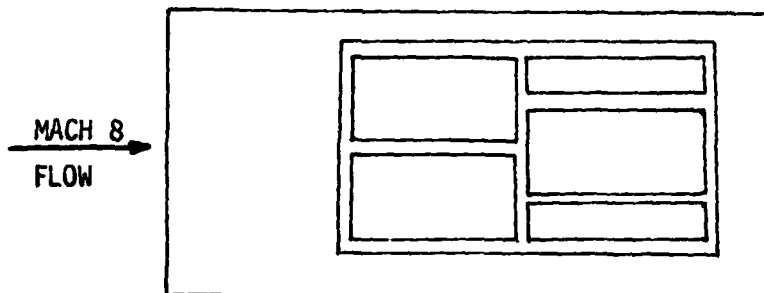
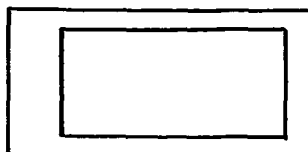


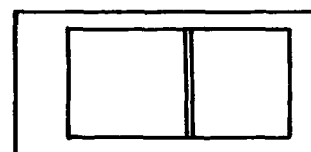
Figure 6

AMES 3.5 FOOT HWT GAP MODELS

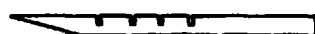
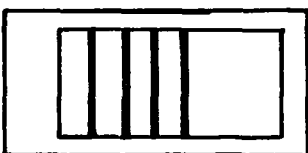
CALIBRATION PLATE



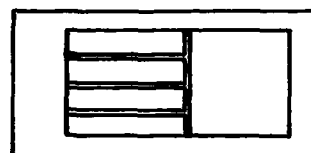
SINGLE TRANSVERSE GAP



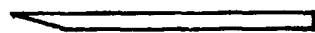
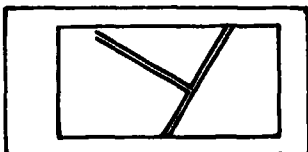
MULTIPLE TRANSVERSE GAP



STAGGERED TILES



30° ORIENTED TILES



- o **TEST VARIABLES**

$10^6 Re/m = 1.4, 2.2, 3.2 \text{ AND } 4.5$
 $m_\infty = 5.1$

GAP WIDTH = 1.59 AND .318 cm

GAP DEPTH = 1, 2, and 4 cm

STEPS = 0, $\pm .159$ AND $+ .317$ cm

- o **81 TEST RUNS ASSIMILATED**



FINAL REPORT
VOLUME I

REPORT MDC E1003
29 JANUARY 1974

4.0 DATA ANALYSIS

4.1 Heat Protection Ability of Candidate Joints - Comparisons of the heat protection performance of candidate RSI joint configurations were made. These comparisons were based on maximum bondline heat-up (temperature rise) rates measured during tests in the NASA JSC 10 MW channel nozzle arc tunnel. Four joint configurations were tested (butt, contoured, inclined and overlap block). The butt joint was tested with forward- and aft-facing steps at the transverse joint and with gap wall emittances of 0.6 (white) and 0.9 (black). The other configurations were tested only with "white" walls. The term "white" walls is used throughout the text and refers to tiles having white gap walls ($\epsilon = 0.6$) except for the first 0.635 centimeters down the gap, which is black ($\epsilon = 0.9$). Gap widths of 0.127, 0.254, 0.381 and 0.762 centimeters were tested for each combination of other test variables. Tile thicknesses of 3.18, 5.08 and 6.35 centimeters were tested, but not for all joint configurations. The high cross range shuttle orbiter A2P entry heating rate-time history was simulated in the NASA JSC channel nozzle for each test run. These test conditions resulted in a laminar boundary layer displacement thickness of approximately 1.02 cm, a Mach number of approximately 4.5, and a theoretical cold wall flat plate heating rate of up to 27.23 watts/cm^2 .

For 5.08 centimeter thick tiles, the rate of bondline heat-up in the transverse gap for candidate joints is shown in Figure 8 as a function of gap width. The contoured joint affords the best heat protection. At large gap widths (up to 0.762 cm) the variation among joint types in heat protection ability is substantial with the forward-facing step (0.381 cm) model experiencing almost 1.78°K/sec at 0.762 cm gap width. This is in contrast to the aft-facing step which affords almost as much heat protection as the contoured joint. Thermal response for transverse and axial gaps are compared in Figure 9. At small gaps (less than 0.381 cm), the forward-facing side of the gap experiences higher bondline temperatures than the shielded aft-facing side of the gap. For the widest gap (0.762 cm), bondline heat-up rate is the same for both sides of the transverse gap. Bondline heat-up rate for this particular model showed that axial gap heating was lower than in the transverse gap.

The data generated with butt joint models having tile thicknesses of 3.18 and 6.35 centimeters and a gap wall emittance of 0.6 (white) are presented in Figures 10 and 11. Figure 10 presents bondline heat-up rates for the 3.18 centimeter butt joints. As was expected, these data show a sharp increase in heat-up rate as the gap was opened. There is no clear differentiation of heating in the transverse

 RSI GAP HEATING
ANALYSIS

GAP CONFIGURATION CONTROLS
BONDLINE TEMPERATURE RESPONSE FOR WIDE GAPS

JSC 10 MW CHANNEL NOZZLE DATA

TEMPERATURE
RESPONSE
 $^{\circ}\text{F}/\text{SEC}$



POINT OF ANALYSIS

FLOW

SYMBOL	GAP TYPE	RUN NO.
○	BUTT, FLUSH	279-282
□	BUTT, FWD. STEP	287-290
△	BUTT, AFT STEP	296-299
◊	CONTOURED	300-303
▽	INCLINED	308-311
◊	OVERLAP	321-324

TILE THICKNESS = 2" (5.08 cm)

TRANSVERSE GAP, FWD. FACING

MAXIMUM TEMPERATURE RESPONSE

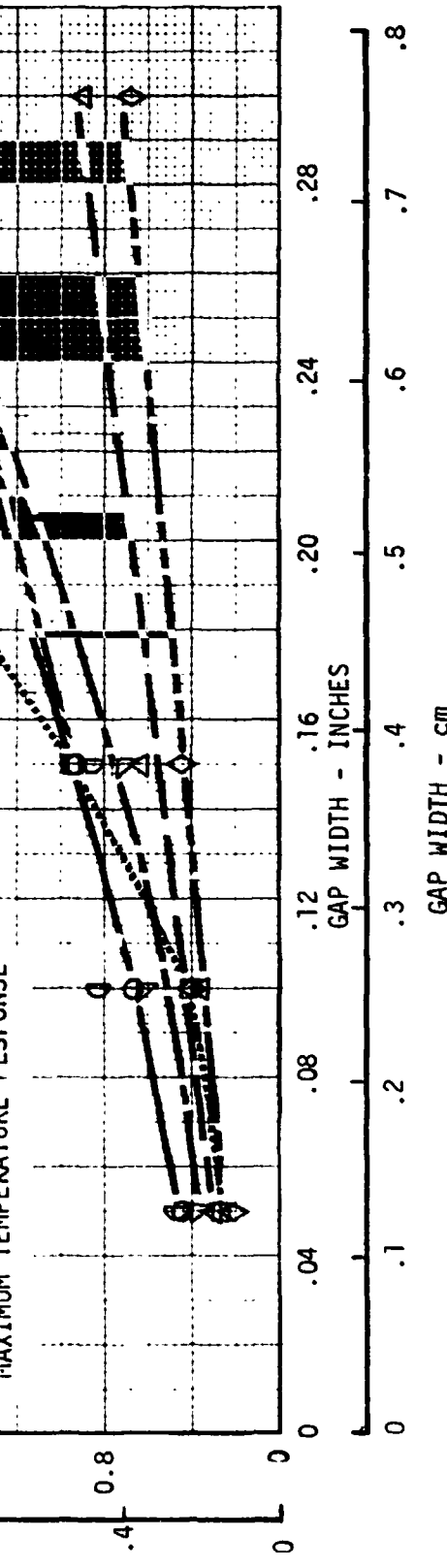


Figure 8



BONDLINE TEMPERATURE RESPONSE VARIES WITH LOCATION

JSC 10 MW CHANNEL NOZZLE TEST

TEMPERATURE
RESPONSE
 $^{\circ}$ F/SEC
 $^{\circ}$ C/SEC

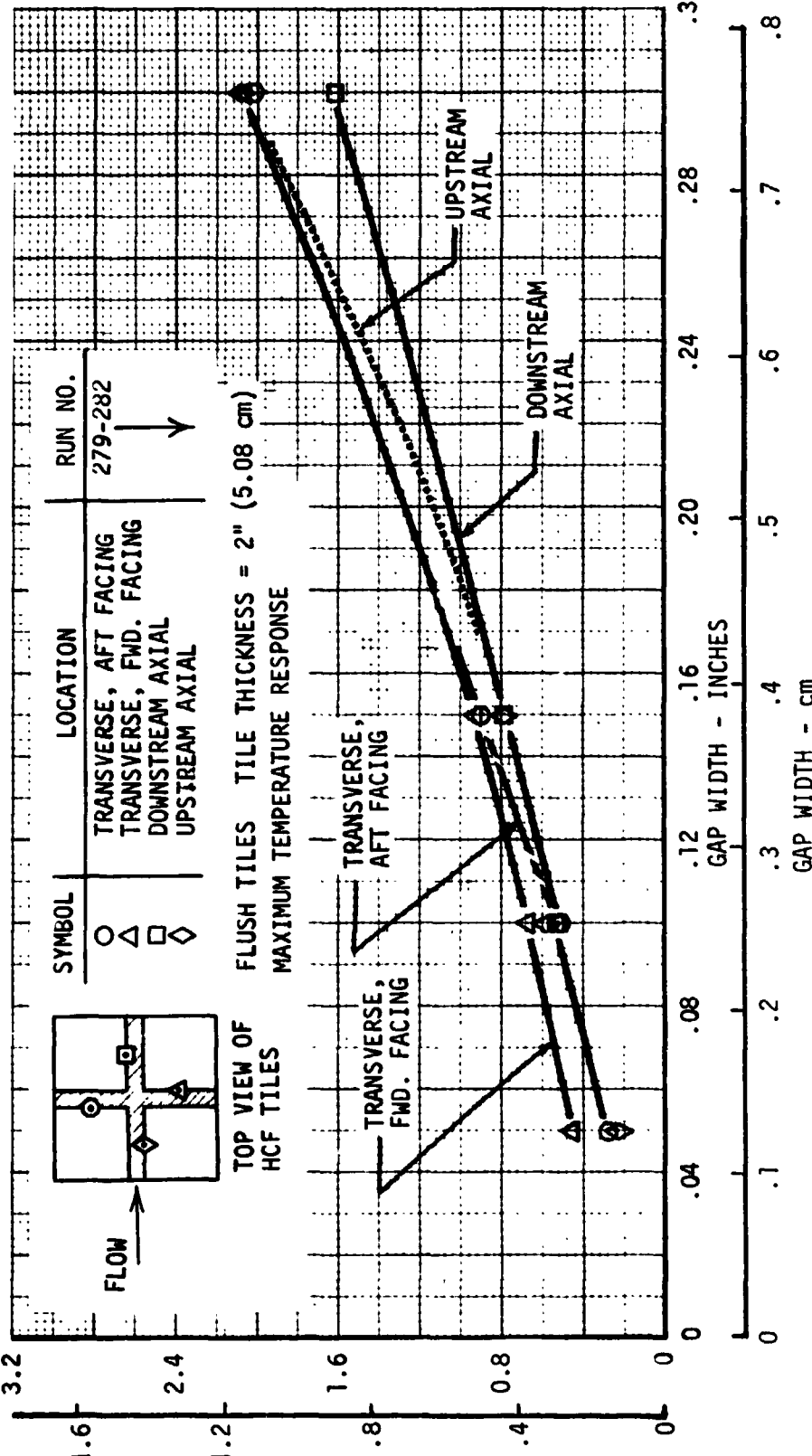


Figure 9

3.18 CM (1.25") BUTT JOINT BONDLINE
TEMPERATURE RESPONSE

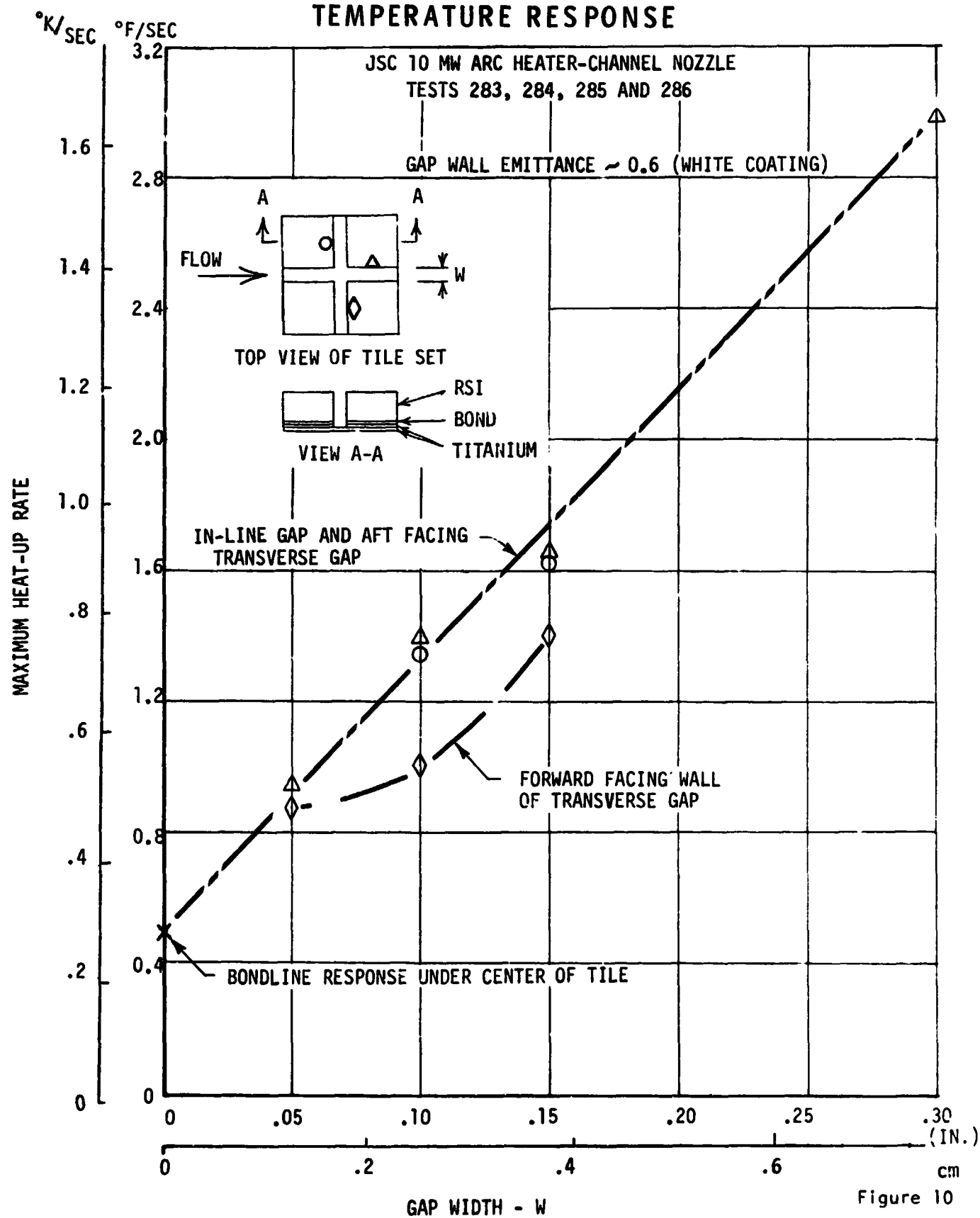


Figure 10

**RSI GAP HEATING
ANALYSIS**

**FINAL REPORT
VOLUME I**

**REPORT MDC E1003
29 JANUARY 1974**

**6.35 CM (2.5") BUTT JOINT BONDLINE
TEMPERATURE RESPONSE**

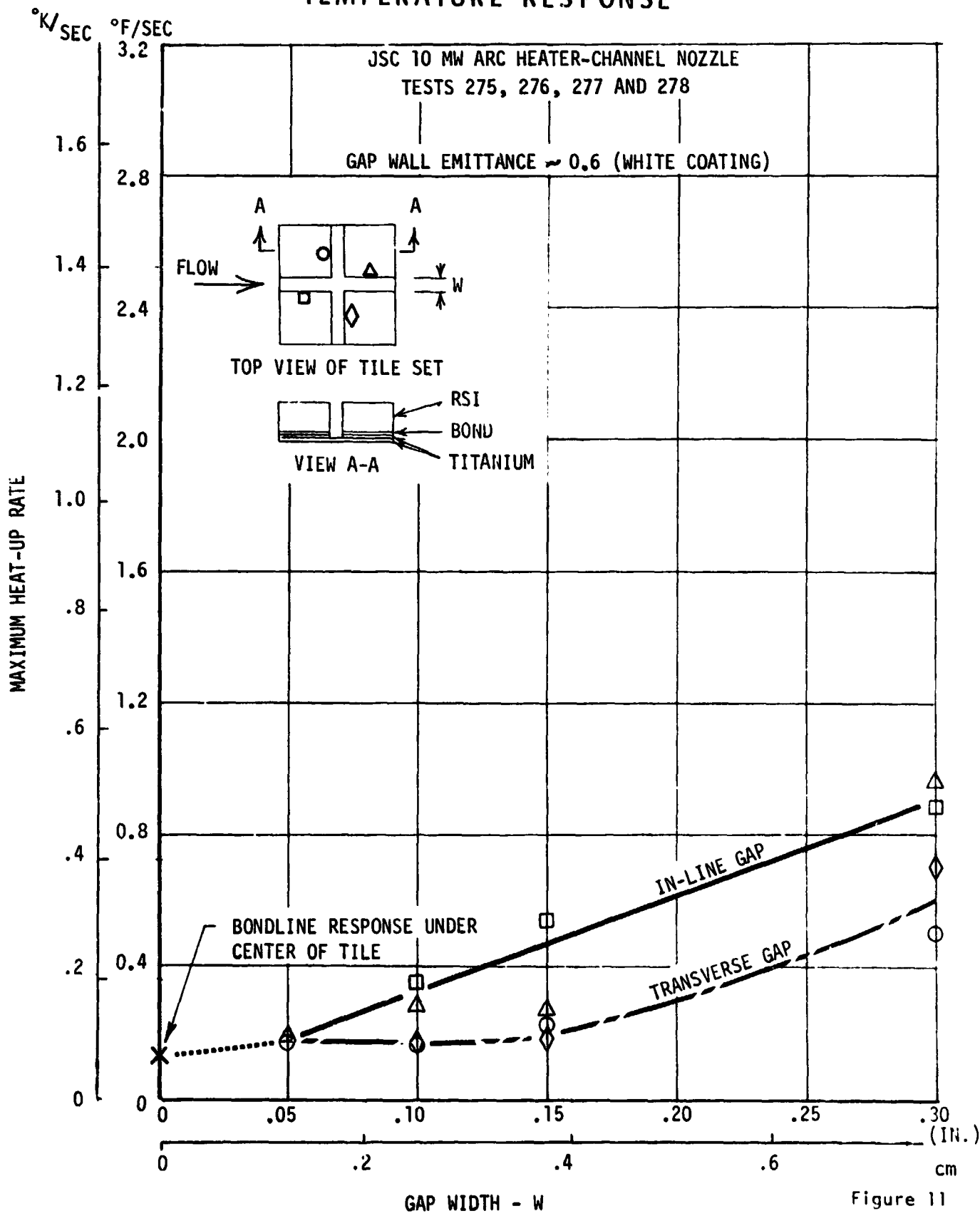


Figure 11

MCDONNELL DOUGLAS ASTRONAUTICS COMPANY - EAST



FINAL REPORT
VOLUME I

REPORT MDC E1003
29 JANUARY 1974

gap as opposed to the axial gap, but the data unexpectedly indicate heating on the upstream wall of the transverse gap to exceed heating on the forward-facing wall. No data are available for the upstream axial location, due to instrumentation failure. The 6.35 centimeter thick tiles (Figure 11) provide more heat protection due not only to increased insulation, but also to a reduced sensitivity to gap width for most locations. Figure 11 shows that the downstream parallel gap location and both of the transverse locations were insensitive to the presence of the gaps for widths of 0.381 centimeters or less. Bondline heat-up rate (6.35 cm tile) at the upstream parallel gap location shows approximately the same sensitivity to increased gap width as do the parallel gap measurements for the 3.18 and 5.08 centimeter thick tiles.

Radiation within the gaps is an important heat transfer mechanism which can be modified by application of emittance-control coatings to the gap walls. Computer simulations have shown that bondline heating can be reduced by increasing gap wall emittance (Reference 4). The mechanism for this reduction is radiation from the high-temperature near-surface areas of the gap walls to the environment. Especially, for the mirror-image temperature distributions of the axial gaps, increased radiation between gap walls will tend to equalize temperatures thus raising the bondline temperature. This equalization could, however, provide some relief for wide transverse gaps where the upstream-facing wall receives significantly higher convective heating than the downstream-facing wall. In that case, radiation from the hot to the cold wall could reduce maximum bondline temperatures.

Figures 12, 13, and 14 present the data generated with butt joint models with tile thicknesses of 3.18, 5.08 and 6.35 centimeters and a gap wall emittance of 0.9. These data also show a strong sensitivity of joint bondline heat-up rate to gap width and do not show either the axial or transverse gap orientation to be consistently hotter.

A direct comparison of the "black" and "white" coatings is made in Figures 15 through 18. These figures show the expected decrease in bondline response with increasing tile thickness for four gap settings. In most cases, the bondline heat-up rates for a given tile thickness are similar for both the black and white coatings. The test data show that bondline heat-up rates were equal or slightly lower for the high emittance walls with two exceptions. One exception could be due to a low response rate (Figure 17 or 14) for the downstream axial gap bondline of the 6.35 centimeter tile set with the 0.381 centimeter gap setting. A more important



**FINAL REPORT
VOLUME I**

**REPORT MDC E1003
29 JANUARY 1974**

3.18 CM (1.25") BUTT JOINT BONDLINE TEMPERATURE RESPONSE

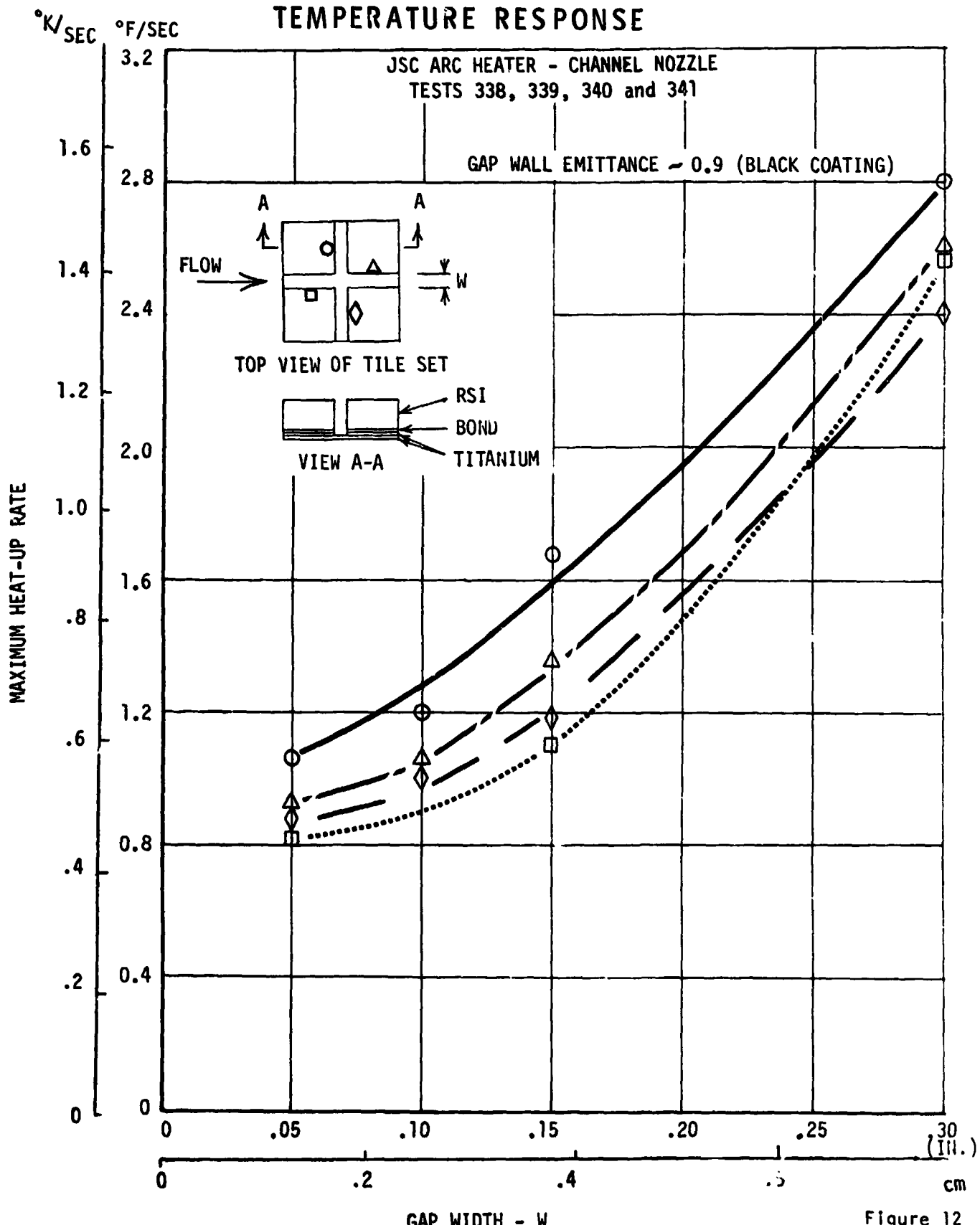


Figure 12

5.08 CM (2") BUTT JOINT BONDLINE
TEMPERATURE RESPONSE

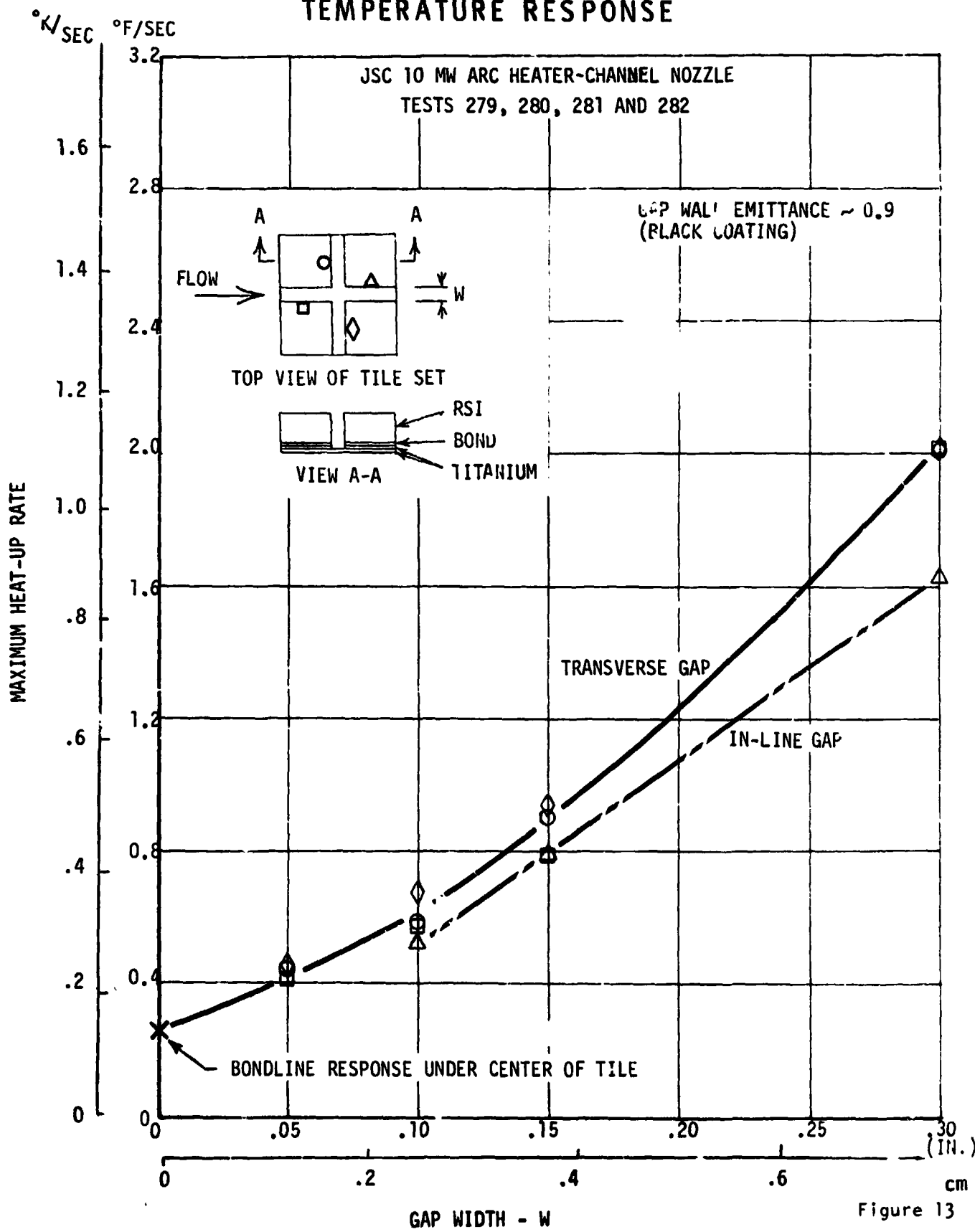
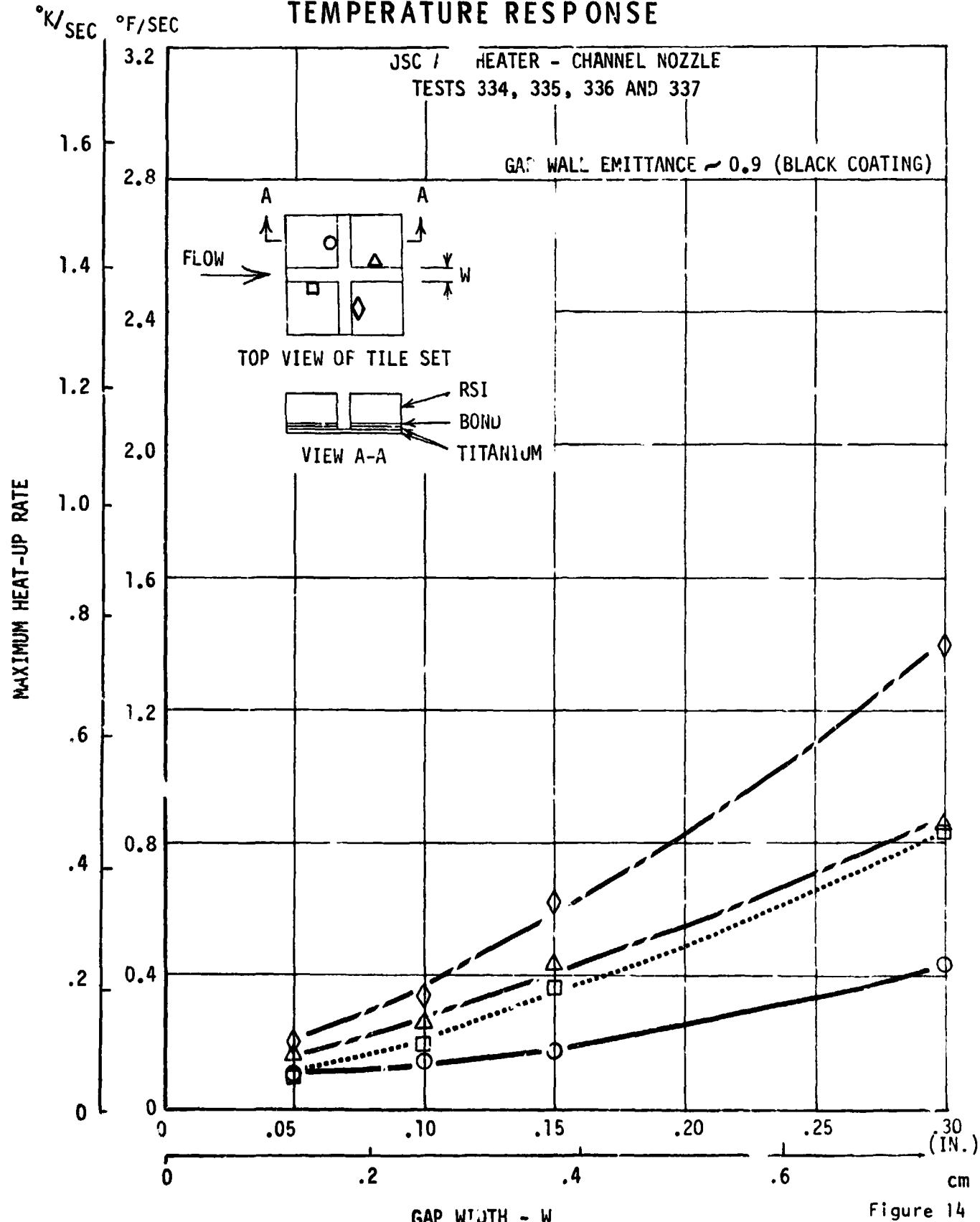


Figure 13

MCDONNELL DOUGLAS ASTROAERONAUTICS COMPANY - EAST

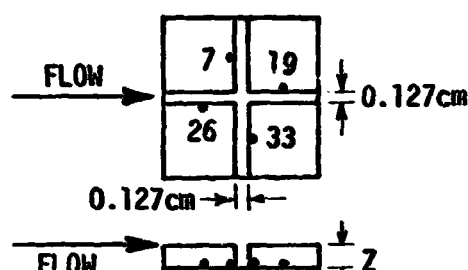
6.35 CM (2.5") BUTT JOINT BONDLINE TEMPERATURE RESPONSE



MCDONNELL DOUGLAS ASTRONAUTICS COMPANY - EAST

EFFECT OF GAP EMITTANCE ON BONDLINE THERMAL RESPONSE

0.127cm GAP



- BLACK COATING (HIGH EMITTANCE)
 - WHITE COATING (LOW EMITTANCE)
- DATA FROM JSC 10 MW ARC TUNNEL

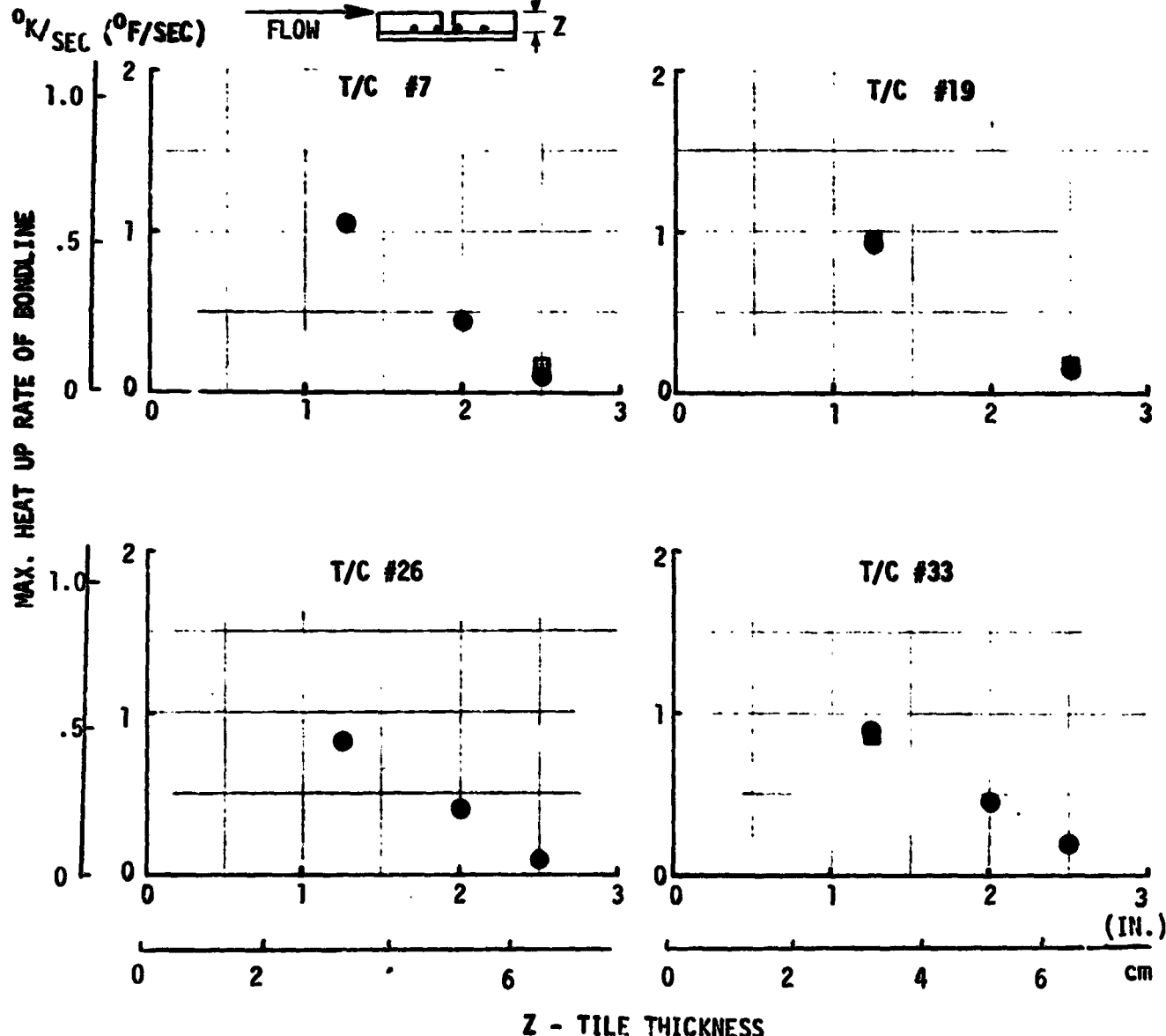
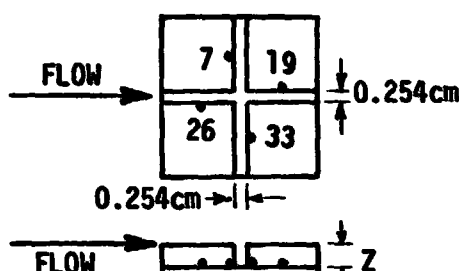


Figure 15

EFFECT OF GAP EMITTANCE ON BONDLINE THERMAL RESPONSE

0.254cm GAP



● BLACK COATING (HIGH EMITTANCE)

□ WHITE COATING (LOW EMITTANCE)

DATA FROM JSC 10 MW ARC TUNNEL

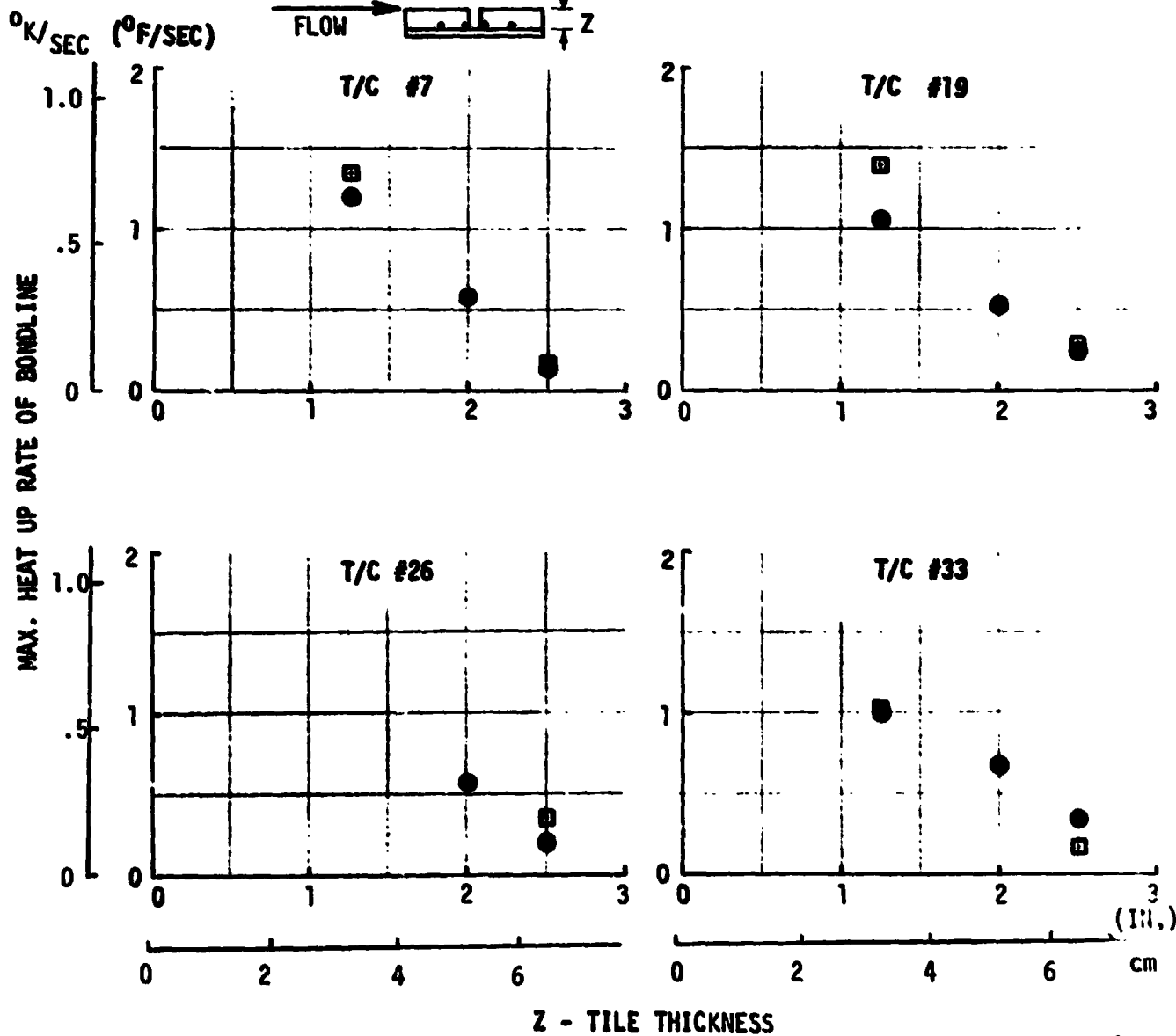


Figure 16

EFFECT OF GAP EMITTANCE ON BONDLINE THERMAL RESPONSE

0.381cm GAP

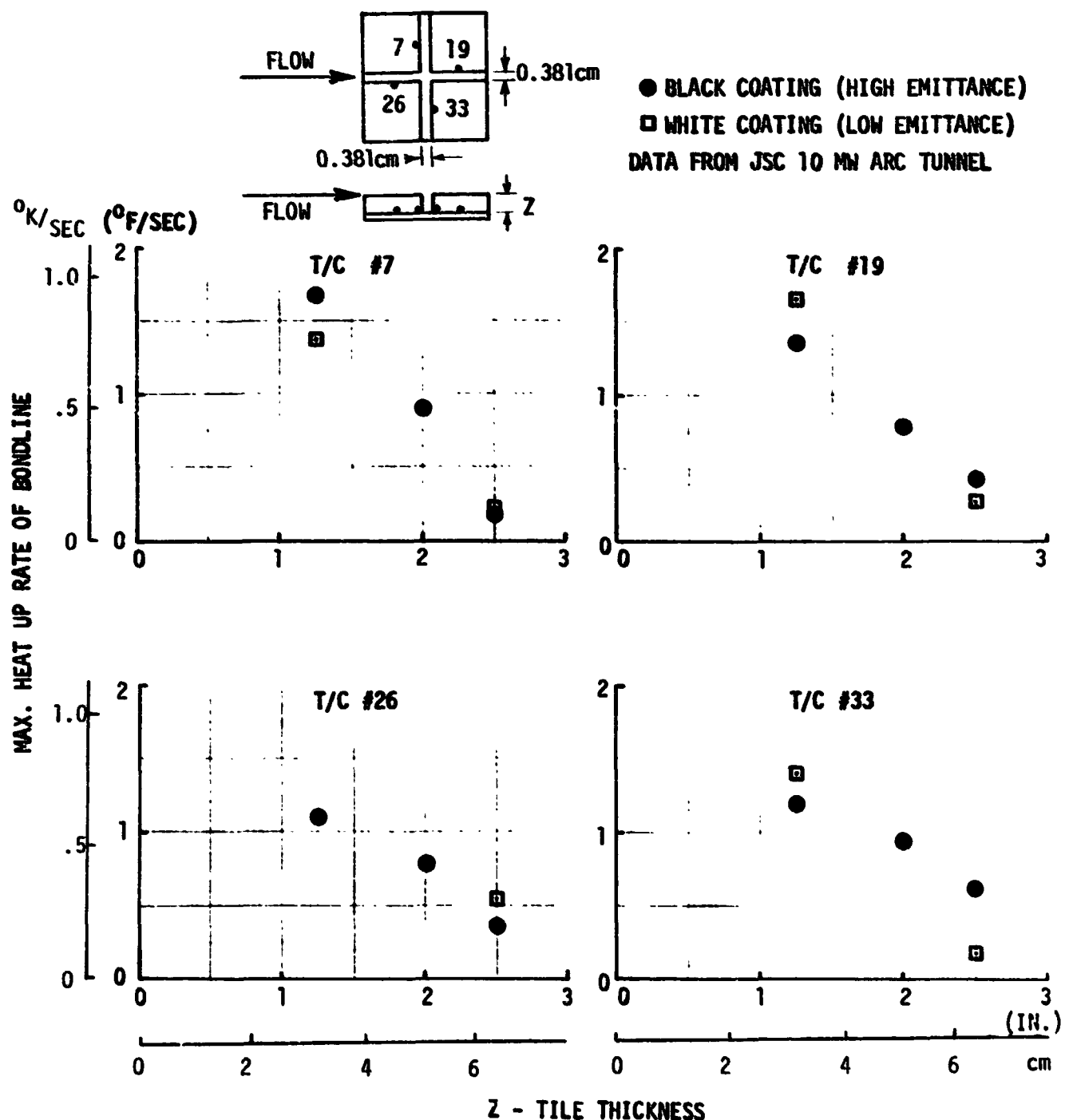


Figure 17

EFFECT OF GAP EMITTANCE ON BONDLINE THERMAL RESPONSE

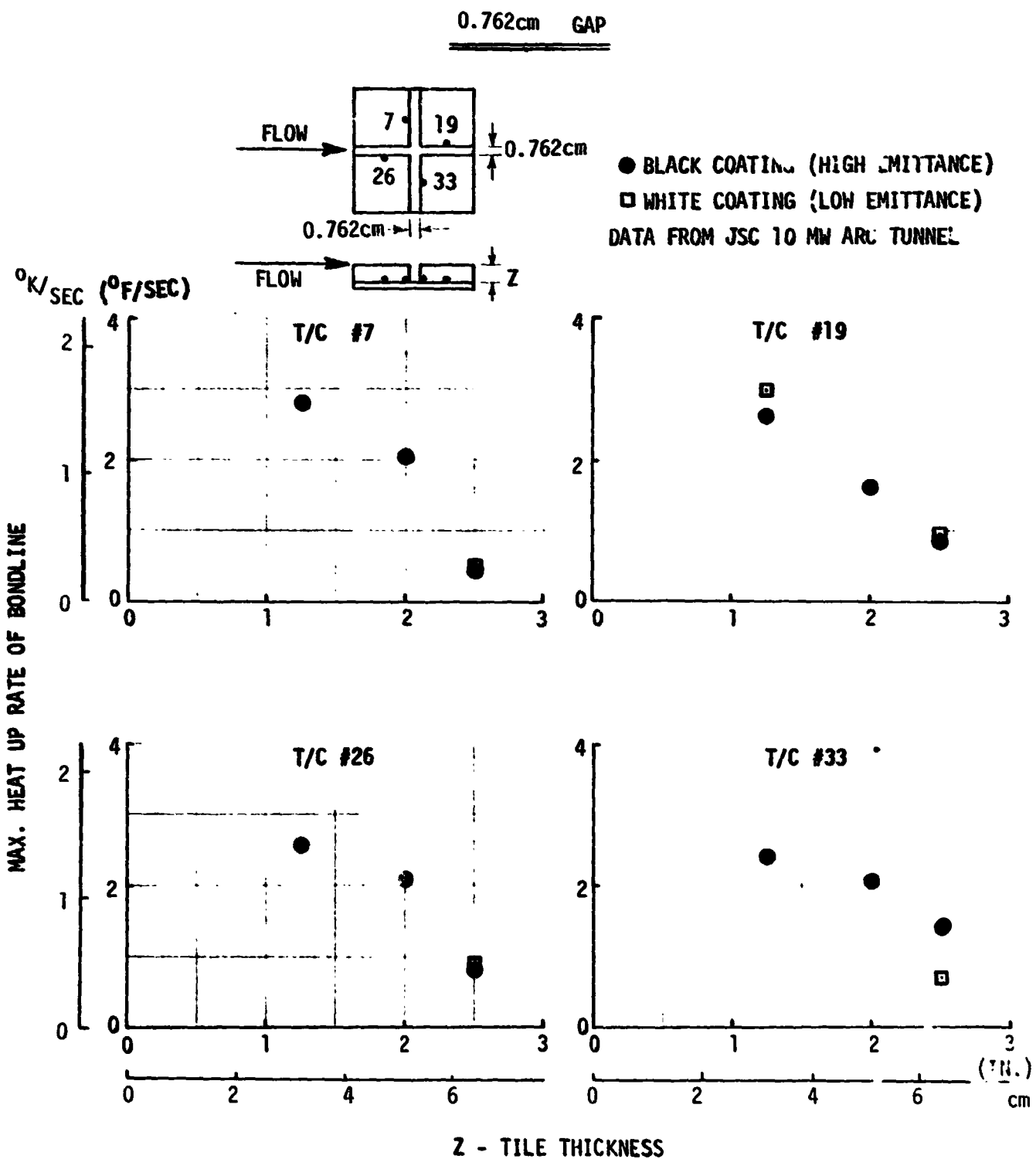


Figure 18



FINAL REPORT
VOLUME I

REPORT MDC E1003
29 JANUARY 1974

exception concerns response of the bondline of the downstream wall in the transverse gap of the 6.35 centimeter thick tile set. For that tile set and location, a higher bondline heat-up rate was recorded after applying a high-emittance coating to the gap walls. This inconsistency is unexplained, but is thought not to be attributable to the increased gap wall emittance. The recorded temperature distribution on the downstream gap wall (point C) is much higher with the "black" coating than for the "white" coating (Figure 19). Two parallel, high temperature, high emittance walls will experience high rates of radiant heat transfer. It would be expected, therefore, that if the "black" coated downstream wall is significantly hotter than the corresponding "white" coated wall, the "black" coated wall should also be hotter than the "white" coated wall on the upstream side of the gap. Comparison of data taken on the upstream (point F) wall of the gap, however, show little difference between the "black" coating and the "white" coating temperatures (Figure 19). instrumentation on the upstream wall of the transverse gap is on the side of the model (starboard side) opposite of that for the downstream wall (port side). There is no reason, however, to expect that the heating to these two locations should differ significantly. As a result, the high bondline heat-up rates measured on the "black" coated downstream wall of the transverse gap of the 6.35 centimeter tile model should not compromise the conclusion that increased gap wall emittance has little effect on bondline heat-up rate.

Review of the behavior of the butt joint data will provide some insight into the observed variations. For these tests, there are three primary parameters which affect bondline response at the gaps; 1) gap width to depth ratio, 2) scale of the gap relative to boundary layer thickness (e.g., the ratio of gap width to boundary layer thickness), and 3) heat transfer within or between tiles (i.e., conduction and radiation). The first of these, gap geometry, has a strong influence on flow structure within the gap (Reference 5) and on radiation exchange between the gap walls. It is therefore important to the distribution of energy deep within the gap. The ratio of gap width to boundary layer thickness is a determinant of the portion of the boundary layer which may be "captured" by the gap which, in turn, defines the energy of the "captured" flow and the heating which results from flow impingement on the gap walls. This parameter is, then, important to near-surface heating distributions and total temperature of the flow within the gap. The third factor, heat transfer within and between the tiles, determines how the convected heat is distributed in the tiles and interacts with the convective heating through

**TEMPERATURE DISTRIBUTION IN .381 CM
TRANSVERSE BUTT JOINT
FOR HIGH AND LOW EMITTANCE COATINGS**

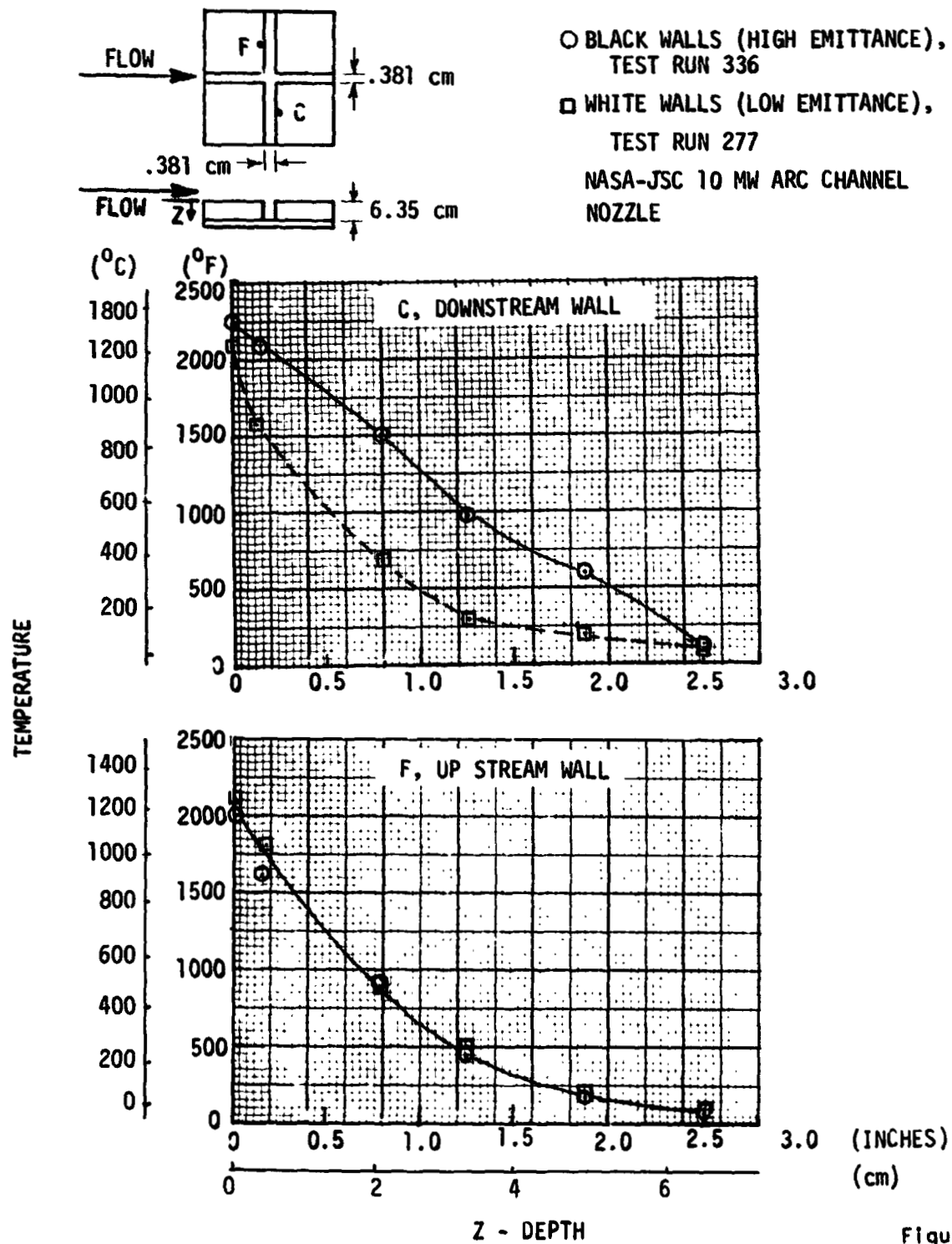


Figure 19



FINAL REPORT
VOLUME I

REPORT MDC E1003
29 JANUARY 1974

the effect of wall temperature or driving potential ($T_{AW} - T_W$). The butt gap bondline heat-up rates consistently increase with gap width (Figures 10 through 14) clearly showing that deep, narrow gaps inhibit penetration of the hot external flow. These data also show a consistent decrease in bondline heat-up rate as tile thickness is increased demonstrating insulative properties even in the presence of joint gaps. This is especially dramatic considering that the largest gap (0.762 cm) tested with the 6.35 centimeter tiles has a heat-up rate which is approximately equal to the heat-up rate of the smallest gap (0.127 cm) with the 3.18 centimeter tiles. In other words, doubling the tile thickness compensates for a six-fold increase in gap width.

Examination of the temperature variations along the gap wall from tile surface to bondline show the expected monotonic decrease. These data indicate, however, that the characteristics of the temperature profiles measured in axial gaps differ from those measured in transverse gaps. Temperature profiles were compared at times corresponding to peak surface temperatures. These comparisons showed the axial gap temperatures to be higher near the surface, but to decay more rapidly than those of the transverse gaps. This is most likely due to a greater penetration of the laminar boundary layer into the long axial gap as opposed to more efficient mixing of the highly vortical flow in the transverse gaps. A general conclusion relating bondline heating severity to joint orientation cannot be based on this observation alone because the variation of gap heating with environment and gap dimensions is not the same for axial and transverse gaps. Figures 10 through 14 show that either gap orientation may be the more severe, depending on the exact circumstances. The axial gaps have a length to depth ratio ranging from 3.7 to 7.5, which approaches geometries for which flow has been observed to reattach on the floor of two-dimensional transverse slots (Reference 6). The heating in the axial gap would, therefore, be much higher if the flow were not restricted by the small width of the slot (less than one boundary layer thickness). In-depth temperature distributions down walls of the axial gap show higher near-surface heating at the upstream location. This is probably due to the proximity (5.74 cm) of the downstream instrumentation to the aft closure of the axial gap. This closure forces the flow in the gap either to recirculate or rejoin the external flow. Since near-surface heating on the walls of the axial gap controls bondline response (Reference 7), the flow which expands into



FINAL REPORT
VOLUME I

REPORT MDC E1003
29 JANUARY 1974

the gap and is attached to the upper surface of the vertical walls is of primary importance. The portion of the vertical wall exposed to the attached heating increases in the downstream direction up to the point where the gap end closure begins to force the flow back out of the gap. This flow structure shifts both with the ratio of gap length to depth and with the ratio of gap width to boundary layer thickness (the boundary layer must "wrap" around the gap corner). This shifting will cause the axial location of the most severe bondline heat-up rate to vary and introduces a sensitivity of test results to instrumentation location. The location of the instrumentation in the transverse gaps should be less important since flow in those gaps is more nearly two dimensional, except in the vicinity of the intersection with the axial gap. As a result, it can be expected that comparisons between axial and transverse gaps may be misleading since the instrumentation in the axial gaps will not always be in the most severe location.

Manufacturing tolerances, structure deflection, etc., can cause either forward- or aft-facing steps at the transverse gaps. Both these configurations were tested by using two upstream butt-gap tiles of 5.08 centimeter thickness and two downstream tiles 5.46 centimeters thick to create forward-facing steps or two downstream tiles 4.70 centimeters thick for aft-facing steps. The results of these tests are illustrated in Figure 20 and compared with results of the tests of 5.08 centimeter thick butt-joint tiles with flush surfaces. For small gap widths, both forward and aft facing steps produced bondline heat-up rates lower than those of the flush tiles. The aft-facing steps provide better thermal protection due to the shielding effect while the forward-facing step is cooler because of the thicker tiles (5.46 cm as opposed to 5.08 cm). As the gap is opened, the aft-facing step maintains lower response rates, but the forward-facing step experiences bondline heat-up rates which increase to levels well above those of the flush tiles.

Alternate gap configurations also offer an opportunity for reduction of gap heating. Three configurations, the contoured, inclined and overlap block in addition to the butt joint were tested in the NASA JSC 10 MW Arc Tunnel. In each case the hot external flow is denied a direct path to the gap bottom. None of these configurations is an unqualified success, yet all achieve a reduction in bondline response at some instrumented location. Test data for 5.08 centimeter thick tiles of each candidate joint configuration are compared next and related to the 5.08 centimeter butt joint.

The measurements taken with the inclined joint tile set (Figure 21) exhibit a particularly wide range of sensitivity to gap width depending on instrument location. All locations are essentially equivalent to the butt joint performance (Figure 11).

EFFECT OF FORWARD- AND AFT-FACING
STEPS ON BONDLINE TEMPERATURE
RESPONSE OF 5.08 CM (2") BUTT JOINTS

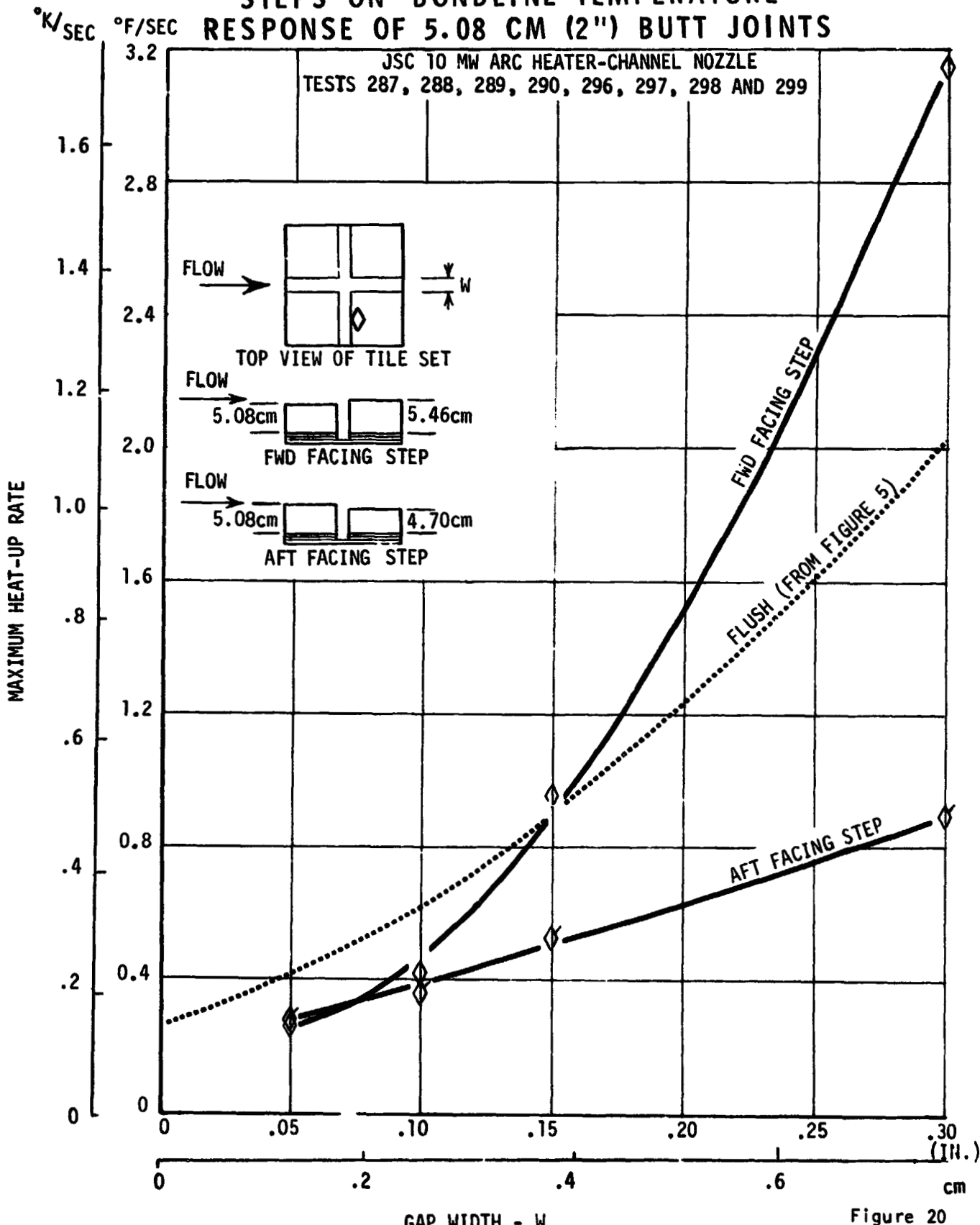


Figure 20

MCDONNELL DOUGLAS ASTRONAUTICS COMPANY - EAST

**RSI GAP HEATING
ANALYSIS**

**FINAL REPORT
VOLUME I**

**REPORT MDC E1003
29 JANUARY 1974**

**5.08 CM (2") INCLINED JOINT BONDLINE
TEMPERATURE RESPONSE**

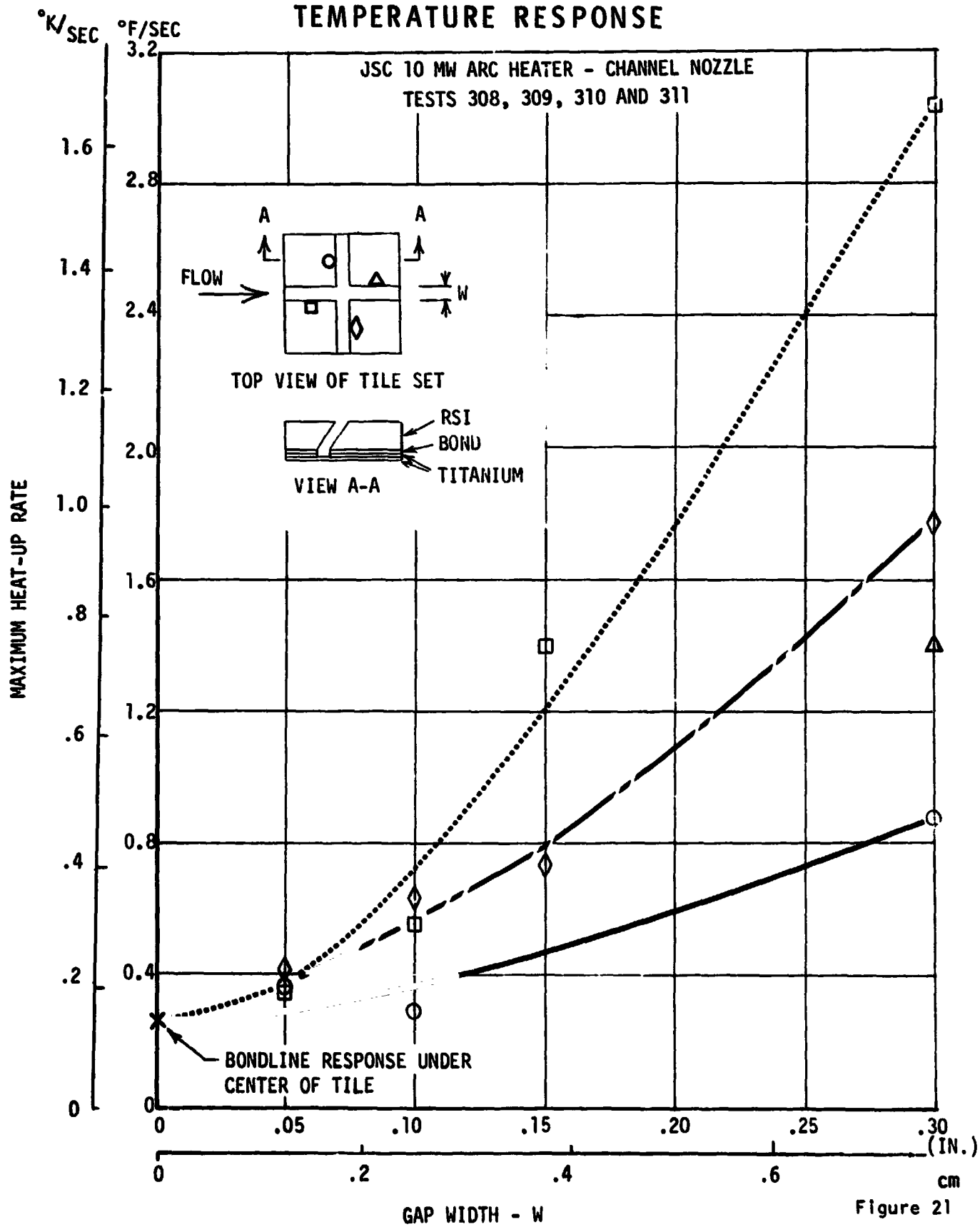


Figure 21

MCDONNELL DOUGLAS ASTRONAUTICS COMPANY - EAST

 RSI GAP HEATING
ANALYSIS

FINAL REPORT
VOLUME I

REPORT MDC E1003
29 JANUARY 1974

at a gap width of 0.127 centimeter. As the gap is opened, however, the heat-up rate of the upstream axial location quickly increases to a level well in excess of the heat-up rates experienced during the butt joint tests. The data taken at the bond-line of the downstream-facing transverse gap wall remain at relatively low levels for all gap widths and data taken at the other two locations are roughly equivalent to those of the butt joint configuration. The contoured joint configuration (which was more complicated) produced the least sensitivity to gap width of any of the configurations tested (Figure 22). It is also the only configuration for which bondline heat-up rate varies significantly with location for the 0.127 centimeter gap width. This configuration does, in fact, experience higher bondline heat-up rates in the downstream axial gap at widths of 0.127 and 0.254 centimeter than does the butt joint. With the largest gap width, though, the contoured joint provided significantly improved heat protection at all locations, compared to the butt joint. The overlap block configuration creates a tortuous path for gas circulating from the surface to the bondline. Figure 23, however, shows that the RSI filier block which is used to create that devious path suffers quite a high bondline heat-up rate. By referring to Figure 13 one may see that the other locations hold no advantage over the simple butt joint configuration. The results of these tests indicate, then, that if small gap widths can be achieved, little can be gained by use of joint configurations more complex than the butt joint. If gap widths approach the local boundary layer displacement thickness (about 1.016 centimeter for these tests), use of the contoured joint configuration may afford considerable relief and forward-facing steps at the joint may exact a considerable penalty.

 RSI GAP HEATING
ANALYSIS

FINAL REPORT
VOLUME I

REPORT MDC E1003
29 JANUARY 1974

5.08 CM (2") CONTOURED JOINT BONDLINE
TEMPERATURE RESPONSE

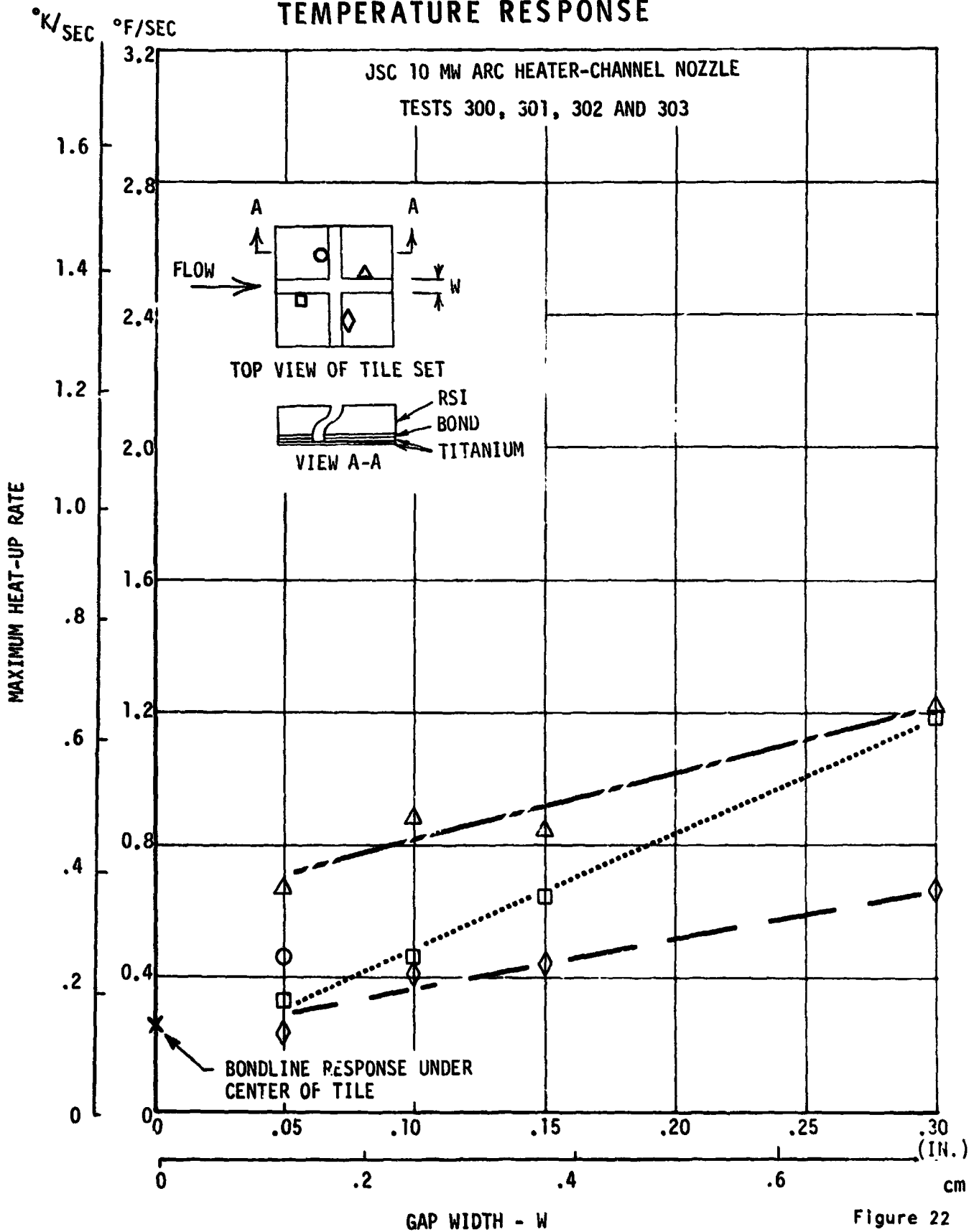


Figure 22

5.08 CM OVERLAP BLOCK BONDLINE TEMPERATURE RESPONSE

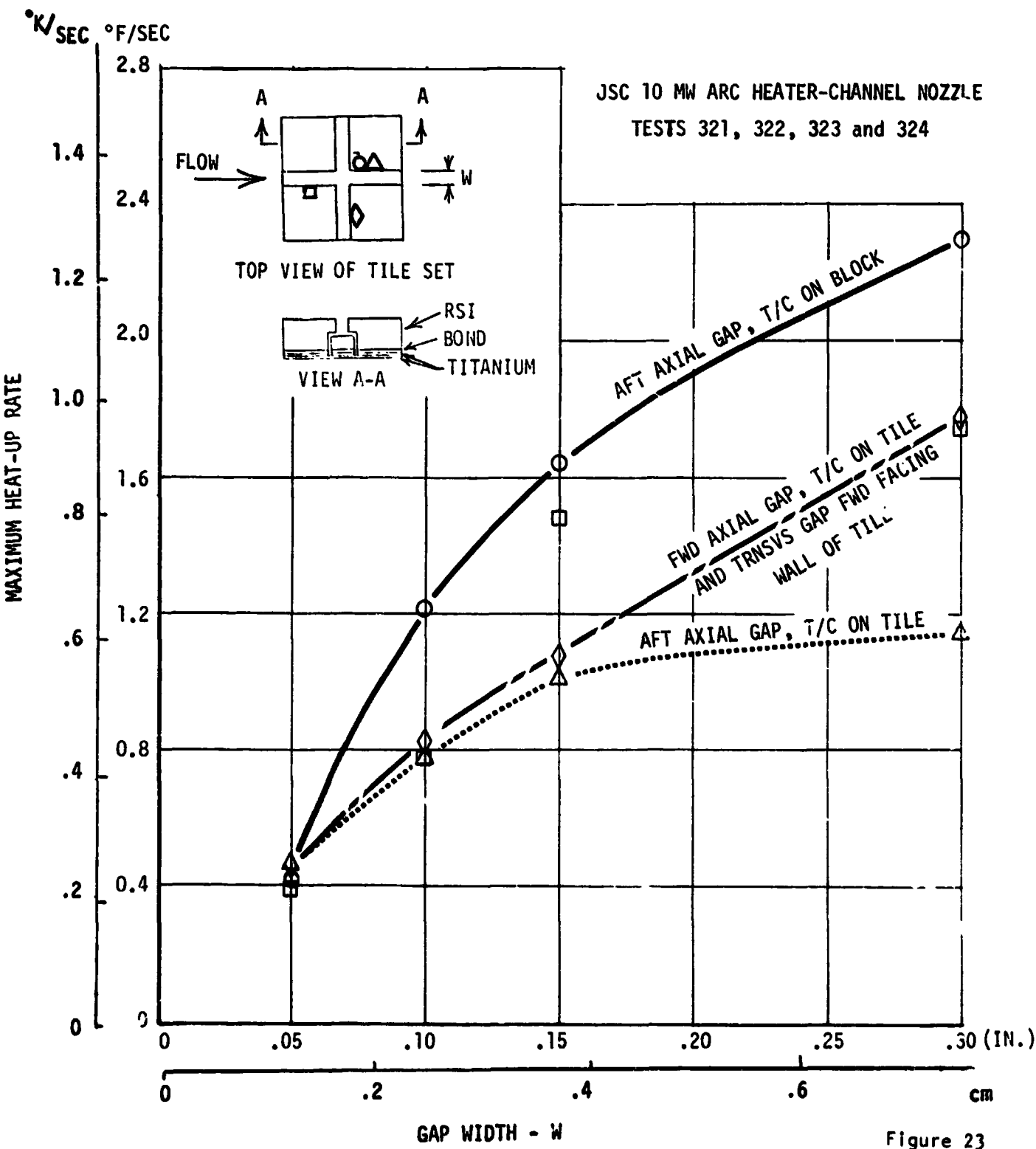


Figure 23



RSI GAP HEATING
ANALYSIS

FINAL REPORT
VOLUME I

REPORT MDC E1003
12 JANUARY 1974

4.2 Heating Rates in RSI Models of Gaps - Heating rate calculations using the RSI-gap thermal response histories measured during a test in the JSC 10 MW Arc Tunnel Channel Nozzle concentrated on a graphical description of the various modes of heat transfer in the gap, and on a detailed description of radiant heat exchange within the gap. Radiation exchange between the faces of a gap is important because relatively high temperatures (816°C or more) are experienced at depths of more than 1.27 centimeter. Preliminary data indicate that convective heating at such depths is on the order of 0.113 watts/cm^2 . For example a 8.3°C difference between two infinite plates (each with a 0.6 emittance) at 816°C produces about 0.113 watts/cm^2 net heat transfer. The 8.3°C is only a 1% change.

The radiation exchange modeling was refined by increasing the number of nodes on the gap wall from 8 to 17. Smaller area nodes are particularly helpful because they allow view factors and the nodal temperatures associated with them to approach the ideal condition of an infinitesimal element model. In modeling a 6.35 centimeter thick specimen, node lengths were decreased from 0.794 to 0.353 centimeters. alleviating the situation where large nodes are used in an analysis of a small gap. In the case of large nodes, the only significant view factor may be with the opposite node, virtually eliminating the opportunity for emitted or reflected energy to be transferred down the gap. Node size in the thermal model was varied so that the smallest nodes occurred in the region of highest temperature.

In Figure 24, the heat transfer for the wall of a typical gap is segregated into its three components: convection, radiation and conduction. Information on this figure was obtained by solving for each component in a series of computer cases. This curve is plotted on cartesian rather than semi-logarithmic paper in order to show the comparative magnitude of each component. The figure is for run 285 in the JSC 10 MW Arc Channel. The specimen was a 3.18 centimeter butt joint with a 0.381 centimeter gap. The location analyzed was a forward facing transverse wall. The test was analyzed using the model with 18 nodes down the gap, using the inverse solution method described in section 4.2.1. Temperatures for the uninstrumented wall of the gap were set equal to the values of the corresponding nodes on the instrumented wall. Heat fluxes less than zero indicate energy leaving the surface at that depth. The conductive flux consists of two parts, the conduction between adjacent coating nodes and conduction into the RSI, normal to the surface of the gap wall.

The convective heating and radiative flux shown in Figure 24 are large at the top of the gap and their distributions approximately mirror one another. By

 RSI CAP HEATING
ANALYSIS

FINAL REPORT
VOLUME I

REPORT MDC E1003
29 JANUARY 1974

HEAT FLUX COMPONENTS COMPUTED FOR
3.18 CENTIMETER RSI BUTT JOINT MODEL

- o NASA JSC 10 MW CHANNEL FACILITY RUN 285
- o ANALYSIS @ PEAK HEATING (460 SECONDS)
- o INSTRUMENTATION ON FORWARD-FACING TRANSVERSE WALL
- o GAP EMITTANCE = 0.6
- o SURFACE HEATING RATE = 22.34 WATTS/cm²

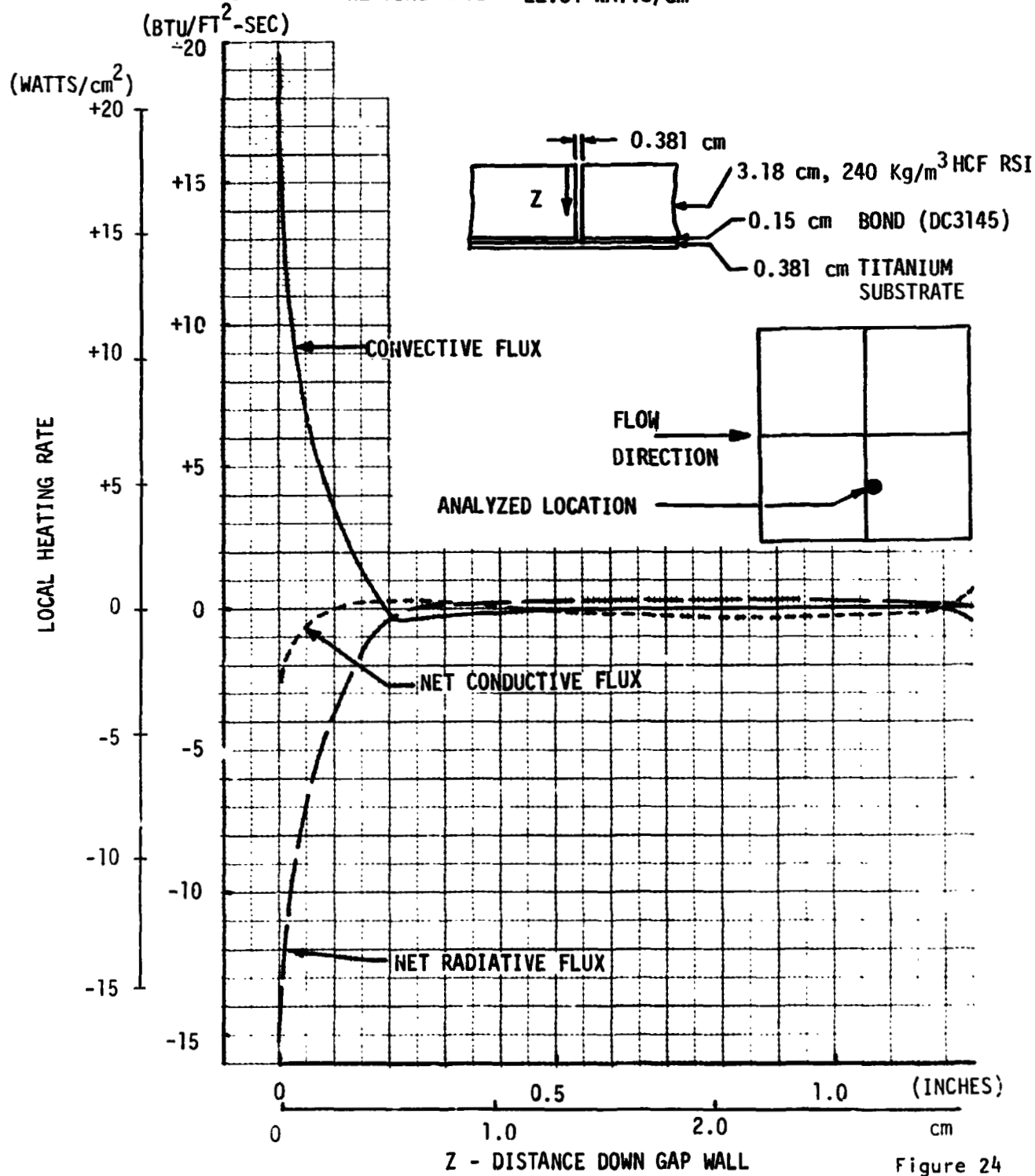


Figure 24



RSI GAP HEATING ANALYSIS

FINAL REPORT VOLUME I

REPORT MDC E1003
29 JANUARY 1974

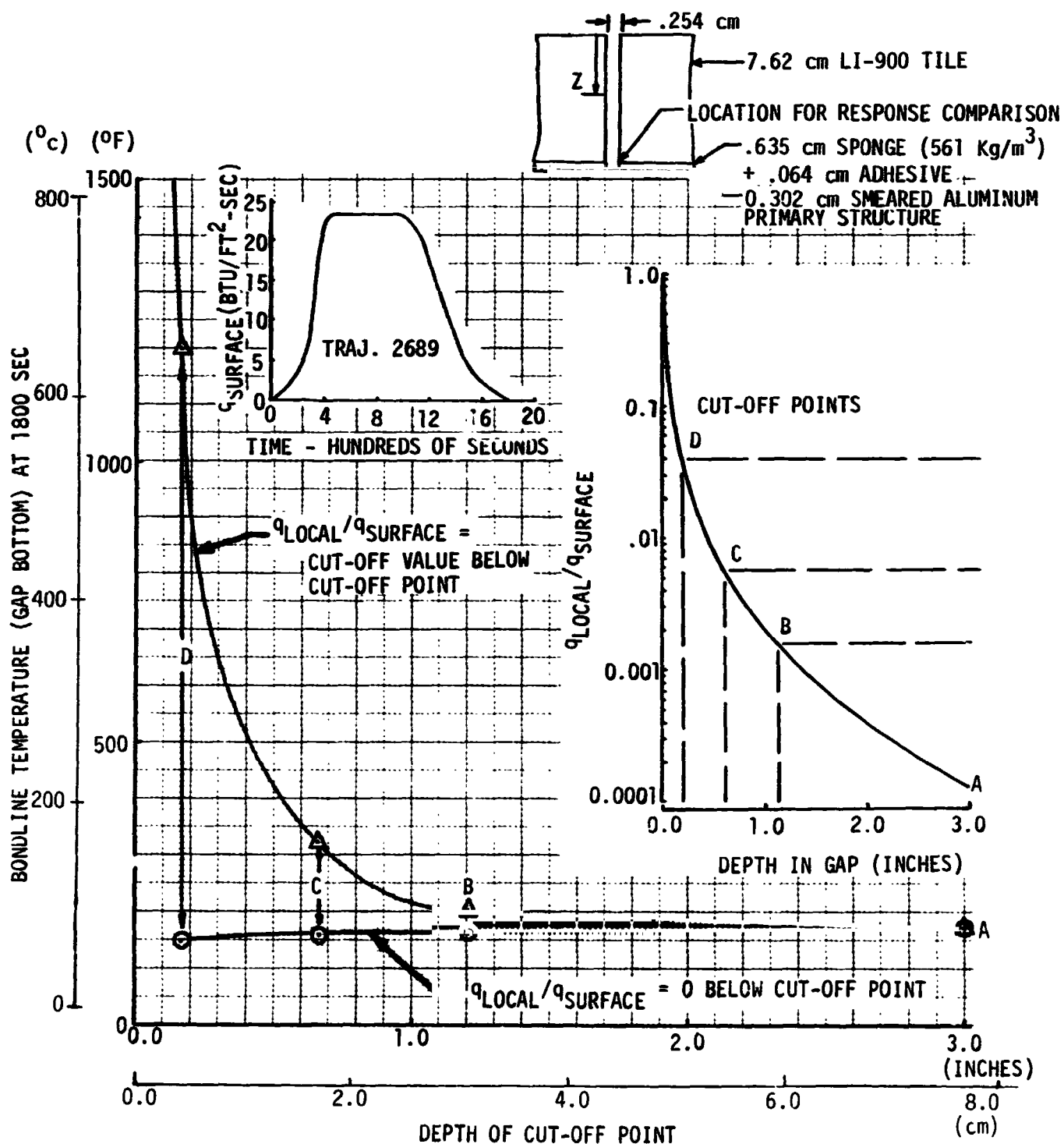
approximately 0.508 centimeters into the gap the convective and radiative heat fluxes are small and their distribution into the depths of the gap can be computed using identical thermal histories for both walls of the gap. The net conductive flux has the greatest magnitude near the top of the gap as expected but much smaller than either the radiative or convective components. The negative net conductive flux at the top of the gap is indicative of a temperature distribution which is approaching steady state and the remainder of the conduction curve is most likely due to the transient thermal response of the RSI. During peak heating, the gap wall is hotter at every depth than laterally adjacent RSI material so the conduction in the normal direction is always negative.

Figure 25 shows the results of a study to determine the impact of uncertainties in gap heating rate distribution on shuttle TPS performance. The TPS system analyzed is depicted on the figure. LI-900 properties were used for the 7.62 centimeter thick RSI tile. A 0.635 centimeter sponge strain isolator was used. Shuttle altitude and reference heating rate histories corresponding to entry trajectory 2689 were used. A heating rate multiplier was applied to the reference heating rate, such that at peak heating a radiation equilibrium temperature of 1260°C was obtained. A ratio of $q_{\text{LOCAL}}/q_{\text{SURFACE}}$ as a function of depth in gap chosen on the basis of preliminary data is shown on this figure.

The heating rate versus depth curve was carried down the full 7.62 centimeters (Point A) in one computer case. The curve was stopped at points B, C, and D for others with a pair of cases run for each point. In one case of the pair, the curve dropped to zero (no heating) below the cut-off point. In the other the $q_{\text{LOCAL}}/q_{\text{SURFACE}}$ value at the cut-off point was retained down to the gap bottom. For these seven cases the temperature at the LI-900/sponge bondline on the gap wall is computed for 1800 seconds and plotted as a function of the cut-off depth.

Bondline temperature is a factor which must be controlled through proper TPS design. The adhesives and strain isolation sponges available for this type of system have relatively low temperature capability compared with the RSI to which they are applied. The results of this analysis give an indication of the level at which gap heating ceases to be a significant factor in determining bondline temperature. The cut-off point can be regarded as a hypothetical point in the gap above which convective heating rates are known, and below which they are uncertain. An extremely conservative design approach would be to assume the value remains constant from that point. A nonconservative approach would be to assume no heating below the cut-off point. The true heating rate distribution, lies between these two

**SENSITIVITY OF MINIMUM HEATING RESOLUTION
IN RIS C.P. BONDLINE TEMPERATURE**





**RSI GAP HEATING
ANALYSIS**

**FINAL REPORT
VOLUME I**

**REPORT MDC E1003
29 JANUARY 1974**

assumptions. For this case the two curves do not diverge strongly unless the cut-off depth is less than 2.54 centimeters. For this situation, it is obvious that if the heating rate distribution is known accurately down to a depth of 2.54 centimeters ($q_{LOCAL}/q_{SURFACE} = 0.002$), the ill effects of uncertainties below that are minimal. The extrapolation to point A is essentially equivalent to setting $q_{LOCAL}/q_{SURFACE} = 0$ at these cut-off points. It should be noted however, that an extrapolation of the heating rate curve into the uncertain region would be more accurate than either extreme alternative. Also the heating rate distribution curve chosen for the analysis is somewhat arbitrary but extremely important in determining the results of this analysis. A more severe curve needs to be known accurately to a greater depth than a less severe one. The effect on bondline temperature is a function both of cut-off point and heating rate magnitude at that point.

4.2.1 Comparison of Heating Rate Distributions in RSI Models of Gaps - The convective heating analyses of gap tests contained in this section were performed in the NASA-JSC 10 MW Arc Tunnel facility utilizing series of adjustable RSI models installed in one wall of a channel nozzle. Convective heating in the gaps between tiles was calculated using the MDC General Heat Transfer Program inverse solution technique. A description and the method of utilizing this technique are given in the following paragraphs.

Data available from RSI tile tests exist in the form of temperature responses from thermocouples situated at known locations on the RSI surface and gap walls. The inverse solution technique uses these measured temperature histories as boundary conditions to compute required heat flux. In the thermal models used for this study all heat transfer mechanisms, except convective heating, are described analytically and the convective heating is computed.

Because previous analysis work done under Contract NAS9-12854 has shown that heating rates deep in RSI gaps will be relatively small, a thermal model is used which can accurately represent modes of heat transfer present during the tests so that the inversely-derived heat flux is due to convective heating alone. Conduction and radiation may account for greater transfer than convection for gap nodes near the TPS bondline, so large errors in modeling these nodes cannot be tolerated. The technique of thermally modeling the RSI joints developed during NAS9-12854 has been improved. The gap thermal model (Figure 26) consists of 130 nodes and contains the RSI tiles, the waterproof coating, the adhesive, supporting substructure, the opposite wall of the channel and the fixture enclosure. This particular model can be easily configured for a butt, inclined or contoured joint by changing only key



FINAL REPORT
VOLUME I

REPORT MDC E1003
29 JANUARY 1974

REPRESENTATIVE TWO DIMENSIONAL
THERMAL MODEL OF RSI JOINT

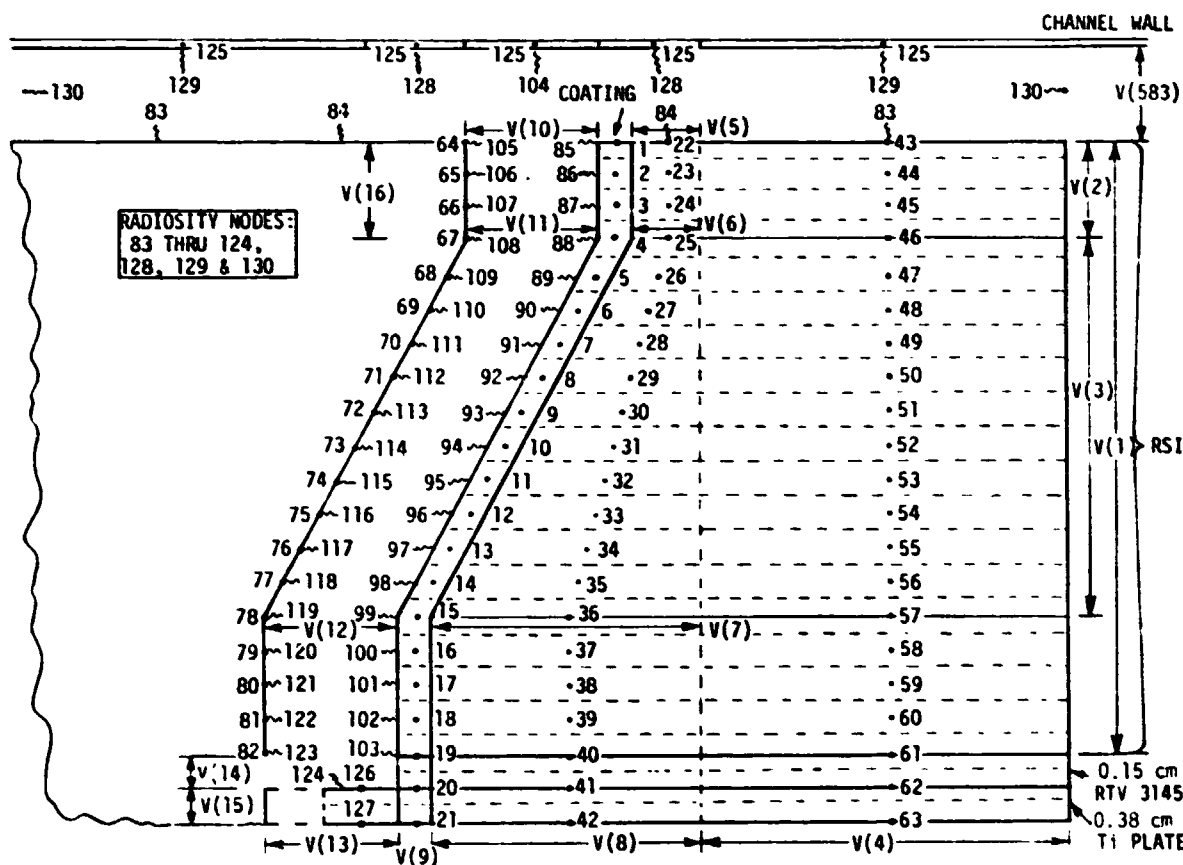


Figure 26



**RSI GAP HEATING
ANALYSIS**

**FINAL REPORT
VOLUME I**

**REPORT MDC E1003
29 JANUARY 1974**

dimensions V(1,2,3,5,6,7 and 8) shown in the figure. A subroutine automatically recomputes nodal dimensions. Conduction is modeled in two dimensions within all materials and between adjacent materials. Heat storage is modeled for all specimen nodes. Radiant heat exchange between all surface nodes is modeled using a radiosity network which accounts for radiant emission, absorption and reflection. The radiation view factors between surface nodes are automatically recomputed by a subroutine to account for thermal expansion which changes the gap width. The gap width is also automatically recomputed and will be used in the data correlation. Data tapes received from the test facilities were converted to binary form for more compact data storage. The measured temperatures which were recorded on magnetic tape during the various tests were input to the computer model. Second-order interpolation of these temperatures is used to obtain temperature boundary conditions for the inverse solution calculation.

The temperatures within the four RSI tiles of the joint model were obtained from measurements through an instrumented plug in one of the tiles. These temperatures within the RSI tiles had a different value than the gap temperatures at a given depth, and therefore were required to account for conduction from the gap wall into the tile. Anomalies in thickness and thermal properties of the RSI coating along the gap wall were accounted for by a nulling process which utilized temperatures obtained during the Argon preheat phase of the test run.

Convective heating results for the transverse and in-line gaps were obtained for the butt and inclined joint configuration. Four gap widths (0.127, 0.254, 0.381, and 0.762 centimeter) and three tile thicknesses (3.18, 5.08, and 6.35 cm) were analyzed for the butt joint configuration. The inclined joint was analyzed for the 6.35 cm tile and all gap widths. Heating distributions for the downstream wall of the transverse gap for the butt joint configuration are shown in Figures 27, 28, and 29. The data on Figures 27 and 28 are presented in rectilinear and semi-log coordinates to emphasize the low magnitude of convective heating in the transverse gap at depths beyond 0.762 centimeter for the arc heater environment produced by the 10 MW facility. In comparing these figures it is seen that heating drops off rapidly down the gap. heating increases with gap width and penetrates deeper into wide gaps, and that for a wide gap (0.762 cm) the heating rate ratio near the top of the gap can be higher than 1.0. Figure 30 is another way of presenting the above data, as a function of gap width, and indicates that for most conditions increasing gap depth lowers the gap heating distribution.



FINAL REPORT
VOLUME I

REPORT MDC E1003
29 JANUARY 1974

BUTT JOINT HEATING RATE DISTRIBUTION
FOR 3.18 CM TILE

- JSC 10 MW CHANNEL NOZZLE TEST
- DOWNSTREAM TRANSVERSE GAP
- HIGH EMMITTANCE COATING 0.635 cm DOWN TILE GAP
- LOW EMMITTANCE COATING REMAINING GAP SURFACE

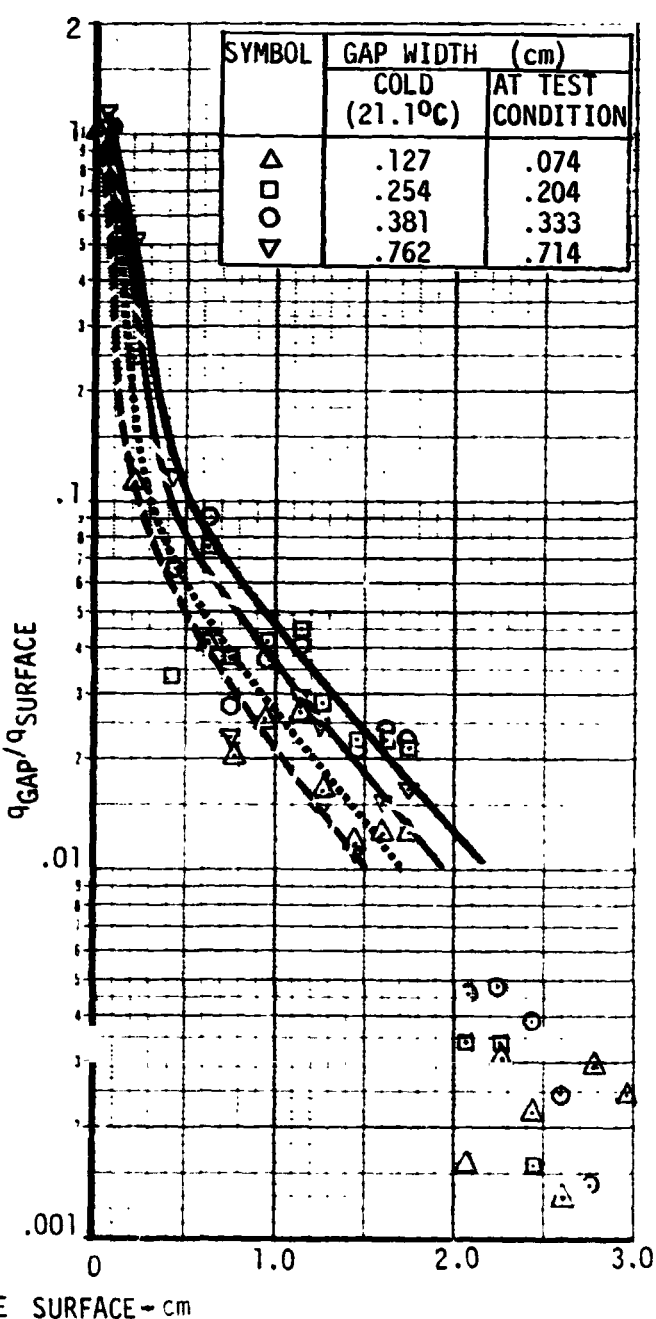
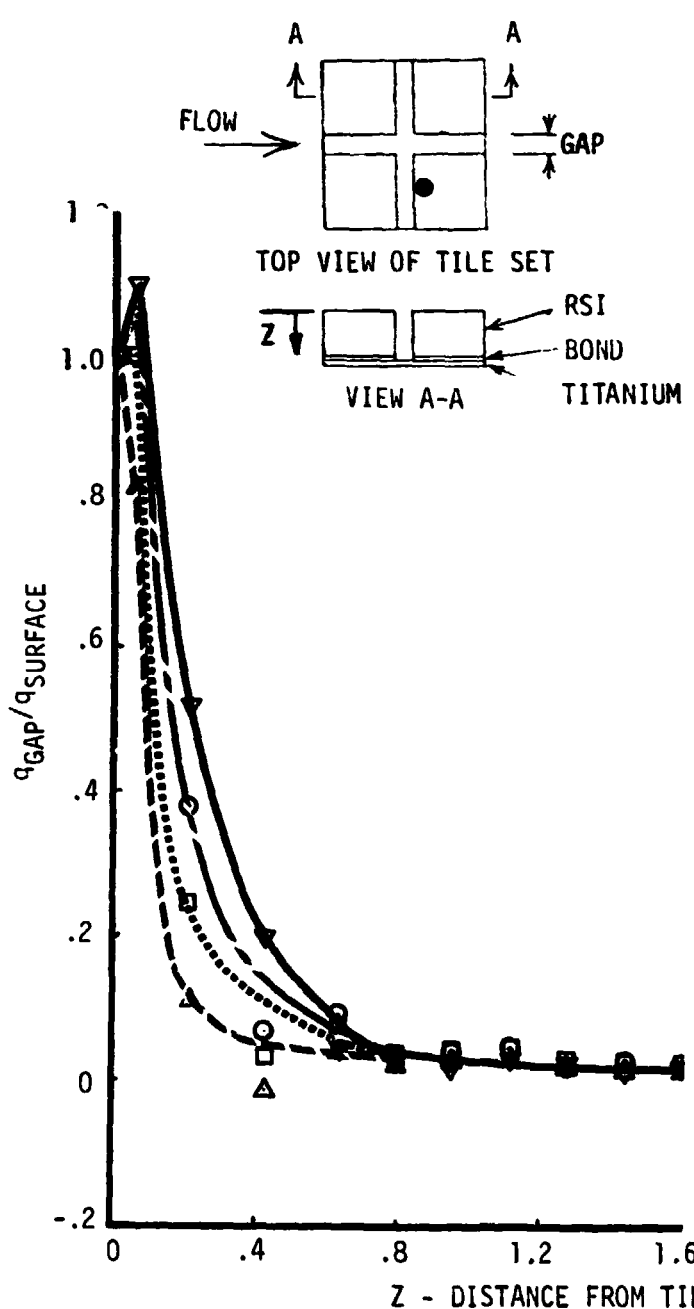
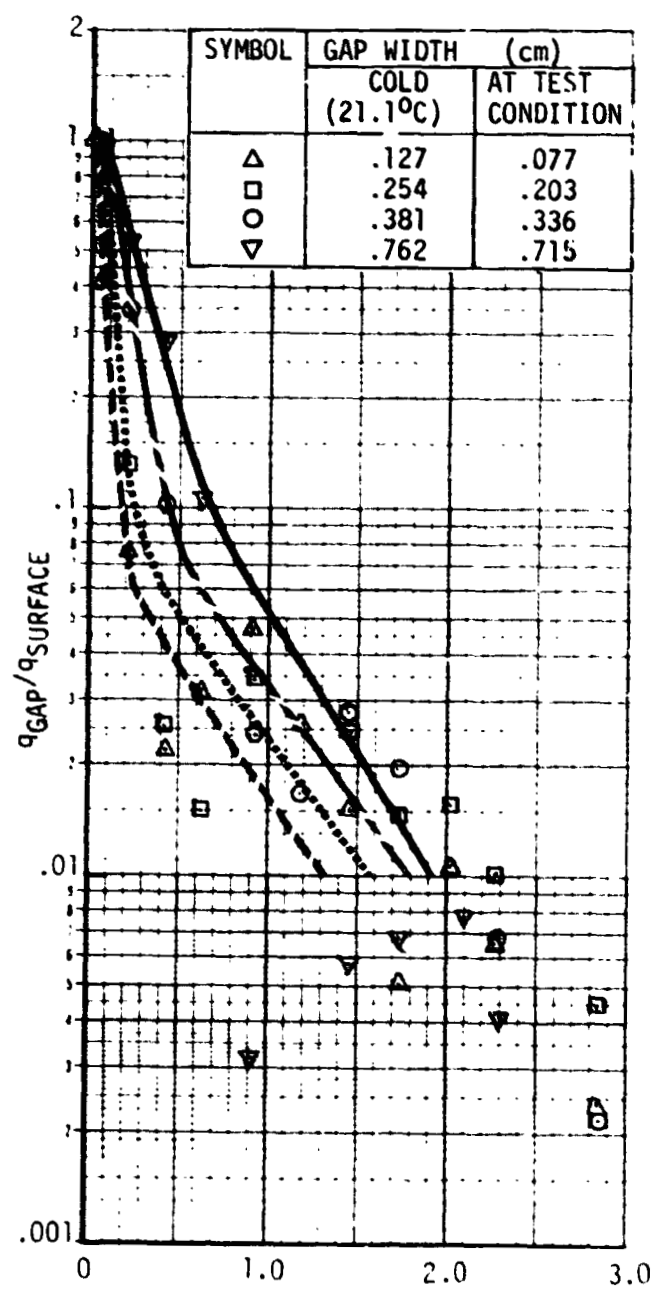
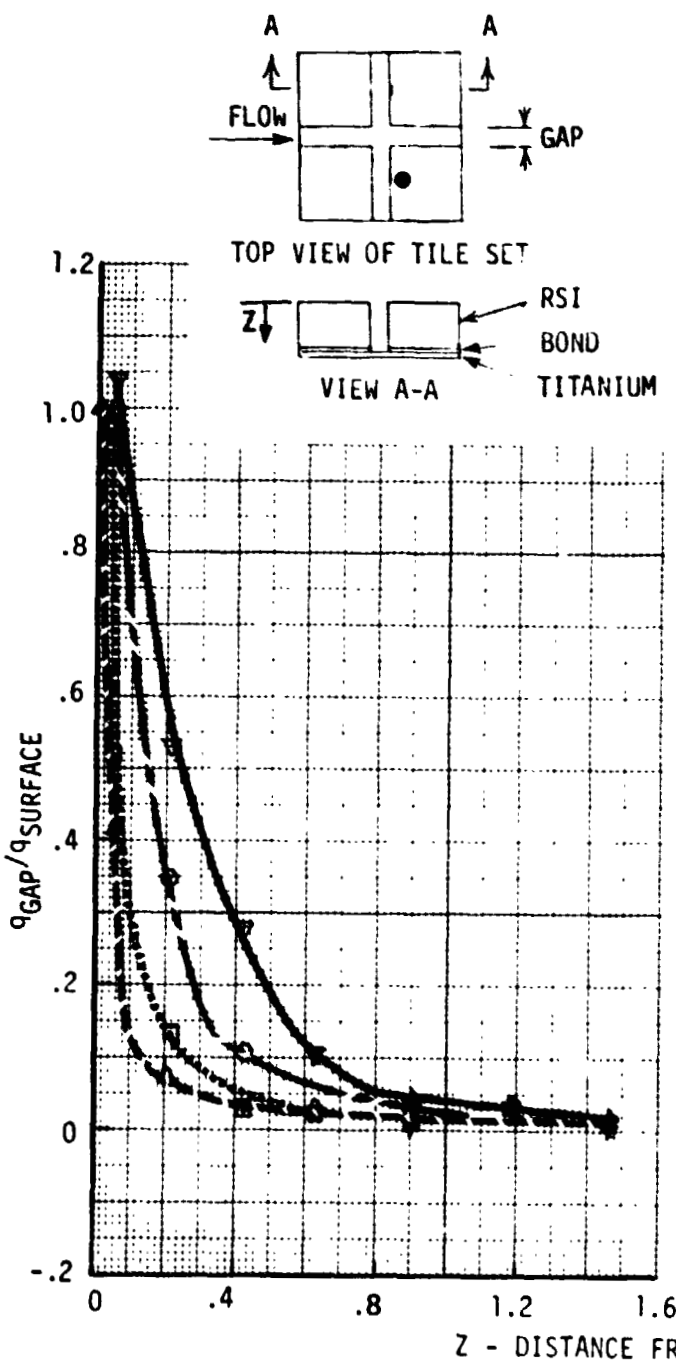


Figure 27

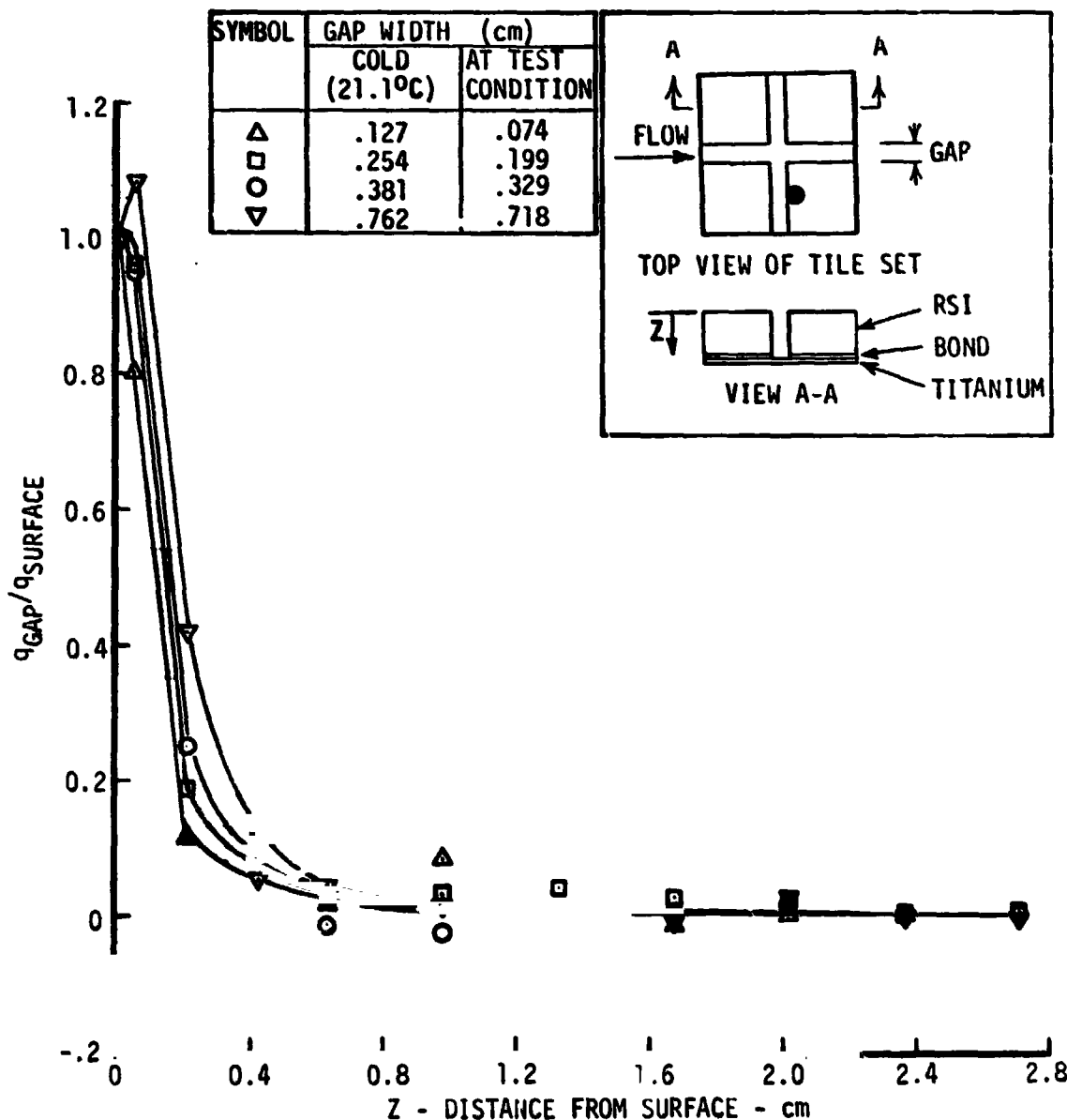
BUTT JOINT HEATING RATE DISTRIBUTION FOR 5.08 CM TILE

- JSC 10 MW CHANNEL NOZZLE TEST
- DOWNSTREAM TRANSVERSE GAP
- HIGH EMITTANCE COATING ON GAP WALLS



BUTT JOINT HEATING RATE DISTRIBUTION IN DOWNSTREAM TRANSVERSE GAP 6.35 CM TILE

- JSC 10 MW CHANNEL NOZZLE TEST
- HIGH EMITTANCE COATING 0.635 cm DOWN TILE GAP
- LOW EMITTANCE COATING REMAINING GAP SURFACE


Figure 29

COMPARISON OF DOWNSTREAM TRANSVERSE GAP
HEAT TRANSFER WITH GAP WIDTH
FOR SEVERAL BUTT JOINT THICKNESSES

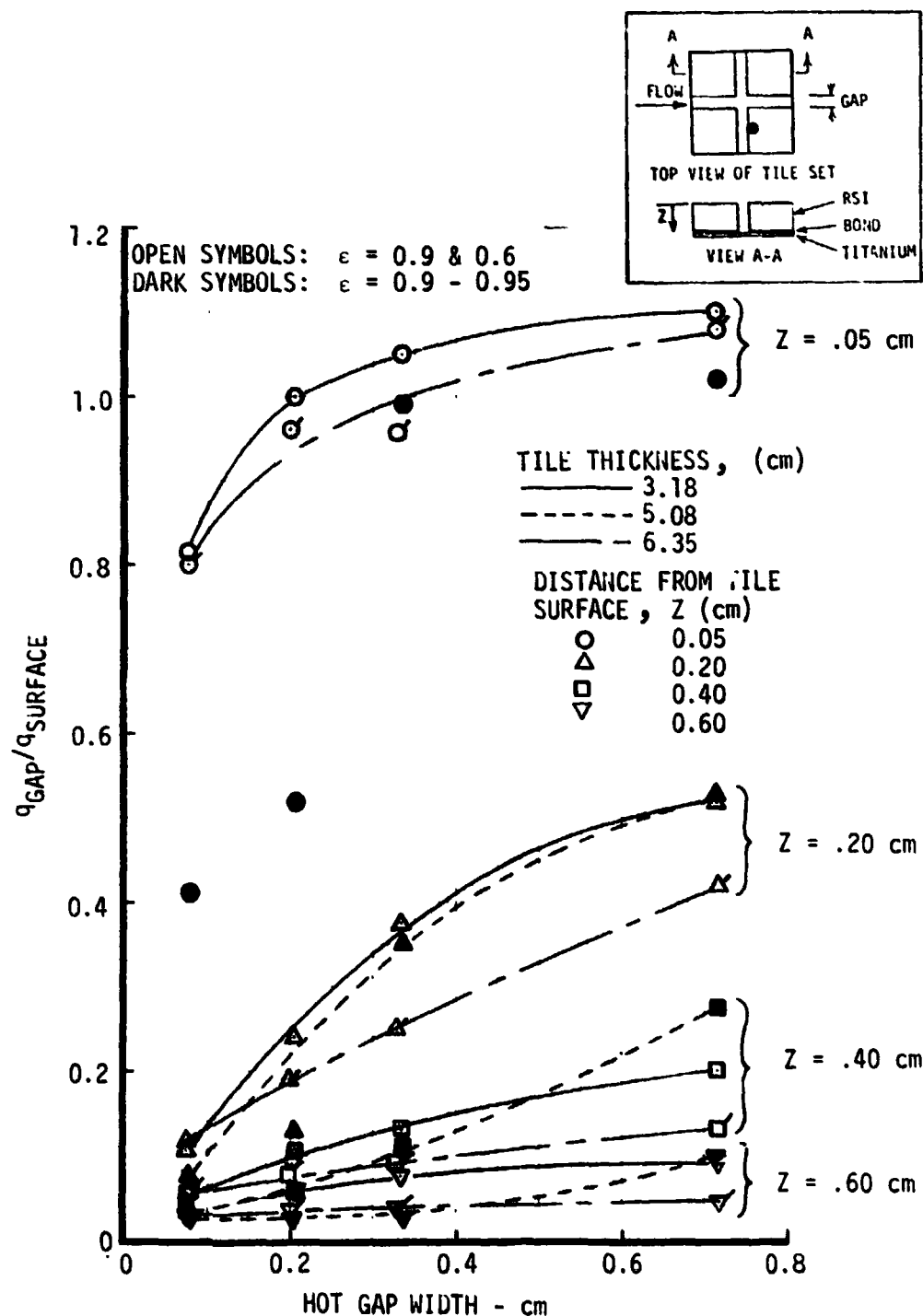


Figure 30

 RSI GAP HEATING
ANALYSIS

FINAL REPORT
VOLUME I

REPORT MDC E1003
29 JANUARY 1974

In-line gap heating distributions are shown in Figures 31, 32, and 33. Figures 31 and 32 are for tiles upstream of the transverse gap for tiles 5.08 and 6.35 centimeter thick. The data presented in Figure 33 is for the 3.18 centimeter tile, but for a location downstream of the transverse gap. The upstream location was not analyzed because of insufficient thermocouple data. A comparison of the data for the two type gaps indicates that heating in in-line gaps is higher than transverse gaps for some combinations of gap width and depth. At a depth of 0.2 centimeters into the gap, the heating is slightly higher than the transverse gap for all gap widths. For the wide gaps (0.381 and 0.762 cm) heating is somewhat higher than the transverse gap from 0.2 to 0.7 centimeters. Heating for the 6.35 centimeter tile and a gap width of 0.762 centimeters is considerably higher than the transverse gap and also considerably higher than the other gap widths when comparing the data to other tile thickness. When comparing Figure 34 to Figure 30 heating down the gap wall from 0.2 to 0.6 centimeter, the in-line gap is more sensitive to gap width than the transverse gap.

Figure 35 is a schematic of the butt joint model with a forward facing step depicting boundary layer flow trends and recirculation patterns in the transverse gap. Heating distributions for a wide and narrow gaps is shown in Figure 36 for a 5.08 centimeter tile. For the narrow gaps (0.064, 0.191, 0.317 cm) the heating near the top of the gap stagnates, increasing the heating rates. Since the gap is small, heating does not penetrate rapidly into the gap, therefore the heating falls off rapidly to 0.9 centimeters with the heating increasing gradually below that point. For the wide gap (0.711cm) the heating takes on a different distribution. Since the gap is wide the heating near the top gets relief from the wide gap below, which causes heating to recirculate and penetrate deep into the gap. This distribution is significantly higher than the narrow gaps. Because the step distorts the gap heating distribution, significant increases in heating occurs. Figure 37 shows a comparison of downstream transverse gap heating for a butt joint model with and without a forward facing step. Heating along the gap wall can be an order of magnitude or more greater than for a flush model.

Convective heating analyses for an inclined joint model were performed for the downstream side of the transverse gap and for an in-line gap upstream of the transverse gap. The tiles were 6.35 centimeters thick. The heating distributions are very similar to the butt joint. The transverse gap as seen in Figure 38 shows that the heating for the inclined joint is slightly greater and more sensitive to gap width from 0.1 to 0.7 centimeter depths. The 0.706 gap width heating is greater than



FINAL REPORT
VOLUME I

REPCRT MDC E1003
29 JANUARY 1974

BUTT JOINT HEATING RATE DISTRIBUTION
UPSTREAM AXIAL GAP
5.08 CM TILE

- o JSC 10 MW CHANNEL NOZZLE TEST
- o HIGH EMITTANCE COATING ON GAP WALLS

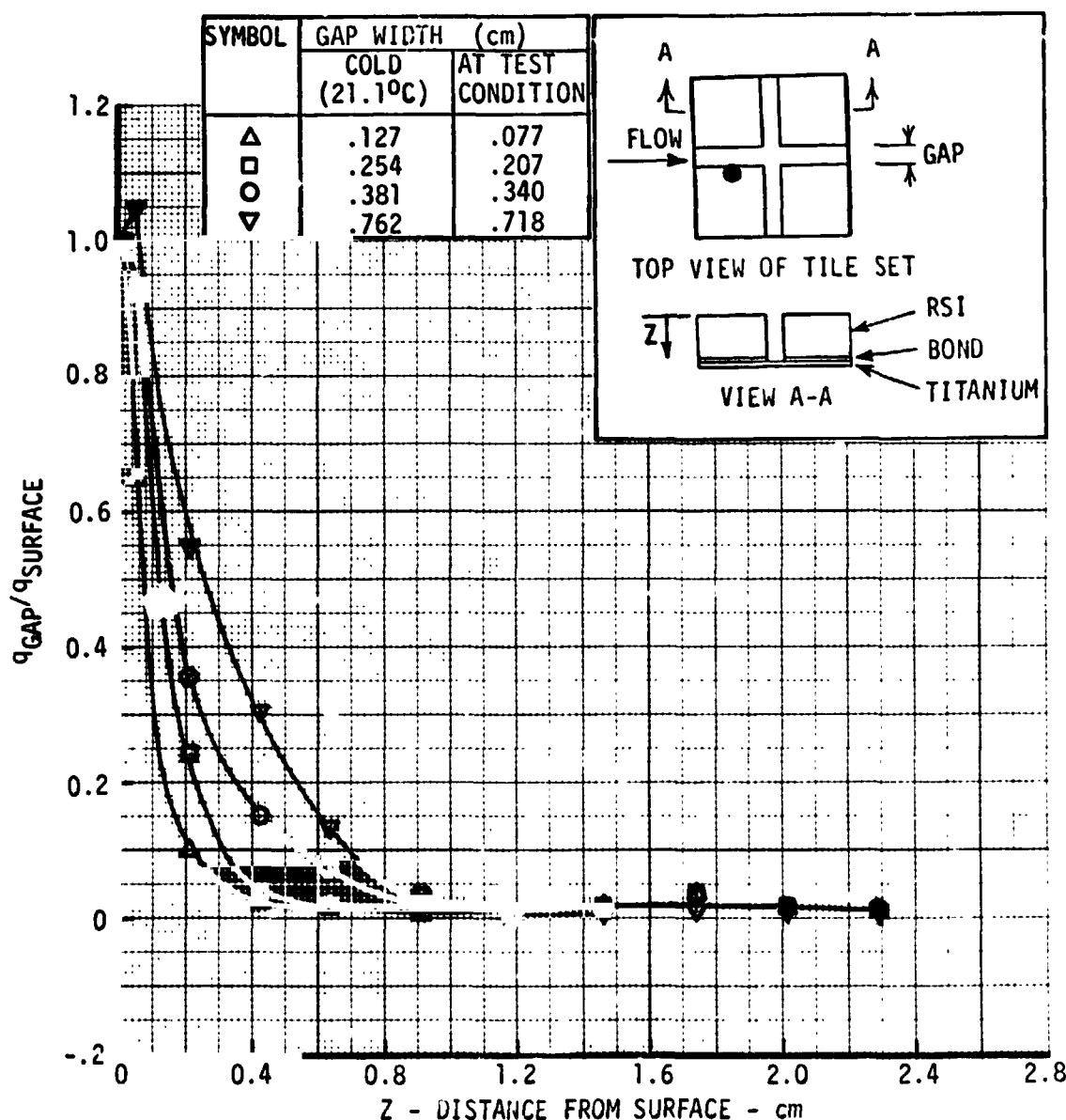


Figure 31

BUTT JOINT HEATING RATE DISTRIBUTION
UPSTREAM AXIAL GAP
6.35 CM TILE

- o JSC 10 MW CHANNEL NOZZLE TEST
- o HIGH EMMITTANCE COATING 0.635 cm DOWN TILE GAP
- o LOW EMMITTANCE COATING REMAINING GAP SURFACE

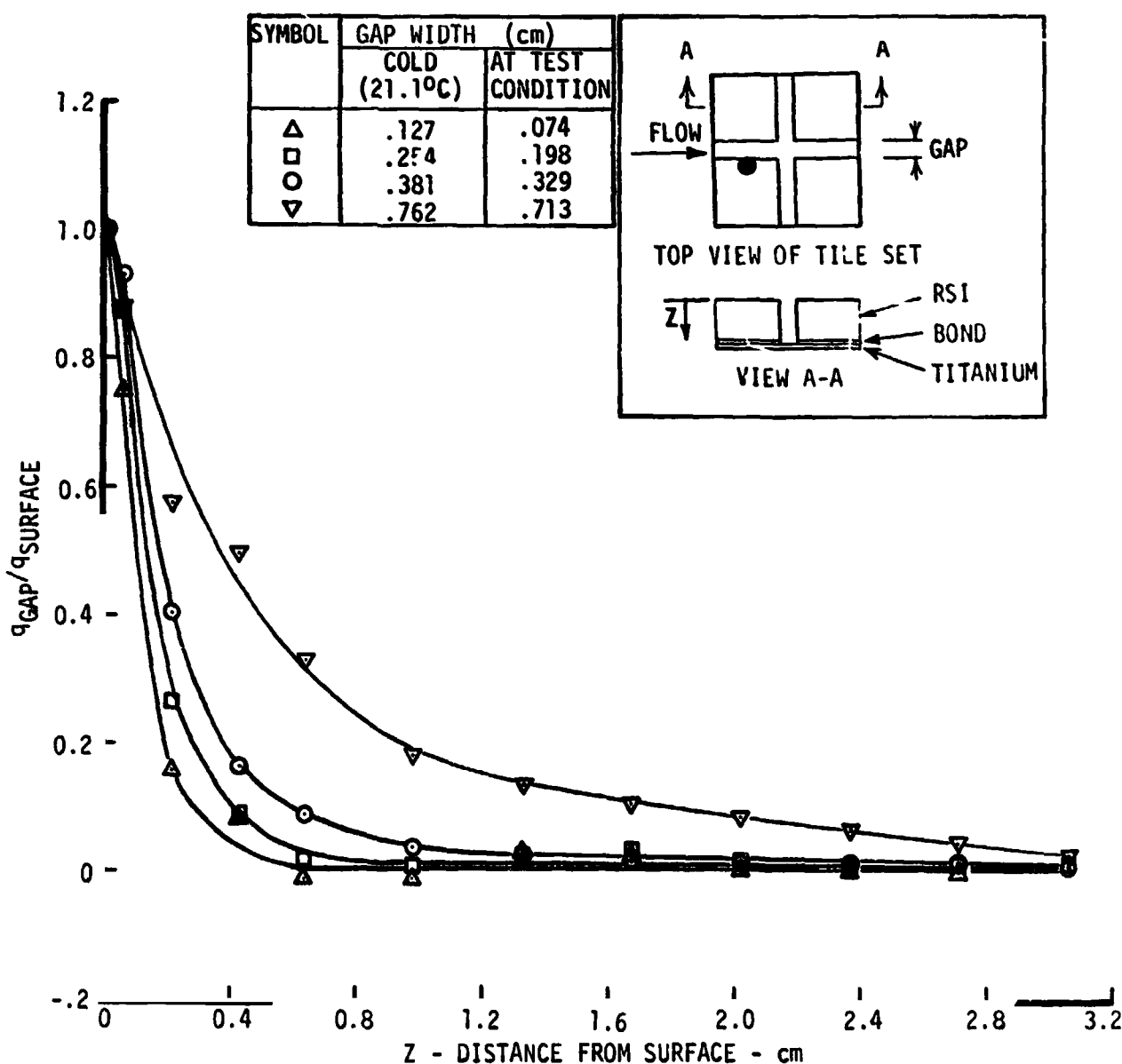


Figure 32



FINAL REPORT
VOLUME I

REPORT MDC E1003
29 JANUARY 1974

BUTT JOINT HEATING RATE DISTRIBUTION
DOWNSTREAM AXIAL GAP
3.18 CM TILE

- o JSC 10 MW CHANNEL NOZZLE TEST
- o HIGH EMITTANCE COATING 0.635 cm DOWN TILE GAP
- o LOW EMITTANCE COATING REMAINING GAP SURFACE

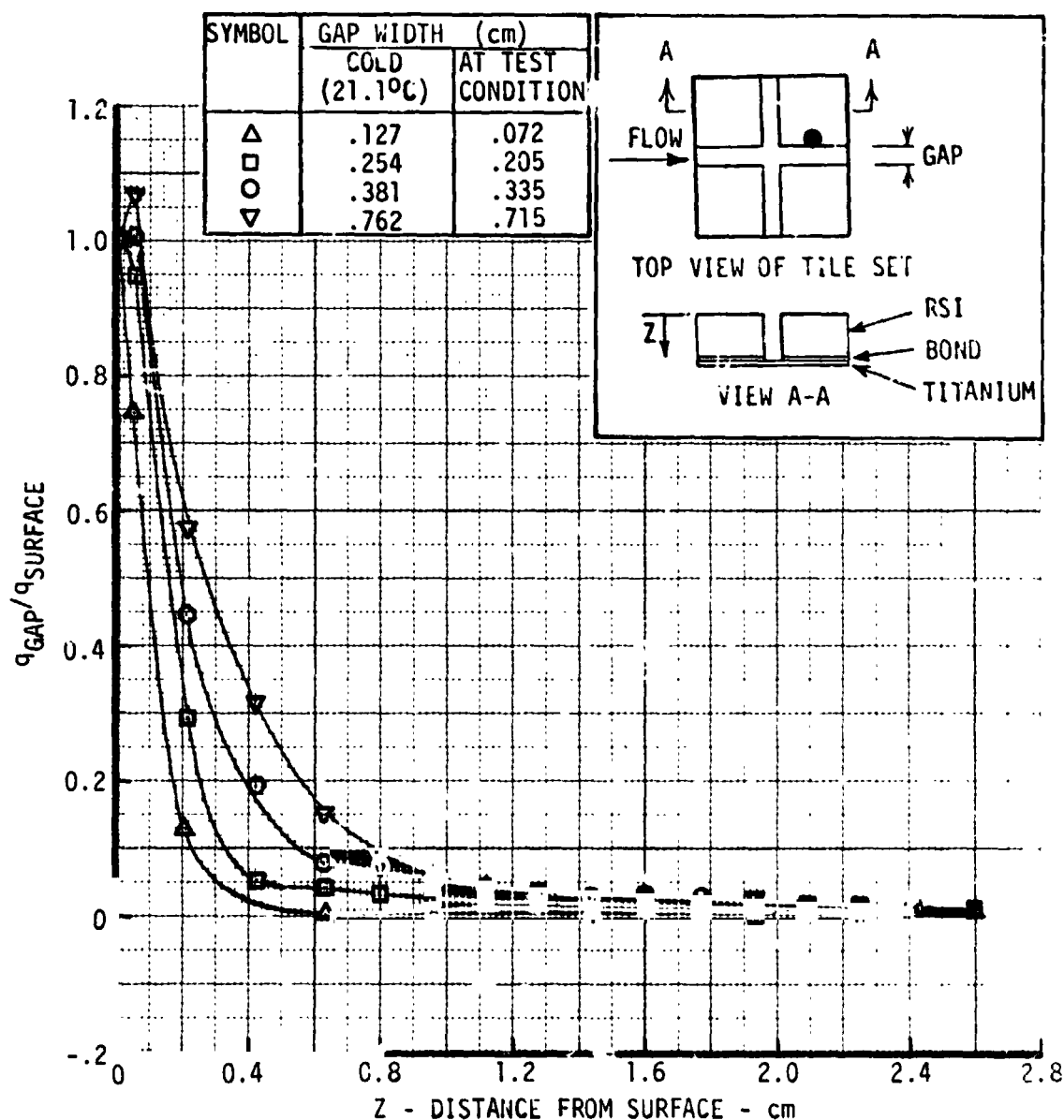


Figure 33

COMPARISON OF AXIAL GAP HEAT TRANSFER WITH GAP WIDTH FOR SEVERAL BUTT JOINT THICKNESSES

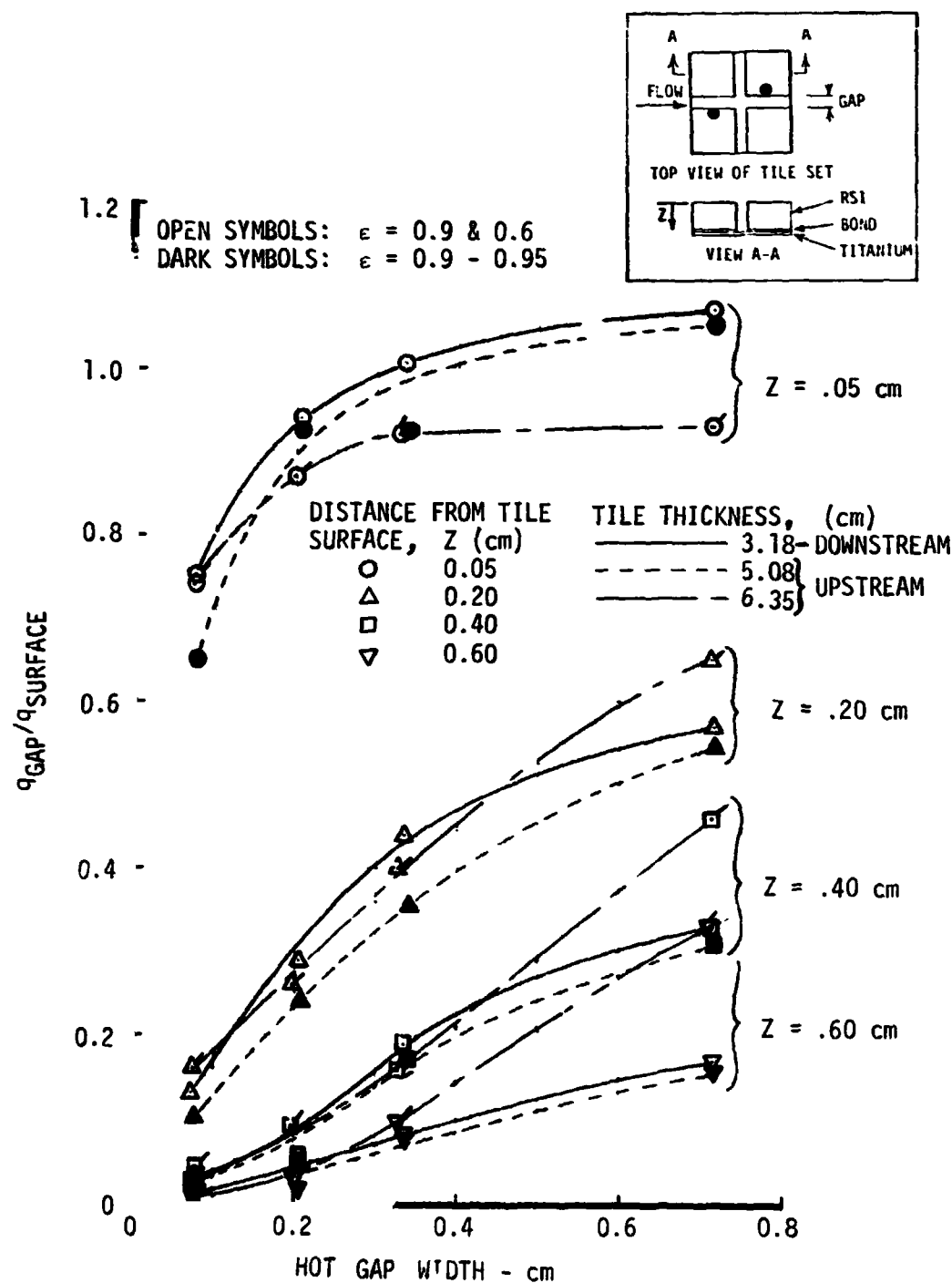


Figure 34

SCHEMATIC OF FORWARD-FACING STEP MODEL

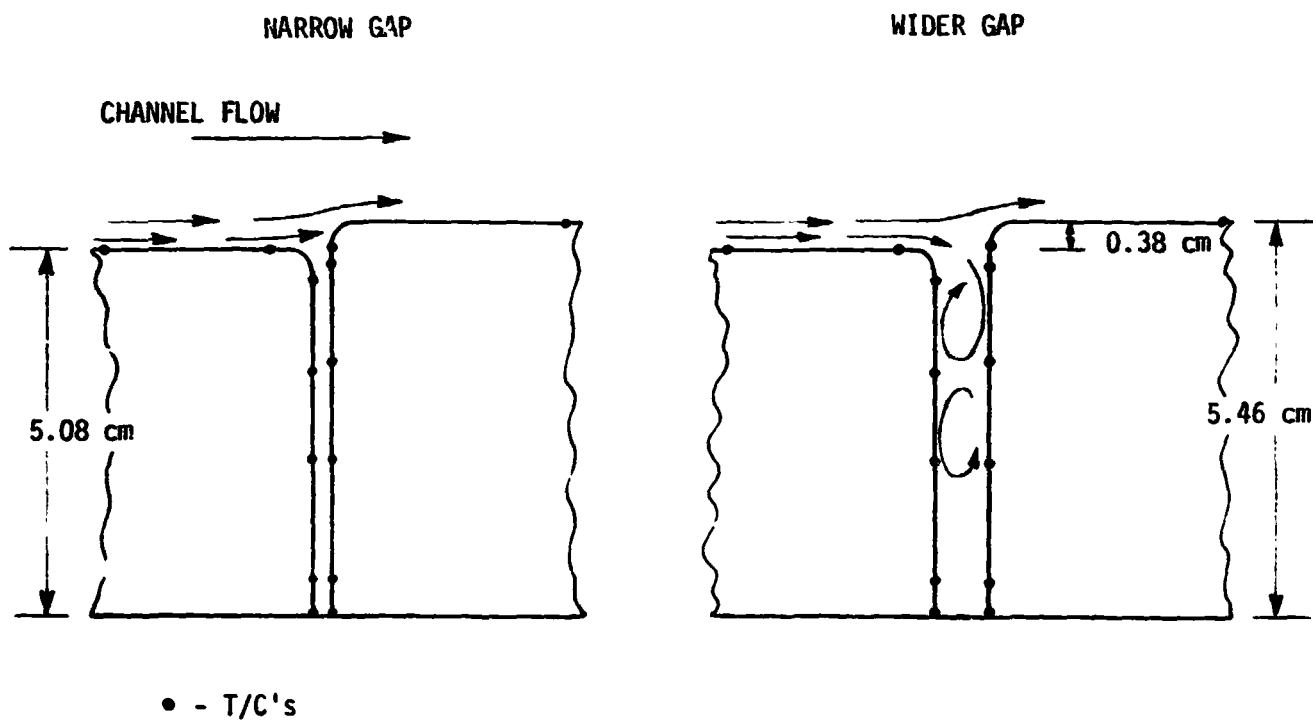


Figure 35



FINAL REPORT
VOLUME I

REPORT MDC E1003
29 JANUARY 1974

BUTT JOINT HEATING RATE DISTRIBUTION
FORWARD-FACING STEP
DOWNSTREAM TRANSVERSE GAP, 5.08 CM TILE

- JSC 10 MW CHANNEL NOZZLE TEST
- HIGH EMITTANCE COATING ON GAP WALLS

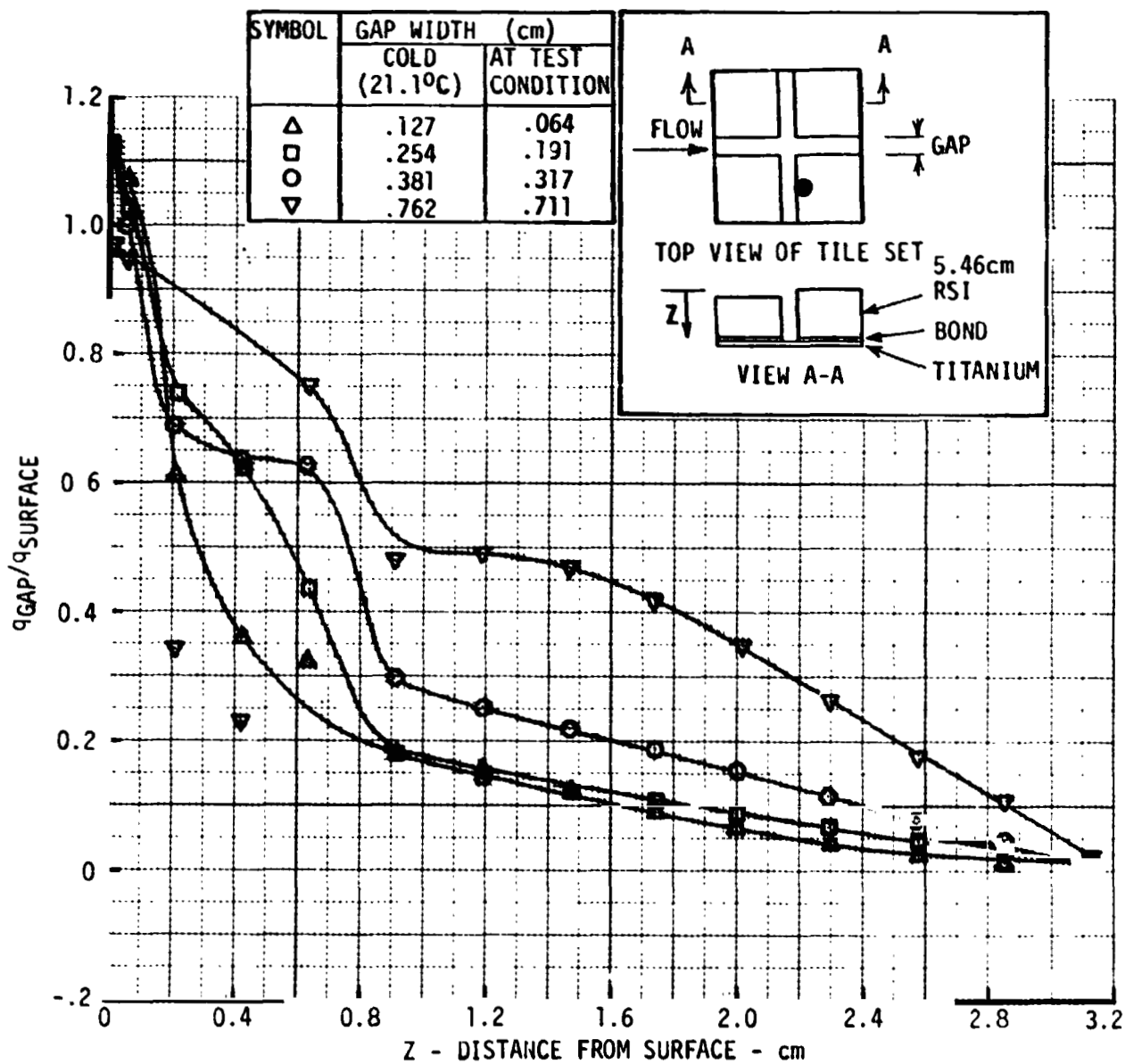
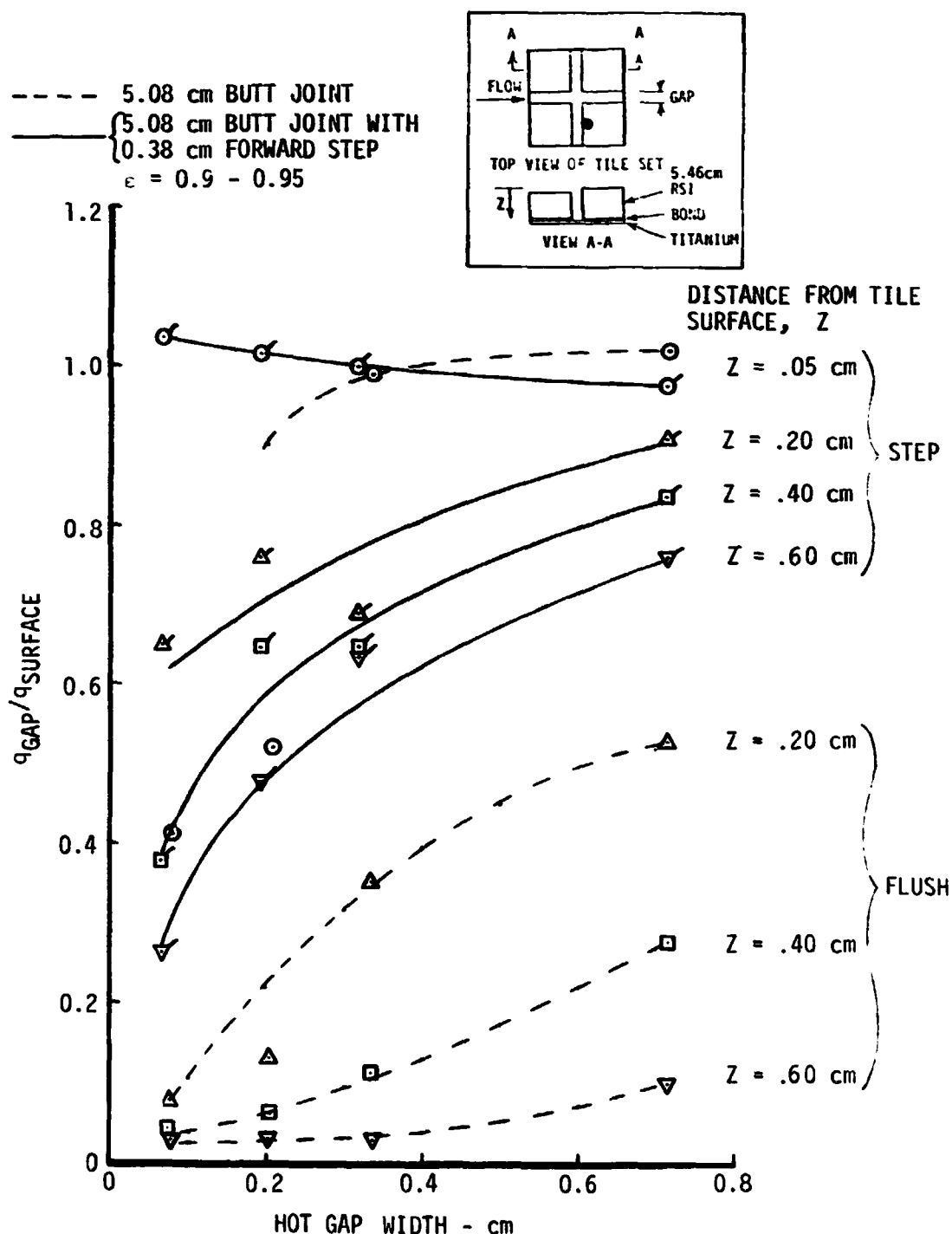


Figure 36

COMPARISON OF DOWNSTREAM TRANSVERSE GAP HEAT TRANSFER WITH GAP WIDTH BUTT JOINT WITH AND WITHOUT FORWARD STEP


Figure 37

INCLINED JOINT HEATING RATE DISTRIBUTION DOWNSTREAM TRANSVERSE GAP 6.35 CM TILE

- o JSC 10 MW CHANNEL NOZZLE TEST
- o HIGH EMITTANCE COATING 0.635 cm DOWN TILE GAP
- o LOW EMITTANCE COATING REMAINING GAP SURFACE

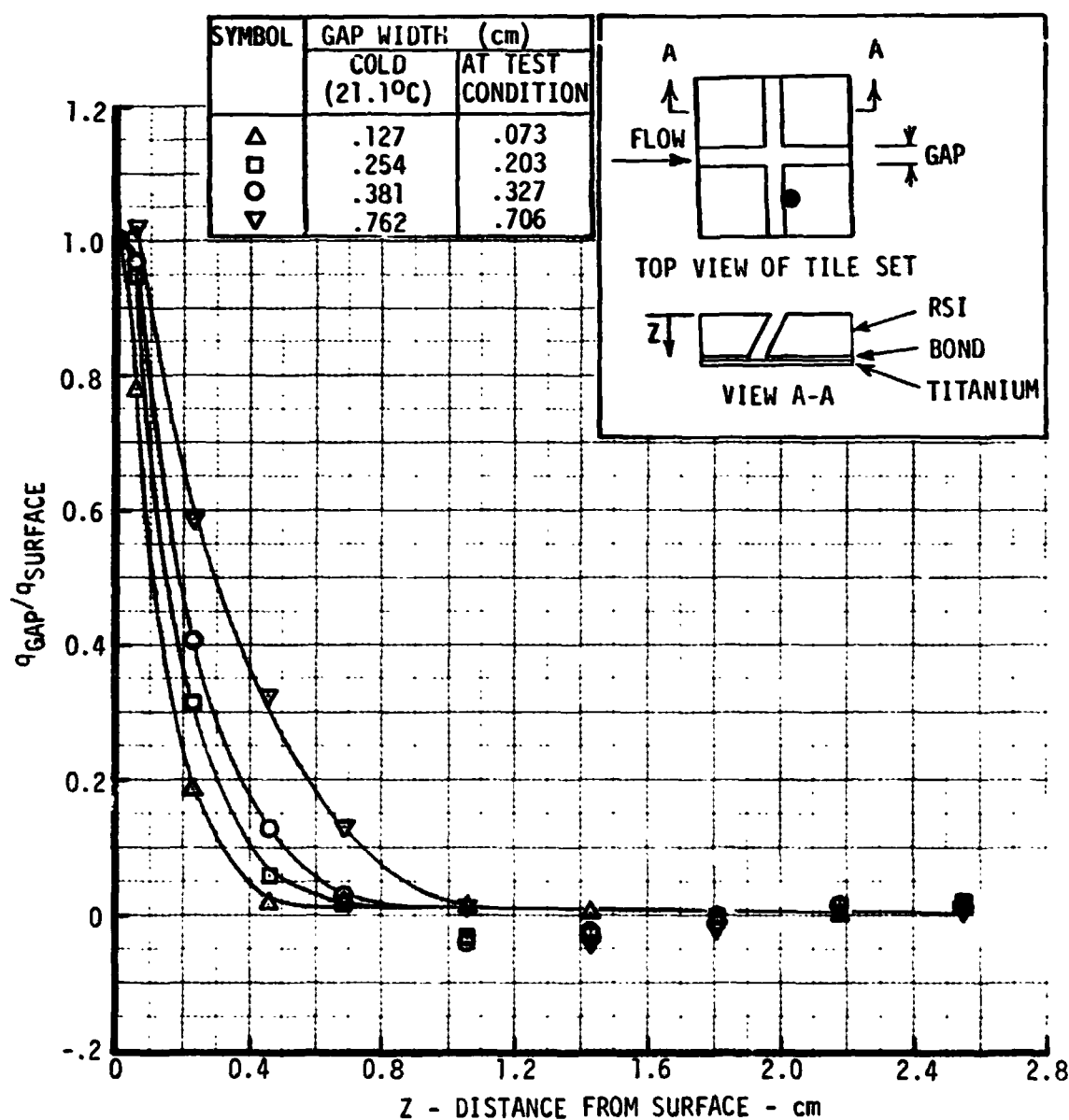


Figure 38

 RSI GAP HEATING
ANALYSIS

FINAL REPORT
VOLUME I

REPORT MDC E1003
29 JANUARY 1974

the butt joint to a depth of 1.0 centimeter into the gap.

The three narrow gap widths (0.099, 0.225, and 0.352cm) for the in-line gap (Figure 39) show that the heating for the inclined joint is also slightly greater and more sensitive to gap width from 0.10 to 1.0 centimeter depth. The wide gap (0.732cm) is nearly the same as the butt joint down to a depth of 0.8 centimeters. The heating below this depth is less than the butt joint configuration.

INCLINED JOINT HEATING RATE DISTRIBUTION UPSTREAM AXIAL GAP 6.35 CM TILE

- o JSC 10 MW CHANNEL NOZZLE TEST
- o HIGH EMITTANCE COATING 0.635 cm DOWN TILE GAP
- o LOW EMITTANCE COATING REMAINING GAP SURFACE

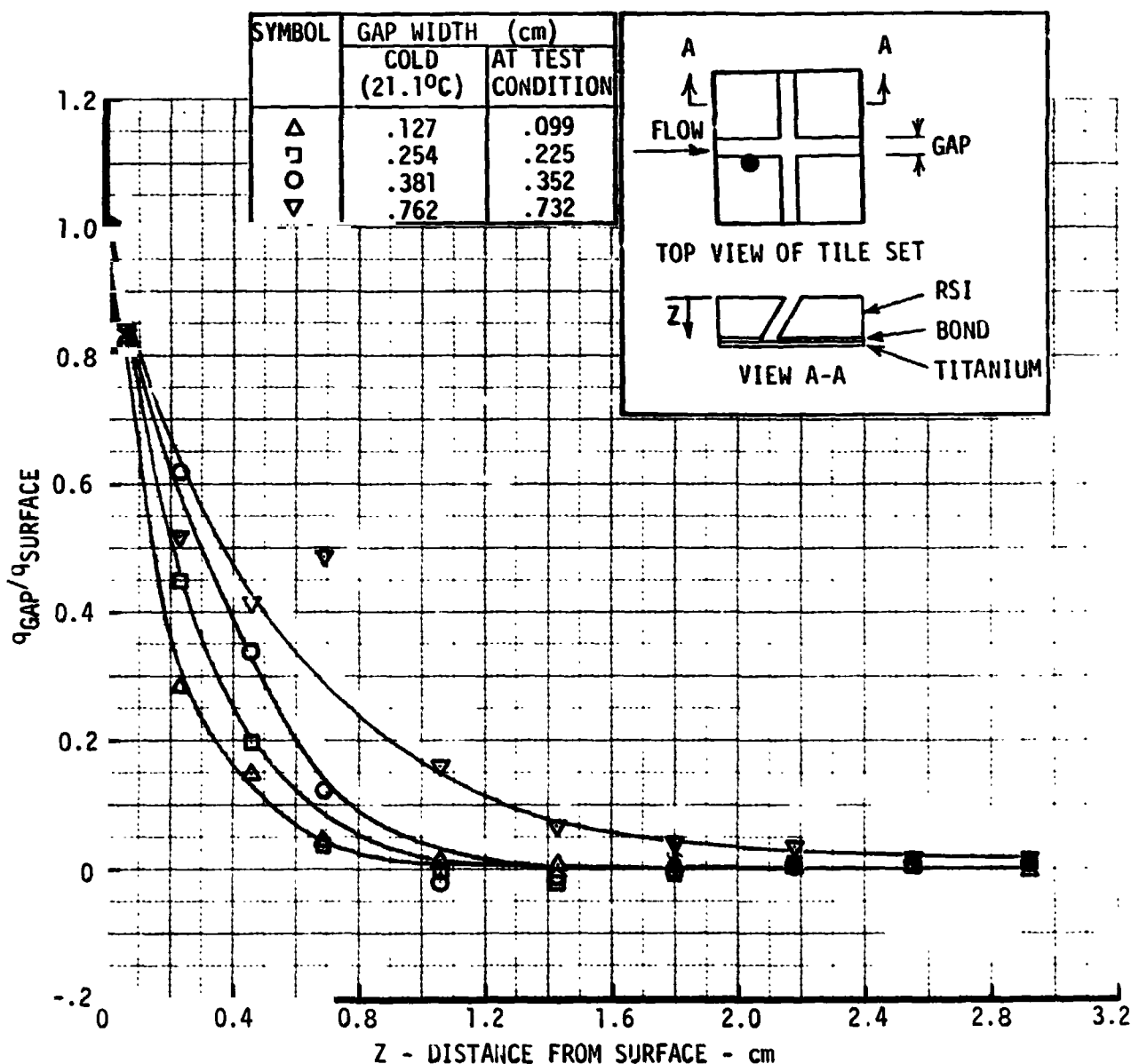


Figure 39



FINAL REPORT
VOLUME I

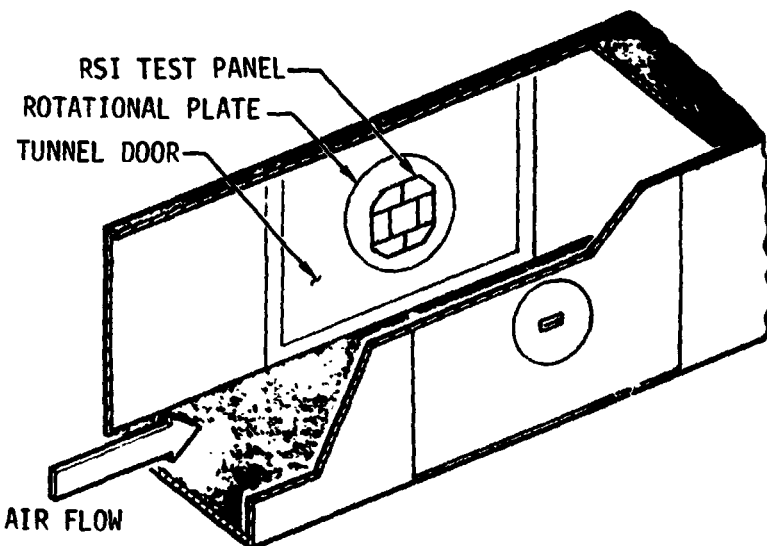
REPORT MDC E1003
29 JANUARY 1974

4.3 Analysis of Mach 10 CFHT Tests of Gap Model - Heat transfer data were taken on a 15.2 x 15.2 x 6.4 cm thin skin tile in the wall of the LaRC CFHT. The test setup is shown in Figure 40. The test article consisted of a panel with six RSI tiles surrounding the highly instrumented thin skin tile. The test panel was located on a rotational plate on the tunnel sidewall such that the flow angle could be varied over the test panel. All tests were conducted at a Mach number of 10 and a unit Reynolds number of 3.3×10^6 . LaRC performed calibration runs in support of a McDonnell Douglas sponsored program to measure heat transfer data on a corrugated panel model mounted on the tunnel sidewall. As part of that effort, flat plate heat transfer data were taken. Figure 41 presents the measured heat transfer distribution in the vertical direction on the flat plate mounted on the tunnel sidewall. The distribution shown is based upon three data runs. A significant variation in the heating across the flat plate is observed. This tunnel characteristic has been attributed to the square nozzle and test section which results in a slight flow convergence toward the center of the tunnel sidewall. Data taken on the corrugated panel exhibited a similar spanwise heating gradient to that observed on the flat plate. Normalizing the corrugated panel heat transfer coefficients by the flat plate coefficients resulted in successful collapsing of the data in the spanwise direction. This result is demonstrated in Figure 42 which compares absolute and nondimensionalized heating distributions on a wave at two spanwise locations. Because of this previous experience in correlating the corrugated panel data, the gap heating data, taken at the same test condition were normalized by the measured flat plate heat transfer coefficients. A representative heating distribution on the thin skin tile is shown in Figure 43. These data were normalized by a constant flat plate heat transfer coefficient measured at the center of the flat plate in the calibration runs. All data received from LaRC were in this form (H/H_0). These data were taken from Run 14 which had a staggered tile arrangement and a gap width of 0.229 cm. Three heating distributions are shown for three spanwise locations. Figure 44 presents the same data normalized by the measured flat plate heat transfer coefficients.

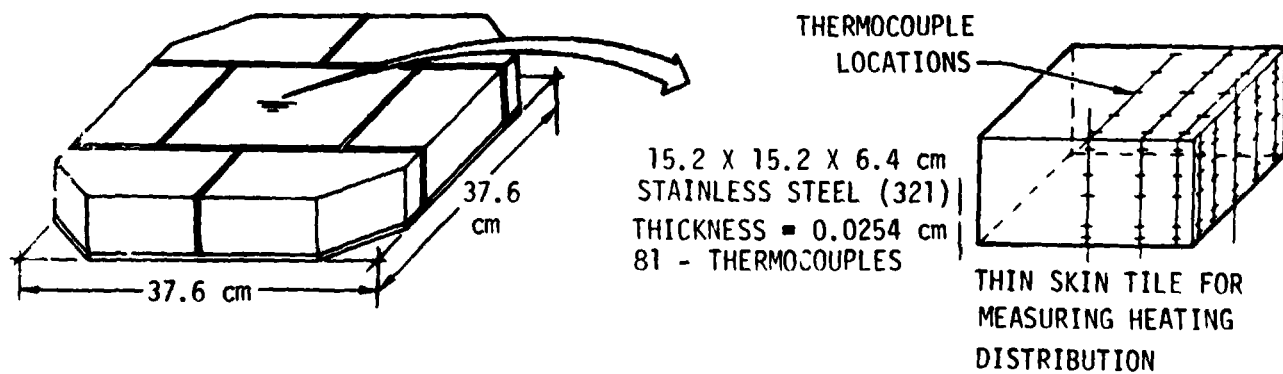
Included in the data analysis are the following:

- a) Evaluation of data reduction methods including the effect of neglecting conduction on measured heating rates.
- b) Inline vs. staggered tile heating patterns.
- c) Effect of gap width on tile heating patterns.

LRC CFHT GAP HEATING EVALUATION



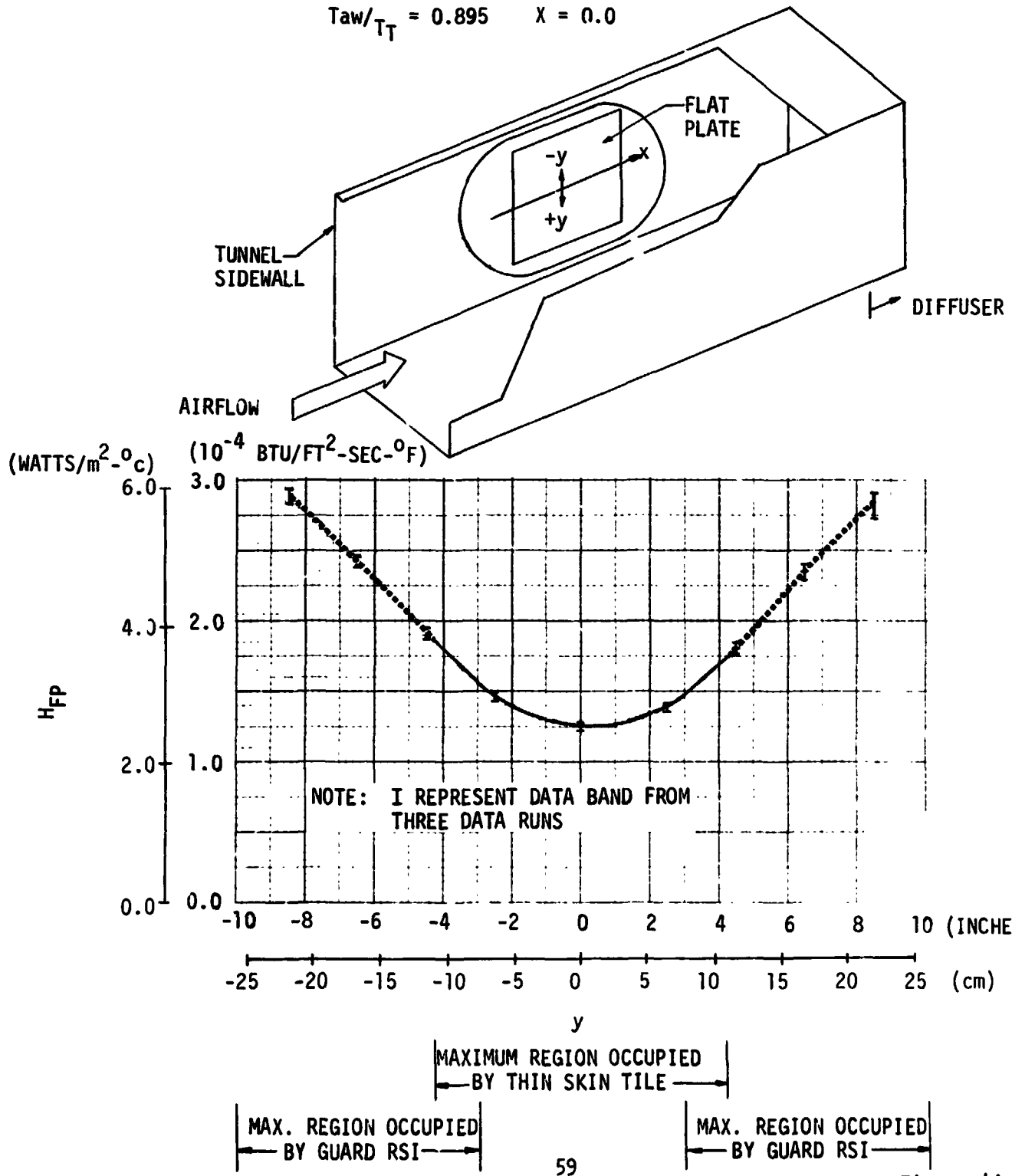
- ADJUSTABLE GAP
- SHIMS FOR STUDYING MISMATCH
- 0 TO $\pm 90^\circ$ ORIENTATION



HEAT TRANSFER DISTRIBUTION [$H_{FP} = f_1(y)$] ON FLAT PLATE MOUNTED ON CFHT SIDEWALL

$M_\infty = 10.33$ $Re_\infty/m = 3.28 \times 10^6$ TEST NO. 93

$T_{aw}/T_T = 0.895$ $X = 0.0$





FINAL REPORT
VOLUME I

REPORT MDC E1003
29 JANUARY 1974

COMPARISON OF ABSOLUTE AND NONDIMENSIONALIZED
HEATING DISTRIBUTIONS IN THE MACH 10 CFHT,
 $RE_\infty/M = 3.3 \times 10^6$

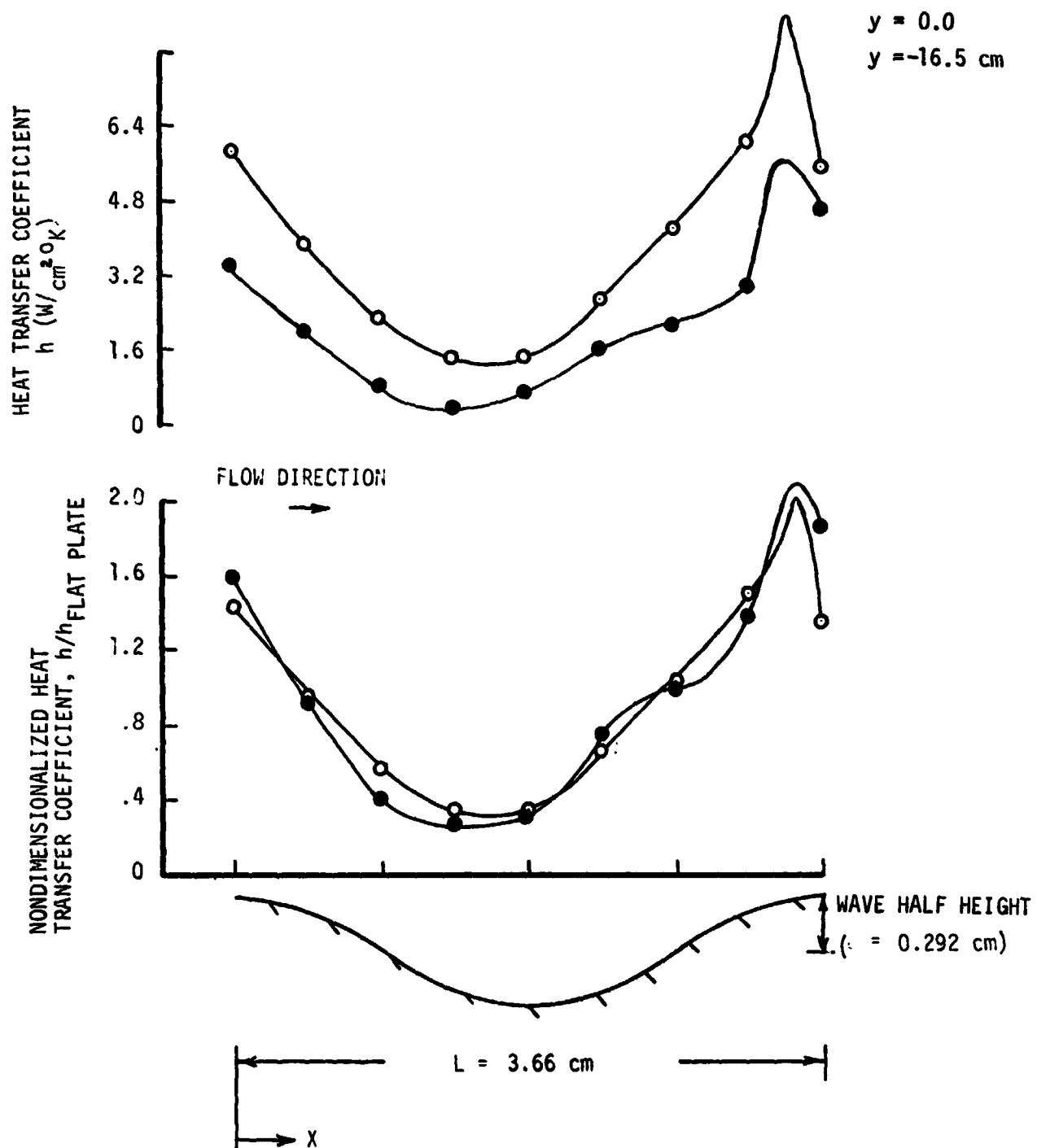


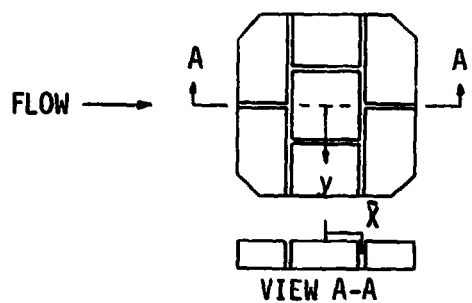
Figure 42

 RSI GAP HEATING
ANALYSIS

FINAL REPORT
VOLUME I

REPORT MDC E1003
29 JANUARY 1974

REPRESENTATIVE HEATING DISTRIBUTION
ON TILE IN CFHT



$$H_0 = 2.55 \text{ WATTS/m}^2 \cdot ^\circ\text{C}$$

STAGGERED TILES
GAP WIDTH = .229 cm
GAMMA = $\pi/2$ RADIAN
RUN NO. 14

O	y = 0.0
□	y = -3.8 cm
△	y = -7.3 cm

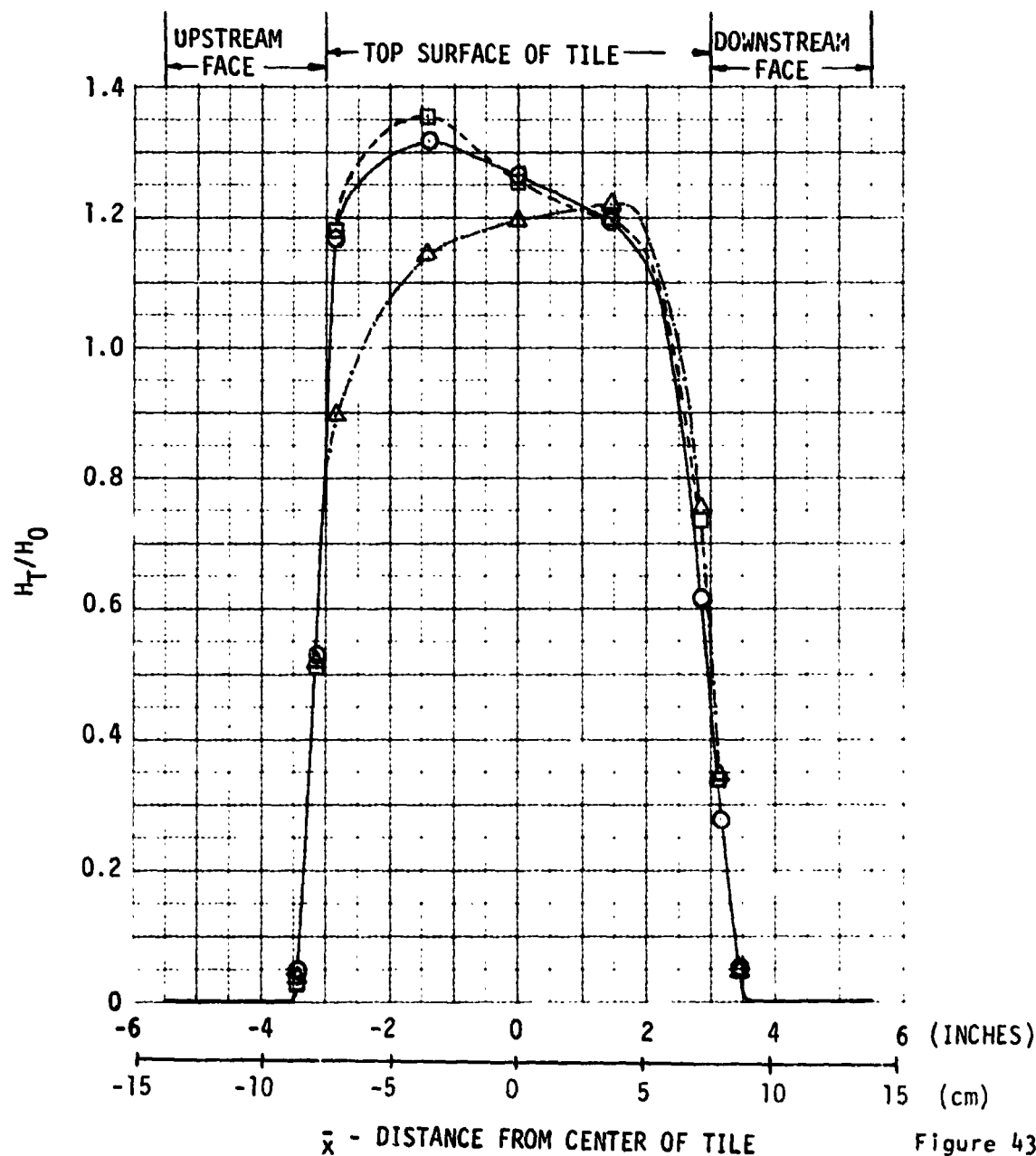


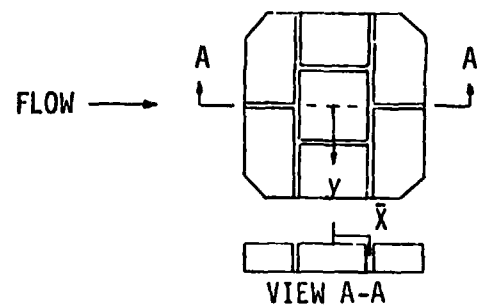
Figure 43



**FINAL REPORT
VOLUME I**

REPORT MDC E1003
29 JANUARY 1974

HEATING ON TILE IN CFHT NORMALIZED BY THE MEASURED FLAT PLATE HEATING



$H_{FP} = F_1(\gamma)$
 STAGGERED TILES
 GAP WIDTH = .229 cm
 GAMMA = $\pi/2$ RADIANS
 RUN NO. 14

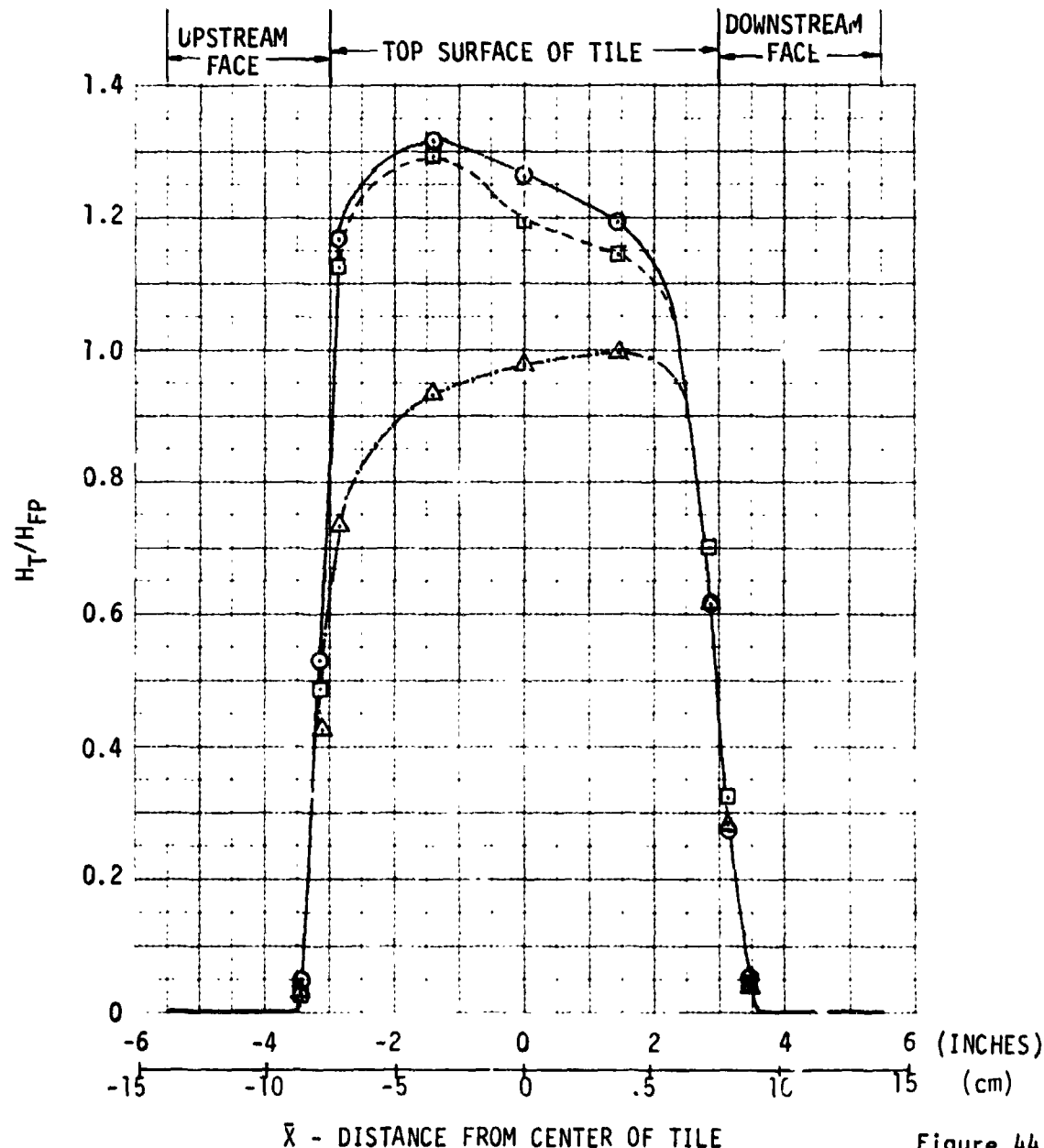


Figure 44



RSI GAP HEATING
ANALYSIS

FINAL REPORT
VOLUME I

REPORT MDC E1003
29 JANUARY 1974

- d) Effect of flow angle on gap heating patterns.
- e) Effect of steps on tile heating patterns.

4.3.1 Analysis of Thin Skin Model - The method used to calculate heat transfer coefficient: for these tests employed the slope of the temperature-time curve at selected times to solve for the heat transfer coefficient using the following equation:

$$h = \frac{\rho C_p X (dT_w/d\theta)}{(T_{aw} - T_w)} \quad \text{where } X = \text{skin thickness}$$

Two times were selected for data reduction for each thermocouple during these tests. By plotting various measured temperatures in the gaps, LaRC personnel determined that erratic temperatures were recorded for many thermocouples during a period of 0.35 to 0.45 seconds after insertion of the test article into the wall. This can be attributed to the finite time required to establish flow in the gaps. Therefore, the first time selected for data reduction was 0.50 seconds after the test article reached the tunnel wall. A second time was also selected which was 0.50 seconds after the first time or 1.0 seconds after tile insertion. The temperature-time derivative ($dT/d\theta$) is obtained by taking the slope of a least squares quadratic curve fit through ten seconds of data obtained for each thermocouple. The initial point of the curve fit interval is the time selected for data reduction, i.e., 0.50 seconds and 1.0 second. Ten seconds was selected as the curve fit interval to obtain data deep in the gaps where heating levels are low. The curve fit expressions are of the form:

$$T_w = a + b \theta + c \theta^2 \quad \text{and } dT/d\theta = b + 2c \theta$$

where a, b, and c are constants. The quantities T_w and $dT/d\theta$ are evaluated at the initial point of each curve fit. Two heat transfer coefficients are computed for each value of $dT/d\theta$ based upon two values of adiabatic wall temperature, i.e., $T_{aw}/T_T = 0.895$ and 1.0. All data in this section are based upon $T_{aw}/T_T = 0.895$ because the boundary layer was turbulent for all tests. Also all data presented in the following figures were evaluated at 0.50 seconds after test article insertion was complete.

Figure 45 presents two typical measured temperature histories on the downstream face of the thin skin tile. The selected data are from Run 4 which employed the staggered tile configuration with gap widths of 0.229 centimeters. The first thermocouple into the gap was channel 20 (0.414 cm from the surface). The slopes evaluated from the curve fit for both 0.50 and 1.0 seconds after insertion are shown and compare favorably with the raw temperature data. Also the two slopes

MEASURED TEMPERATURES IN GAPS AT CFHT

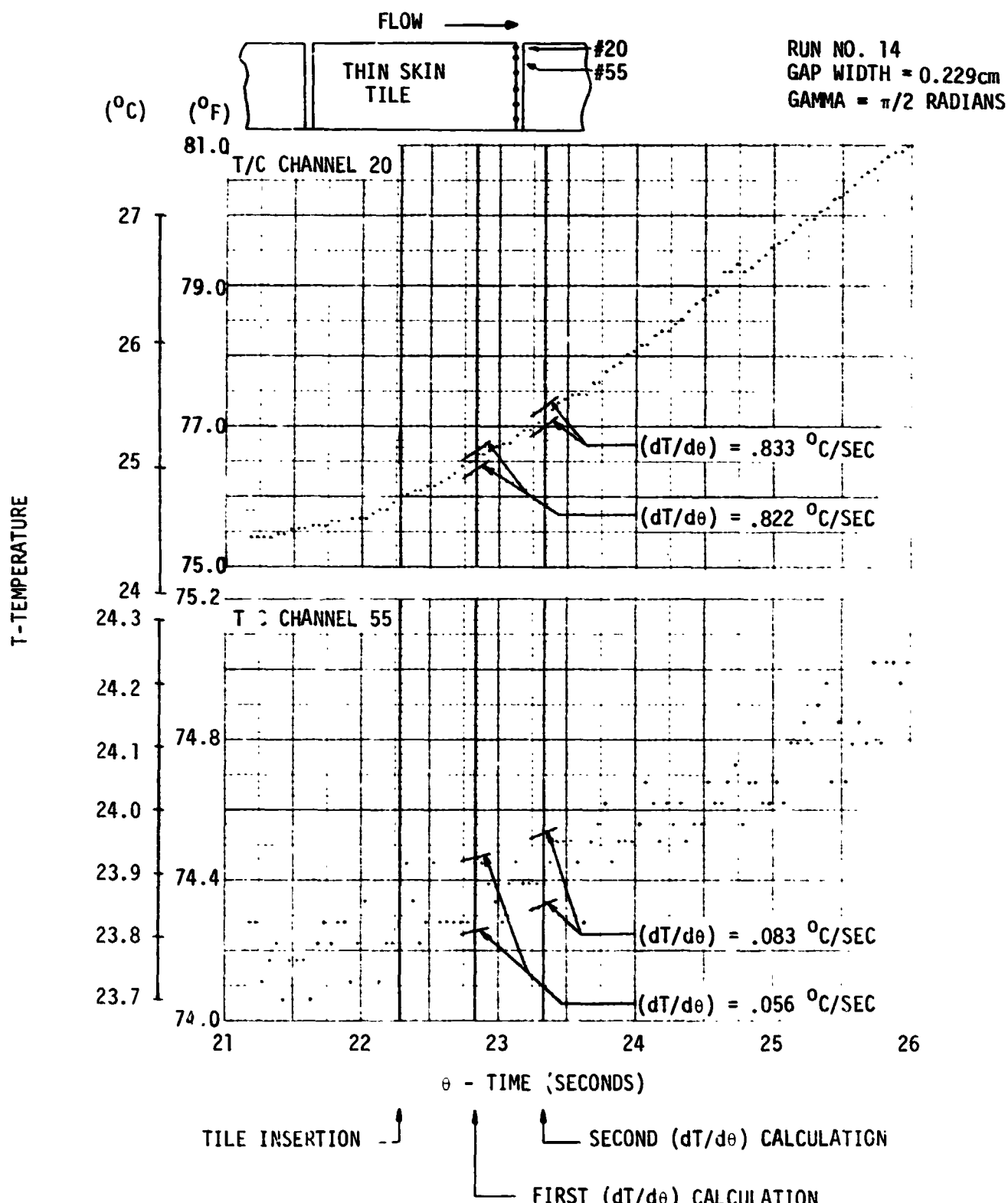


Figure 45



FINAL REPORT
VOLUME I

REPORT MDC E1003
29 JANUARY 1974

are nearly equal indicating a linear temperature response. All thermocouples where a significant temperature rise occurred exhibited this type of temperature response. Thermocouple channel 55 is on the next level into the gap 1.113 cm from the surface). The measured data for channel 55 shows a temperature response which is an order of magnitude lower than channel 20. Also, the temperature response was low enough that the "noise" from the data recording system was observed in the data. By taking a large data sampling (10 seconds) the data could be curve fit and $dT/d\theta$ evaluated at the two selected times. The slopes derived from the two curve fits are reasonable when compared with the raw temperature data. The third through the sixth rows of thermocouples had a temperature response so low that the "noise" from the data recording system was greater than the temperature rise over a ten second time interval. A significant number of thermocouples in the gaps had such a low signal to noise ratio that the data were not included in the analysis.

4.3.1.1 Conduction Sensitivity Study - A study was made to examine the effect of including conduction in the calculation of heating rates from wind tunnel tests that employ thin skin tiles. Data from Run 14 of the CFHT were selected for this purpose. An eight (8) node thermal model was formulated to describe the heat storage and heat conduction characteristics of a section through the thin skin tile for the temperature distributions shown in Figure 46. For each node in the thermal model there is a corresponding thermocouple on the thin skin tile which was used to define the nodes' temperature history. Hand fairings of the temperature histories were input into the General Heat Transfer Computer Program along with the thermal model descriptors and an inverse solution was performed to calculate a heating rate for each node. Figure 46 depicts the spanwise temperature distribution across the top and down the side of the tile. Two distributions are shown which correspond to the two times when LaRC provided heating rate data. These times are 0.5 seconds and 1.0 second after the test article insertion. Significant feature of the temperature distributions are the two sharp "knees" in the curve which indicate transient conduction effects might be expected at those nodes.

Figure 47 shows the effect on calculated heating rates of excluding and including conduction in the thermal model. This figure is for 0.5 second after insertion. The heating rates for the "no conduction" case consider only the heat storage term and are comparable with the data reported by LaRC. The differences between these data are due to the techniques used in fairing the temperature histories. The technique utilized by LaRC consisted of least squares

TYPICAL SPANWISE TEMPERATURE DISTRIBUTION
ON TILE IN CFHT

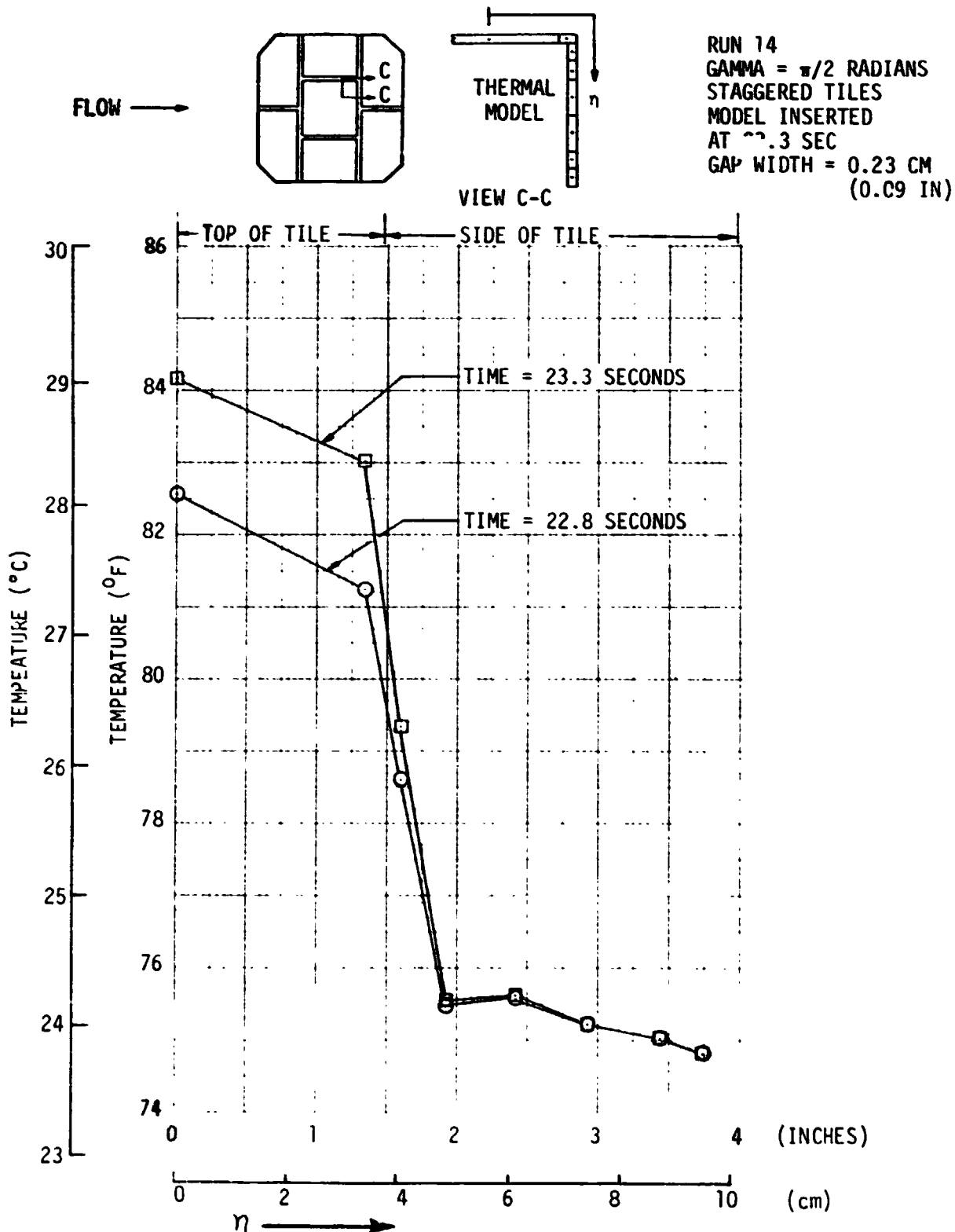


Figure 46

EFFECT OF INCLUDING CONDUCTION ON CALCULATED HEATING RATES IN CHFT

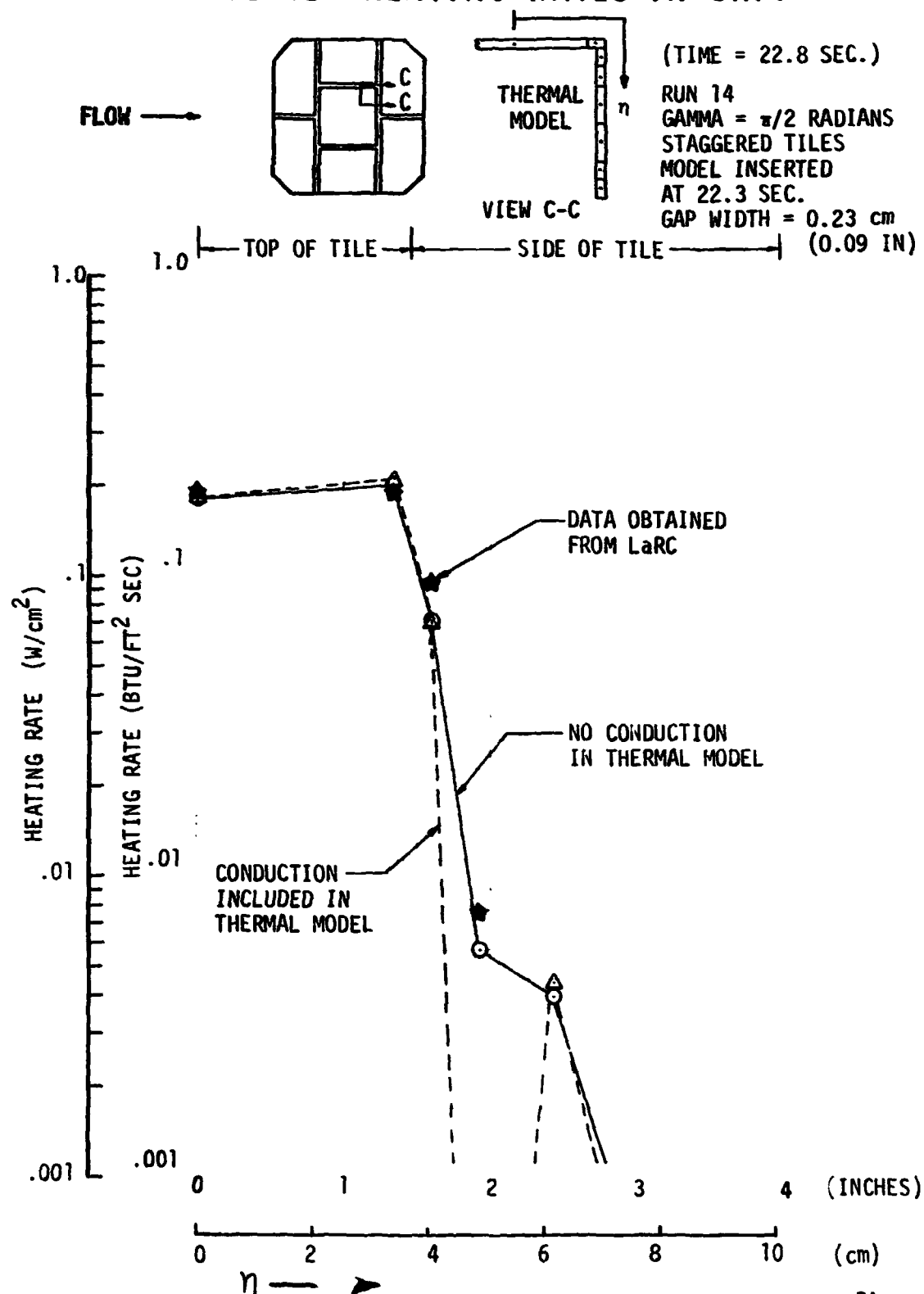


Figure 47



FINAL REPORT
VOLUME I

REPORT MDC E1003
29 JANUARY 1974

curve fit of the temperature histories while hand-faired histories were used with the 8 node thermal model. When conduction between nodes is included in the analyses, the surface node near the top edge of the tile and the second node into the gap were the only nodes to show any appreciable effect. The top surface node showed a 5% increase in the calculated heating rate when conduction was included. The first node down the gap showed no effect of conduction. This is because the heat being conducted away from the node is nearly equal to the heat being conducted into the node (see Figure 46). The second node down the side of the tile shows a significant effect of conduction on calculated heating rate. When conduction is included in the thermal model the calculated heat flux is negative (cooling). This means that the measured temperature rise of the thermocouple with time is too small to account for the net heat gain of the node due to conduction alone. Therefore, cooling was required to balance energy at that node. The remaining nodes showed no appreciable effect of conduction on calculated heating rates. Figure 48 shows heating rates calculated 1.0 second after insertion of the test article into the wall. The same trends appear at this time as in the earlier time. The top surface node near the edge of the tile has a 7% increase in calculated heating rate when conduction is included. The second node down the side of the tile has a negative heating rate when conduction is included in the thermal model. The other nodes show no appreciable effect of conduction on calculated heating rates.

The data reduction method customarily used in thin skin model testing considers only the temperature rise rates and the local heat storage characteristics of the thin skin material. Therefore, the thermocouple/recording system is not generally calibrated against known temperatures. In order to include conduction effects, the absolute value of the temperature is required such that temperature differences between adjacent thermocouples can be computed. NASA LaRC has investigated the characteristics of the thermocouple/recording system used in the CFHT tests to provide additional information to aid in evaluating conduction effects.

A test was conducted by NASA LaRC to investigate the characteristics of the thermocouple/recording system consisted of measuring temperatures on the thin skin tile at essentially isothermal conditions. The thin skin tile was suspended in an insulated box which was equipped with heaters. The thermocouples were connected to the recording system in exactly the same manner as during the CFHT tests. The box was heated until the tile reached 65.9°C and then the heaters were turned off. Figure 49 presents data taken at half hour intervals after the heaters were turned

EFFECT OF INCLUDING CONDUCTION ON CALCULATED HEATING RATES IN CFHT

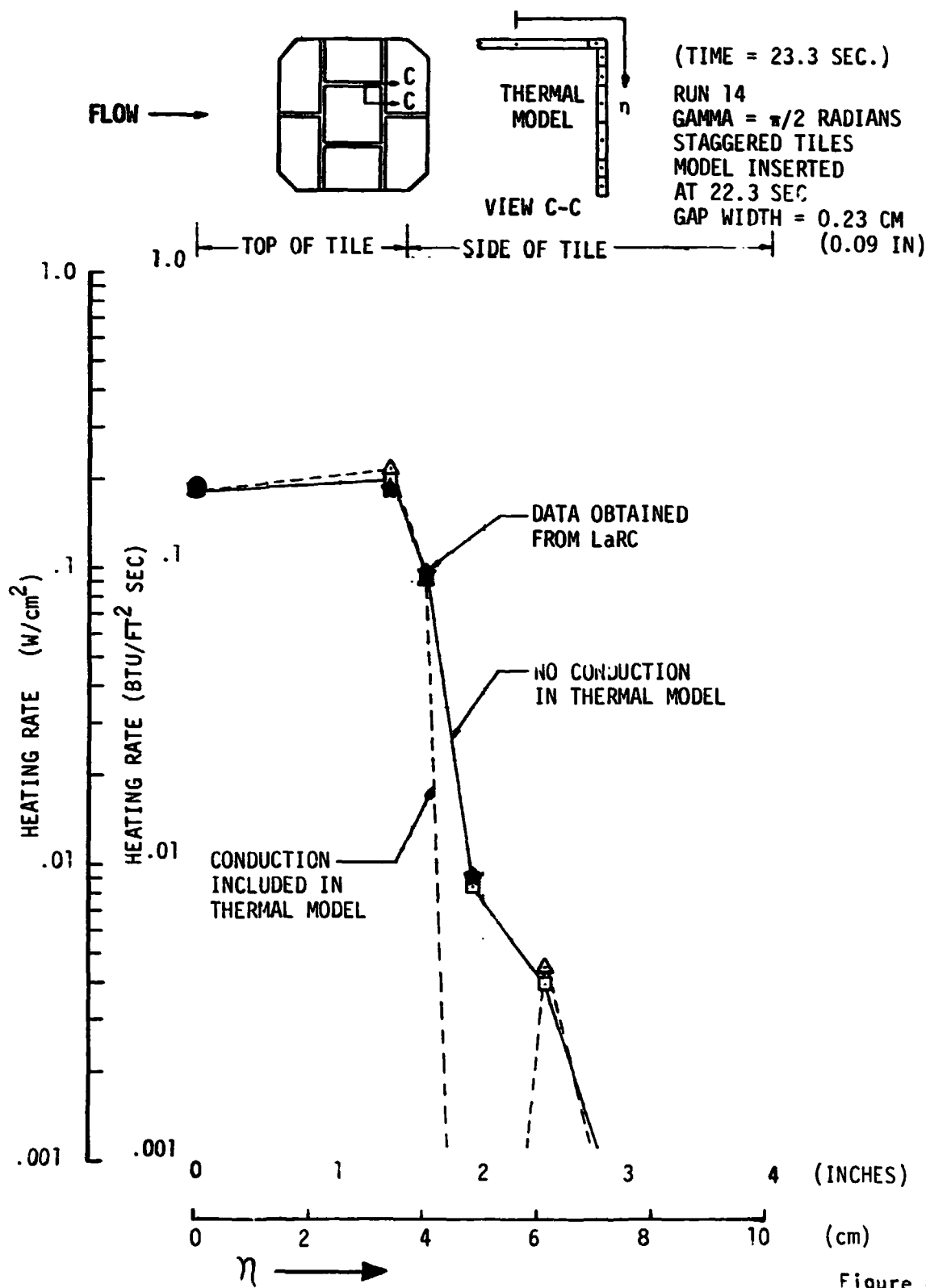


Figure 48



FINAL REPORT
VOLUME I

REPORT MDC E1003
29 JANUARY 1974

ISOTHERMAL TEST DATA FOR THIN SKIN TILE
USED IN CFHT TESTS

		TIME (HRS)		
		0.5	1.0	1.5
AVERAGE TEMPERATURE (°C)		38.667	31.494	28.339
MAXIMUM ADJACENT ΔT (°C)		.7556	.7222	.7222
AVERAGE ADJACENT ΔT (°C)		.1456	.1356	.1322
NODE 1 TEMPERATURE - T/C #27 (°C)		38.533	31.399	28.138
2	44	38.171	31.122	28.012
3	70	39.078	32.032	28.923
4	75	38.473	31.373	28.232
5	74	39.229	32.095	28.923
6	73	39.319	32.064	28.986
7	72	39.199	31.969	28.734
8	71	39.319	32.064	28.892

Figure 49

 RSI GAP HEATING
ANALYSIS

FINAL REPORT
VOLUME I

REPORT MDC E1003
29 JANUARY 1974

off. The average temperature, maximum temperature difference between adjacent thermocouples and the average temperature difference are shown for all thermocouples on the tile. Individual data readings shown are for each thermocouple used to define the thermal model temperatures. It can be seen that the temperature recorded for node 4 (second node down the gap) is considerably lower than the rest of the gap nodes (nodes 3 through 8). This node is where negative heating (cooling) was computed when conduction effects were included in the thermal model. It was decided to re-run the sensitivity study using the thermal model with a ΔT applied to each nodes' temperature history. The delta temperature (ΔT) that was used was the difference between the average temperature of the tile and the individual thermocouple temperature at 1.5 hours after the heaters were shut off. This time was selected because the temperatures were nearest the tile temperature when heat transfer data were taken during the test. Also the box is nearly adiabatic at the later time. Figure 50 shows the temperature distribution used in the previous study at 0.5 seconds after tile insertion and the revised distribution after the ΔT was applied to each node. The revised temperature distribution is seen to be much smoother than the original distribution with the resultant elimination of the "knee" in the curve that existed at node 4.

Figure 51 shows the effect on calculated heating rates of excluding and including conduction in the thermal model using the revised temperature distributions. The data shown in this figure is for 0.5 second after tile insertion. The heating rates for the "no conduction" case consider only the heat storage term and are comparable with the data reported by LaRC. The differences between these data are due to the techniques used in the fairing of the temperature histories. The technique used by LaRC consisted of least squares curve fit of the temperature histories while hand-faired histories were used with the 8 node thermal model. When conduction is included in the thermal model analysis, the surface node near the top edge of the tile showed an increase in calculated heating rate of 8.5%. The calculated heating rates in the gap are generally lower when conduction is included. The negative heating rate that was calculated at the second node into the gap in the previous analysis (node 4) has been eliminated by using the revised temperature distributions. However, the heating distribution down the gap is still not a smooth function when the heating rate reaches very low values.

It has been shown that by including conduction in the data reduction of thin skin tiles can affect the resultant data. However, the best technique for including such a calculation in the data reduction program is not obvious. It would be advisable in future tests of thin skin tiles where low heating rates are expected

TYPICAL SPANWISE TEMPERATURE DISTRIBUTION
ON TILE IN CFHT

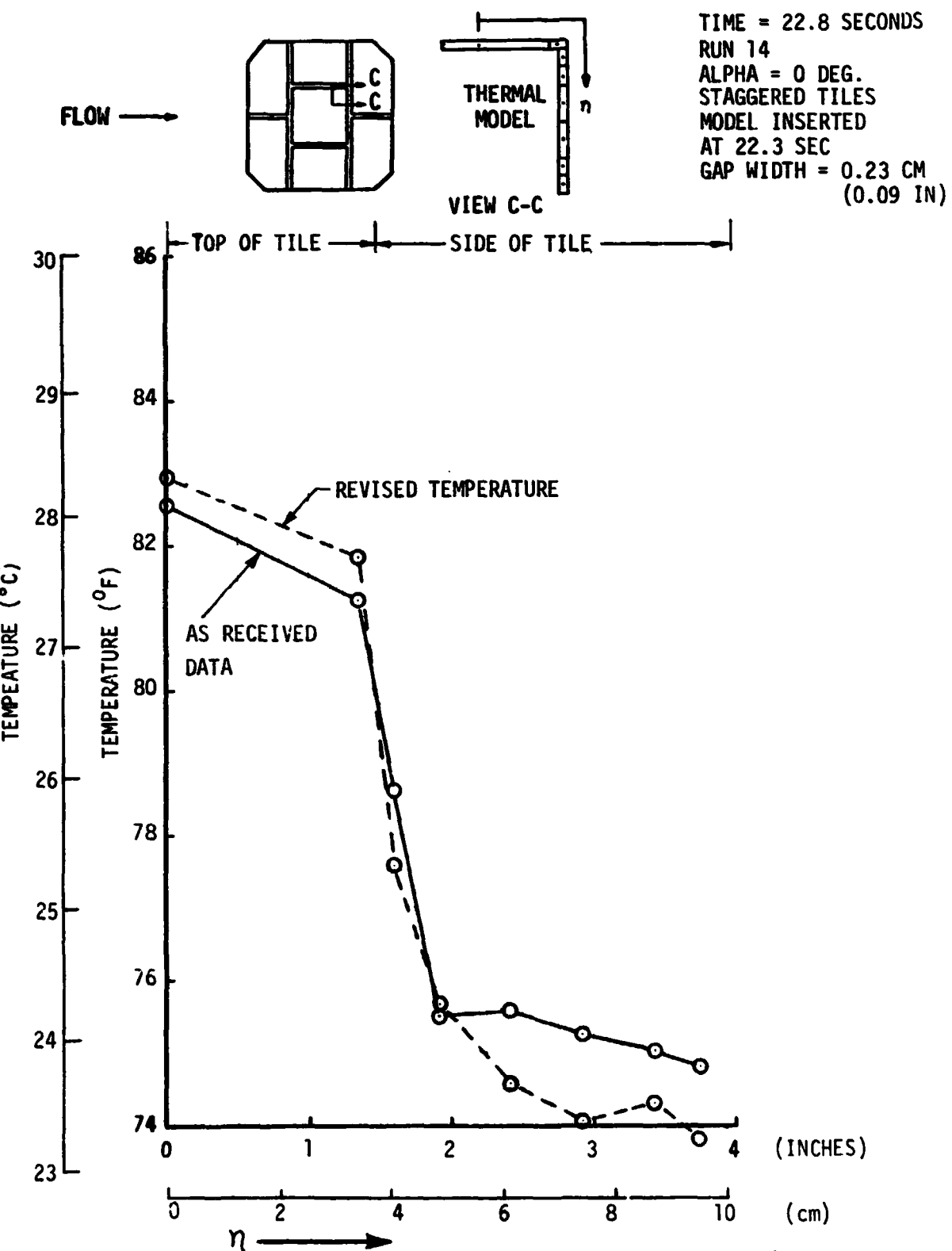


Figure 50

EFFECT OF INCLUDING CONDUCTION ON CALCULATED HEATING RATES IN CFHT

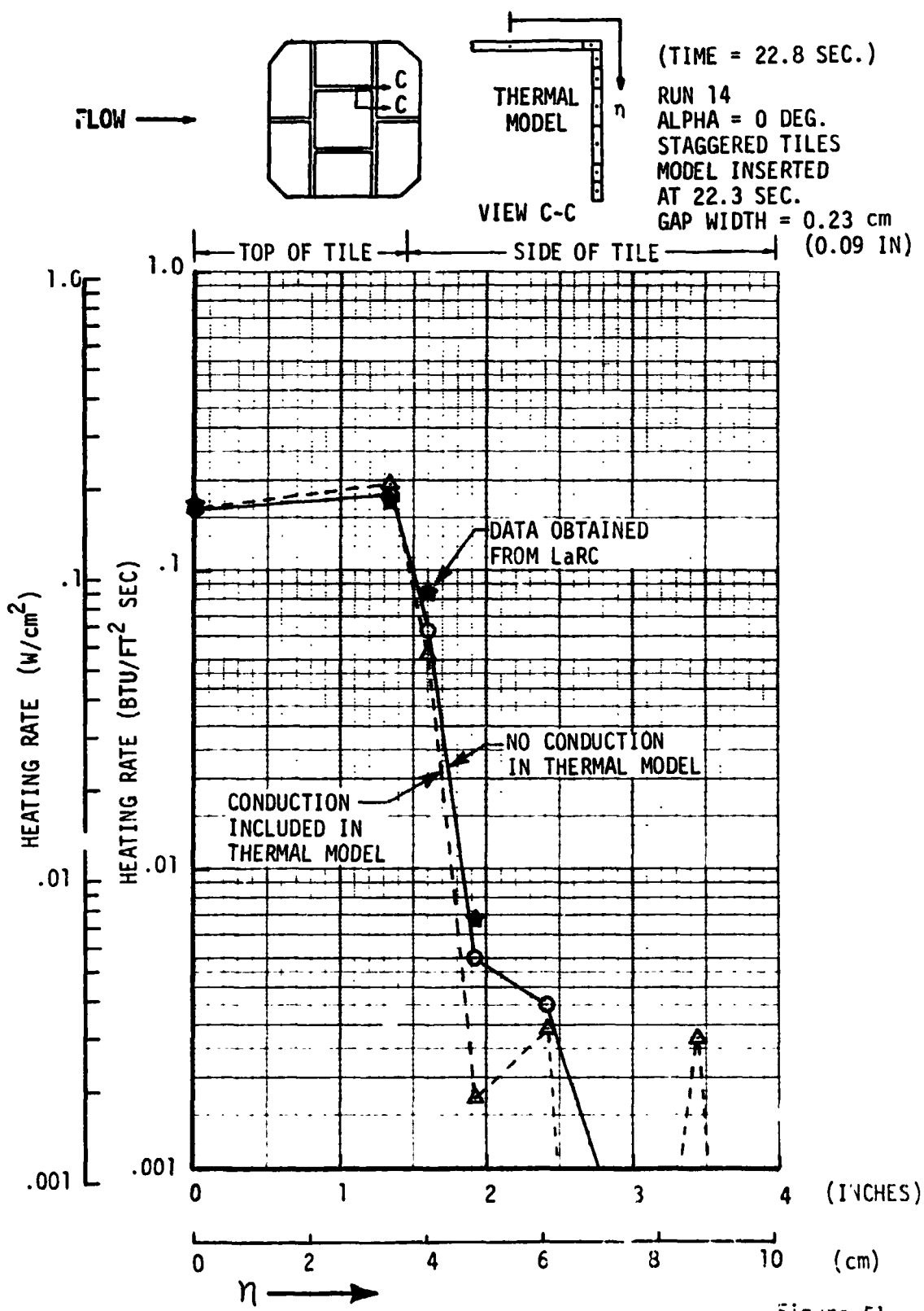


Figure 51



FINAL REPORT
VOLUME I

REPORT MDC E1003
29 JANUARY 1974

(i.e., deep in the gaps) that the thermocouple/recording system be calibrated to a known temperature such that conduction effects can be better evaluated. It is recommended that the heating rates neglecting conduction (i.e. data obtained from Langley) be used in gap heating data correlation because this gap heating data is higher than when conduction is included in the analysis.

4.3.2 Heating Patterns, Inline versus Staggered Tiles - Data were taken on the thin skin tile with two basic tile arrangements. These arrangements are referred to as staggered and in-line. Figure 52 shows the orientation of the test article with respect to the flow for both arrangements. The in-line arrangement is achieved by rotating the test article 90 degrees from the staggered tile orientation. It should be noted that for the in-line arrangement, the tiles are in-line in the axial direction only. In the spanwise direction (normal to the flow) the tiles are staggered. Comparisons of the axial heating distributions for the staggered and in-line tile arrangements at $y = 0.0$, -3.8 and -7.3 cm are presented in Figures 52, 53, and 54, respectively. These figures present data for tile gap width of 0.23 cm. Heating on both the upstream and downstream faces of the tile does not appear to be significantly affected by the surrounding tile arrangement for a gap width of 0.23 cm. Heating on the top surface of the thin skin tile is higher (4% to 24%) for the staggered arrangement than for the in-line arrangement. This trend is most pronounced at the centerline ($y = 0.0$ cm) of the tile and decreases near the edge ($y = -7.3$ cm) of the tile. Also the magnitude of the heating on the top of both tile configurations decreases near the tile edges. The trends shown in these figures are for the 0.23 cm gap width only.

4.3.3 Effect of Gap Width - Comparisons of heating distributions for four gap widths at $y = 0.0$, -3.8 and -7.3 cm are presented for the staggered tile arrangement in Figures 55, 56, and 57, respectively. Data for gap widths of 0.13, 0.23, 0.46 and 0.71 cm are shown in each figure. These figures show that the effect of gap width on tile heating changes with location on the tile. Figure 55 presents data along the centerline of the tile ($y = 0.0$). On the upstream face, the gap heating increases slightly with increasing gap width. This trend is reversed on the top surface and downstream face with the exception of the upstream edge of the tile top surface. Examination of the axial distribution at $y = -3.8$ cm shows a much greater increase in gap heating with increasing gap width on the upstream face than was shown at $y = 0.0$. On the top surface of the tile the heating at the upstream edge of the tile increased dramatically with increasing gap width. Over the rest of the top surface, the heating appears essentially independent of gap width.

STAGGERED AND IN-LINE TILE HEATING DISTRIBUTIONS IN CFHT ($Y = 0.0$)

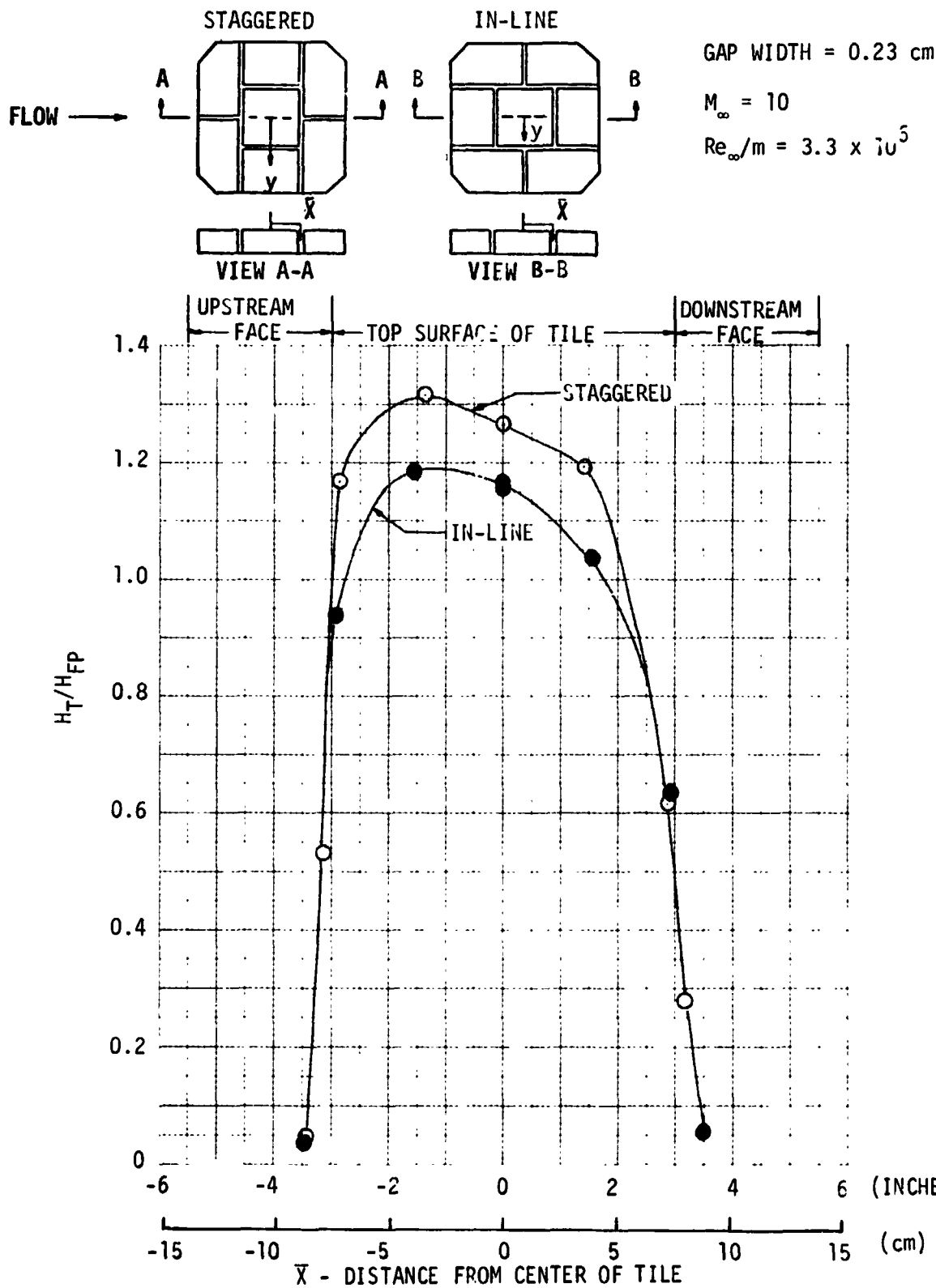
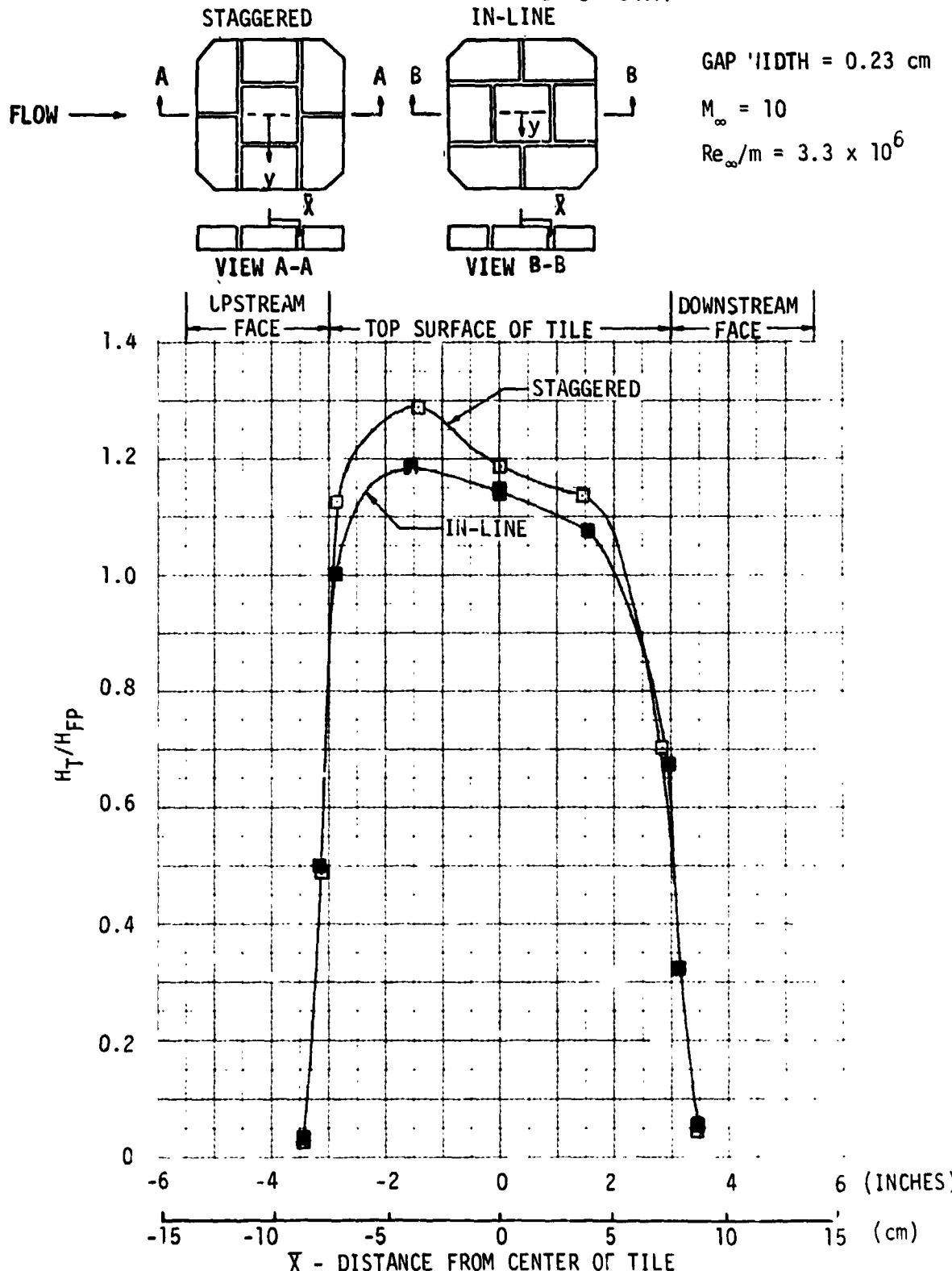
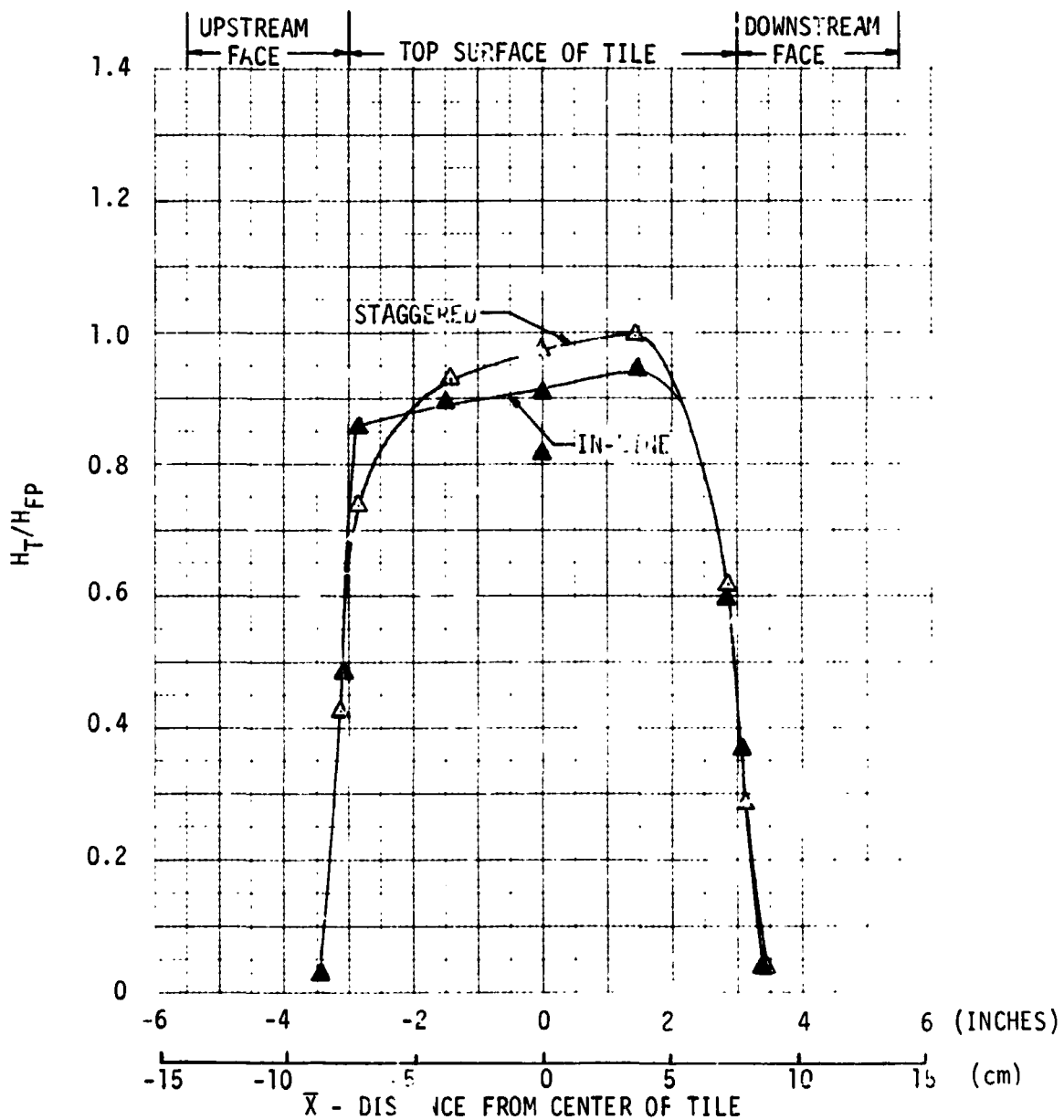
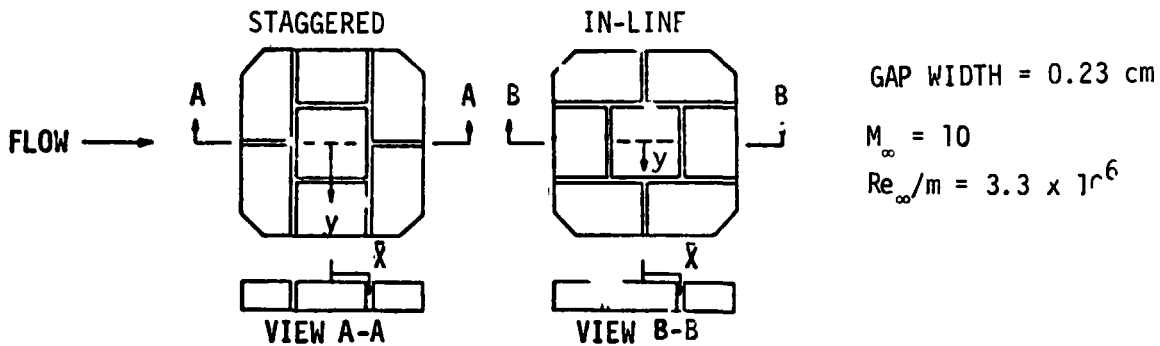


Figure 52

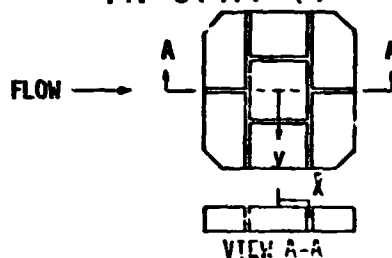
STAGGERED AND IN-LINE TILE HEATING DISTRIBUTIONS
IN CFHT ($Y = -3.8$ CM)



STAGGERED AND IN-LINE TILE HEATING DISTRIBUTIONS
(IN CFHT ($y = 7.3$ CM))



EFFECT OF GAP WIDTH ON STAGGERED TILE HEATING
IN CFHT ($Y = 0.0$)

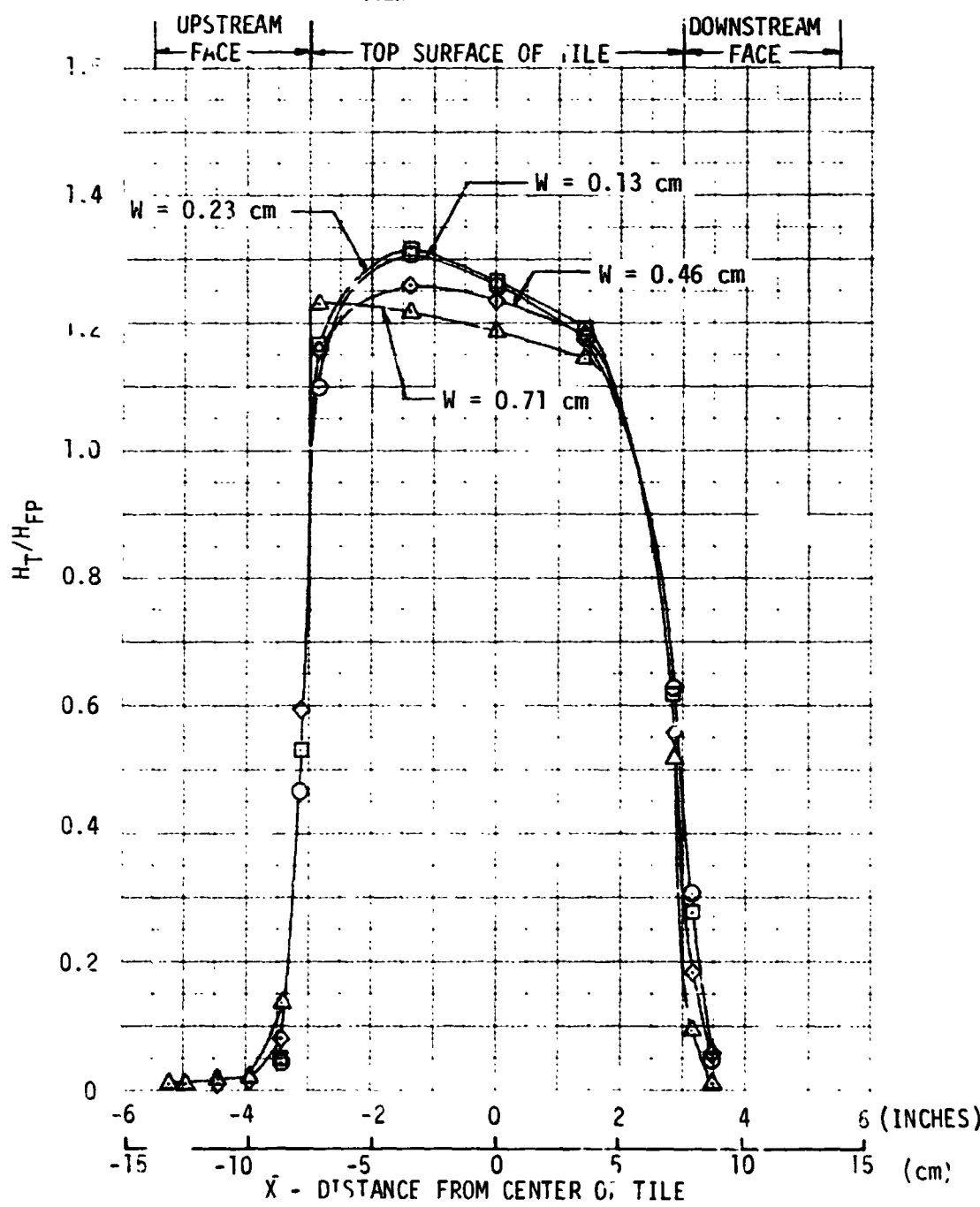


$\Gamma = \pi/2$ RADIANS

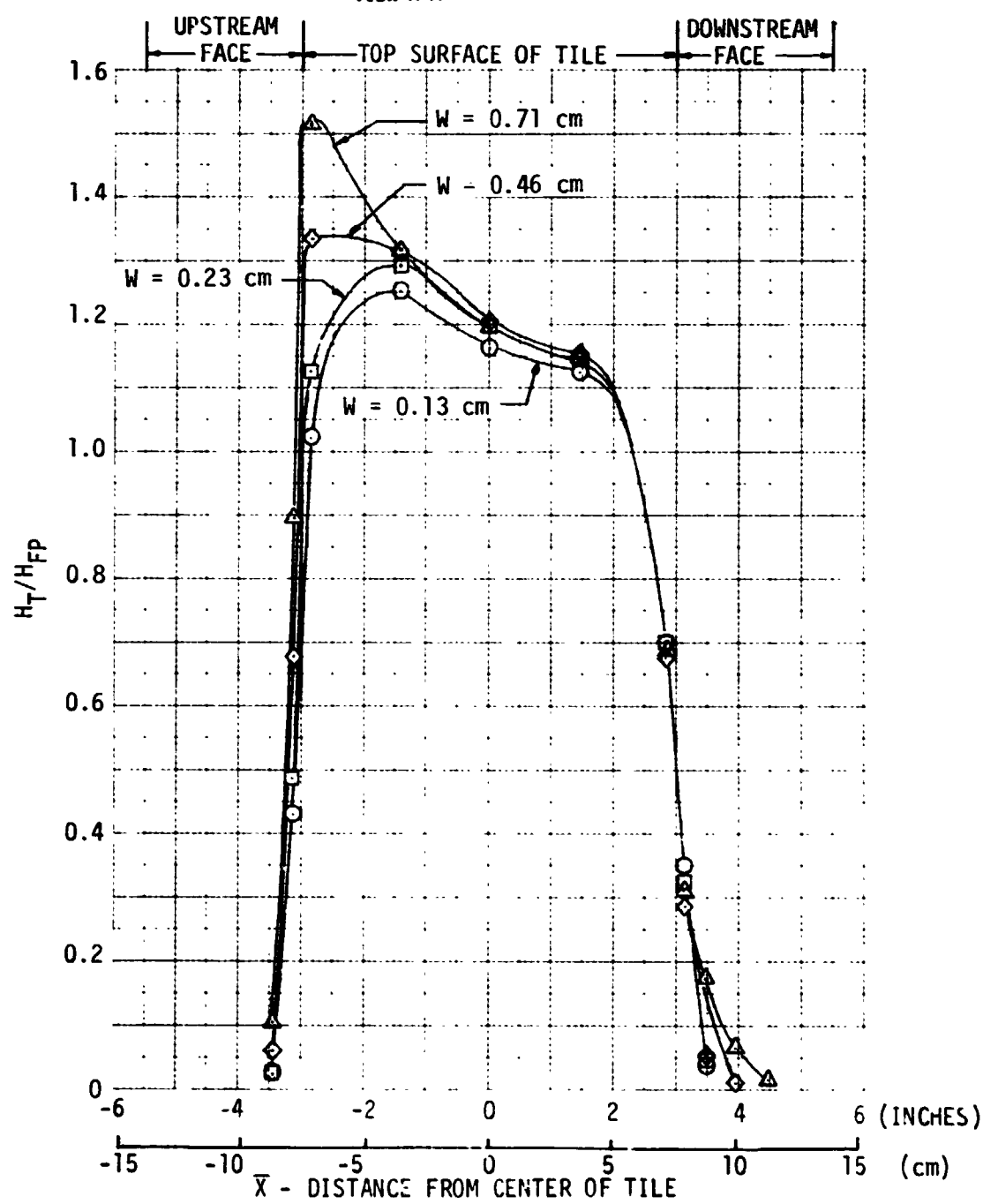
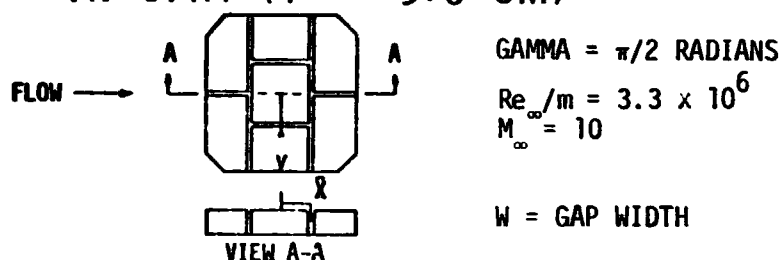
$Re_\infty/m = 3.3 \times 10^6$

$M_\infty = 10$

$W =$ GAP WIDTH



EFFECT OF GAP WIDTH ON STAGGERED TILE HEATING
IN CFHT ($Y = -3.8$ CM)



**EFFECT OF GAP WIDTH ON STAGGERED TILE HEATING
IN CFHT ($Y = -7.3$ CM)**

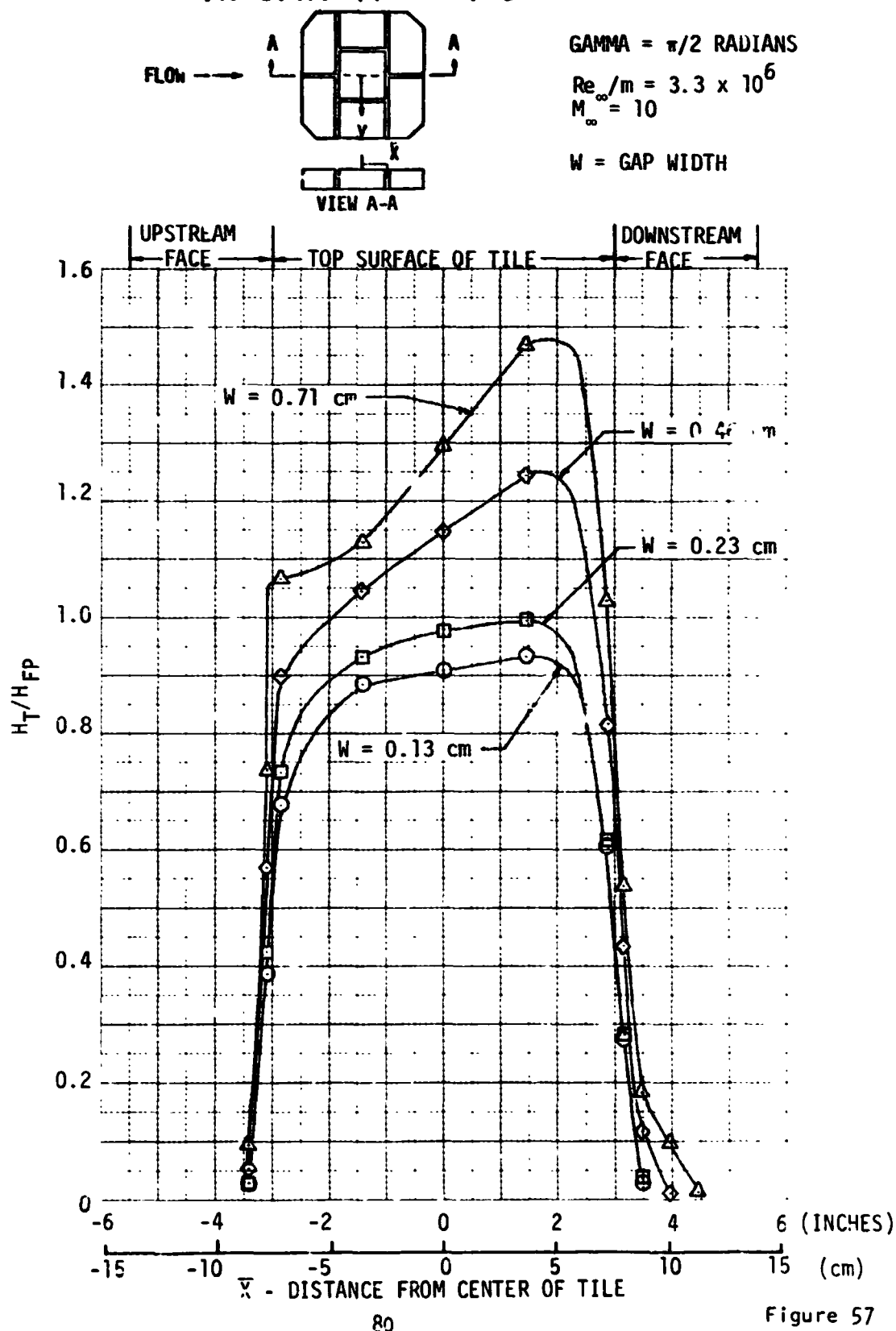


Figure 57



FINAL REPORT
VOLUME I

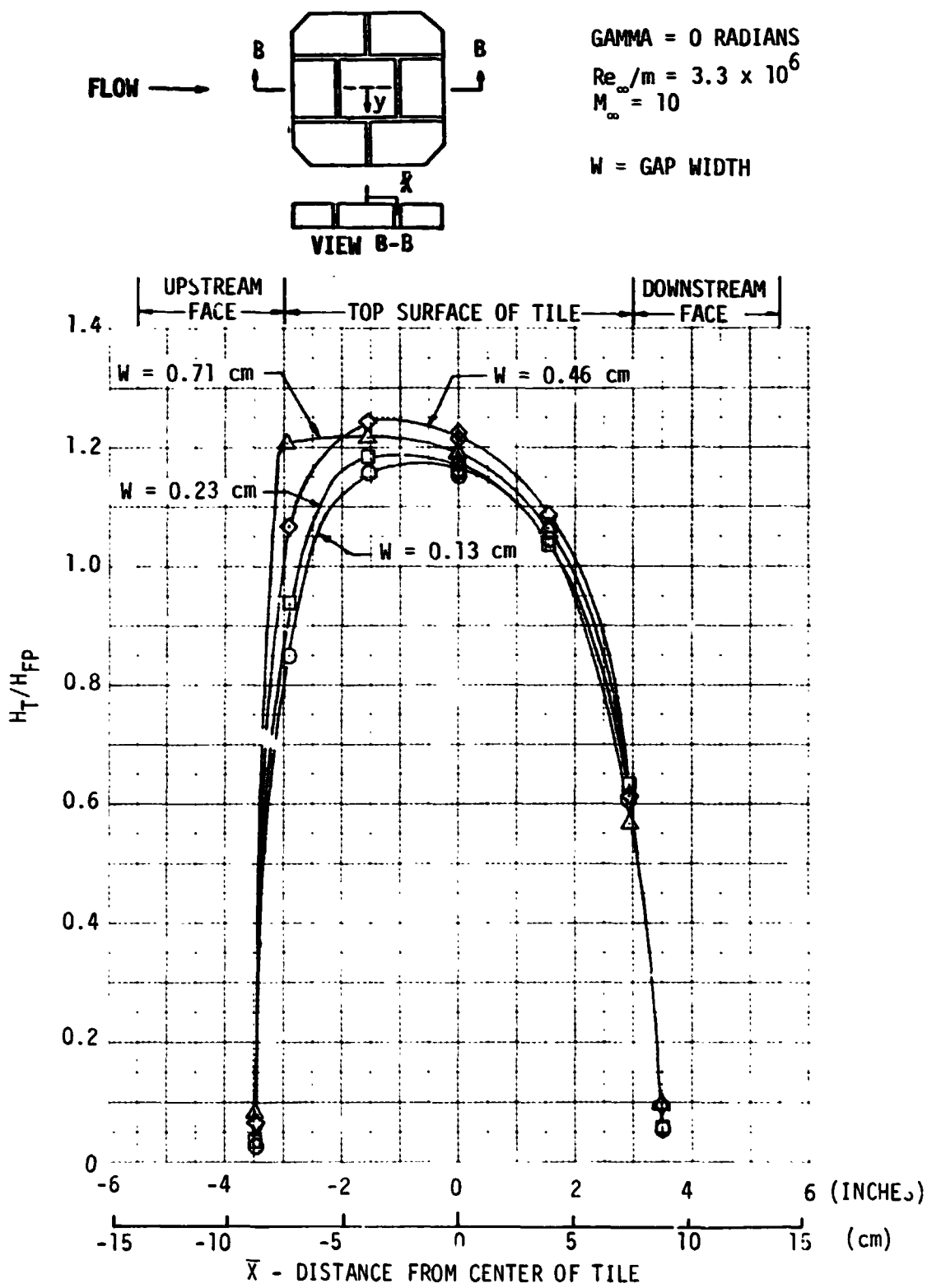
REPORT MDC E1003
29 JANUARY 1974

On the downstream face the trend is mixed with the gap heating either increasing or decreasing with gap width depending on the depth into the gap. The data near the outer edge of the tile ($y = -7.3$ cm) shows the heating on the upstream face, top surface, and downstream face all increasing significantly with increasing gap width.

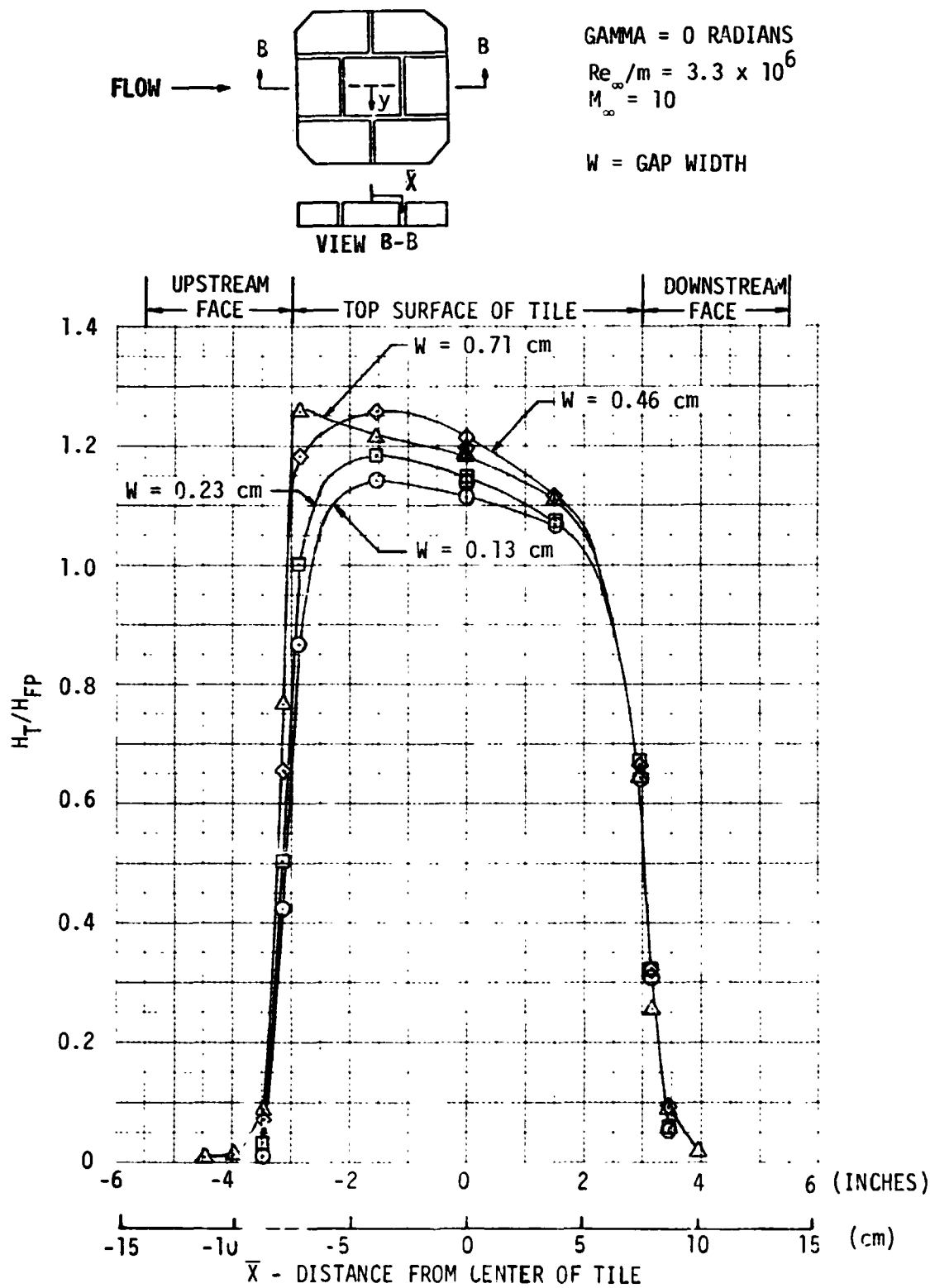
In general for the three (y) stations examined, it appears that the gap heating is related to the heating on the top surface near the gaps. The same trends that apply to the gap heating also apply to the top surface heating near the edges of the tile. This can be seen in all the figures presented for the staggered tile arrangement.

Figures 58, 59, and 60 present comparisons of heating distributions for the four gap widths at $y = 0.0$, -3.8 and -7.3 cm, respectively, for the in-line tile arrangement. It should be noted that two tunnel runs are required to produce the axial distributions for the in-line arrangement because only one half of the tile was instrumented. The front half of the thin skin tile is instrumented for one run and then the test article is rotated 180 degrees and data taken for the aft half of the tile for the second run. This results in a redundant set of data points at $\bar{X} = 0$. Figure 58 shows the axial heating distribution for the centerline of the tile. There are no data at the top of the upstream and downstream faces of the tile due to an inoperative thermocouple. The data taken in the gap show slightly increasing heating as the gap width increases for both upstream and downstream faces. The heating on the top surface generally increases with increasing gap width. This effect is greatest at the forward edge of the tile and actually reverses itself slightly at the aft edge. The heating distribution at $y = -3.8$ cm is presented in Figure 59 and shows essentially the same trends as were observed along the centerline. Figure 60 shows the heating distributions along the outer edge of the tile ($y = -7.3$ cm). It is observed that heating on all surfaces increase with increasing gap width. A review of the figures showing the effect of gap width on both staggered and in-line tile arrangements indicates that the in-line tile arrangement results in lower and more uniform heating on the top surface of the tile. The gap heating on the upstream faces of the tile do not appear to be significantly different for the two tile arrangements. A similar conclusion can be drawn for the downstream face. Gap width, as expected, significantly affects gap heating. However, the magnitude of the effect is dependent on the location in the gap.

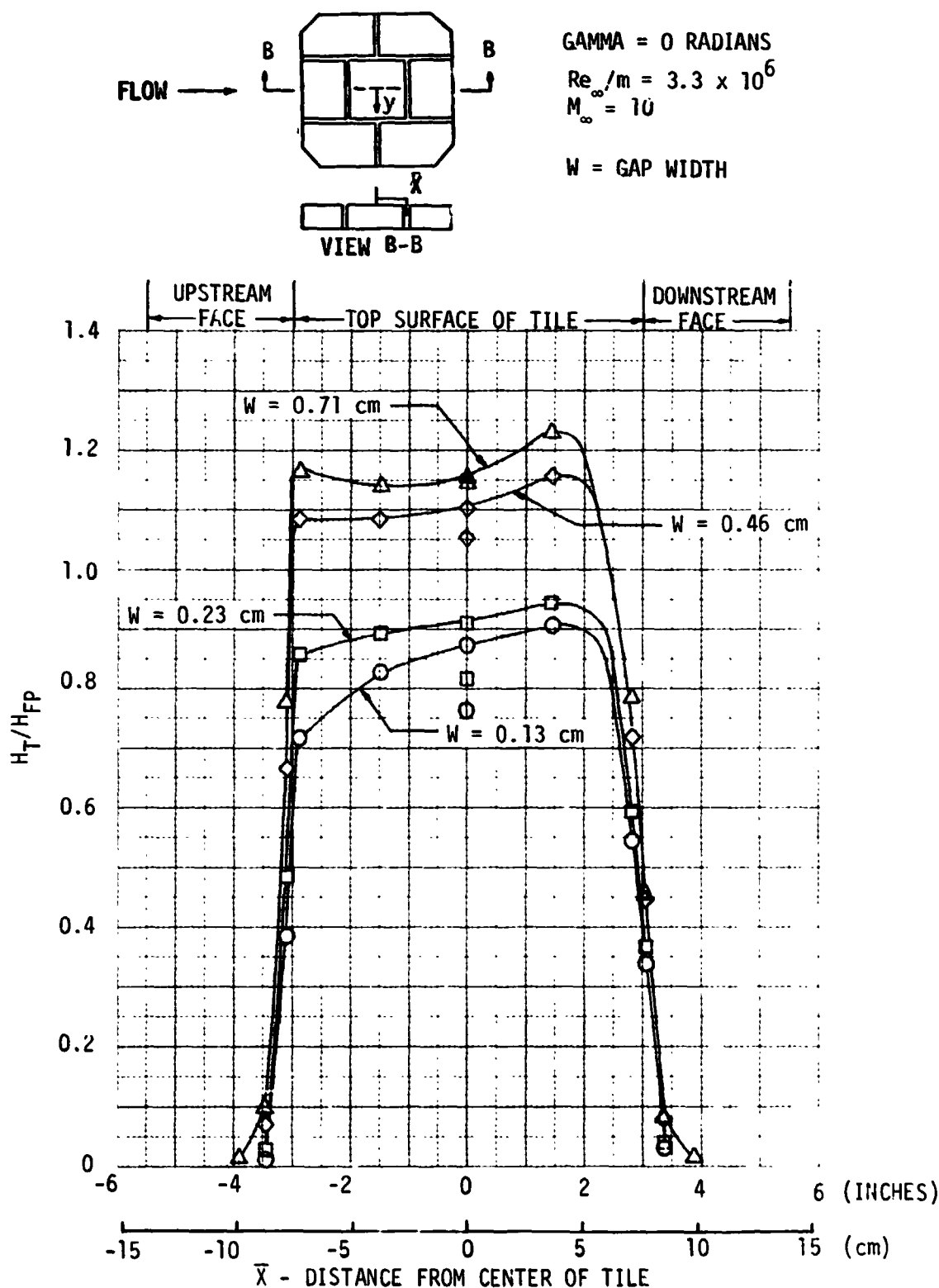
EFFECT OF GAP WIDTH ON IN-LINE TILE HEATING
IN CFHT ($Y = 0.0$)



EFFECT OF GAP WIDTH ON IN-LINE TILE HEATING IN CFHT ($Y = -3.8$ CM)


Figure 59

EFFECT OF GAP WIDTH ON IN-LINE TILE HEATING IN CFHT ($Y = -7.3$ CM)





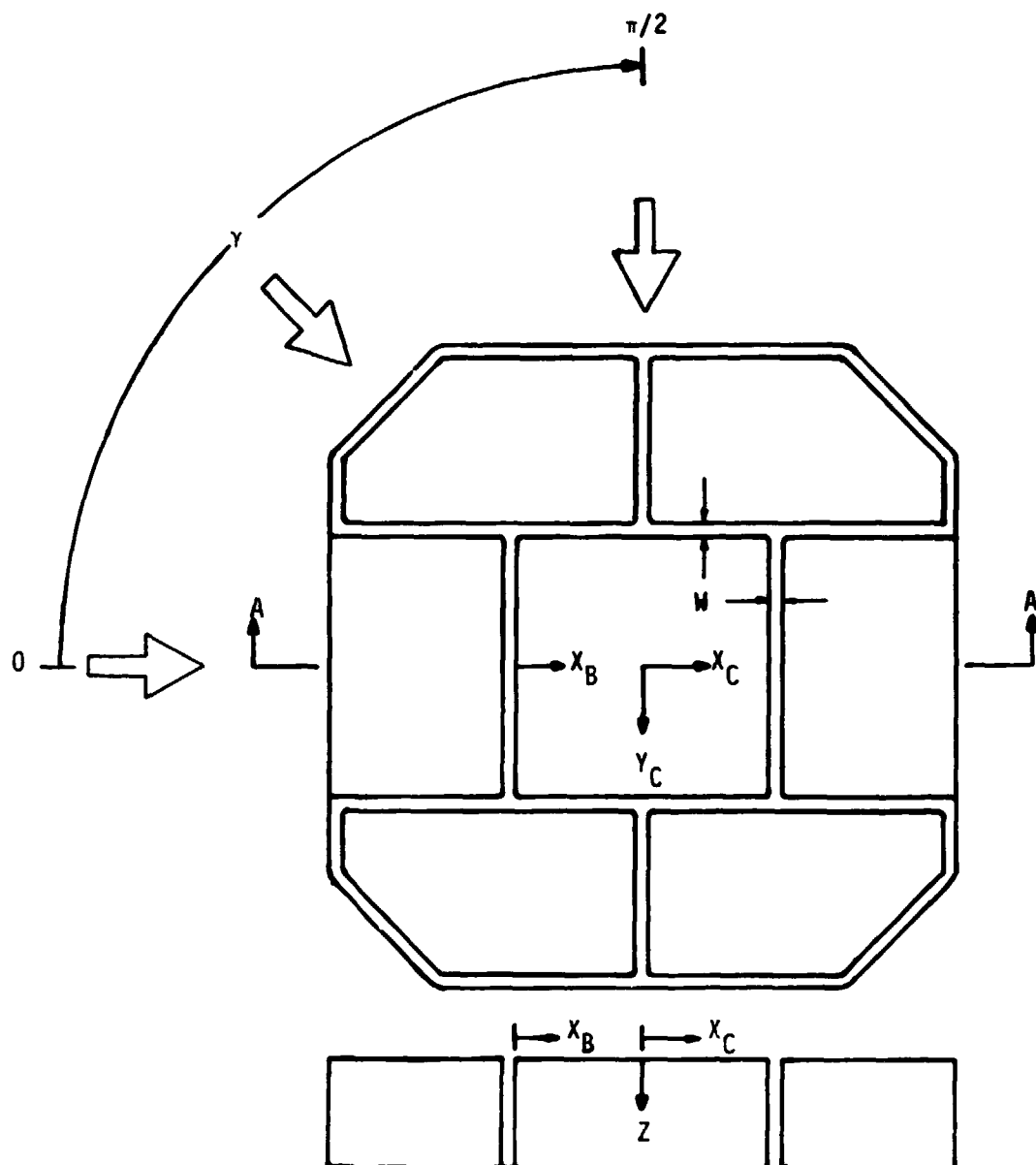
FINAL REPORT
VOLUME I

REPORT MDC E1003
29 JANUARY 1974

4.3.4 Effect of Flow Orientation - A different coordinate system was used during the execution of the CFHT tests to describe instrumentation locations on the thin skin tile for each basic tile position. This resulted in four separate coordinate systems. Using these systems, the flow angle (α) over the test article varies from 0 to $\pi/4$ radians. In examining the effect of flow angle on gap heating trends, it becomes apparent that these systems made the selection of data groups unwieldy. Therefore, a consistent coordinate system was defined which is fixed in the thin skin tile. A new flow angle variable (γ) was defined which varies from 0 radians (in line configuration) to $\pi/2$ radians (staggered configuration). By using a single coordinate system with respect to a fixed tile, the data from several tests were combined to describe heating on the entire tile as a function γ . Figure 61 shows the coordinate system.

The effect of flow angle on gap heating was examined on two faces of the thin skin tile for a 0.229 cm gap. Figure 62 presents data for the $X_C = -7.62$ cm face of the tile at four Y_C locations for the first thermocouple into the gap. This figure is an upstream face for inline tiles ($\gamma = 0$) which becomes a parallel face for staggered tiles ($\gamma = \pi/2$). It should be noted that the distance from the surface (Z) varies significantly for the data used in this figure. The heating level in the gap is a strong function of Z and therefore continuous curves are shown only for constant Z data. The data show that heating in the gaps is significantly affected by flow angle. The dependency of gap heating on flow angle changes with location along the gap. The minus Y_C data show the heating to decrease as γ is varied from 0 to $\pi/6$ radians and then increases as γ is varied from $\pi/4$ to $\pi/2$ radians. The plus Y_C data show the opposite trend with the heating increasing and then decreasing as γ is varied between 0 and $\pi/2$ radians. It appears that for this face of the tile the heating in the gap is either at a maximum or a minimum at $\gamma = \pi/4$ depending on the Y_C location. No data are shown for $Y_C = 0.0$ due to an inoperative thermocouple at that location. Heating data for the $Y_C = -7.62$ cm face of the tile are presented in Figure 63. Data for the first thermocouple down the gap for the X_C locations are shown for a gap width of 0.229 centimeters. This face is parallel to the flow for inline tiles ($\gamma = 0$) and faces the flow for staggered tiles ($\gamma = \pi/2$). The minus X_C data show decreasing heating as γ goes from 0 to $\pi/6$ radians. This trend is reversed as γ goes from $\pi/4$ to $\pi/2$ radians. The plus X_C data again show the opposite trends of the minus X_C data. As γ goes from 0 to $\pi/6$ radians the heating level increases. The heating then decreases as γ varies from $\pi/4$ to $\pi/2$ radians. The $X_C = 0.0$ data shows basically the same trend as the

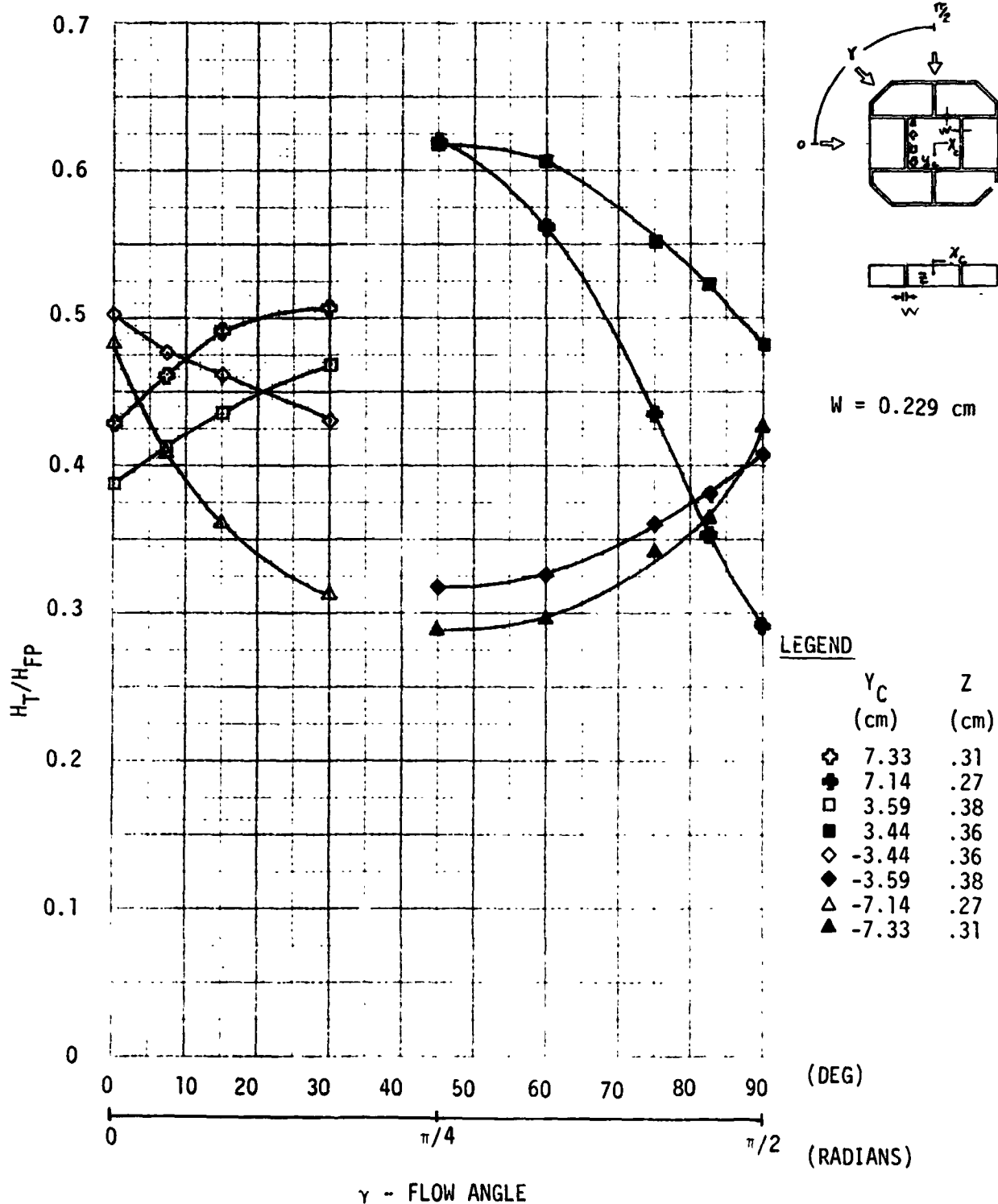
CFHT "TILE FIXED" COORDINATE SYSTEM



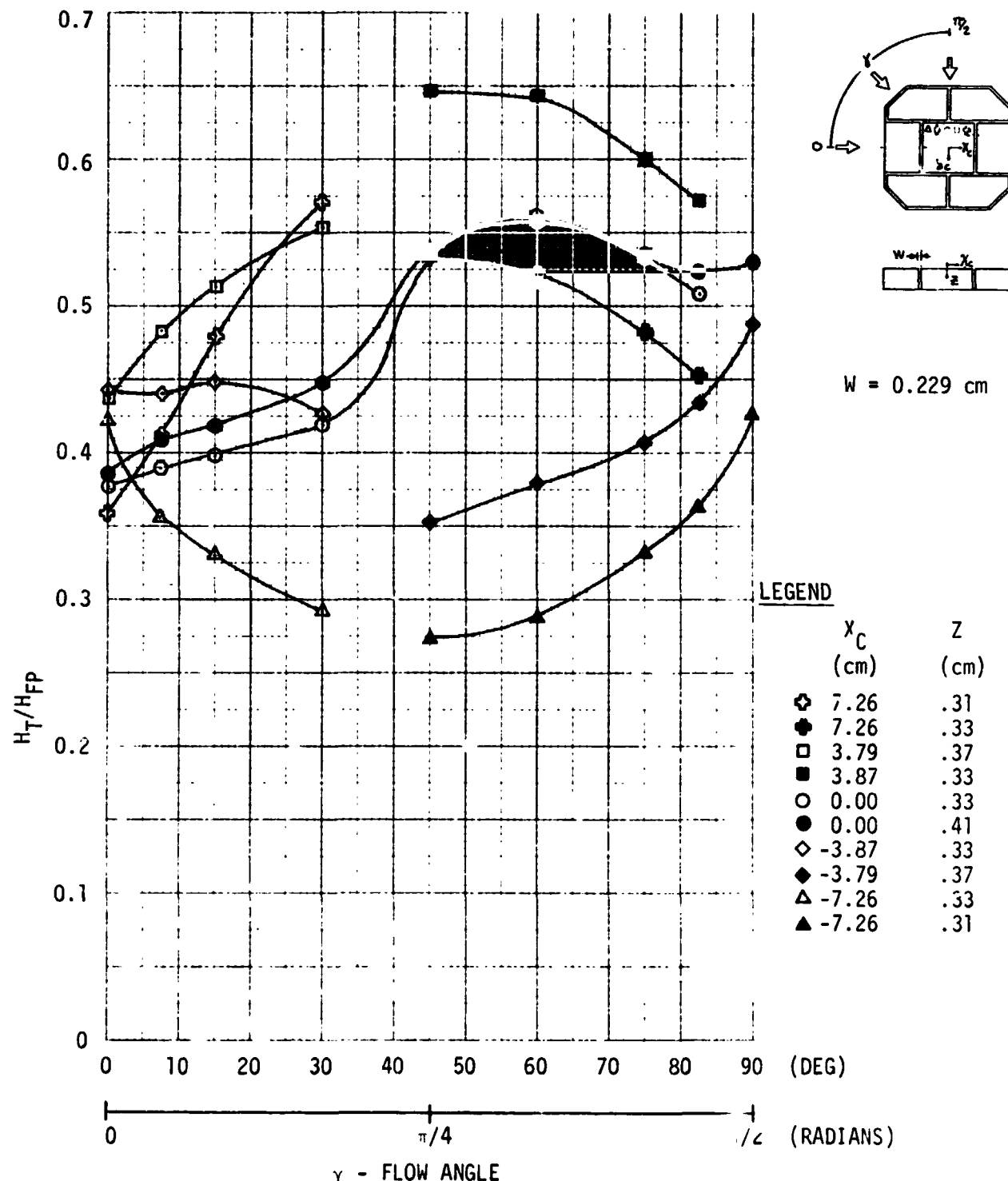
VIEW A - A

Figure 61

GAP HEATING VARIATIONS CAUSED BY FLOW ORIENTATION, ($X_C = -7.62$ CM)


Figure 62

GAP HEATING VARIATIONS CAUSED BY FLOW ORIENTATION, ($Y_C = -7.62$ CM)


Figure 63



FINAL REPORT
VOLUME I

REPORT MDC E1003
29 JANUARY 1974

plus X_C data between γ of 0 and $\pi/6$ radians. However, the heating level remains relatively constant between γ of $\pi/4$ and $\pi/2$ radians. The greatest variation in heating along this face of the tile occurs at $\gamma = \pi/4$ radians.

Figures 62 and 63 indicate that either an inline tile arrangement ($\gamma = 0$) or a staggered tile arrangement ($\gamma = \pi/2$) is more desirable than other possible flow orientations. The spread in gap heating in the X_C and Y_C direction is minimized at $\gamma = 0$ and $\pi/2$ radians. Also, the peak heating in the gaps are minima at these flow angles. These conclusions are based on data for a 0.229 cm gap width. Figure 64 shows the locations and levels of maximum gap heating at various flow angles for a gap width of 0.71 centimeters. The data were measured approximately 0.3 cm from the tile surface. These data support the conclusion that peak heating in the gaps are minima at flow angles of 0 and $\pi/2$ radians. The heating distributions along gaps at a depth of 0.3 cm for gap widths of 0.23 cm and 0.71 cm is presented in Figure 65 for a flow angle of $\pi/4$ radians. The heating rate gradients that occur at this flow angle are illustrated in this figure and appear to become more severe as the gap width increases.

4.3.5 Effect of Steps - The effect of tile mismatch was examined during testing by employing shims to raise and lower the thin skin tile. Tests were run with the tile raised 0.254 cm above the surrounding RSI tiles and lowered 0.168 cm below the surrounding tiles. Figure 66 presents inline tile heating distributions ($Y_C = 0.0$) for the step-up, flush and step-down tile configurations with a gap width of 0.23 centimeters. The step-up configuration resulted in a 55% increase in the peak heating rate measured on the tile surface when compared to the flush tile. The peak heating location appears to move nearer the upstream edge of the tile as the tile is raised above the flush position. Raising the tile increased heating on the upstream face of the gap and entire tile surface while having little effect on the downstream face. The step-down tile configuration resulted in lower heating on the upstream half of the thin skin tile and similar heating on the downstream half when compared with the flush tile. The peak heating rate was only 4.5% lower for the step-down tile. Figure 67 presents heating distributions for the three tile positions when the surrounding tiles are in the staggered configuration ($\gamma = \pi/2$). Similar conclusions can be drawn from the staggered tile data that were found in the inline tile data.

LOCATIONS OF MAXIMUM GAP HEATING

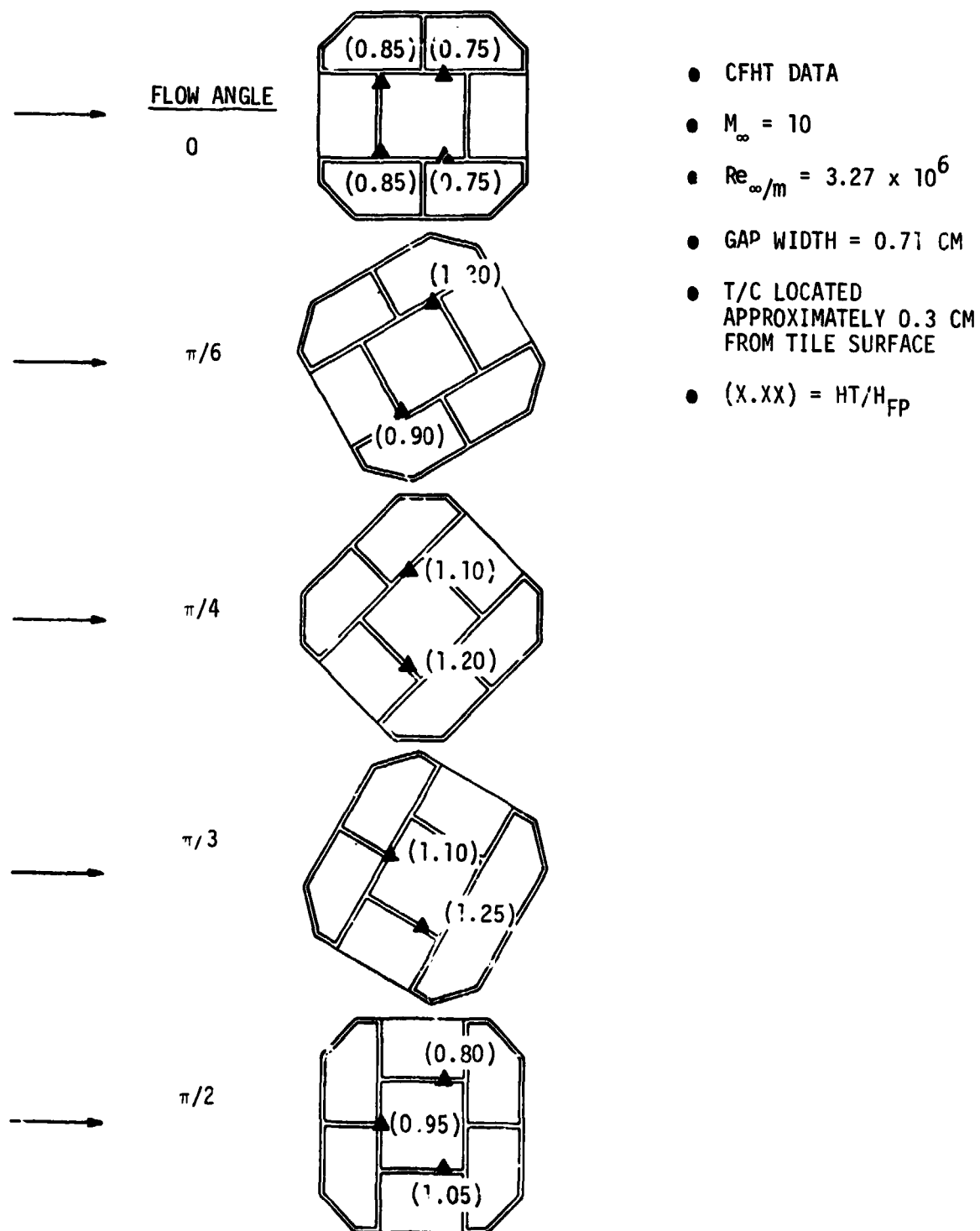


Figure 64

HEATING ALONG GAPS AT A DEPTH OF 0.3 CM

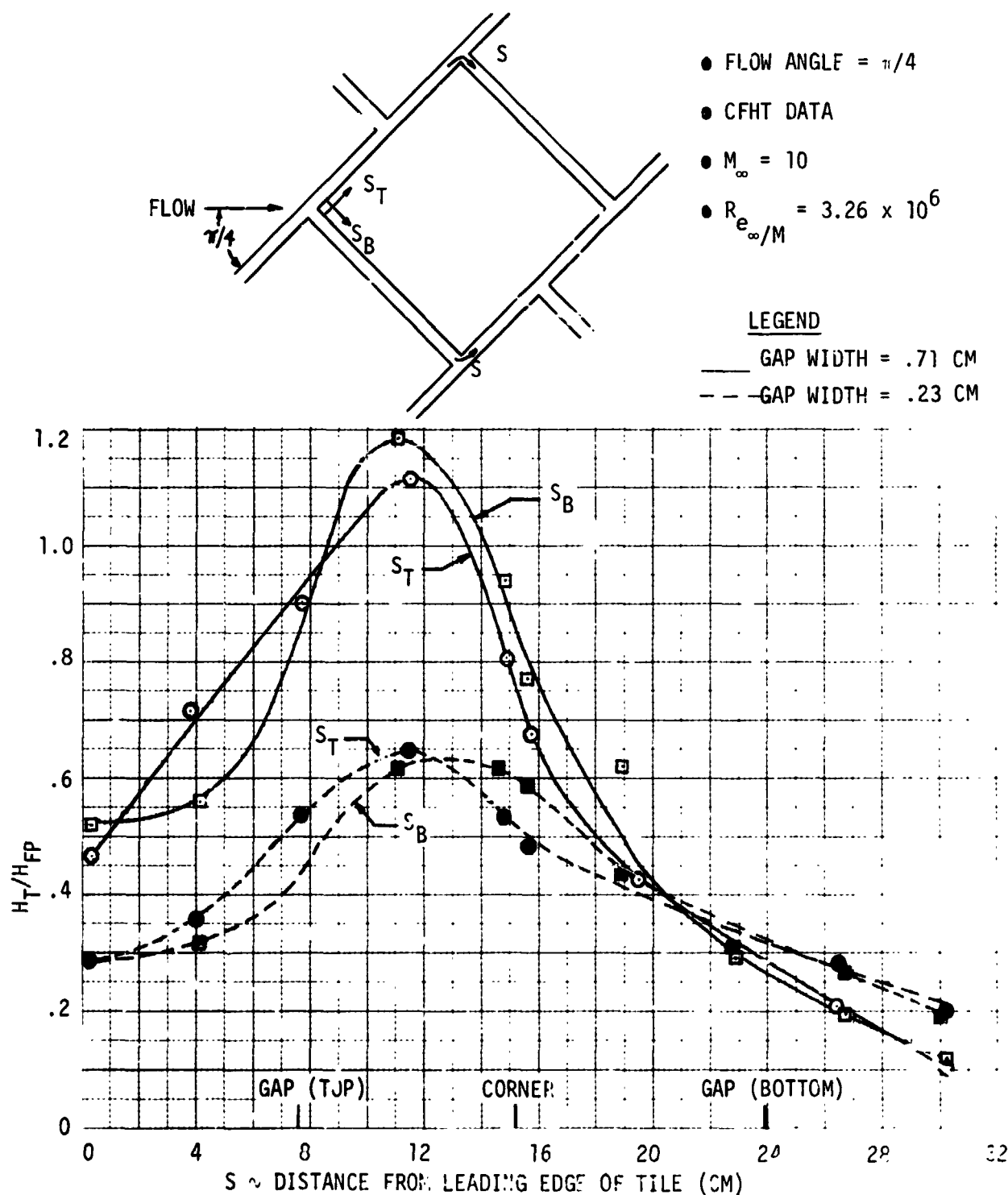


Figure 65



FINAL REPORT
VOLUME I

REPORT MDC E1003
29 JANUARY 1974

IN-LINE TILE HEATING DISTRIBUTIONS
IN CFHT ($Y_C = 0.0$)

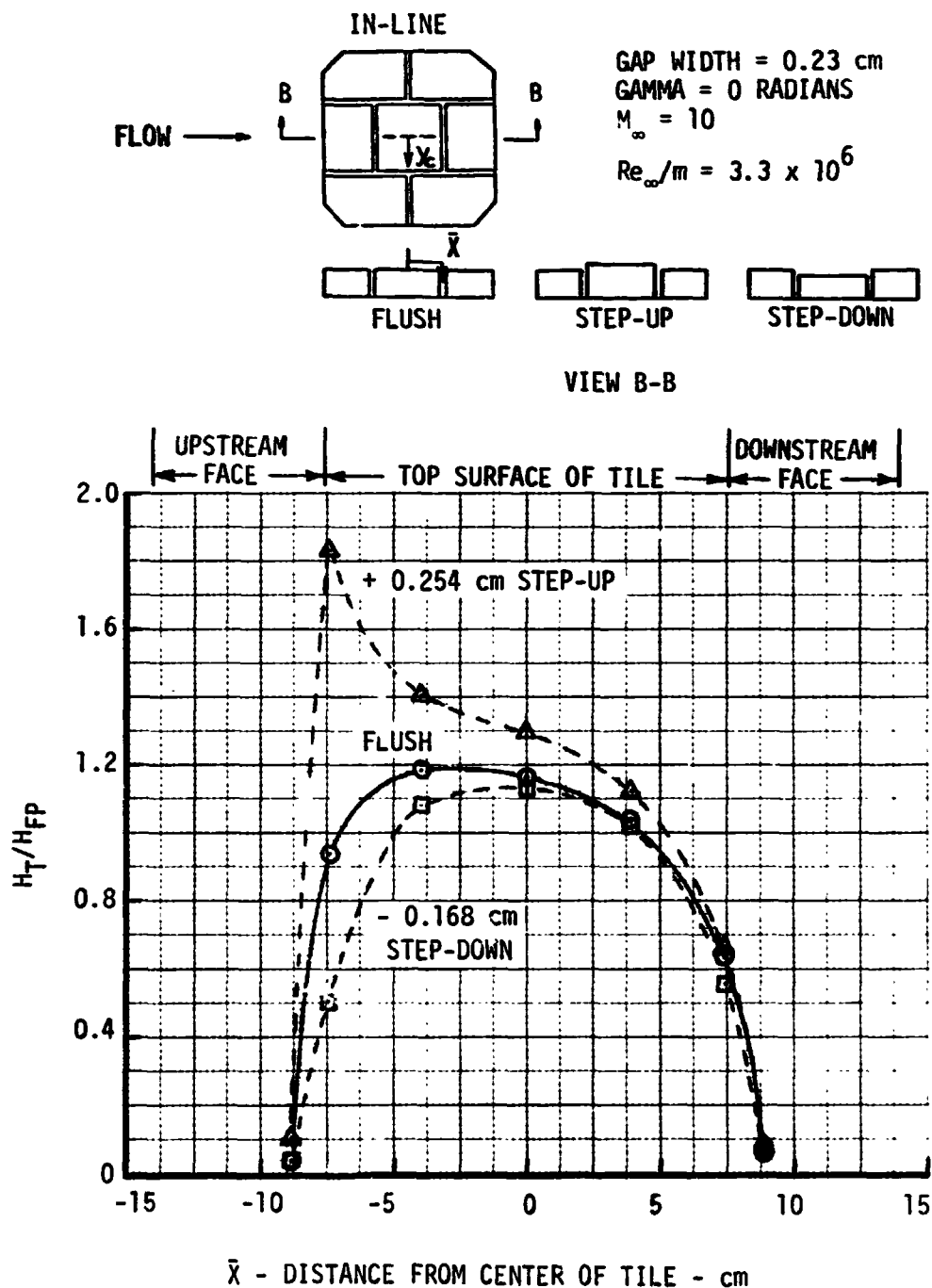
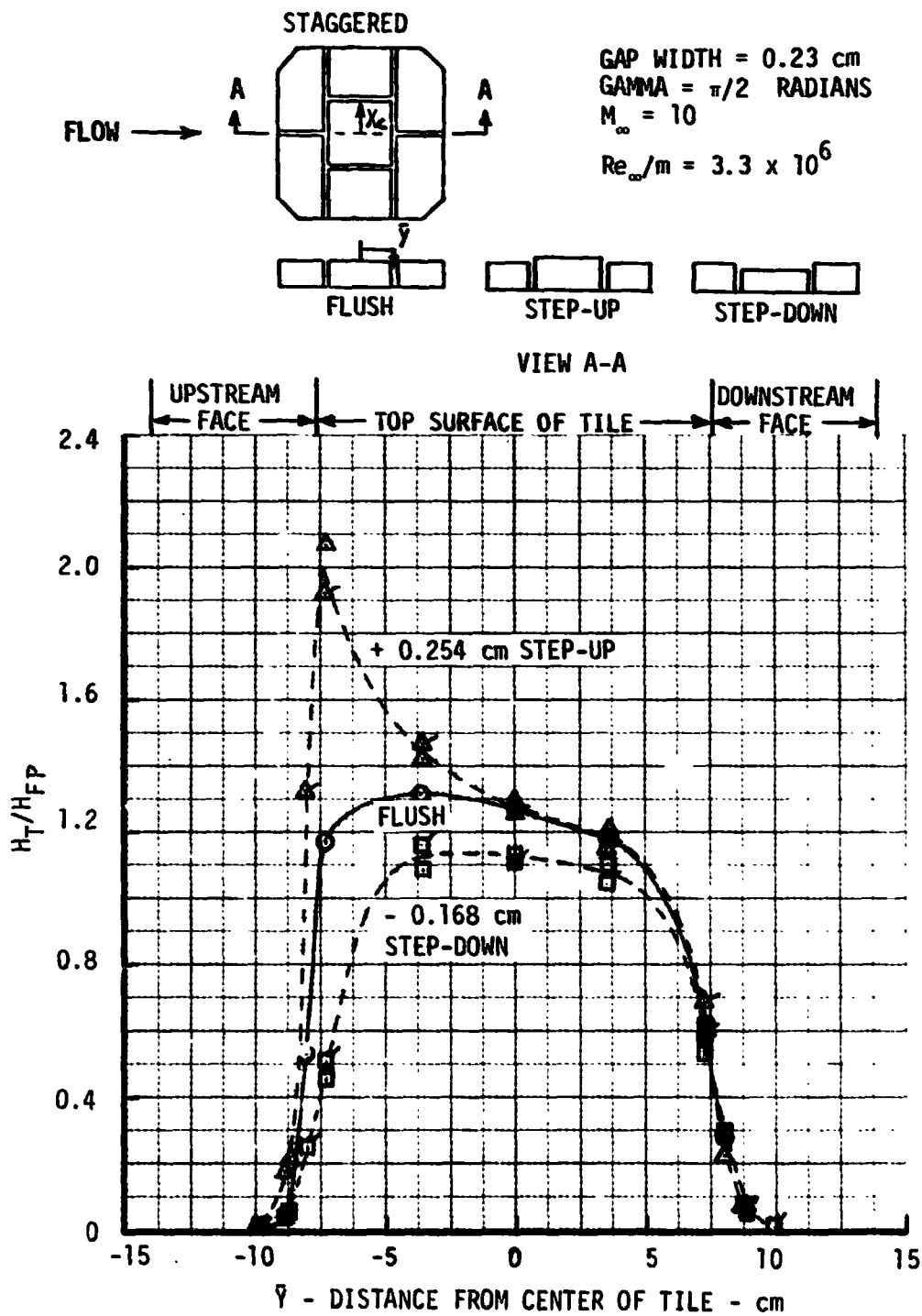


Figure 66

STAGGERED TILE HEATING DISTRIBUTIONS IN CFHT ($X_C = 0.0$)


Figure 67



FINAL REPORT
VOLUME I

REPORT MDC E1003
29 JANUARY 1974

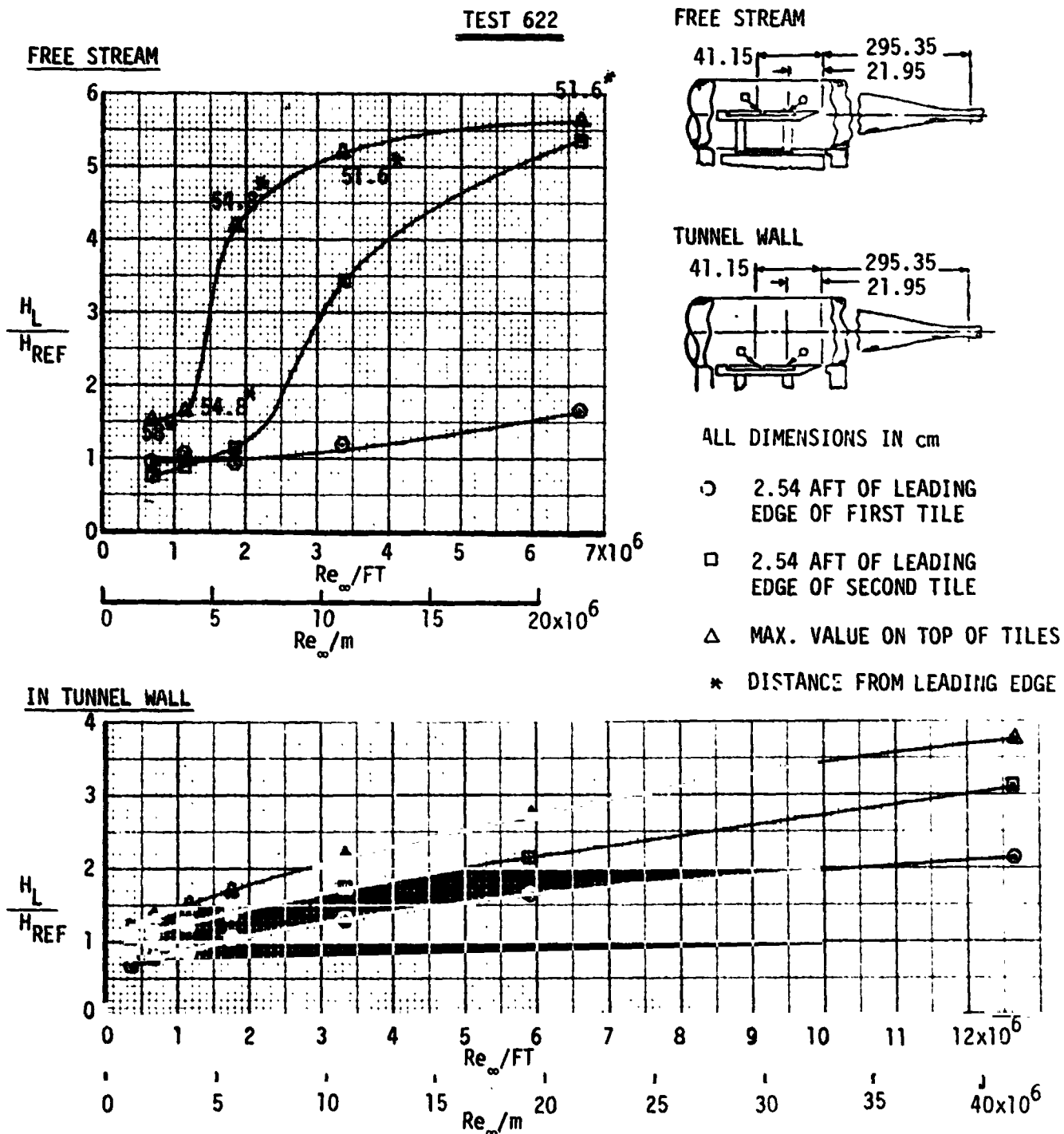
4.4 Analysis of Mach 8 Variable Density Tunnel Tests - Heat transfer measurements were performed for both in-line and staggered tiles (thin skin) positioned on the center line ("Free Stream") and in the wall of the Mach 8, Variable Density Tunnel. The tiles were 10.16 x 20.32 centimeters. Tests were conducted at Reynolds number (Re_∞/m) from 1.16×10^6 to 41.4×10^6 . A data tape containing test conditions, measured data and derived heat transfer parameters was prepared for facilitating analysis and for the Multiple Regression Analysis computer program. Listing of the data is contained in Volume II.

As a first step in the data analysis, heating on the top of the panel was examined to establish a reference for correlation. Heat transfer coefficient ratios obtained for the top of the panel at the most forward (2.54 cm aft of tile leading edge) instrumentation on the tiles and the maximum values are shown in Figure 68. A laminar recovery factor was used to compute a heat transfer coefficient (H_L) as well as laminar boundary layer theory to compute (H_{ref}) which was based on distance from model leading edge. This type of ratio is used to investigate transitional flow. If a value of unity is obtained, the flow is considered laminar. For the "Free Stream" tests, conditions were laminar on the forward portion of the model only at low Reynolds number. Plots of (H_L/H_{ref}) show a monotonic increase with distance along the panel and indicate no discernable effects caused by the transverse gap (0.159 cm) at the panel center. The high ratios indicate transition on the aft portion of the panel when in the Free Stream position. Also indicated on the figure is the position of maximum heating which moves forward as Reynolds number was increased indicative of transitional flow.

Figure 68 also contains similar data for the tunnel wall tests. The "maximum value" was near the trailing edge of the panel. When the data are presented, using (H_L/H_{ref}) significant increase in heating is indicated with distance along the panel. This is due to using H_{ref} in the ratio. For the tunnel wall tests, length Reynolds number was varied from 3.7×10^6 to 136×10^6 with boundary layer thicknesses ranging from 5 cm to 10 cm which was characteristic of a turbulent boundary layer. Sub-layer dimensions ranged from 0.15 cm to 0.30 cm.

In Figure 69 the same information is presented for the tunnel wall tests except the heat transfer coefficients are ratioed to the heating at point A at the lowest test Reynolds number. The shaded zone is based on ratioing to a laminar distribution and indicates a failure to collapse the data. When the laminar correction is removed, the measured data falls on the indicated line. The measured heating, (indicated by the "I" symbol) on the panel is nearly uniform, with only a 5% to 10% increase along the panel.

HEAT TRANSFER MEASURED ON TOP SURFACE OF TILES IN MACH 8 VARIABLE DENSITY TUNNEL



NOTE: H_{REF} = FLAT PLATE, LAMINAR HEAT TRANSFER COEFFICIENT, $r = \sqrt{\rho r}$

Figure 68

EFFECT OF CORRELATING HEAT ON
TOP OF TILE TO LAMINAR HEATING THEORY
MACH 8, VARIABLE DENSITY TUNNEL

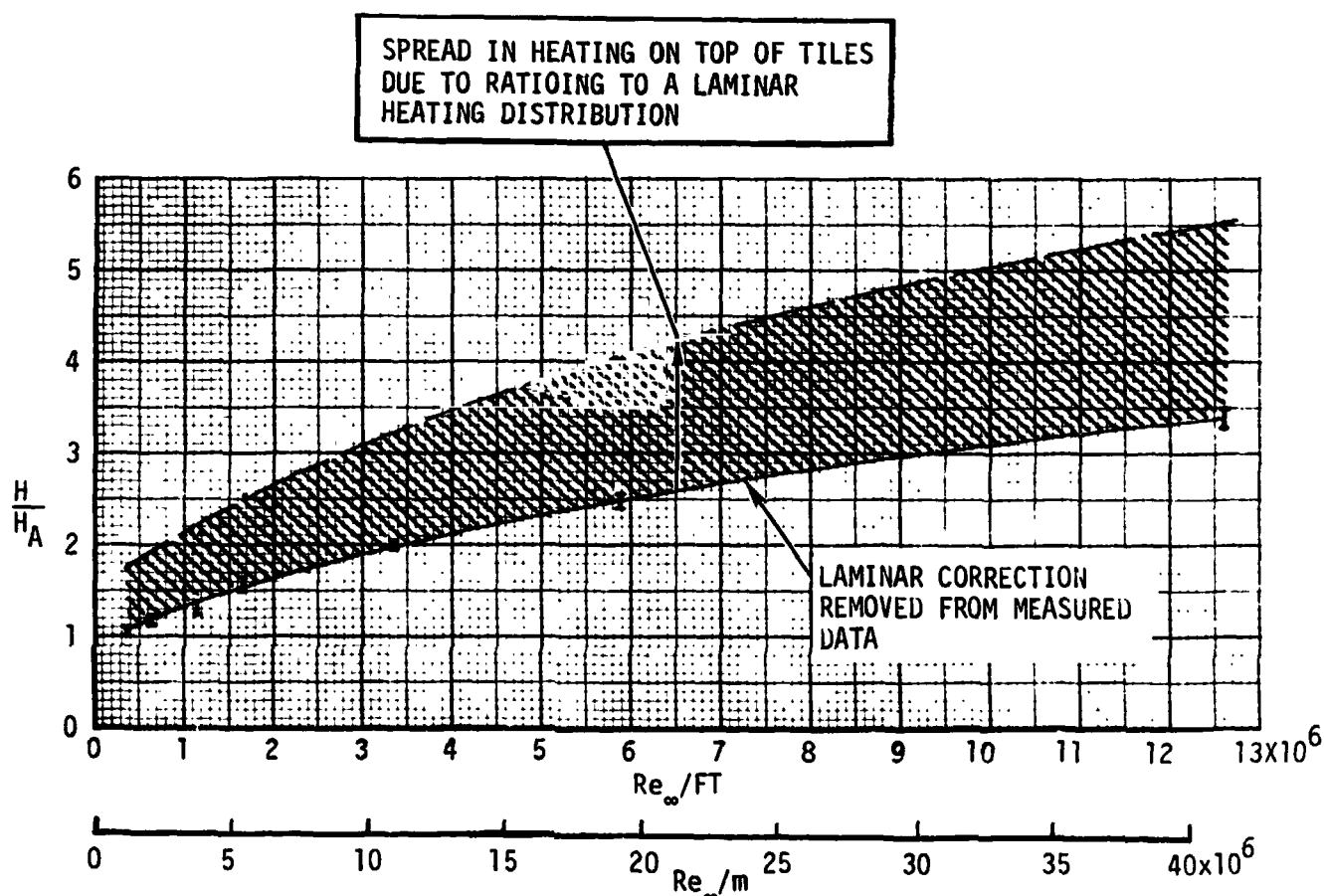
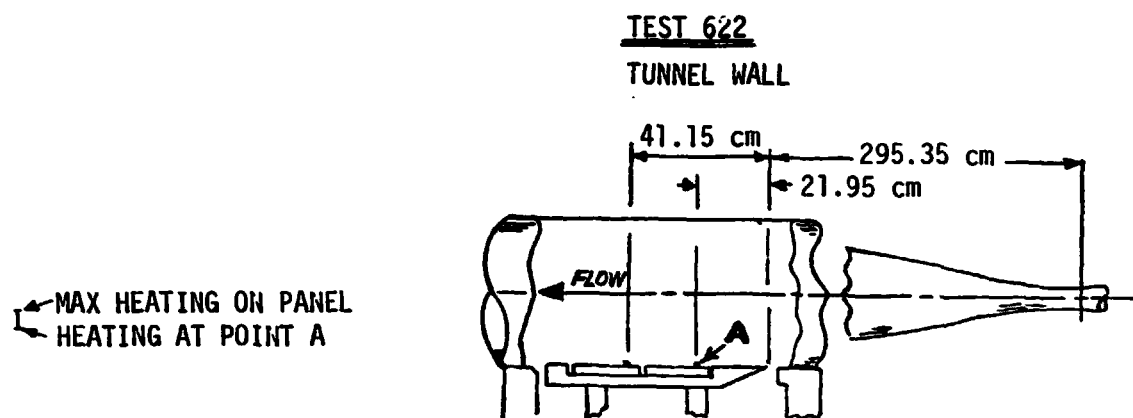


Figure 69



FINAL REPORT
VOLUME I

REPORT MDC E1003
29 JANUARY 1974

4.4.1 Heating Patterns on In-Line Tiles - The measured heating distributions along the length of the panel for the in-line tile configuration when the panel was positioned on the centerline (freestream) of the tunnel are shown in Figure 70. Heat transfer coefficients for each run are ratioed to that measured at point "B". Data are presented for unit Reynolds number/m from 2.3×10^6 to 21.8×10^6 . A variety of heating patterns is exhibited on the top of the tiles indicating laminar flow on tile #1 for the lower Reynolds number and transitional flow for the higher Reynolds numbers. For tile #2 the two lower Reynolds number tests exhibit a trend toward transitional flow. For $Re_\infty/m = 21.8 \times 10^6$ the data for the top of tile #2 suggests that the flow is fully turbulent. The gap at the center of the panel does not affect the heating on the top of the panel except for the $Re_\infty/m = 6.1 \times 10^6$ test where the gap produces transition onset. Transverse gap heating is relatively low compared to that measured on top of the panel and does not show a strong dependence on Reynolds number for the forward facing wall. The aft facing walls experienced a slight heating distribution change with Reynolds number. Even though significant changes in heating on top of the tile occurred, heating in the gaps remained well behaved. The larger gaps (0.318 cm) experience higher heating than the smaller gap (0.159 cm).

Heating distributions for the in-line gap model positioned flush with the tunnel wall are shown in Figure 71. Heat transfer coefficients for each tunnel run are ratioed to that measured at point "B". Tests were performed at unit Reynolds number/m from 1.16×10^6 to 41.4×10^6 . Heating on top of the tiles is relatively uniform with the higher Reynolds number data being almost constant. The lower Reynolds number data show a 10% heating increase on the tile top. Heating in the transverse gaps do not show as sharp a drop off with distance into the gap as the freestream test (Figure 70). For both the free stream and tunnel wall position, the upstream side of the transverse gap experiences equal or higher heating than the downstream side of the gap. Again the heating is higher for the larger gap. Increasing Reynolds number tends to lower the gap heating for the 0.159 cm gap.

4.4.2 Heating Patterns on Staggered Tiles - Heating distributions were measured also for a staggered tile configuration with the model in the freestream position and flush with the tunnel wall. Figure 72 contains the heating data for the freestream tests. Heating distributions on the top surface of the tiles are similar to those obtained for the in-line gap model (Figure 70) over the range of Reynolds numbers investigated. The staggered tile configuration had only the

HEATING DISTRIBUTION ALONG MACH 8 V.D.T. GAP MODEL, (IN-LINE GAP CONFIGURATION, FREE STREAM POSITION)

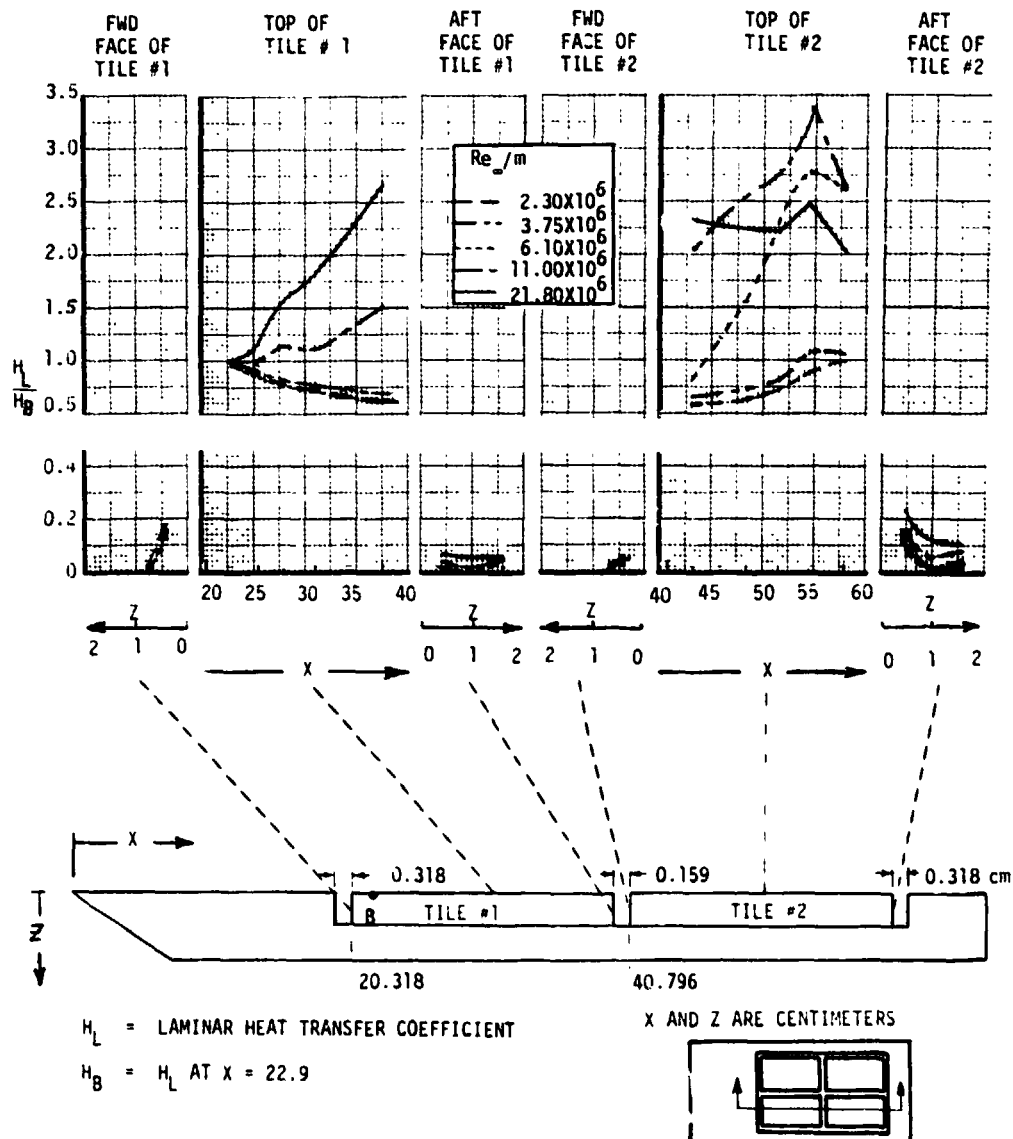


Figure 70



FINAL REPORT
VOLUME I

REPORT MDC E1003
29 JANUARY 1974

HEATING DISTRIBUTION ALONG MACH 8 V.D.T. GAP MODEL, (IN-LINE GAP CONFIGURATION, TUNNEL WALL POSITION)

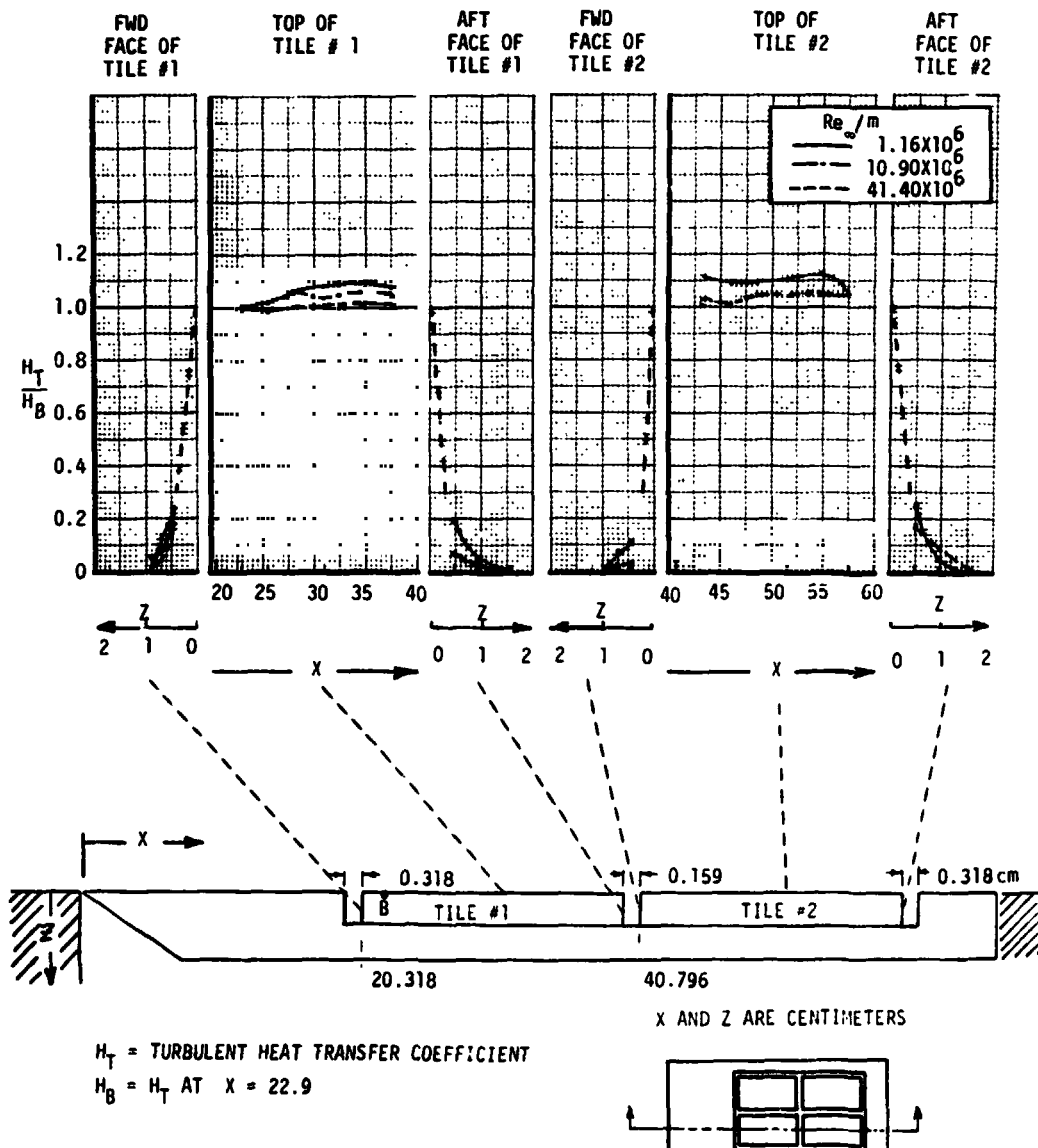


Figure 71



FINAL REPORT
VOLUME I

REPORT MDC E1003
29 JANUARY 1974

HEATING DISTRIBUTION ALONG MACH 8 V.D.T. GAP MODEL.
(STAGGERED GAP CONFIGURATION, FREE STREAM POSITION)

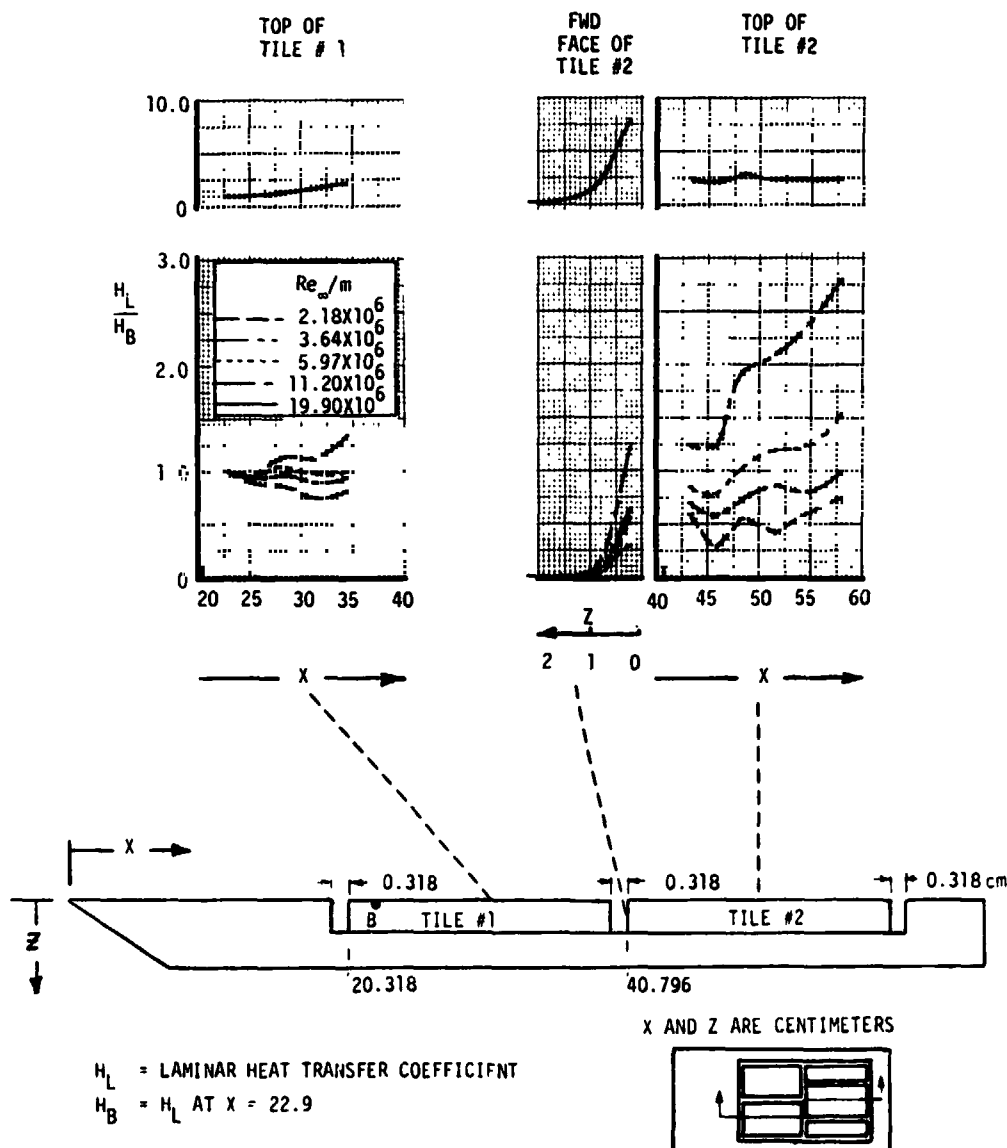


Figure 72



FINAL REPORT
VOLUME I

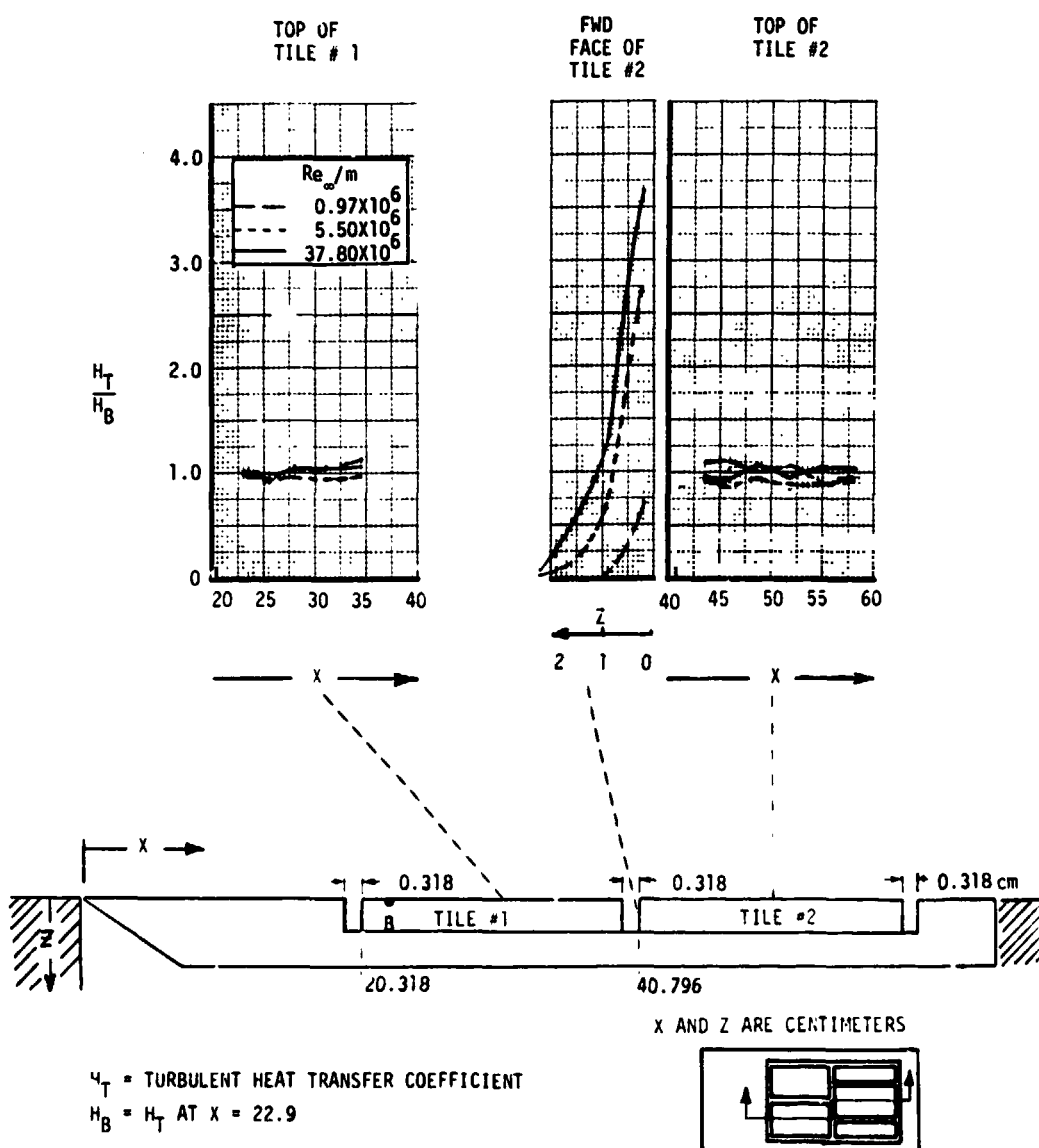
REPORT MDC E1003
29 JANUARY 1974

downstream face of the center transverse gap instrumented. This gap (0.318 cm) was twice the width of that in the in-line model. Gap heating at the center of the model (stagnation region) is presented in Figure 72 and shows a strong dependency on Reynolds number. For Reynolds numbers greater than 11.2×10^6 per meter, heating in the gap is greater than the top surface. The gap heating for $\text{Re}_{\infty}/m = 19.6 \times 10^6$ is as great as eight times the surface value.

Heating data for the staggered tile configuration flush with the tunnel wall (Figure 73) show that the turbulent boundary layer produced essentially uniform heating on the top of the panel which is similar to that experienced by the in-line tile model (Figure 71). As with the freestream tests of the staggered tiles, the downstream face of the transverse gap experienced significant heating with a distribution strongly dependent on Reynolds number.

Figure 74 shows a remarkable set of heating distributions measured across the gap face of the downstream tile for the staggered tile configuration. Indicated on the figure is the half width of the parallel gap which terminates at the tile face. The heating is almost constant across the half gap width and then decreases consistently in the lateral direction similar to a "normal" distribution. Also shown are heat flux contours which show the size of the hot spot. The size of the hot spot, where the heating ratio (H_T/H_B) is greater than 0.5, is approximately 1.5 centimeter radius.

HEATING DISTRIBUTION ALONG MACH 8 V.D.T. GAP MODEL, (STAGGERED GAP CONFIGURATION, TUNNEL WALL POSITION)


Figure 73



FINAL REPORT
VOLUME I

REPORT MDC E1003
29 JANUARY 1974

GAP HEATING DISTRIBUTION ON THE FACE OF THE
DOWN STREAM TILE-STAGGERED CAP CONFIGURATION,
TUNNEL WALL

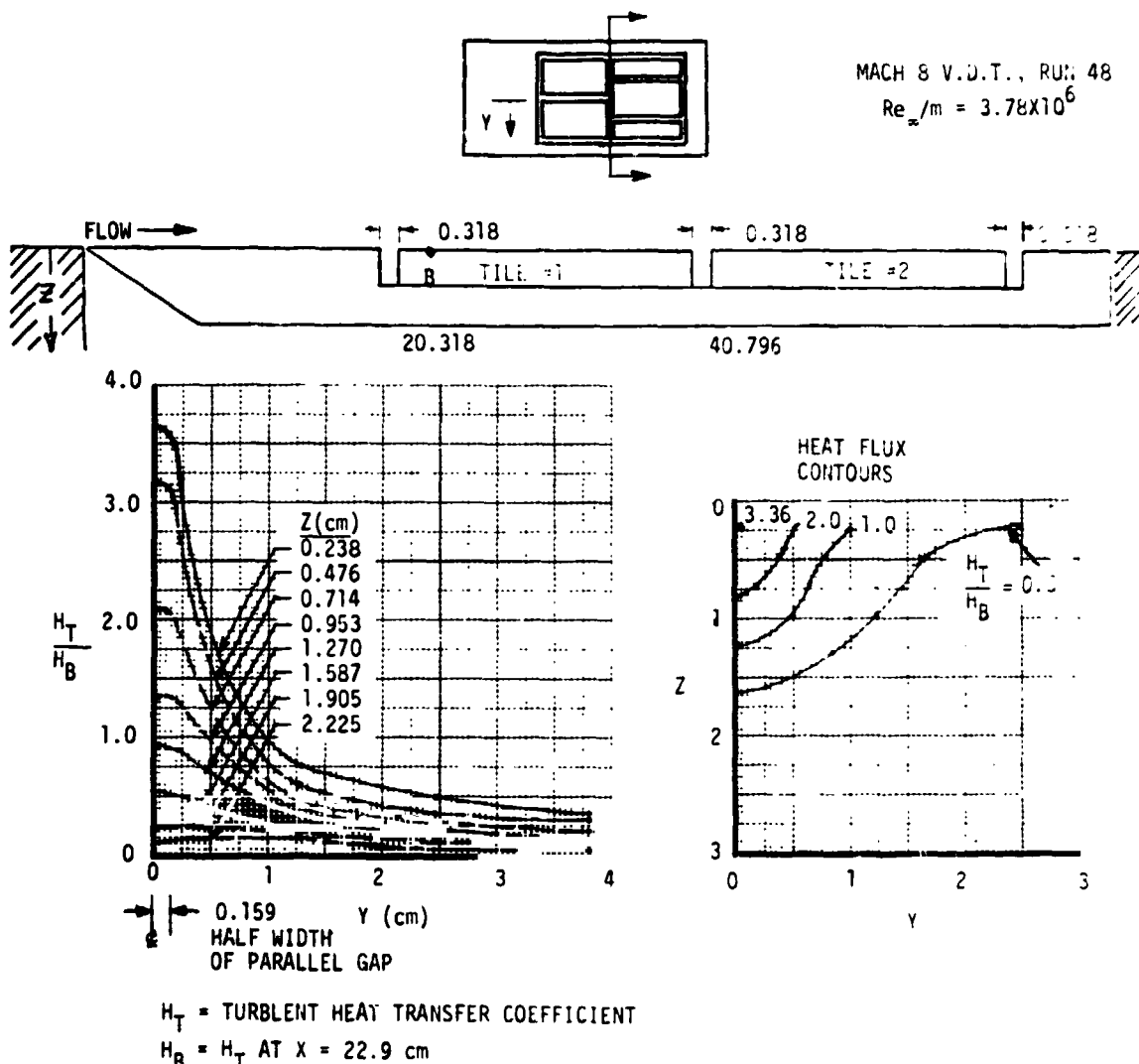


Figure 74



FINAL REPORT
VOLUME I

REPORT MDC E1003
29 JANUARY 1974

4.5 Analyses of Ames 3.5 Foot HWT Tests of Gap Models - Analyses were performed on the data from the Rockwell International Gap Heating Test 158 (OH-2) conducted in NASA-Ames 3.5 Foot Hypersonic Wind Tunnel. Figure 75. is a summary of the gap heating models that were tested. The tests were run at Mach 5.1 at four unit Reynolds numbers. The Reynolds numbers were 1.4, 2.2, 3.3, and 4.5×10^6 per meter. A total of five gap widths and three gap depths were investigated. All tests employed a flat plate model at zero angle-of-attack. A complete description of the test as well as a listing of the data are contained in Section 5.0 of Volume II of this report.

4.5.1 Calibration Plate Heating Pattern - The test configuration consisted of a 68.6 152.4 cm carrier plate (Figure 76) into which 70 x 106.7 cm instrumented test article inserts were placed. Total temperature and pressure probes were mounted on the downstream end of the carrier plate at three spanwise locations. These probes were used to define the freestream conditions for the tests. Four calibration runs (Runs 38 thru 41) were made to characterize the flow over the test configuration utilizing the smooth heat transfer calibration plate. Three rows ($y = -20.54$, 0.0, and 20.54cm) of Chromel-Constantan thermocouples and three corresponding total temperature probes were used to measure the heating environment along and across the test article. Figure 77 presents the heat transfer coefficient along the calibration plate ($y = -20.54$) for the four test unit Reynolds numbers. The heat transfer coefficient (H_L) is based on a recovery factor of 0.874 Companion data was also received for a recovery factor of 0.907. The low Reynolds number heating data decrease approximately with the square root of distance along the panel which is characteristic of a laminar boundary layer. The higher Reynolds number data show a decrease and then a sharp rise in heating along the panel characteristic of transitional flow. The heat transfer data measured on inserts with simulated RSI gaps are referenced to the flat plate calibration data. A two-dimensional interpolation in the x and y directions was performed on the calibration data for each test condition to determine the reference heat transfer coefficient at the locations where gap heating data were measured. Figure 78 is a typical plot of Stanton number along the calibration plate and shows amplified separation of data due to a Reynolds number effect. The laminar and transitional heating patterns are obvious from this figure.

4.5.2 Gap Heating Distributions - A cursory analysis of the data was performed mainly consisting of comparisons of data trends with trends observed in the CFHT data. Figure 79 presents heating distributions at three Reynolds number



FINAL PORT
VOLUME I

REPORT MDC E1003
29 JANUARY 1974

AMES 3.5 FOOT HWT GAP MODELS

- TEST VARIABLES

$10^6 Re/m = 1.4, 2.2, 3.3 \text{ AND } 4.5$

$M_\infty = 5.1$

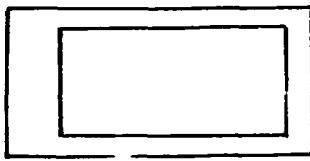
GAP WIDTH = .159 AND .318 cm

GAP DEPTH = 1, 2, AND 4 cm

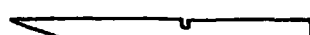
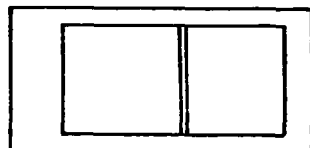
STEPS = 0, $\pm .159$ AND $\pm .318$ cm

- 71 TEST RUNS ASSIMILATED

CALIBRATION PLATE



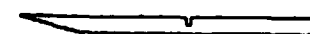
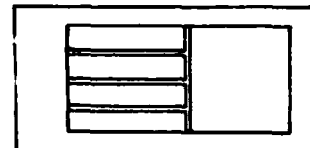
SINGLE TRANSVERSE GAP



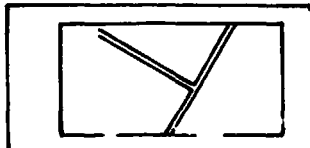
MULTIPLE TRANSVERSE GAP



STAGGERED TILES



30° ORIENTED TILES



CARRIER PLATE FOR AMES GAP HEATING TESTS

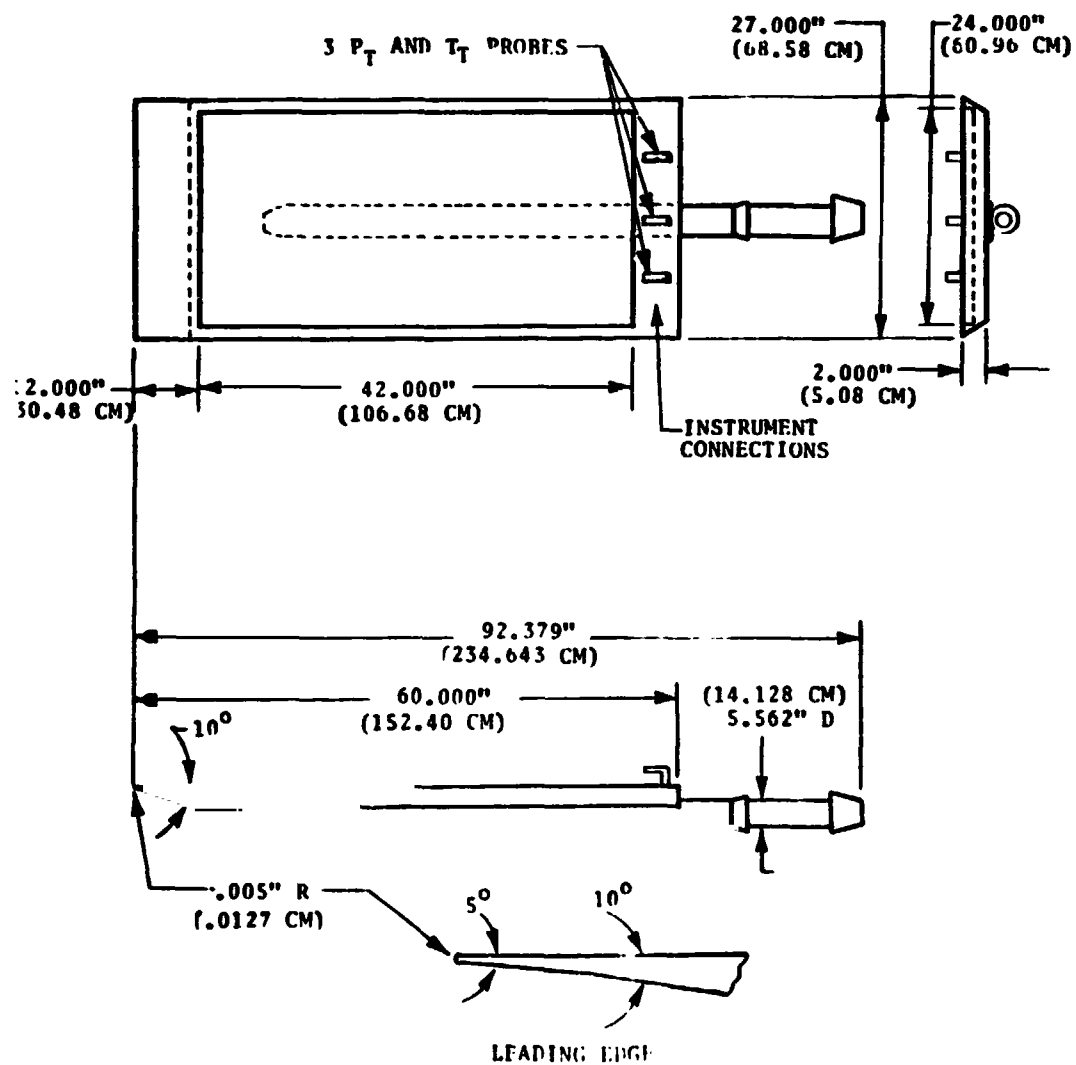
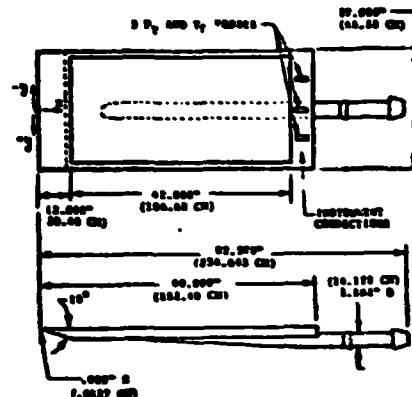


Figure 76

HEAT TRANSFER COEFFICIENT (LAM) ALONG AMES WEDGE

SYM	Re_{∞}/m	RUN
□	$1.450800E+06$	38
○	$2.322100E+06$	39
▲	$3.347600E+06$	40
+	$4.511900E+06$	41



Y - LATERAL DISTANCE (CM) = -20.536

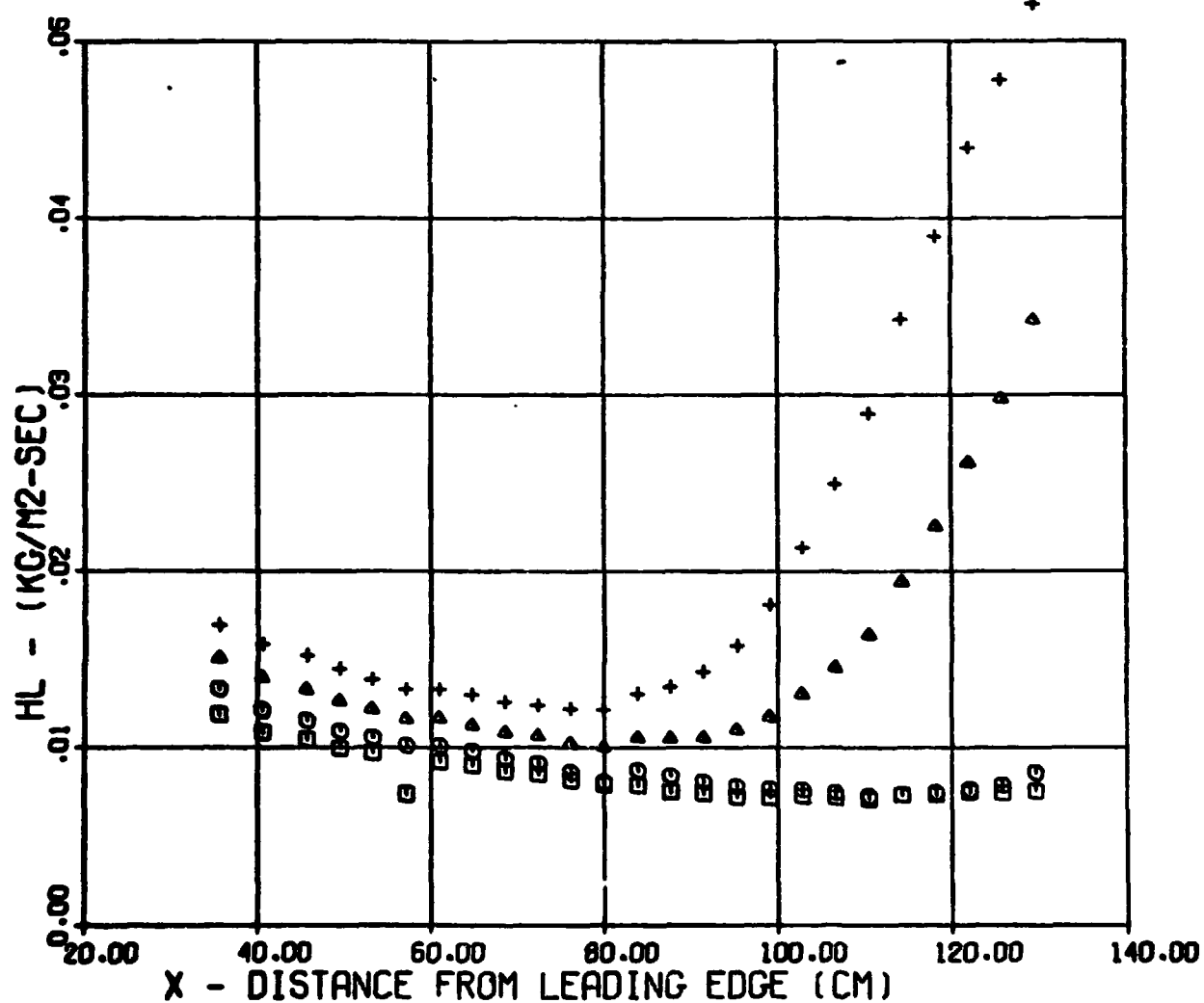
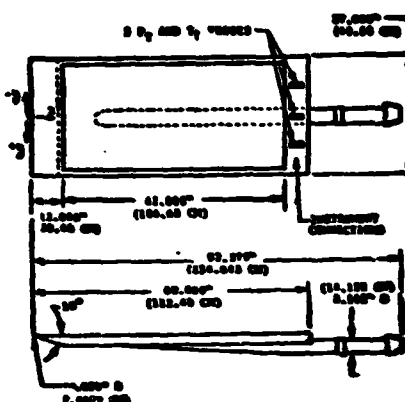


Figure 77

STANTON NUMBER (LAM) ALONG AMES WEDGE

SYM	Re_∞/m	RUN
□	1.4508E+06	38
○	2.1991E+06	39
▲	3.2607E+06	40
+	4.5119E+06	41



Y - LATERAL DISTANCE (CM) = 0.000

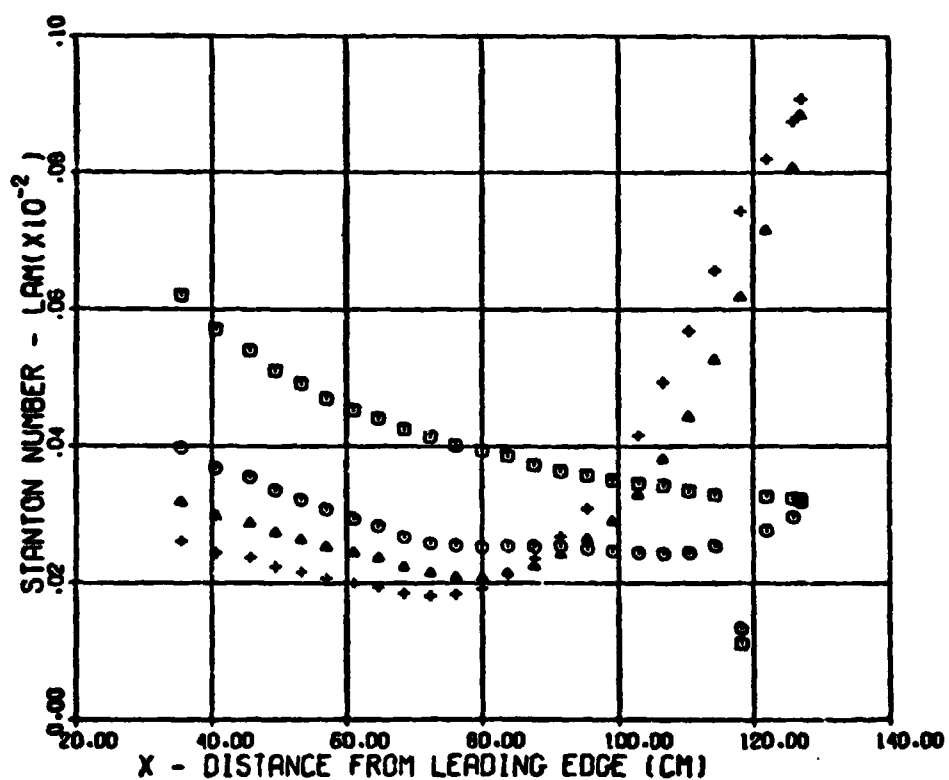


Figure 78

HEATING DISTRIBUTION MEASURED AT 0.254 CM TRANSVERSE GAP (AMES 3.5 FOOT HWT)

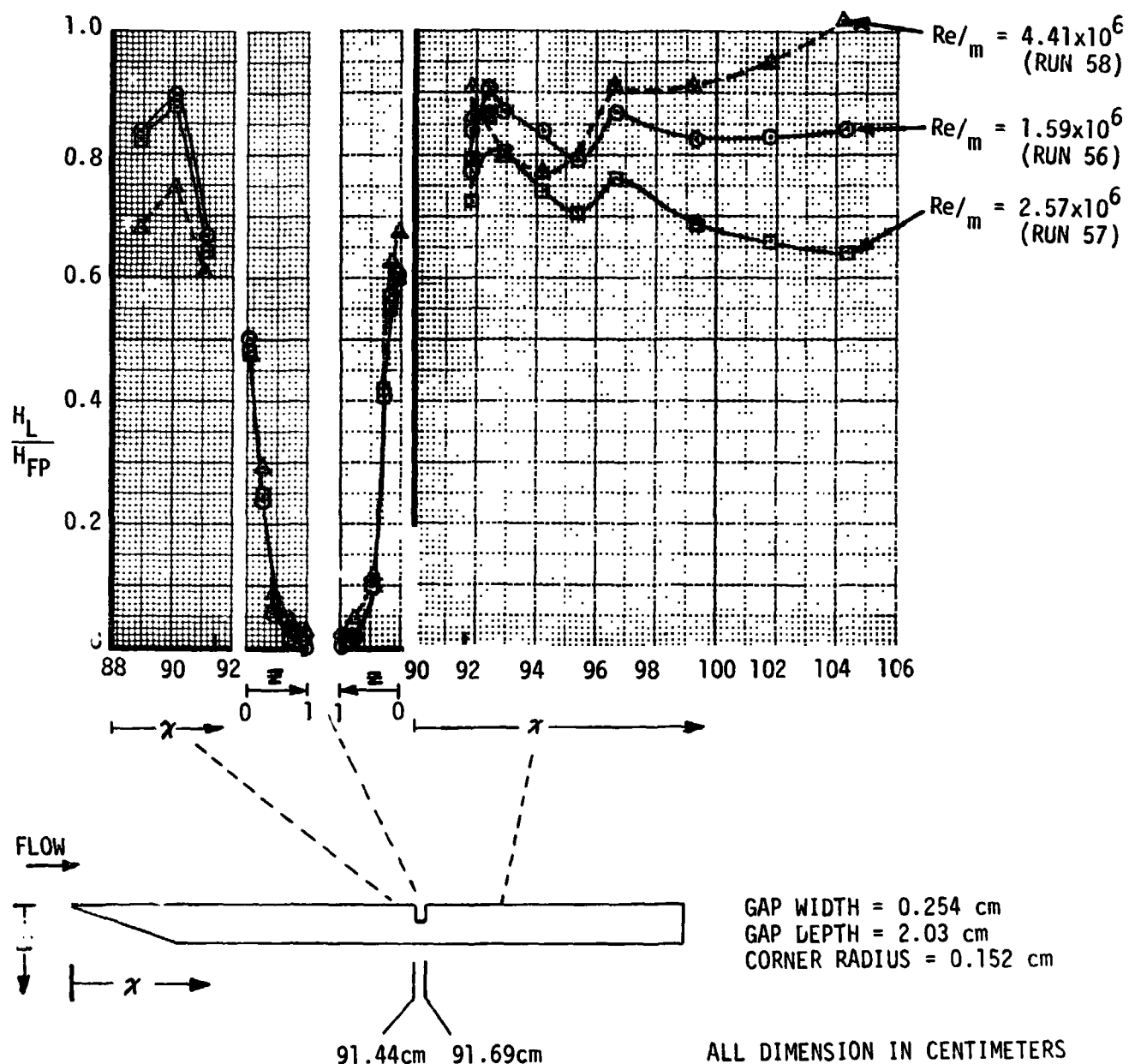


Figure 79



**RSI GAP HEATING
ANALYSIS**

**FINAL REPORT
VOLUME I**

**REPORT MDC E1003
29 JANUARY 1974**

conditions on the single transverse gap model. The gap width was 0.254 cm and the gap depth was 2.03 cm. The heat transfer coefficients were normalized to the calibration plate coefficients at the same x and y locations. Heating distributions are shown on the surface of the model both forward and aft of the gap as well as both faces in the gap. The heating forward of the gap increases and then decreases with distance for all Reynolds number conditions. The heating parameter (H_L/H_{FP}) consistently decreases with increasing Reynolds number. The heating in the gap shows consistent Reynolds number trends with the effect of Reynolds number much less than is observed in the surface heating data. The surface heating aft of the gaps has irregular distributions with an apparent inconsistent Reynolds number trend. It can also be noted that the surface heating rates on the single transverse gap model were generally less than that measured on the calibration plate, i.e., $H_L/H_{FP} < 1.0$.

The models used in these tests had an ample number of thermocouples on the surface to define the surface heating rate distribution near the gaps. Figure 80 compares surface heating distributions on the downstream side of a transverse gap from the Ames 3.5 foot HWT test and the LaRC CFHT test. The Ames data indicate that the peak surface heating rate occurs approximately one edge radius downstream of the tile leading edge. The model used in the CFHT did not have the same instrumentation density to adequately measure the heating distribution near the edge of the tile. A dashed curve has been added to the CFHT portion of the figure to illustrate a plausible heating distribution which would be consistent with the AMES data. The AMES data show a level of sensitivity to unit Reynolds number. As the Reynolds number is increased, the heating ratio (h/h_{FP}) intensifies. Other data obtained during the AMES tests were examined to determine the effect of unit Reynolds number on the tile heating distribution.

Heating distributions for the upstream and downstream sides of gaps oriented at 30 degrees and 60 degrees to the flow (Figure 81 and 82) show similar dependency on unit Reynolds number. As the Reynolds number increases, the heating distribution intensifies. At 30 degrees, heating on the panel is monotonic with distance with a sharp drop near the gap. Heating on the downstream side of the gap shows a definite enhancement due to the gap. Reynolds number effects are evident on the downstream side of the gap. For the 60 degree orientation, heating on both sides of the gap is dependent on Reynolds number. It should be noted that the 60 degree data are downstream of the disturbance caused by the 30 degree gap. Also spotted on both figures are comparable data measured during the CFHT tests.

HEATING DISTRIBUTION ON LEADING EDGE ON DOWNSTREAM SIDE OF GAP

FLOW DIRECTION →

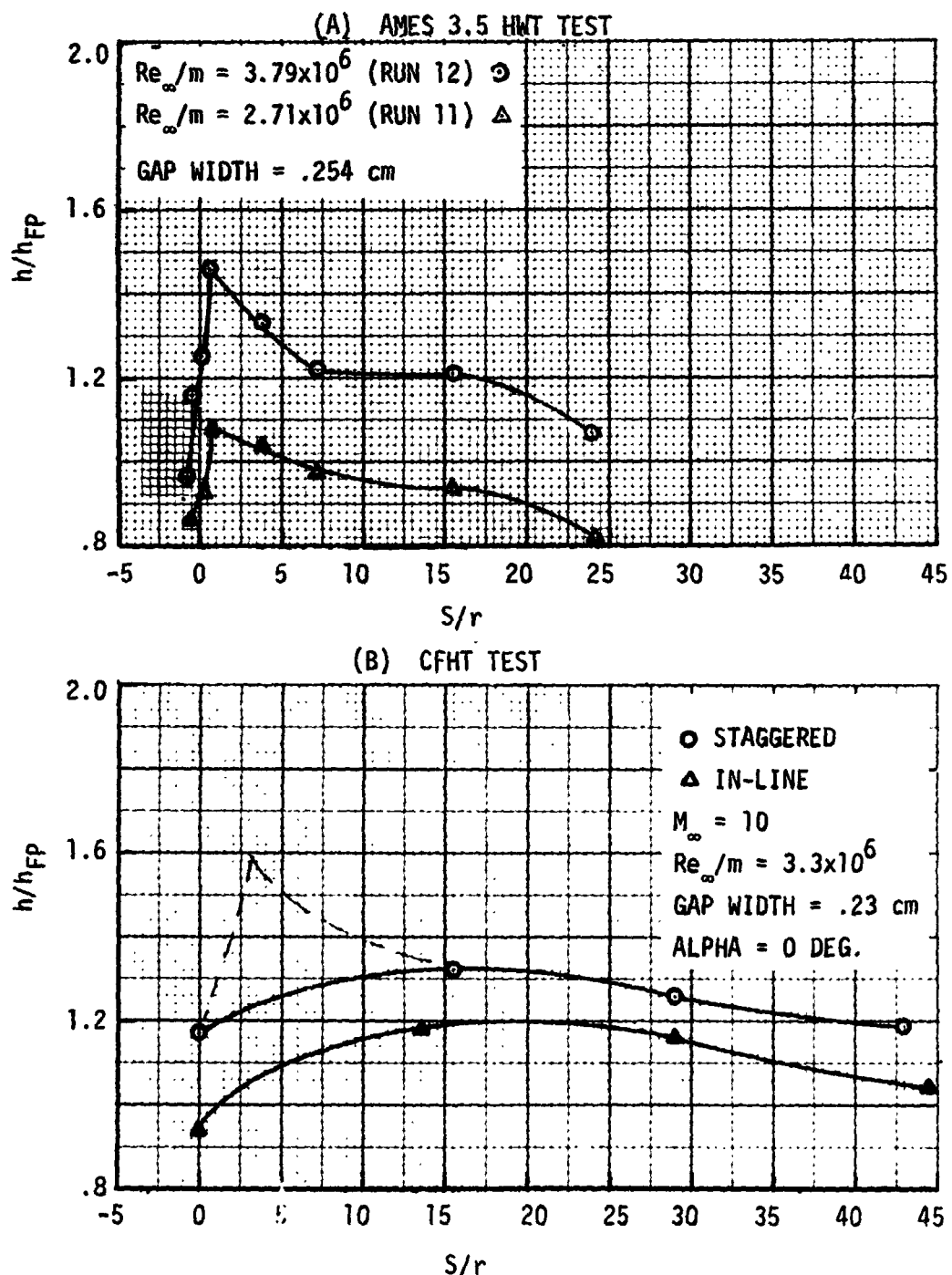
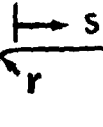


Figure 80

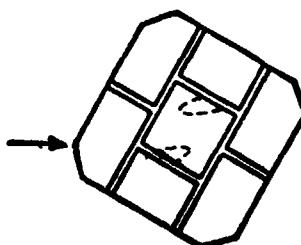
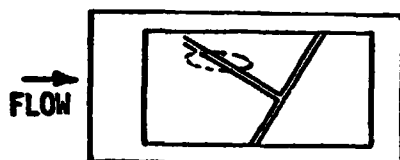
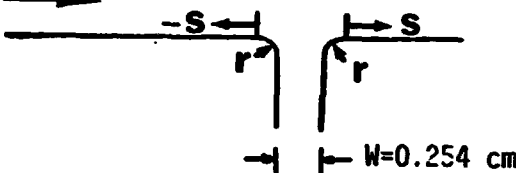


FINAL REPORT
VOLUME I

REPORT MDC E1003
29 JANUARY 1974

HEATING NEAR GAP AFFECTED BY REYNOLDS NUMBER
AND BOUNDARY LAYER STATE
FLOW ANGLE = 30°

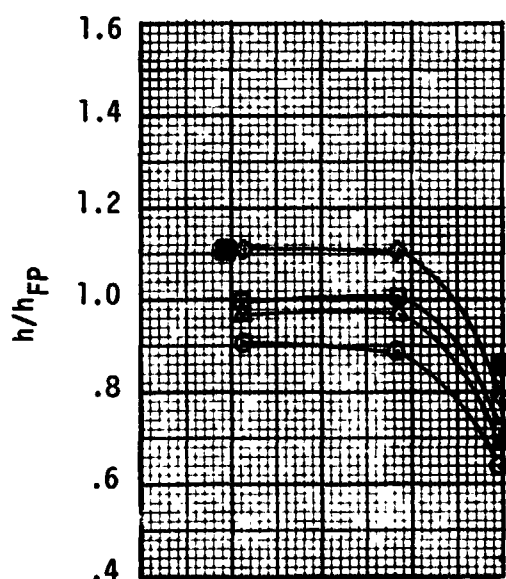
FLOW DIRECTION →



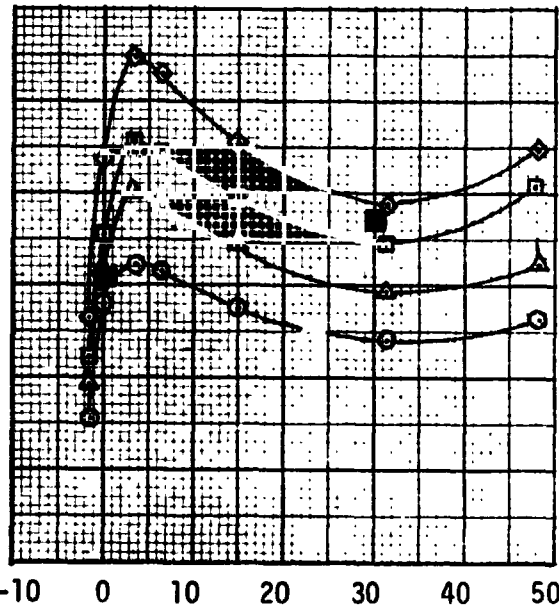
$\circ \text{Re}_{\infty}/m = 1.688 \times 10^6$
 $\triangle \text{Re}_{\infty}/m = 2.815 \times 10^6$
 $\square \text{Re}_{\infty}/m = 3.587 \times 10^6$
 $\diamond \text{Re}_{\infty}/m = 4.685 \times 10^6$
} AMES
 $M_{\infty} = 5.1$

$\blacksquare \text{Re}_{\infty}/m = 3.3 \times 10^6, M_{\infty} = 10.3, \text{CFHT}$

(TURBULENT B.L.)



(UPSTREAM SIDE)



(DOWNSTREAM SIDE)

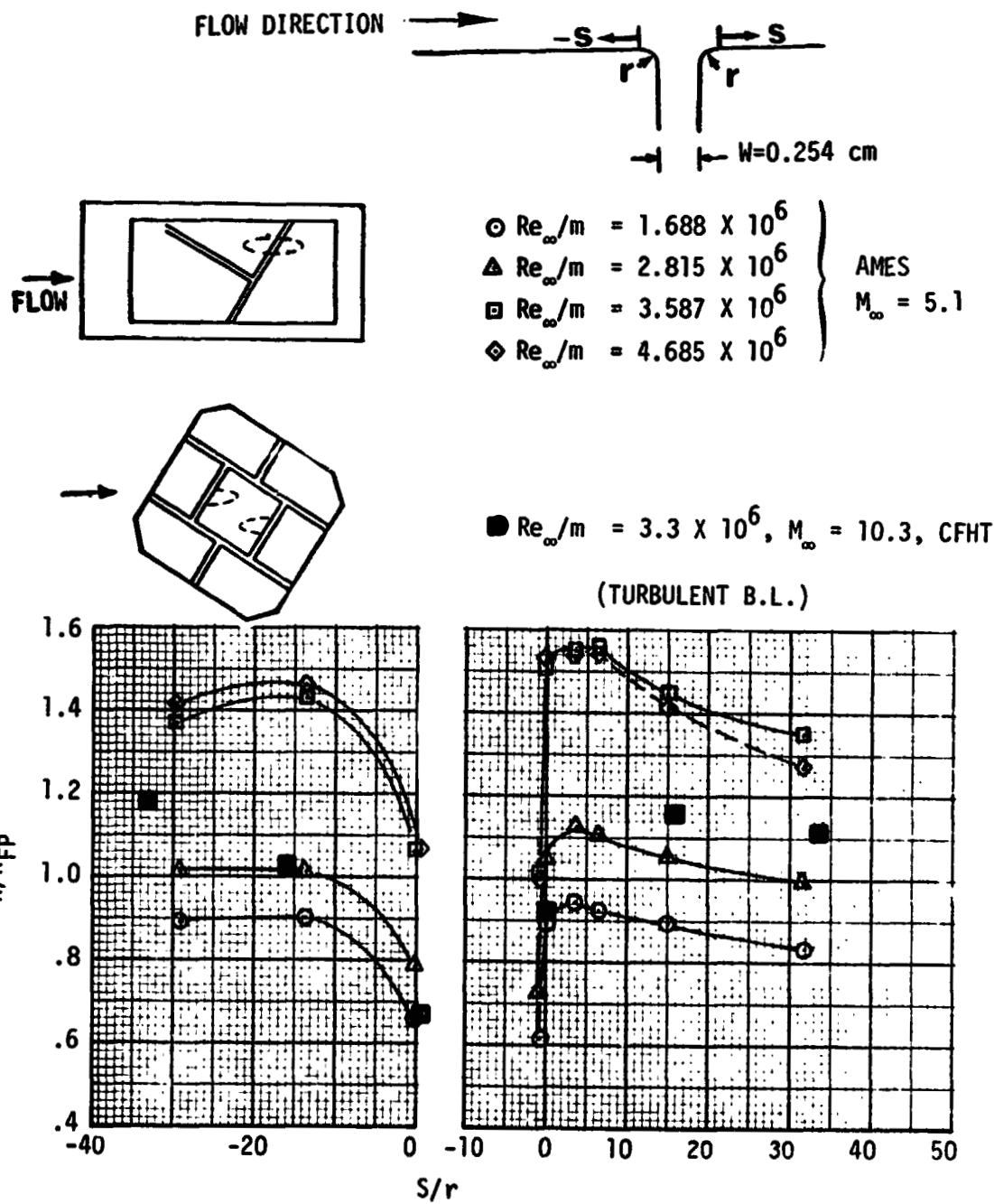
Figure 81



FINAL REPORT
VOLUME I

REPORT MDC E1003
29 JANUARY 1974

HEATING NEAR GAP AFFECTED BY REYNOLDS NUMBER
AND BOUNDARY LAYER STATE
FLOW ANGLE = 60°



(UPSTREAM SIDE)

(DOWNSTREAM SIDE)

Figure 82



**RSI GAP HEATING
ANALYSIS**

**FINAL REPORT
VOLUME I**

**REPORT MDC E1003
29 JANUARY 1974**

At the 30 degree orientation, the heating distributions from the CFHT and the AMES 3.5 foot tunnel are similar. At the 60 degree orientation the distribution measured at AMES is higher than measured at the CFHT. This is probably due to the transitional flow present in the AMES tests and the fully turbulent conditions in the CFHT.

Data for the in-line gap from the AMES 3.5 foot HWT and the CFHT were also compared (Figure 83). These data are for the top of the tile near the gap where effects of gap flow should be evident. Both sets of data show an increase in (H/H_{FP}) with distance along the gap. Also, the in-line gap data increase with Reynolds number as do the other data measured at AMES.

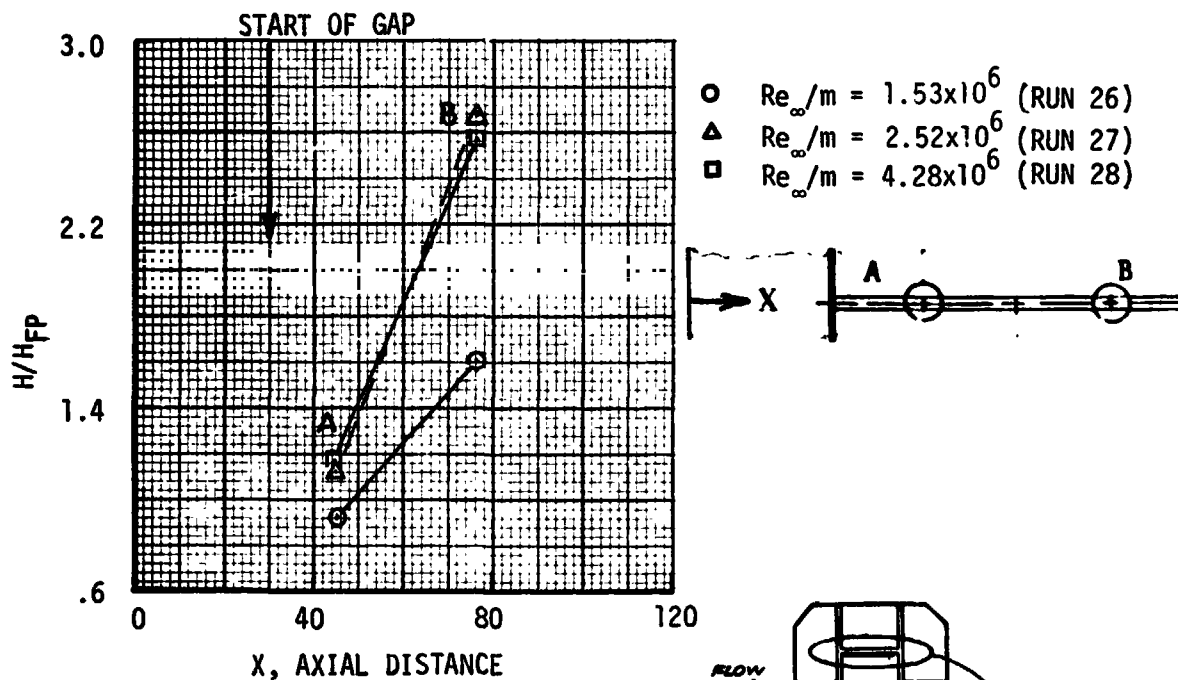


FINAL REPORT
VOLUME I

REPORT MDC E1003
29 JANUARY 1974

HEATING DISTRIBUTION ON TOP SURFACE OF GAP
ALIGNED WITH FREE-STREAM FLOW DIRECTION

(A) AMES TEST



(B) CFHT TEST

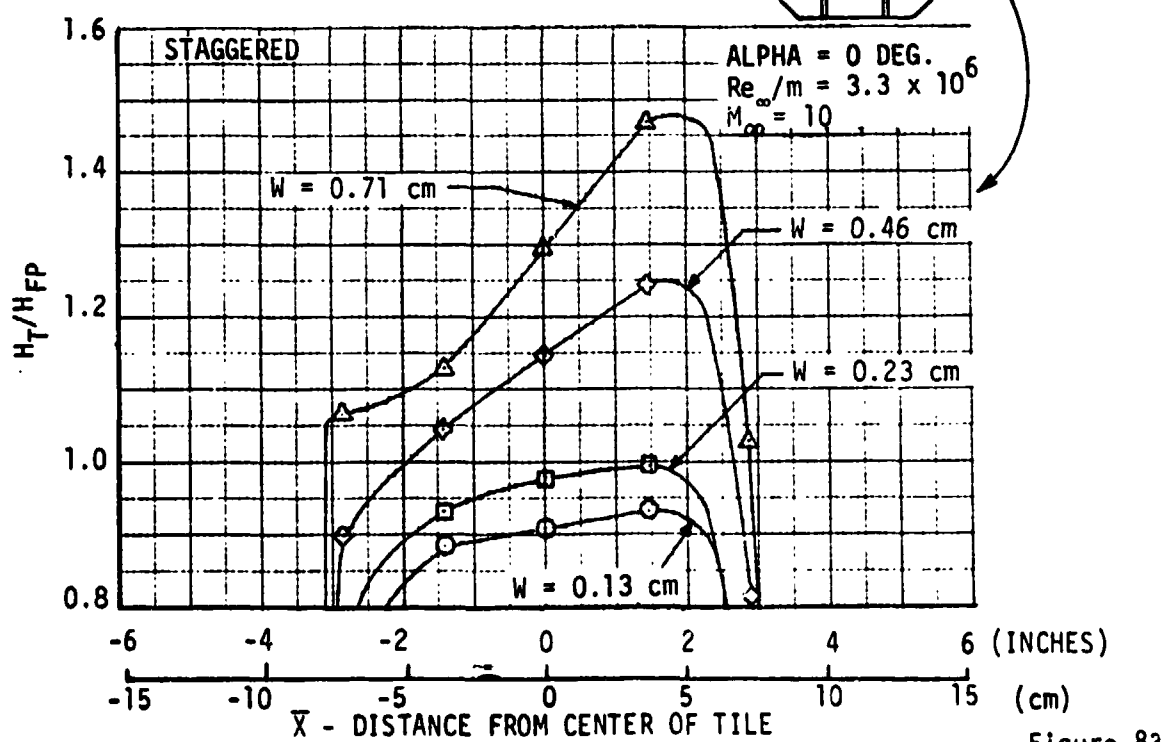


Figure 83



FINAL REPORT
VOLUME I

REPORT MDC E1003
29 JANUARY 1974

4.6 Boundary Layer Analyses - Boundary layer analyses were performed to characterize the environments at the various tunnel test conditions. Basic boundary layer parameters were computed for use in correlating the heat transfer results from the test facilities. These parameters will aid in extrapolating the test results to Shuttle flight conditions. The basic boundary layer parameters determined for the various test conditions are:

- 1) Type of boundary layer (laminar, transitional, turbulent)
- 2) Local unit Reynolds number (edge condition)
- 3) Local Mach number (edge condition)
- 4) Displacement thickness (δ^*)
- 5) Momentum thickness (θ)
- 6) Laminar sublayer thickness for turbulent boundary layers (δ_s)
- 7) Temperature ratio across the boundary layer

A summary of the boundary layer analyses that were performed is shown in Figure 84. The boundary layer parameters for the JSC 10 MW channel nozzle and the LaRC Mach 8 Variable Density Tunnel wall tests were provided by the facility investigators. The analyses for the remaining tests were performed by MDAC-E using numerical solution of the boundary layer equations.

4.6.1 JSC 10 MW Arc Tunnel Boundary Layer Parameters - Boundary layer parameters assuming both frozen and non-equilibrium flow in the JSC 10 MW channel nozzle were determined by JSC using the "NATA" computer program. These parameters were furnished along with the basic temperature response data for assimilation into the program. The boundary layer parameters for non-equilibrium flow were selected because the flow produced by the Arc heater was not in equilibrium. The boundary layer in the channel nozzle is laminar and relatively thin. Displacement thickness varied between 0.43 cm and 0.55 cm over the test panel. The local Mach number and local Reynolds number/meter were 4.2×10^4 and 5.7×10^4 , respectively for this series of tests. The momentum thickness was not provided by JSC.

4.6.2 LaRC Mach 10 CFHT Boundary Layer Parameters - LaRC performed tunnel calibration runs for a prior McDonnell-Douglas sponsored program to measure heat transfer on a flat plate mounted flush with the tunnel sidewall. As part of that effort, pitot pressure distributions were measured through the turbulent boundary layer at three vertical locations on the tunnel sidewall: (a) tunnel centerline, (b) 16.51 cm above centerline, and (c) 16.51 cm below centerline. Pitot pressure distributions for the three vertical locations are shown in Figure 85. The boundary layer profile is distorted, but is symmetrical about the



BOUNDARY LAYER ANALYSES PERFORMED

FINAL REPORT VOLUME I

REPORT MDC E1003
29 JANUARY 1974

FACILITY	B. L. STATE	INVESTIGATOR	COMMENTS
JSC 10 M ^w (CHANNEL NOZZLE)	LAMINAR	JSC (J.E. GRIMAUD)	EQUILIBRIUM AND NON-EQUILIBRIUM FLOW IN NOZZLES, (NATA COMPUTER PROGRAM)
LaRC CFHT (TUNNEL WALL)	TURBULENT	MDAC	QUADRATIC RELATIONSHIP BETWEEN TEMPERATURE AND VELOCITY ASSUMED
LaRC M=8 V.D.T. (TUNNEL WALL)	TURBULENT	LaRC (C.B. JOHNSON)	MEASURED TEMPERATURE AND PRESSURE PROFILES USED TO CALCULATE B.L. PARAMETERS
LaRC M=8 V.D.T. (FREE STREAM)	LAMINAR, TRANSITIONAL, TURBULENT	MDAC	EXACT NUMERICAL SOLUTION FOR FLAT PLATE B.L. ANALYSIS MODIFIED EQUATION EXTEND REYNOLDS NUMBER (CHEN AND THYSON); USFD TO DEFINE TRANSITION ZONE
AMES 3.5 FT. H.W.T. (FREE STREAM)	LAMINAR, TRANSITIONAL	MDAC	EXACT NUMERICAL SOLUTION FOR FLAT PLATE B.L. ANALYSIS TRANSITION EXTEND REYNOLDS NUMBER (CHEN AND THYSON) USED TO DEFINE TRANSITION ZONE

Figure 84



FINAL REPORT
VOLUME I

REPORT MDC E1003
29 JANUARY 1974

tunnel centerline. This distortion has been attributed to the inviscid flow development in the square nozzle. The measured pitot pressure distributions was used to determine the displacement thickness (δ^*) and momentum thickness (θ) on the tunnel sidewall by assuming a quadratic relationship between velocity and temperature through the boundary layer that is,

$$\frac{T_T - T_w}{T_{T_\infty} - T_w} = \frac{u}{u_\infty}^2$$

where:

T_T = local total temperature

T_{T_∞} = total temperature in free stream

T_w = wall temperature

u = local velocity in boundary layer

u_∞ = free stream velocity

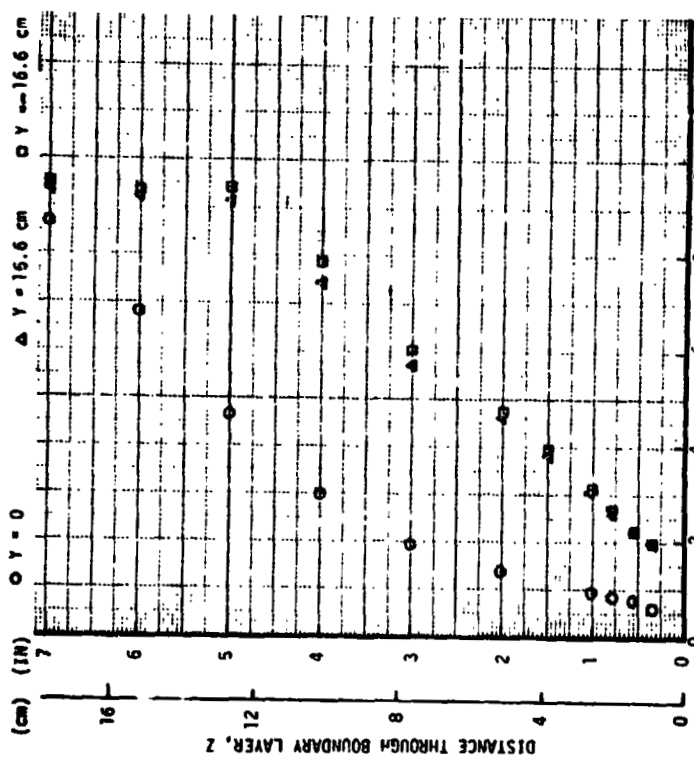
The computed displacement and momentum thicknesses are presented in Figure 85. It was necessary to describe the temperature profile because the total temperature distribution in the boundary layer was not measured. The quadratic relationship between the total temperature and velocity is frequently observed in hypersonic wind tunnel boundary layers as a consequence of unheated walls (Reference 8) and substantiated by experimental measurements in the CFHT (Reference 9). For the CFHT, the stilling chamber, the throat region, and the entire nozzle are water cooled. A more exact calculation of δ^* and θ for the CFHT wall would require measurement of the total temperature profile in the wall boundary layer.

4.6.3 LaRC Mach 8 V.D.T., Boundary Layer Parameters - Gap heating tests were performed with the test article positioned in both the freestream (tunnel centerline) and wall of the Mach 8 Variable Density Tunnel. The boundary layer on the tunnel wall was turbulent. Displacement thickness and momentum thickness were measured in the turbulent wall boundary layer and are presented in Figure 85 as a function of the freestream unit Reynolds number. The experimental boundary layer thickness, δ , is also shown in the figure for comparison. The parameters δ and θ are strong functions of Reynolds number for Re_∞/m less than 13×10^6 , and appear to approach a constant value for Re_∞/m greater than 13×10^6 . On the other hand, the displacement thickness is essentially independent of Reynolds number. The data presented in Figure 86 were obtained from C. B. Johnson of NASA-LaRC.

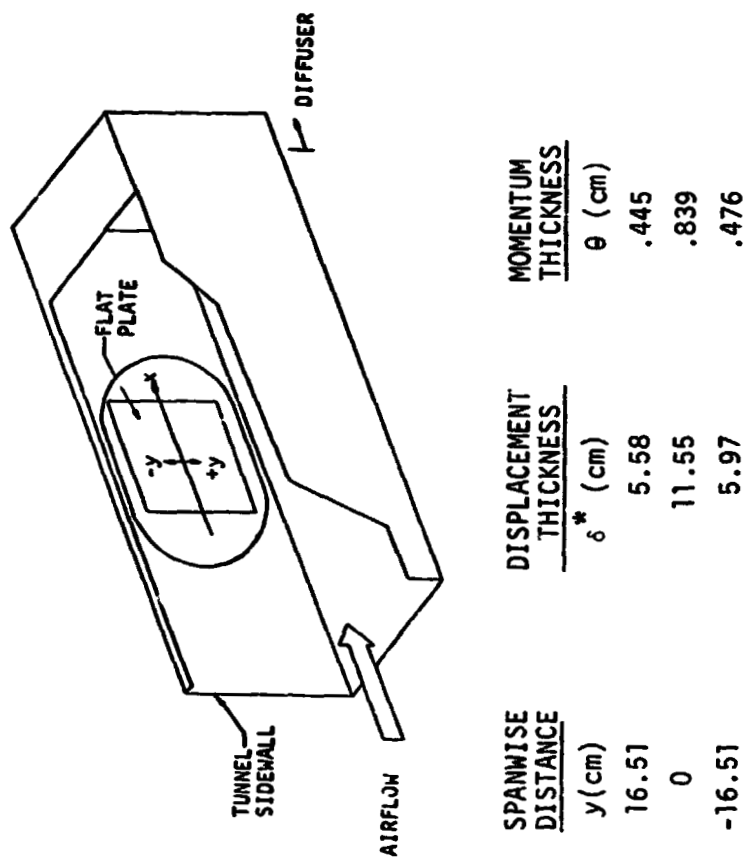
 RSI GAP HEATING
ANALYSIS

DISPLACEMENT AND MOMENTUM THICKNESSES FOR
MACH 10 CFHT, $Re_\infty/M = 3.28 \times 10^6$

MEASURED PRESSURE DISTRIBUTION
ACROSS BOUNDARY LAYER



REPORT MDC E1003
29 JANUARY 1974



SPANWISE DISTANCE y (cm)	DISPLACEMENT THICKNESS δ^* (cm)	MOMENTUM THICKNESS	
		θ (cm)	δ (cm)
16.51	5.58	.445	
0	11.55	.839	
-16.51	5.97	.476	

PITOT PRESSURE RATIO THROUGH BOUNDARY LAYER, $\frac{P_{T_2}}{P_{T_1}}$

$$\bullet \frac{T_T - T_W}{T_{T_\infty} - T_W} = (u/u_\infty)^2$$

Figure 85

EXPERIMENTAL WALL BOUNDARY LAYER PARAMETERS FOR MACH 8 VARIABLE DENSITY TUNNEL

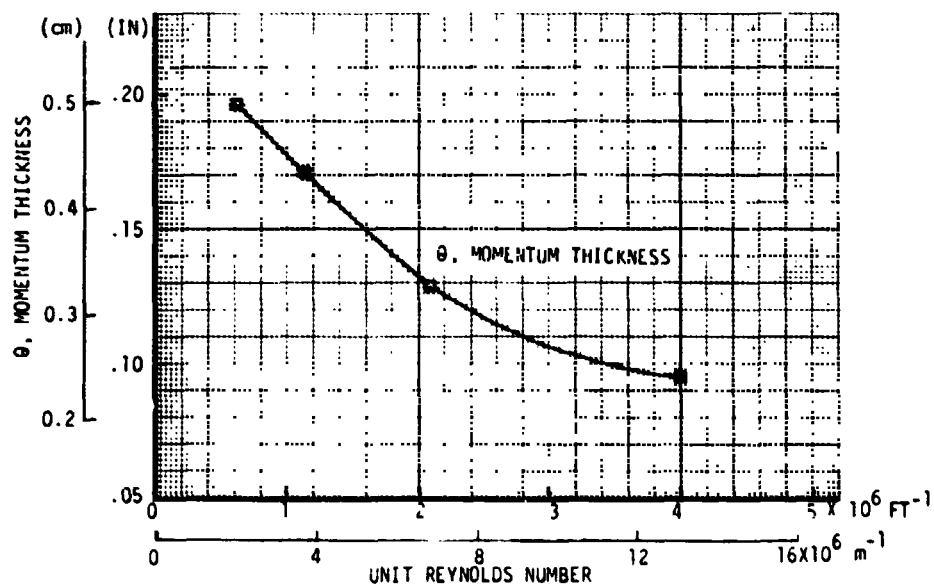
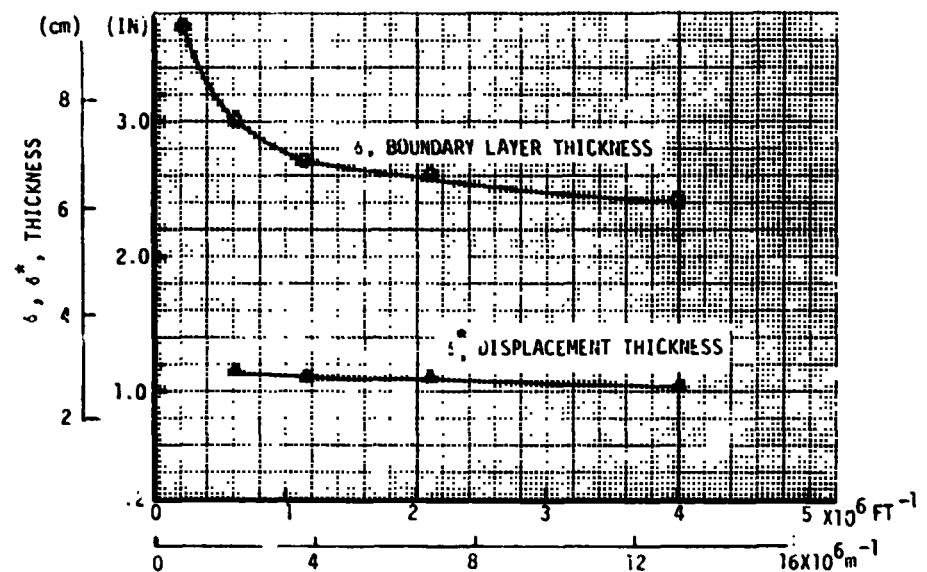


Figure 86



FINAL REPORT
VOLUME I

REPORT MDC E1003
29 JANUARY 1974

Beckwith, et al, (Reference 10) recently developed a correlation to predict the laminar sublayer thickness for hypersonic nozzle wall boundary layers. This correlation which shows that the sublayer thickness is a function of the boundary layer thickness, a free-stream Mach number, and the momentum thickness Reynolds number is presented in Figure 87. This correlation was formulated by analyzing velocity profile data over a wide range of wind tunnel flow conditions. In the analysis of the velocity profile data, the sublayer thickness was defined as the distance from the wall to the edge of the region where the velocity profile remained approximately linear.

Using Beckwith's correlation, the laminar sublayer thickness (δ_s) has been calculated for the Mach 8 V.D.T. and the Mach 10 CFHT wall boundary layers. The results of the calculations are also presented in Figure 87. For the Mach 8 V.D.T., δ_s decreases with increasing free-stream Reynolds number. For the Mach 10 CFHT, δ_s is a function of the spanwise location because of the nonuniform flow on the wind tunnel side-wall.

Boundary layer parameters were not measured for the flow over the model for the tests conducted in the freestream of the Mach 8 Variable Density Tunnel. Therefore, it is necessary to calculate the boundary layer flow for these tests. The technique used in this study is a solution the compressible boundary layer equations using the numerical method described by Keller and Cebeci (Reference 11). This method has been extended to compressible ideal gas flows by T. Cebeci and has been used in many boundary layer analyses. For turbulent flow, the eddy viscosity formulation of Cebeci (Reference 12) were used. For transitional flow, the intermittency factor given by Chen and Thyson (Reference 13) were employed.

To establish the validity of the computed boundary layer parameters, the calculated heat transfer rates have been compared with the measured values on the top surface model in the freestream. Measured and predicted heating distributions are compared in Figure 88 for freestream conditions $M_\infty = 8$ and $Re_\infty/m = 21.8 \times 10^6$. The agreement between theory and experiment is quite good for the case in which laminar, transitional, and turbulent flow are considered in the analysis.

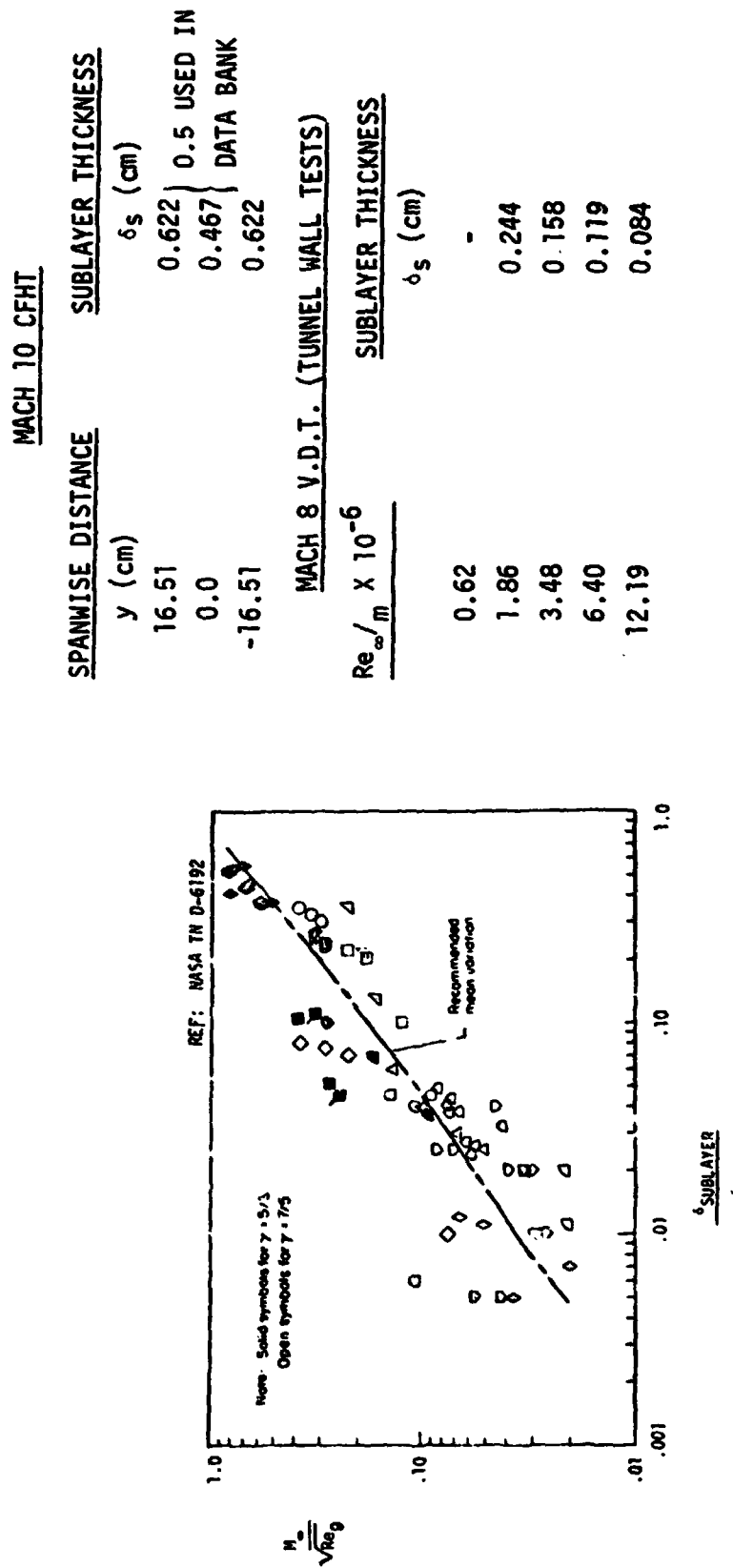
The predicted displacement and momentum thicknesses for the same freestream wind tunnel run are shown in Figure 89 by assuming (a) fully laminar, (b) fully turbulent, and (c) laminar, transitional, and turbulent flow. The parameters δ^* and θ are very different for laminar and turbulent flow. These results show that the effect of transitional flow must be included in determining the boundary layer parameters for the freestream tests.

**RSI GAP HEATING
ANALYSIS**

**LAMINAR SUBLAYER THICKNESSES ON TUNNEL WALL
IN MACH 10 CFHT AND MACH 8 V.D.T.**

**FINAL REPORT
VOLUME I**

**REPORT MOC E1003
29 JANUARY 1974**



COMPARISON OF MEASURED AND PREDICTED
HEATING DISTRIBUTIONS FOR
THE MACH 8 VARIABLE DENSITY TUNNEL

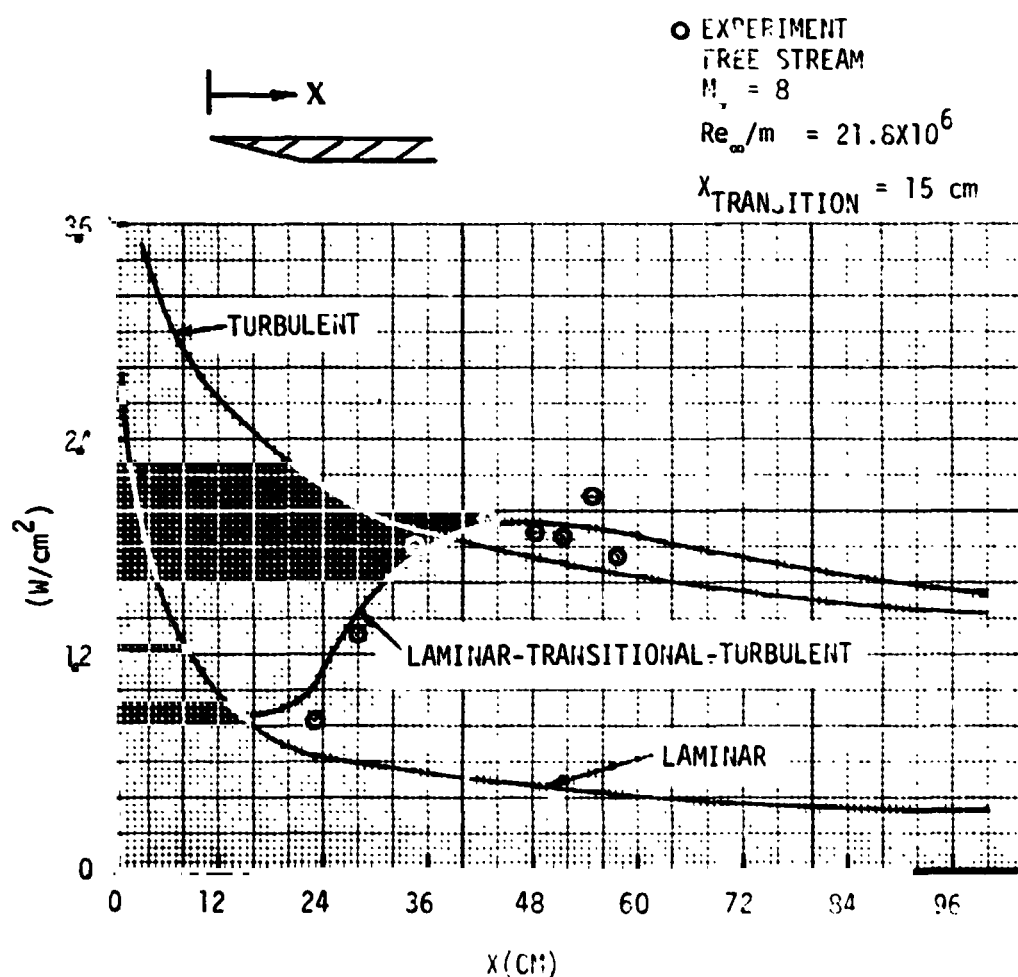
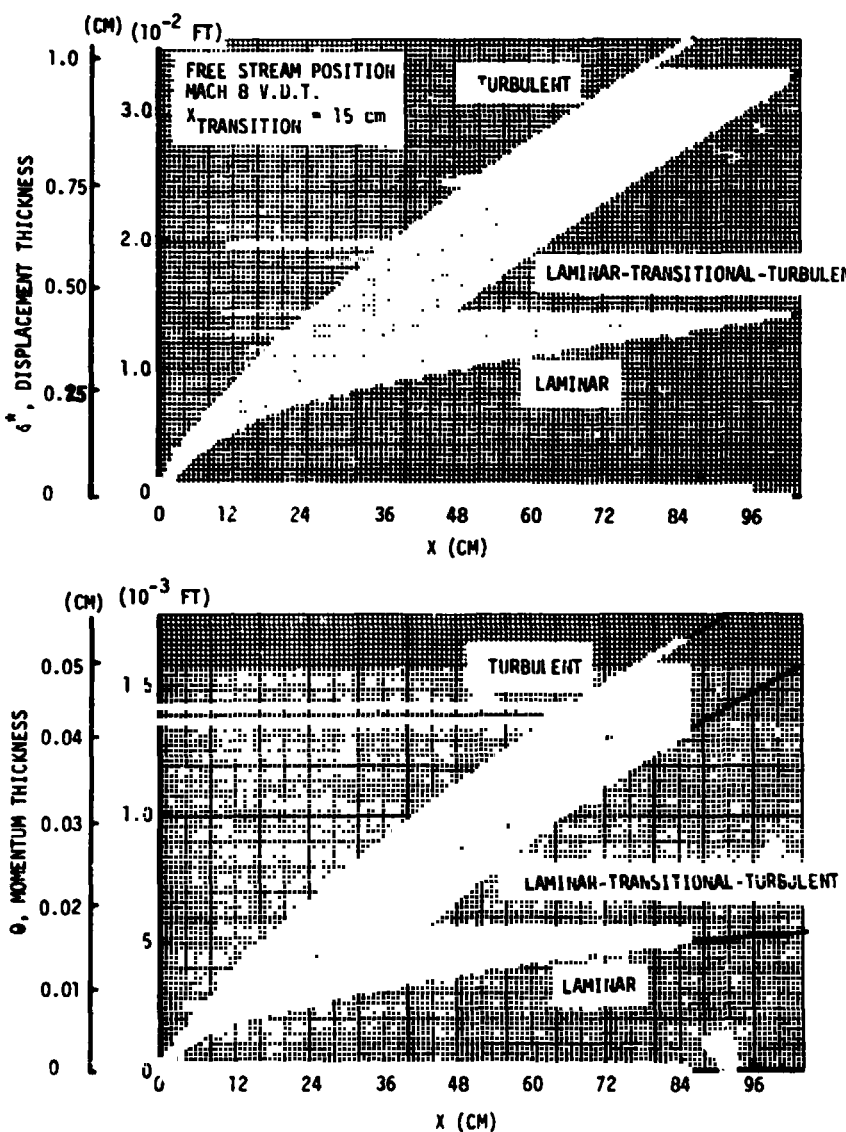


Figure 88

PREDICTED DISPLACEMENT AND MOMENTUM THICKNESSES,

$$M_{\infty} = 8.0, Re_{\infty} / m = 21.8 \times 10^6$$


Figure 89



FINAL REPORT
VOLUME I

REPORT MDC E1003
29 JANUARY 1974

Boundary layer calculations were made for two additional freestream conditions: (a) $M_\infty = 7.7$, $Re_\infty/m = 2.30 \times 10^6$, and (b) $M_\infty = 7.87$, $Re_\infty/m = 6.06 \times 10^6$. For these two cases it was found that the "transition extent Reynolds number" used in the boundary layer computer program was not valid. This was not surprising because the transition correlation used in the analysis is the formulation suggested by Chen and Thyson which is based on experimental data for freestream Mach numbers less than 5.0. The transition extent Reynolds number is evaluated at the onset of transition flow. Chen and Thyson's equation for the extent of transition is

$$Re_{\Delta X} = A Re_{tr}^{.67}$$

$$A = 60 + 4.68 M_\infty^{1.92}$$

$Re_{\Delta X}$ = Reynolds number based on the extent of the transition zone

Re_{tr} = Reynolds number based on the physical location of the transition onset point

For these two cases it was found that

$$A = 0 + 1.85 M_\infty^{1.92}$$

gave the best fit for the transition zone. It is not implied that this relationship for the parameter "A" is valid for all freestream Mach numbers greater than 5.0. The above relationship is probably only valid for the two cases considered in this report. A detailed study is certainly needed to refine Chen and Thyson's correlation for freestream Mach numbers greater than five.

The validity of the boundary layer calculations has been established by comparing the measured heating values on the smooth model surface with the calculated heat transfer rates. Measured and predicted heating distributions are shown in Figure 90 for the two above freestream conditions. The agreement between theory and experiment is quite good. The predicted displacement and momentum thickness for the same freestream conditions are shown in Figure 91.

4.6.4 Ames 3.5 Foot HWT, Boundary Layer Parameters - Boundary layer calculations were made for the four freestream conditions of the gap heating tests: (a) $Re_\infty/m = 1.45 \times 10^6$, (b) $Re_\infty/m = 2.20 \times 10^6$, (c) $Re_\infty/m = 3.26 \times 10^6$, and (d) $Re_\infty/m = 4.51 \times 10^6$. All calculations were made at a freestream Mach number of 5.10. The validity of the boundary layer calculations was established by comparing the measured heating values on the calibration plate with the calculated heating

COMPARISON OF MEASURED AND PREDICTED HEATING DISTRIBUTIONS FOR THE MACH 8 V.D.T.

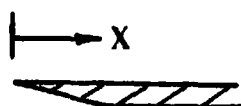
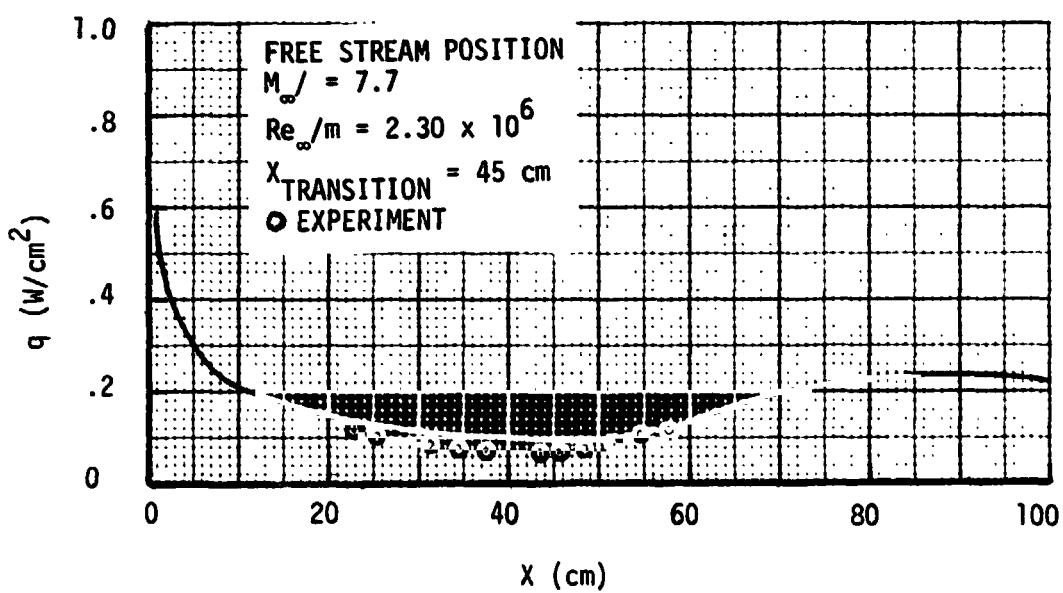
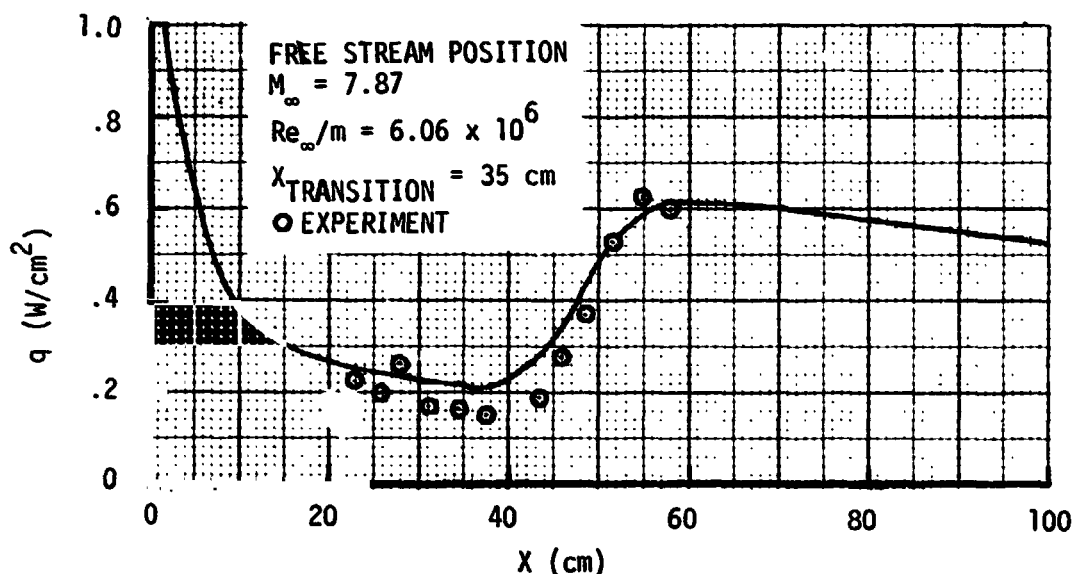
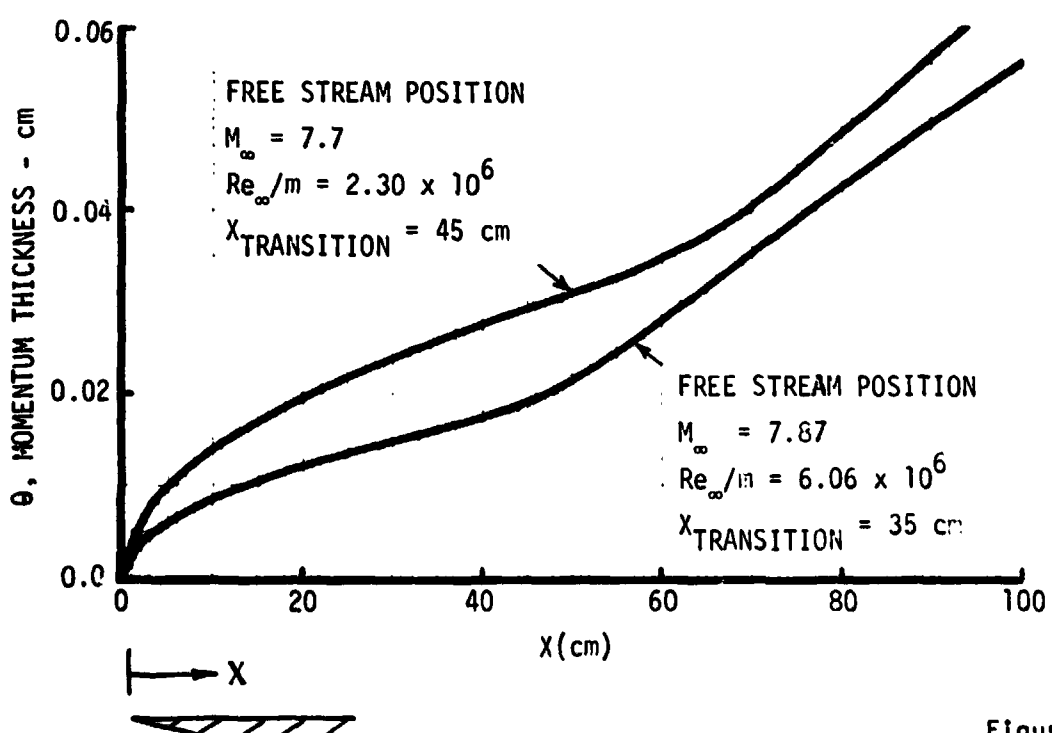
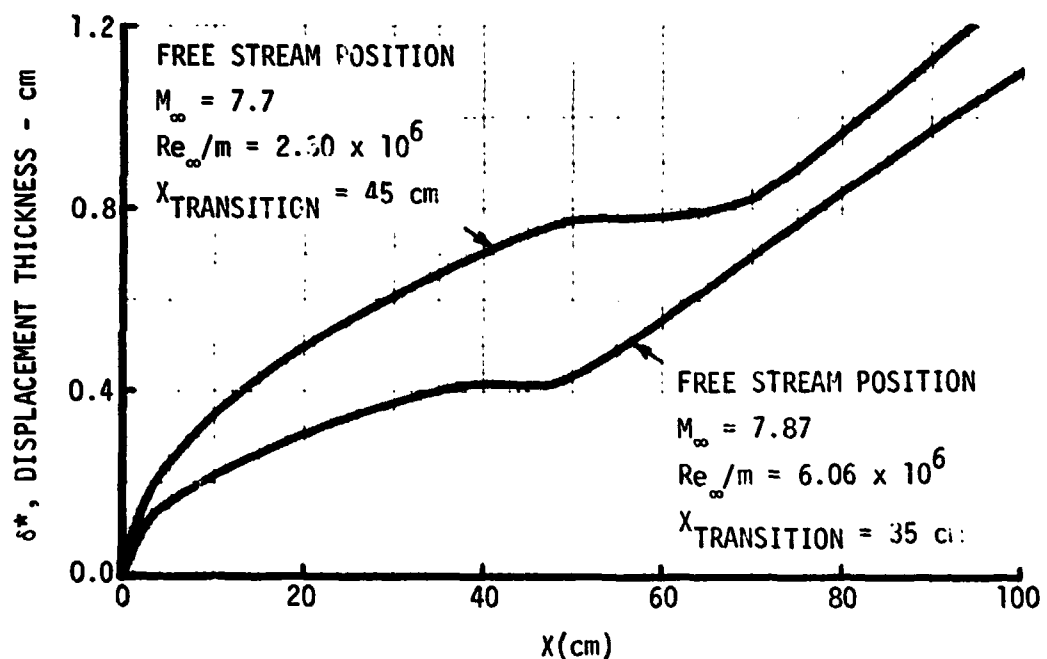


Figure 90

PREDICTED DISPLACEMENT AND MOMENTUM THICKNESS FOR MACH 8 V.D.T. FOR MACH 8 V.D.T.


Figure 91



FINAL REPORT
VOLUME I

REPORT MDC E103
29 JANUARY 1974

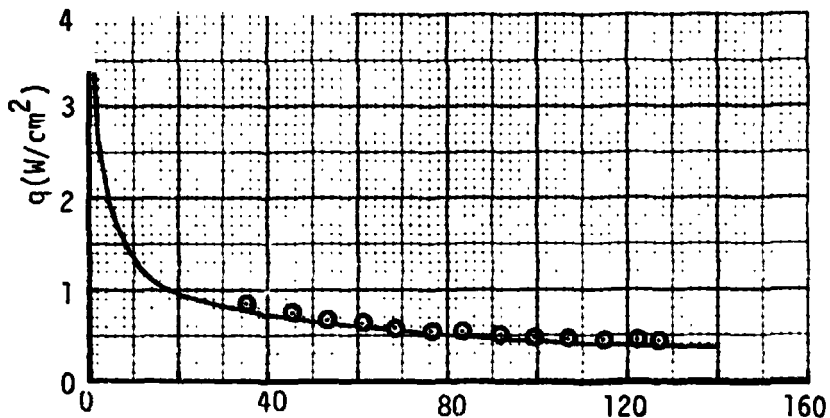
rates. Measured and predicted heating distributions are compared in Figure 92, for the above four freestream conditions. The predicted displacement and momentum thicknesses for the same four freestream conditions are shown in Figure 93. These boundary layer parameters were used in the data correlation activity.

An interesting result of the present calculations is that the transition correlation used in the boundary layer computer program was found to be valid for the Ames data. The transition correlation used in the analysis is the formulation suggested by Chen and Thyson (Reference 13) which is based on experimental data under nearly adiabatic wall conditions. The Ames data were taken under cold wall conditions. It therefore appears that the Chen-Thyson transition correlation is valid for both cold and hot wall conditions, at least at the upper Mach number limit of the correlation ($M = 5$). The effect of cooling on the transition extent Reynolds number needs further investigation for $M < 5$.

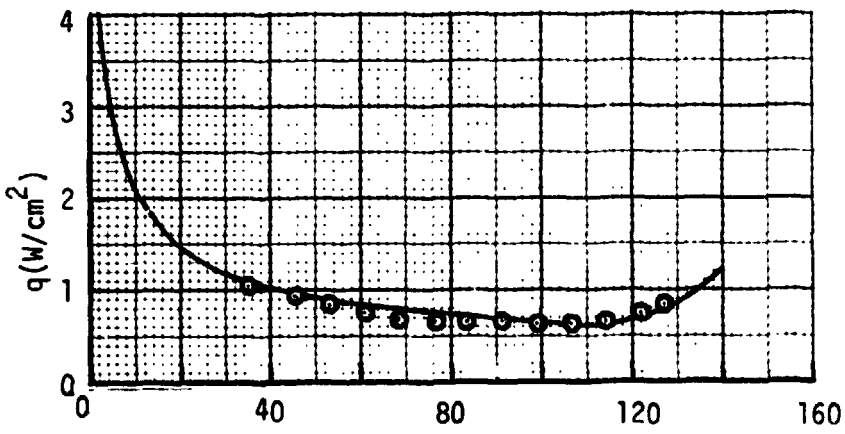
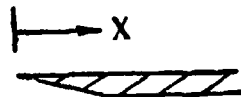
COMPARISON OF MEASURED AND PREDICTED HEATING DISTRIBUTIONS FOR THE MACH 5.1 AMES TEST

O EXPERIMENT

— THEORY



A) $Re_{\infty}/m = 1.4508 \times 10^6$, LAMINAR



B) $Re_{\infty}/m = 2.1991 \times 10^6$, $X_{TRANSITION} = 110$ cm

Figure 92

 RSI GAP HEATING
ANALYSIS

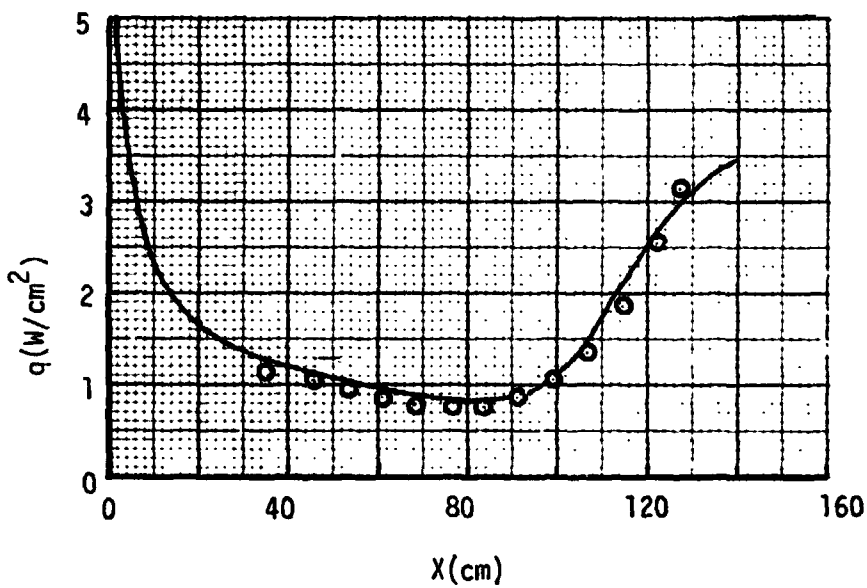
FINAL REPORT
VOLUME I

REPORT MDC E1003
29 JANUARY 1974

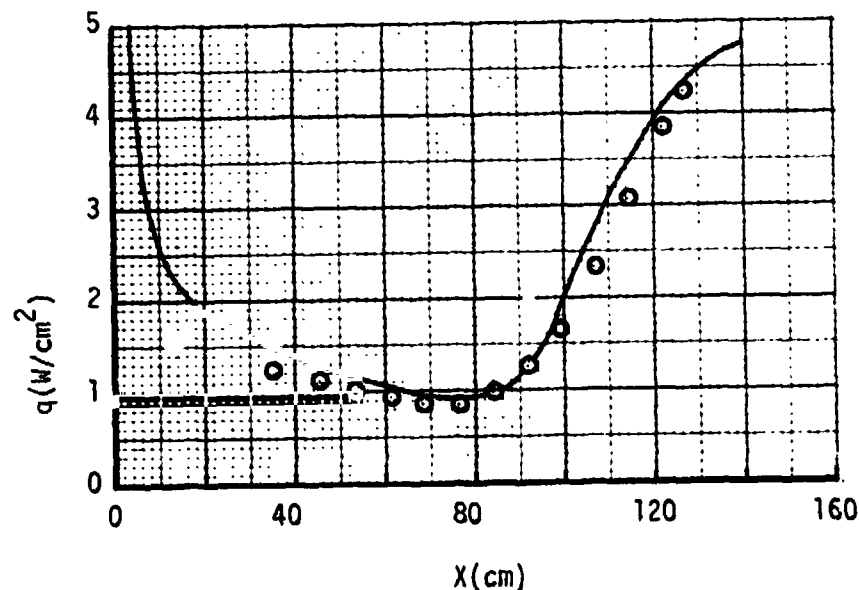
COMPARISON OF MEASURED AND PREDICTED HEATING DISTRIBUTIONS FOR THE MACH 6.1 AMES TEST

O EXPERIMENT

— THEORY



A) $\text{Re}_\infty/\text{m} = 3.2607 \times 10^6$, $X_{\text{TRANSITION}} = 85 \text{ cm}$



B) $\text{Re}_\infty/\text{m} = 4.5119 \times 10^6$, $X_{\text{TRANSITION}} = 80 \text{ cm}$

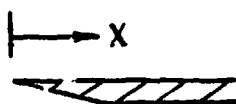


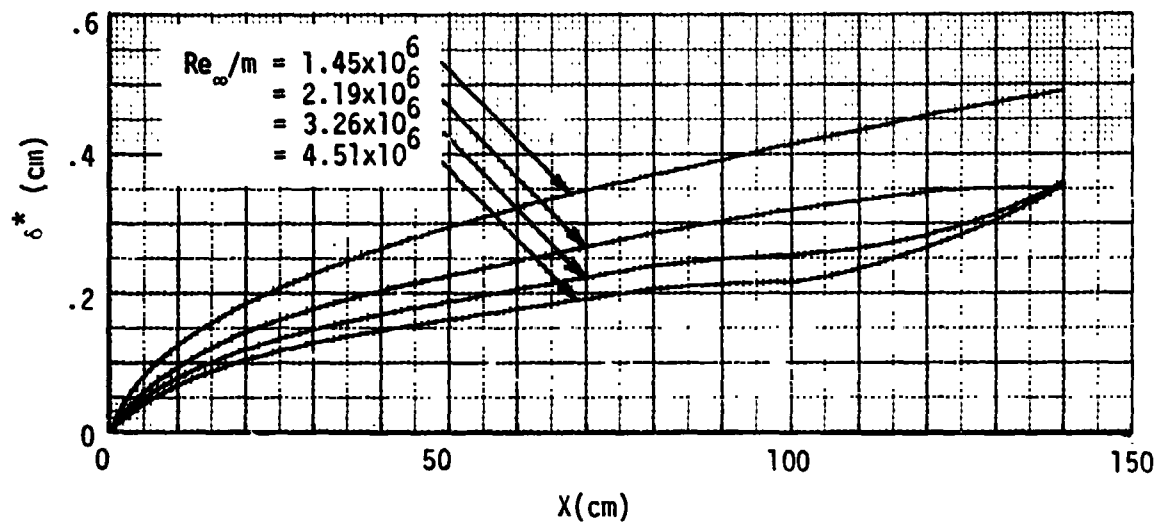
Figure 92 Concluded



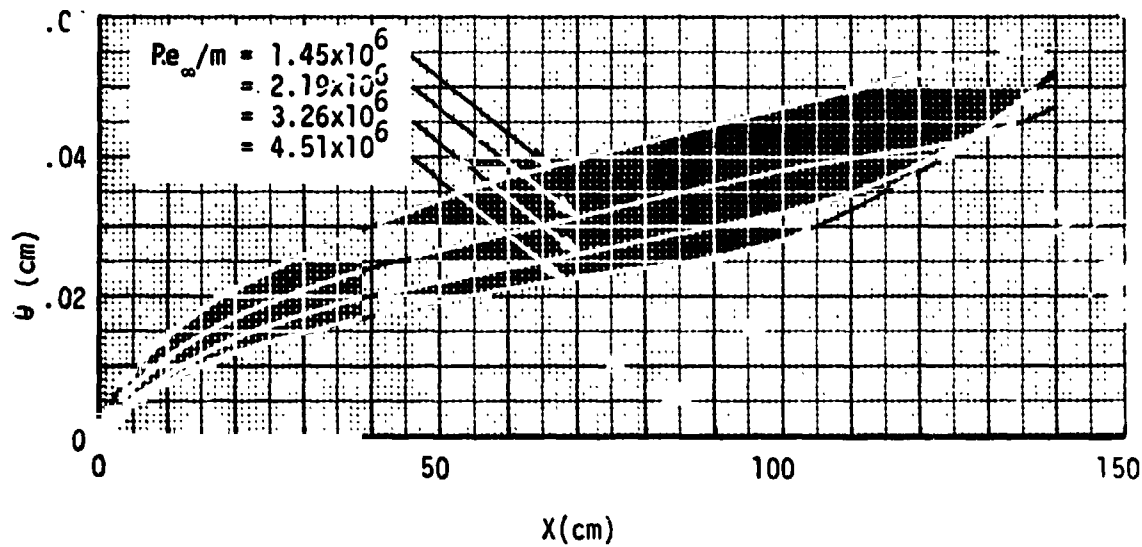
FINAL REPORT
VOLUME I

REPORT MDC E1003
29 JANUARY 1974

PREDICTED DISPLACEMENT AND MOMENTUM THICKNESS FOR THE MACH 5.1 AMES TEST



A) DISPLACEMENT THICKNESS



B) MOMENTUM THICKNESS

Figure 93



FINAL REPORT
VOLUME I

REPORT MDC E1003
29 JANUARY 1974

4.7 Flow Field Simulation - The gap heating data collected during this study are to be correlated in terms of the flow field parameters defined in Section 4.6 (Boundary Layer Analyses). The wind tunnel parameters are compared with available Shuttle flight parameters in Figures 94 thru 96. These figures provide an insight into the flight simulation capabilities of the wind tunnels where gap heating data were taken.

A local Reynolds number-local Mach number map comparing wind tunnel and flight conditions is presented in Figure 94. The wind tunnel data are represented by open symbols for turbulent flow, flagged symbols for transitional flow, and closed symbols for laminar flow. Also shown in this figure are two sets of Shuttle flight calculations. The shaded zone represents theoretical flight calculations computed by Fivel (Reference 14) using a non-equilibrium, real gas boundary layer computer program. Fivel performed analysis of the flow over 0.524 and 0.698 radian half angle cones having a nose radius of 61 cm at an altitude of 70.2 km while flying at a velocity of 7.32 km/second. Detailed inviscid flow field and boundary layer calculations were performed along the entire axial length of the cone (30.5 meters). The shaded zone combines calculated conditions for both laminar and turbulent flow that are expected on Shuttle's lower surface. The crosshatched zone represents theoretical flight calculations by Rockwell International (Reference 15) for Shuttle Trajectory 89212 between X/L of 0.1 and 0.5 on the Orbiter lower centerline. It can be noted that the local Mach number on the lower centerline does not exceed 6.0. This is due to the strong shock which develops when the Orbiter enters at 30° angle of attack. The NASA JSC arc tunnel flow conditions provide a good simulation of Shuttle flight Re/m and Mach number with the other tunnels producing slightly more severe conditions.

The displacement thickness and momentum thickness are shown in Figures 95 and 96 versus the local Mach number. The Fivel and Rockwell International calculations are also shown in these figures for comparison. In addition, the displacement thicknesses measured in the wall boundary layer of the Langley Unitary Plan Wind Tunnel are also shown to demonstrate the effectiveness of the UPWT in simulating the flight conditions. As shown on Figure 95 the displacement thickness of the Shuttle boundary layer is simulated on the various gap panels tested. Displacement thicknesses range from 0.1 to 10 centimeters. On the other hand, only the CFHT and Mach 8 V.D.T. produced boundary layers with momentum thicknesses as large as expected in flight. Momentum thicknesses of 0.17 and higher are expected during flight.

COMPARISON OF LOCAL MACH NUMBER AND REYNOLDS NUMBER FOR WIND TUNNEL AND FLIGHT

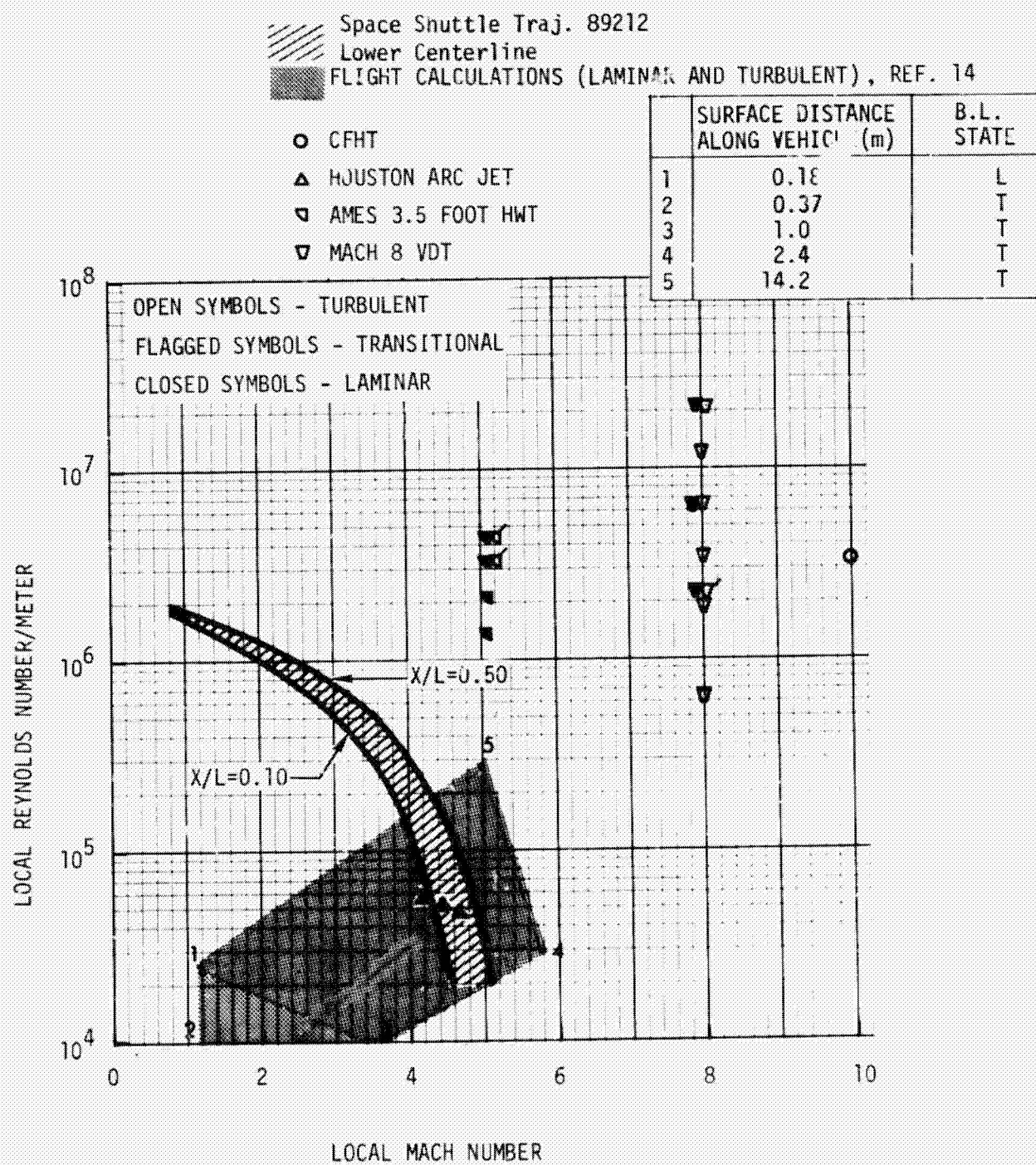


Figure 94

COMPARISON OF DISPLACEMENT THICKNESS AND LOCAL MACH NUMBER FOR WIND TUNNEL AND FLIGHT

- FLIGHT CALCULATIONS (TURBULENT), REF. 14
 - FLIGHT CALCULATIONS (LAMINAR), REF. 14
 - CFHT
 - △ HOUSTON ARC JET
 - AMES
 - ▽ MACH 8 VDT
 - ◆ UPWT WALL BOUNDARY LAYER
- Traj. 89212 Laminar — Turbulent

	SURFACE DISTANCE ALONG VEHICLE(m)	B.L. STATE
1	0.18	L
2	0.28	L
3	0.37	T
4	2.4	T
5	15.0	T
6	21.0	T
7	36.0	T

OPEN SYMBOLS - TURBULENT

FLAGGED SYMBOLS - TRANSITIONAL

CLOSED SYMBOLS - LAMINAR

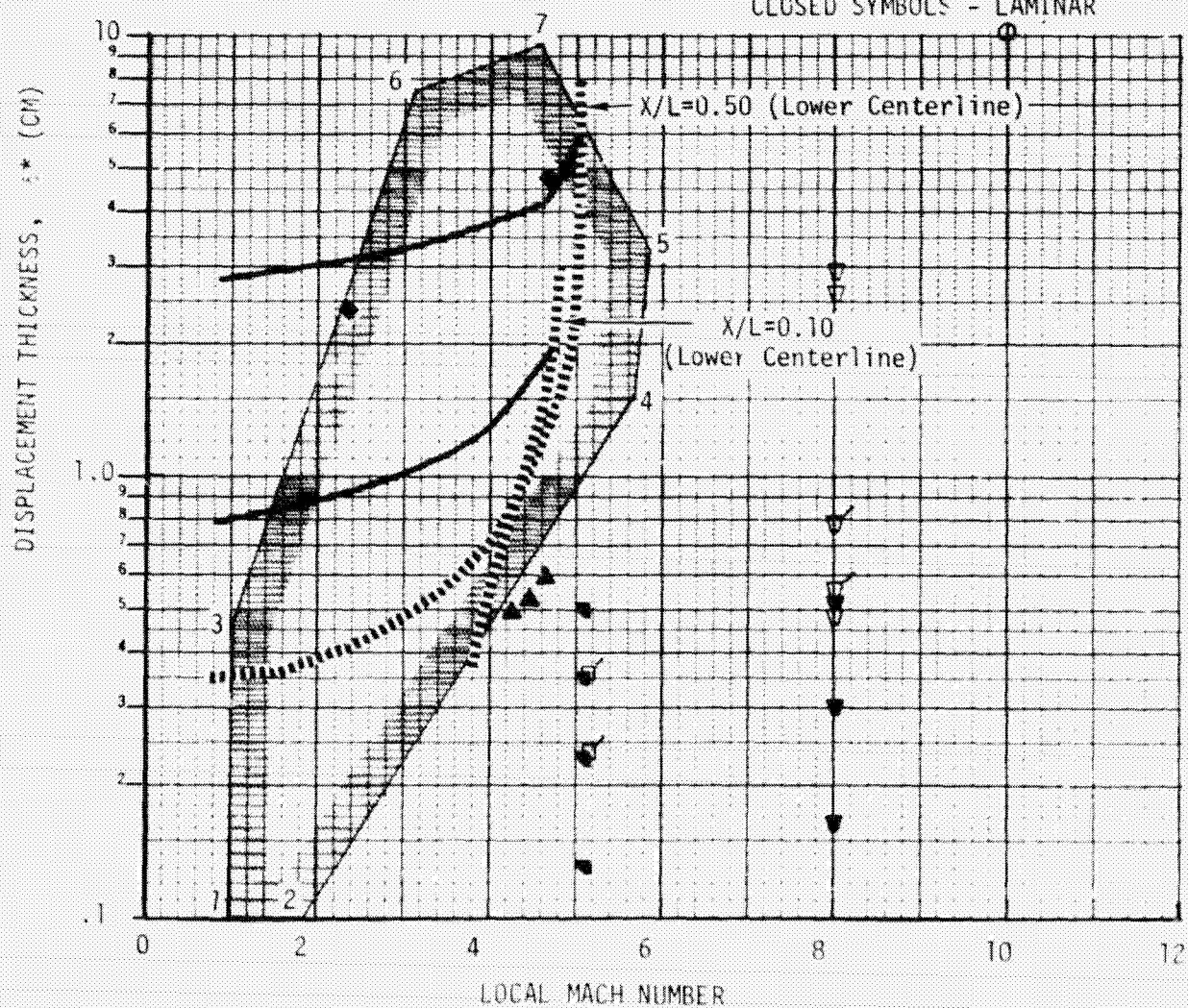


Figure 95

COMPARISON OF TURBULENT THICKNESS AND
LOCAL MACH NUMBER FOR WIND TUNNEL AND FLIGHT

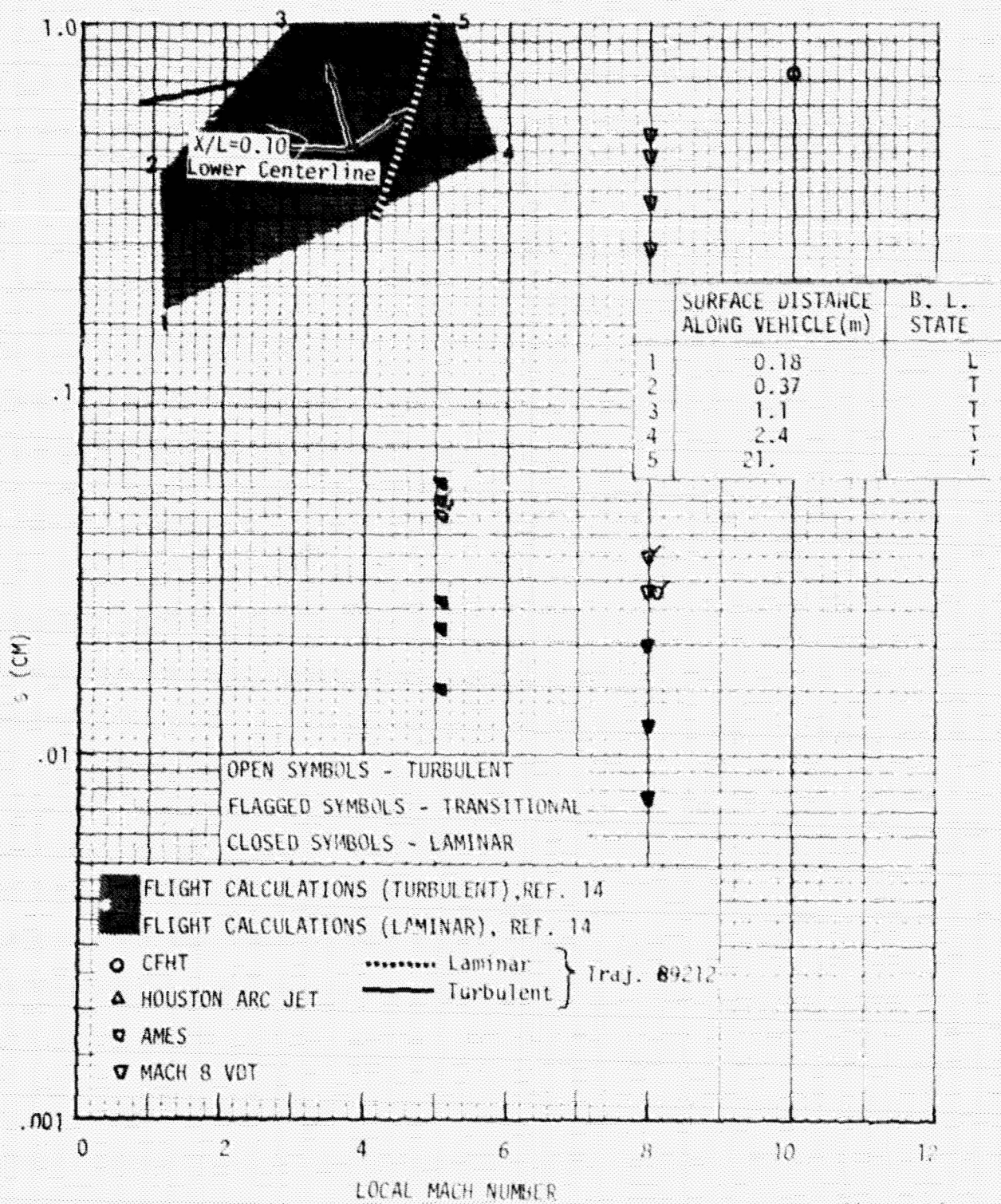


Figure 96



FINAL REPORT
VOLUME I

REPORT MDC E1003
29 JANUARY 1974

4.8 Comparison of Gap Heating Data from Arc Tunnel and Wind Tunnel Tests -

The gap heating data which have been assimilated come from both an arc tunnel and wind tunnels. Arc tunnels provide high energy (temperature and enthalpy) flow to test articles while wind tunnels provide a considerably lower energy flow. The effect of this difference in flow energy on gap heating was investigated by comparing data from arc and wind tunnels. Figure 97 summarizes the gap heating test environments and transverse gap geometry for which data have been assimilated. As can be noted, the wide variety in conditions makes direct comparisons difficult. The check marks denote the data which were selected for comparison. Two gap widths from the JSC 10 MW arc tunnel tests were compared with the wind tunnel data. These gap widths bound the selected gap widths from the wind tunnels. The arc tunnel had the lowest freestream unit Reynolds number of any of the facilities. Therefore, the lowest Reynolds number data available from each wind tunnel facility were selected for comparison. A laminar boundary layer existed in the arc facility and two of the wind tunnel tests while it was turbulent for the other two wind tunnel tests.

Gap heating data from each wind tunnel test were compared individually with data from the arc tunnel test in Figures 98 thru 101. A comparison of gap heating data from the Ames 3.5 foot Hypersonic Wind Tunnel and the JSC 10 MW Arc Tunnel is shown in Figure 98. Both tests were conducted in a laminar boundary layer environment with similar edge Mach numbers. Generally good agreement exists in the level of heating down the gap, although the shapes of the heating distributions are different. Figure 99 presents the comparison of gap heating distributions for the arc tunnel and the "freestream" tests in the LaRC Variable Density Tunnel (VDT). Both tests were run with a laminar boundary layer over the test article. The Mach number in the V.D.T. was 8.0 while the Mach number in the arc tunnel was 4.2. Also, the freestream unit Reynolds number is considerably higher in the wind tunnel than in the arc tunnel. The wind tunnel data agree well with the arc tunnel data at a depth into the gap of the 0.7 cm and below. The only data taken higher in the gap were taken at 0.5 cm and here the dimensionless heating was considerably higher than in the arc tunnel. Gap heating data were also taken in the wall of the V.D.T. to expose the test article to a turbulent boundary layer. These data are compared with the arc tunnel data in Figure 100 and are considerably higher than the laminar arc tunnel data. Figure 101 compares the arc tunnel data and data taken in the wall of the Mach 10 Continuous Flow Hypersonic Tunnel (CFHT). The boundary layer in the CFHT tests was turbulent and the data for these tests are again higher than the arc tunnel data.



FINAL REPORT
VOLUME I

REPORT MDC E1003
29 JANUARY 1974

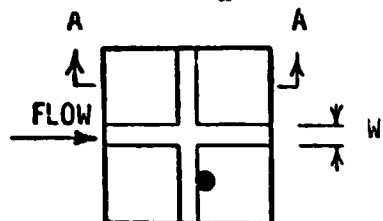
SUMMARY OF GAP HEATING TEST ENVIRONMENTS
AND GEOMETRY (TRANSVERSE BUTT JOINT)

TESTING FACILITY	TEST ARTICLE POSITION	GAP DEPTHS (CENTIMETERS)	GAP WIDTHS (CENTIMETERS)	M_∞	Re_∞/m	B.L. STATE
JSC 10 MW ARC TUNNEL	CHANNEL NOZZLE WALL	$\sqrt{3.78}$ 5.08 6.35	.074 $\sqrt{.204}$ $\sqrt{.333}$.714	$\sqrt{4.2}$	$\sqrt{.06} \times 10^6$	LAMINAR
AMES 3.5 FOOT WIND TUNNEL	FREE STREAM	1.016 2.032 $\sqrt{4.064}$	$\sqrt{.254}$	$\sqrt{5.1}$	$\sqrt{1.6} \times 10^6$ $\sqrt{2.6} \times 10^6$ $\sqrt{4.4} \times 10^6$	LAMINAR
LANGLEY VARIABLE DENSITY WIND TUNNEL	FREE STREAM	$\sqrt{2.54}$.159 $\sqrt{.318}$	$\sqrt{8}$	$\sqrt{2.3} \times 10^6$ $\sqrt{21.8} \times 10^6$	LAMINAR
LANGLEY VARIABLE DENSITY WIND TUNNEL	TUNNEL WALL	$\sqrt{2.54}$.159 $\sqrt{.318}$	$\sqrt{8}$	$\sqrt{1.16} \times 10^6$ $\sqrt{41.4} \times 10^6$	TURBULENT
LANGLEY CONTINUOUS FLOW HYPERSONIC WIND TUNNEL	TUNNEL WALL	$\sqrt{6.35}$.13 $\sqrt{.23}$.46 .71	$\sqrt{10}$	$\sqrt{3.28} \times 10^6$	TURBULENT

Figure 97

COMPARISON OF TRANSVERSE GAP HEATING (JSC 10 MW AND AMES 3.5 FT)

JSC 10 MW $M = 4.2 \text{ Re}_{\infty}/m = .06 \times 10^6$



AMES 3.5 FT. $M = 5.1 \text{ Re}_{\infty}/m = 1.6 \times 10^6$

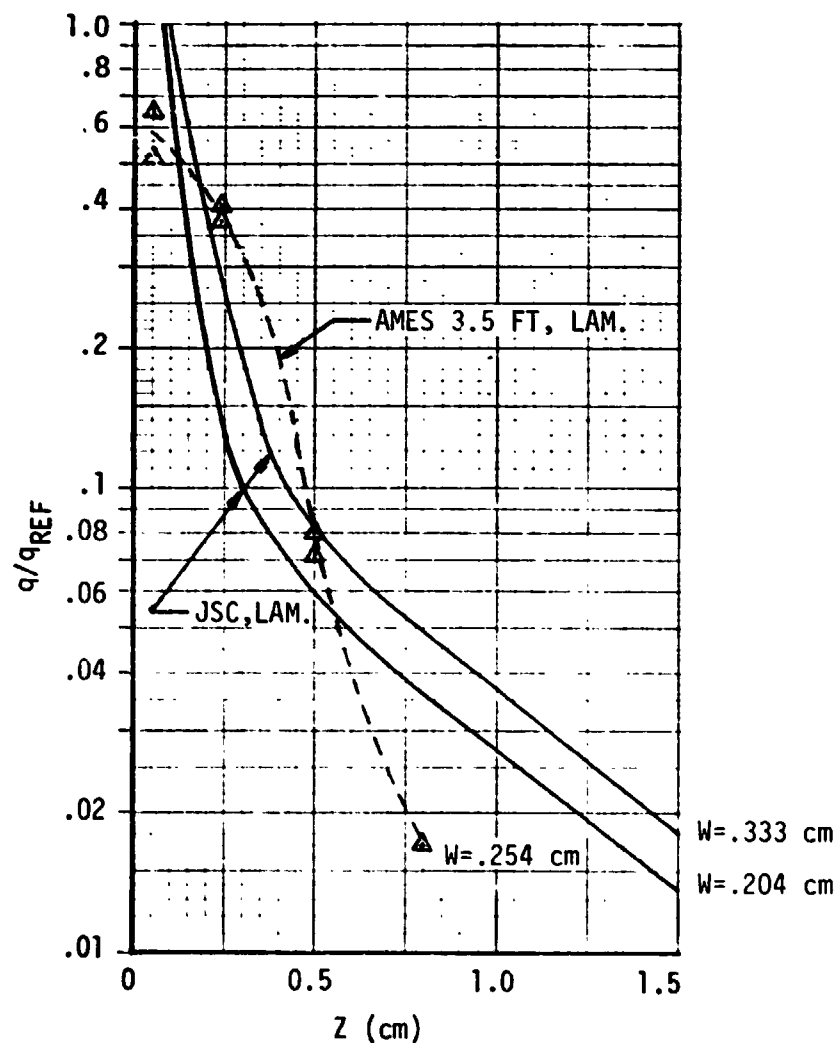
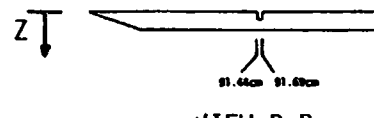
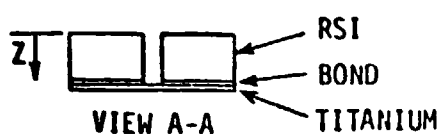
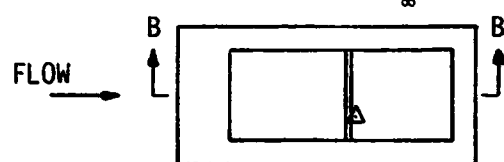
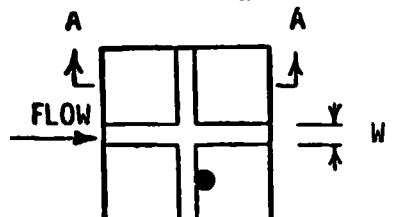


Figure 98

COMPARISON OF TRANSVERSE GAP HEATING (JSC 10 MW AND V.D.T. - FREE STREAM)

JSC 10 MW $M = 4.2 \text{ Re}_{\infty}/m = .06 \times 10^6$



$M=8$ V.D.T. (FREE STREAM) $\text{Re}_{\infty}/m = 2.3 \times 10^6$

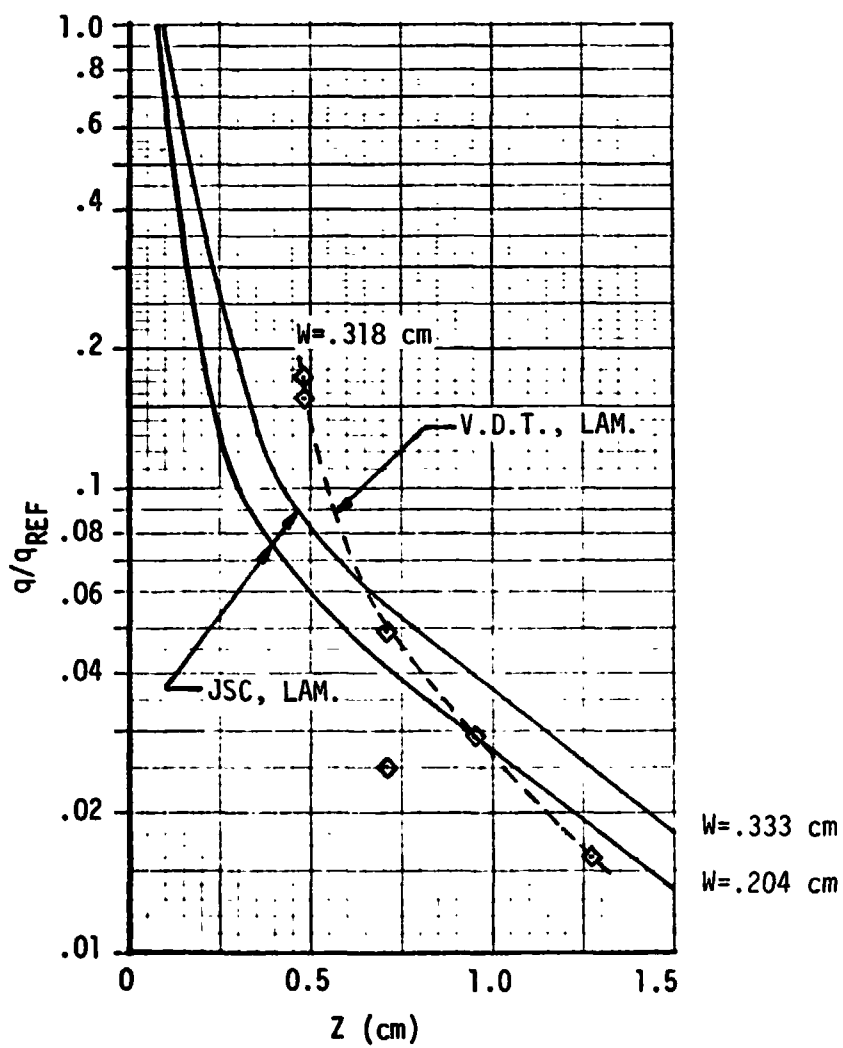
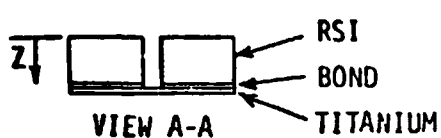
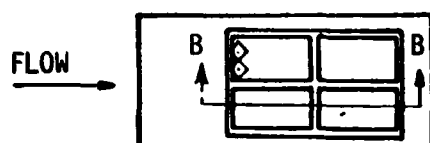


Figure 99

COMPARISON OF TRANSVERSE GAP HEATING (JSC 10 MW AND V.D.T. - TUNNEL WALL)

JSC 10 MW $M = 4.2$ $Re_{\infty}/m = .06 \times 10^6$

$M = 8$ V.D.T. (TUNNEL WALL)
 $Re_{\infty}/m = 1.16 \times 10^6$

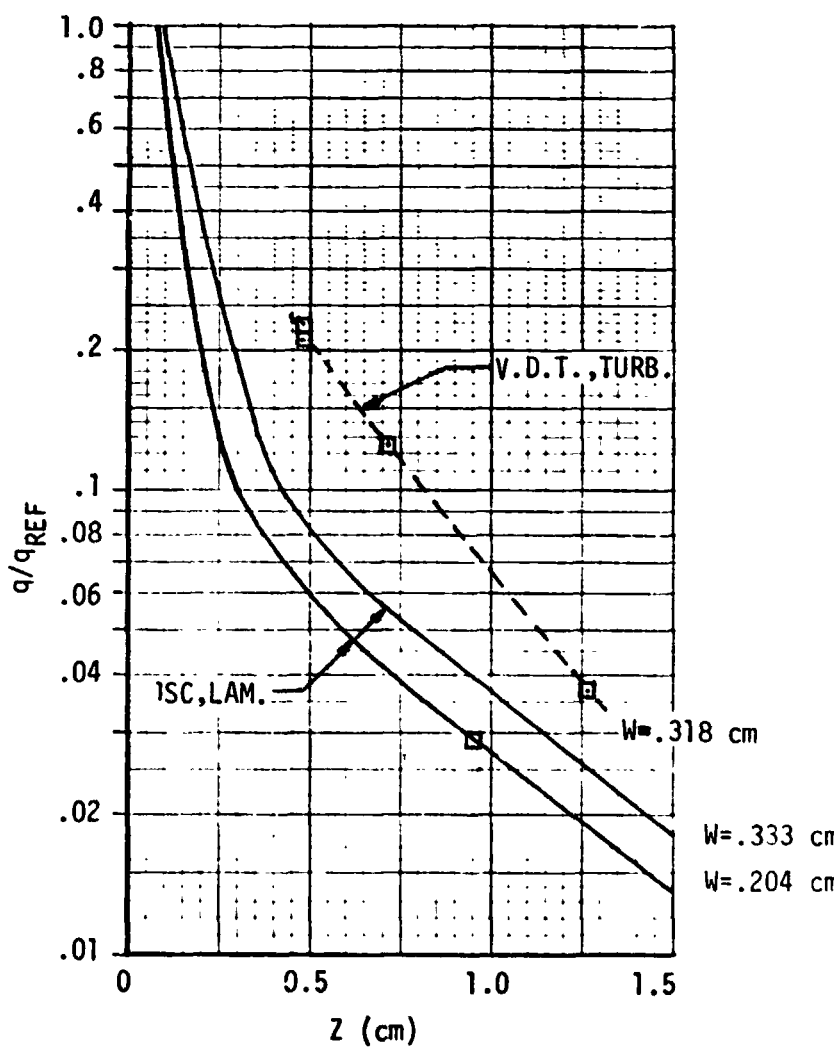
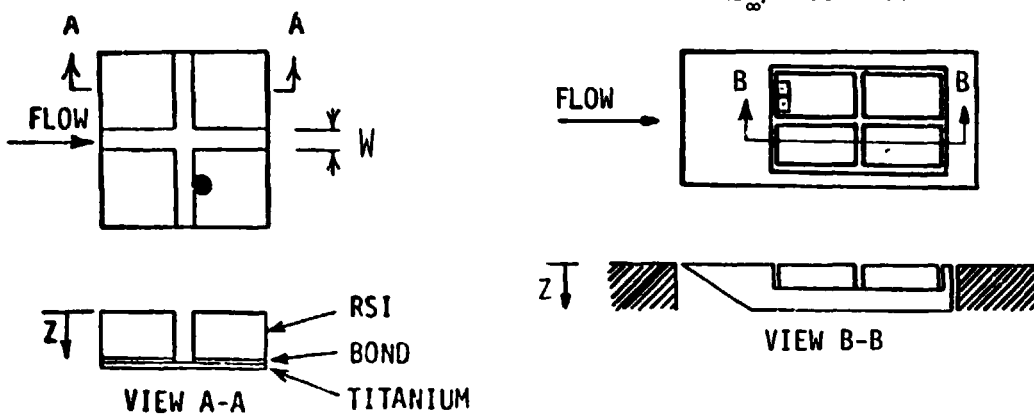


Figure 100

COMPARISON OF TRANSVERSE GAP HEATING (JSC 10 MW AND CFHT)

JSC 10 MW $M = 4.2 \text{ Re}_{\infty}/m = .06 \times 10^6$

CFHT $M = 10 \text{ Re}_{\infty}/m = 3.28 \times 10^6$

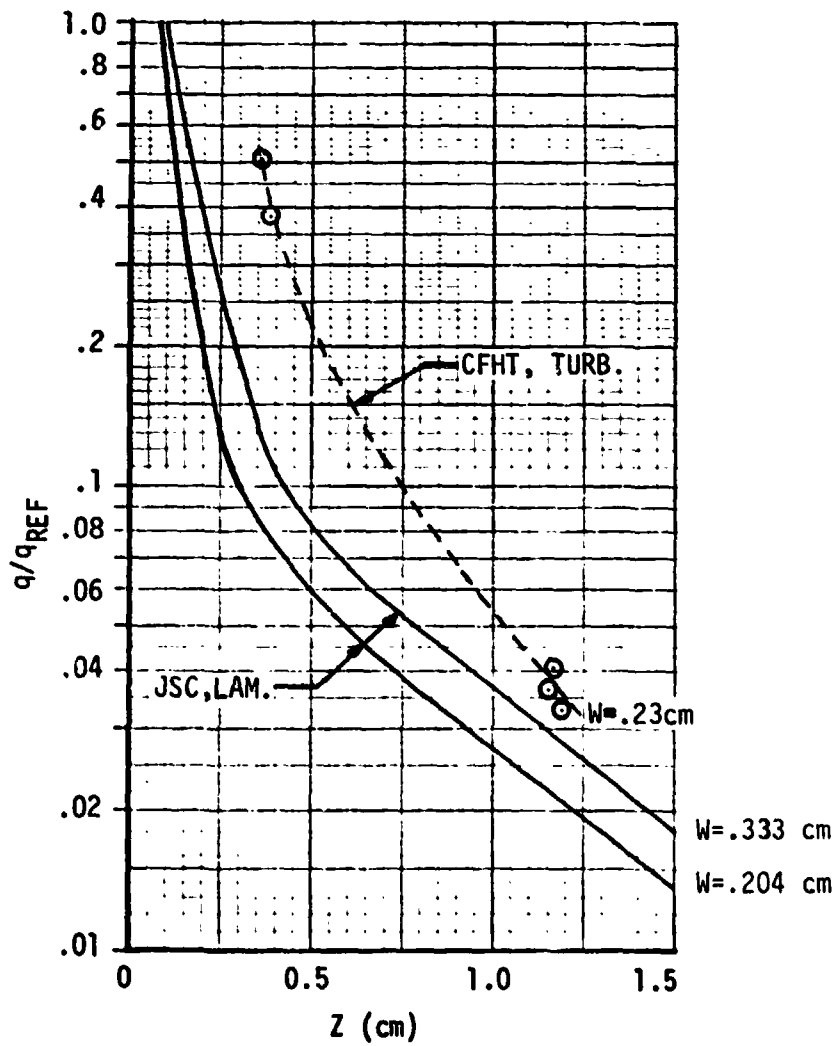
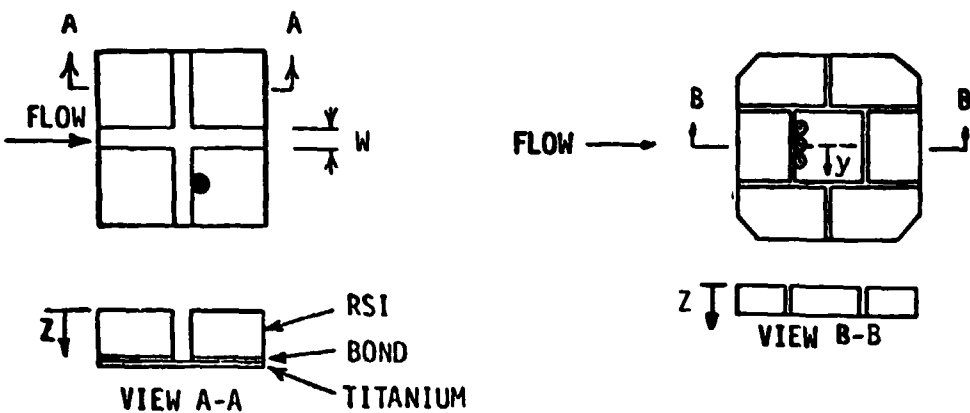


Figure 101



FINAL REPORT
VOLUME I

REPORT MDC E1003
29 JANUARY 1974

The difference in enthalpy between arc tunnels and wind tunnels does not appear to significantly affect gap heat transfer when normalized by the reference surface heating rate. The laminar wind tunnel data agree reasonably well with the laminar arc tunnel data. However, the boundary layer state does affect the heating in gaps. The data indicate that turbulent boundary layers result in higher dimensionless heating in gaps than laminar boundary layers.



FINAL REPORT
VOLUME I

REPORT MDC E1003
29 JANUARY 1974

4.9 Comparison of Gap Heating Data with Available Theories - Heating profiles obtained from the Arc tunnel and wind tunnels tests were compared with theoretical calculation methods to determine the adequacy of the theories. The forms of theoretical expressions were examined for parameters to be used in correlating test results. The three most appropriate theories which were examined are; Burggraf (Reference 16), Hodgson (Reference 17) and Nestler, et al,(Reference 18).

Burggraf developed a relationship for heating to the wall of a cavity exposed to steady separated flow in two-dimensional rectangular cavities at high Reynolds number. The external flow was separated from the inviscid rotating flow in the gap by a recirculating flow which was defined, using a modification of Chapman's theory. Figure 102 contains the important calculation steps for Burggraf's theory. The heating ratio turns out to be a pure function of gap dimensions and characteristic flow length. Parameters used in the theory include, flow length divided by gap width, gap width to depth ratio and distance down the downstream face of the gap normalized by the sum of gap width and depth.

Hodgson (Reference 17) formulated a two dimensional model for laminar flow in cavities. The model includes an upstream boundary layer to establish a cavity shear layer and the effect of compressibility on reattachment length. Figure 103 contains the calculation procedure used and includes a corrected expression for reattachment length (Reference 18). Parameters entering into the calculation include, the wall temperature to boundary layer edge temperature ratio, Mach number, Reynolds number based on gap width and boundary layer thickness.

Heating distributions down the gap wall computed using Burggraf's method, Hodgson's method and Hodgson's method referenced to Eckert's flat plate heating are compared with measured data in Figures 104 and 105. Wind tunnel data (Figure 104) from the M=8 V.D.T. and the AMES 3.5 foot H.W have a sharp drop in heating with distance into the gap. Predictions based on Hodgson's method overestimates gap heating and Burggraf's method produces a different shaped heating distribution. Hodgson's method (Figure 105) significantly overestimates the gap heating distributions obtained from Arc tunnel tests. Burggraf's method shows a higher sensitivity to gap width than measured.

Nestler (Reference 18) developed a correlation of gap heating using heating for attached flow in terms of gap width to flow length ratio and gap depth to gap width ratio. Data from the JSC 10 MW channel nozzle tests and from NASA TN D-5908 have been added to Nestler's chart (Figure 106). These data show higher heating ratios that decrease, rather than increase, with gap width.

BURGGAF LAMINAR CAVITY HEATING EQUATIONS

$$Re_{x_0} = \frac{\rho_e U_e x_0}{\mu_e}$$

$$Re_{cr} = 240 \left(\frac{x_0}{W} \right)^{4/3} \left(1 + \frac{T}{W} \right)$$

If $Re_{x_0} > Re_{cr}$ then

$$\frac{q(z)}{q_s} = \frac{.21}{\sqrt{1 + T/W}} \left[\zeta \left(\frac{1}{2}, \frac{z}{2(W+T)} \right) - \zeta \left(\frac{1}{2}, \frac{z+W}{2(W+T)} \right) \right]$$

RIEMAN ZETA FUNCTION $\zeta \left(\frac{1}{2}, x \right) = \frac{1}{\sqrt{x}} + \sum_{n=0}^5 a_n (x+1)^n$

$$a_0 = + 0.803323$$

$$a_1 = - 3.89728$$

$$a_2 = + 2.55002$$

$$a_3 = - 1.19121$$

$$a_4 = + 0.308284$$

$$a_5 = - 0.0335024$$

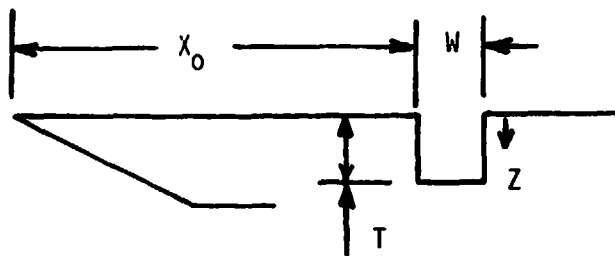


Figure 102



FINAL REPORT
VOLUME I

REPORT MDC E1003
29 JANUARY 1974

HODGSON LAMINAR CAVITY HEATING EQUATIONS

DIVIDING STREAMLINE VELOCITY:

$$U_d/U_e = f(W/X_0) = a_0 + a_1 \xi + a_2 \xi^2 + a_3 \xi^3 + a_4 \xi^4 + a_5 \xi^5$$

$$\text{WHERE } \xi = \log_{10}(W/X_0)$$

$$a_0 = + .51706 \quad a_1 = + .088707 \quad a_2 = - .049822$$

$$a_3 = - .0020116 \quad a_4 = + .0047757 \quad a_5 = + .0006549$$

$$T_d = T_w + (U_d/U_e)(T_{aw} - T_w) - (U_d/U_e)^2 \sqrt{P_R} (U_e^2/2C_p)$$

$$T_c = .5(T_d + T_w)$$

$$L = L_i \left\{ 1 + .447 [(\gamma-1)/2] M_e^2 / \left[5.22 + 4.41 \left(T_w/T_e - 1 \right) \right] \right\}$$

$$L_i = 11.8 W / Re_w^{1/2}; \quad Re_w = \rho_e U_e W / \mu_e$$

FOR Z/L ≤ 1

$$\frac{v}{U_d} = 1 - .189 \exp(-5.3Z/L) - 10.6 \sum_{n=1}^{\infty} \frac{\exp[-Z/L(9.87n^2 + 28.1)^{1/2}]}{9.87n^2 + 28.1}$$

$$StRe_L^{1/2} = C_1 \left(\frac{v}{U_d} \right)^{C_2} / \left[\int_0^{Z/L} \left(\frac{v}{U_d} \right)^{C_3} d\left(\frac{z}{L} \right) \right]^{1/2}$$

$$\text{WHERE FOR } P_R = 0.7: \quad C_1 = .418, \quad C_2 = .435, \quad C_3 = 1.87$$

FOR Z/L > 1, v = U_d AND

$$StRe_L^{1/2} = C_1 / (Z/L - A)^{1/2}$$

$$\text{AND FOR } P_R = 0.7, \quad A = .178$$

$$Re_L = \frac{P_c U_d L}{\mu_c}$$

$$q = St_p v C_p (T_d - T_w)$$

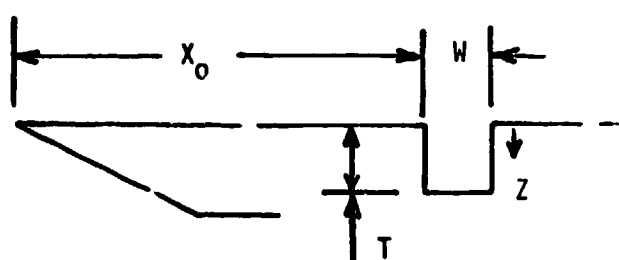


Figure 103



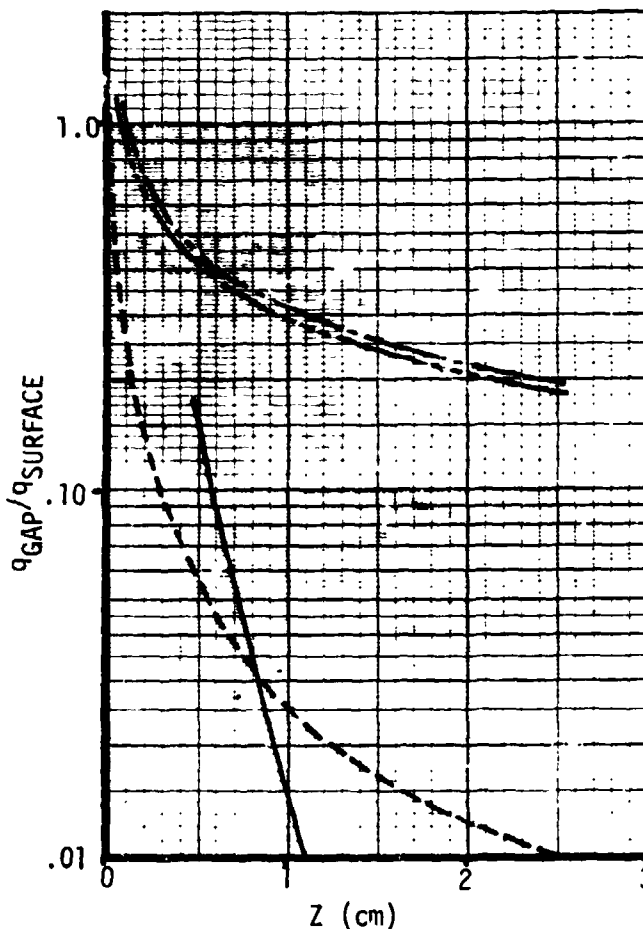
FINAL REPORT
VOLUME I

REPORT MDC E1003
29 JANUARY 1974

COMPARISON OF LAMINAR THEORIES WITH WIND TUNNEL DATA

- DATA FAIRING
- - - BURGGRAF
- - - HODGSON q/q_S
- - - HODGSON q/q_{ECK}

LaRC MACH 8 VDT RUN 10
 $Re_\infty/M = 2.30 \times 10^6$
 $W = .318 \text{ cm}$



AMES 3.5 FT HWT RUN 56
 $Re_\infty/M = 1.59 \times 10^6$
 $W = .254 \text{ cm}$

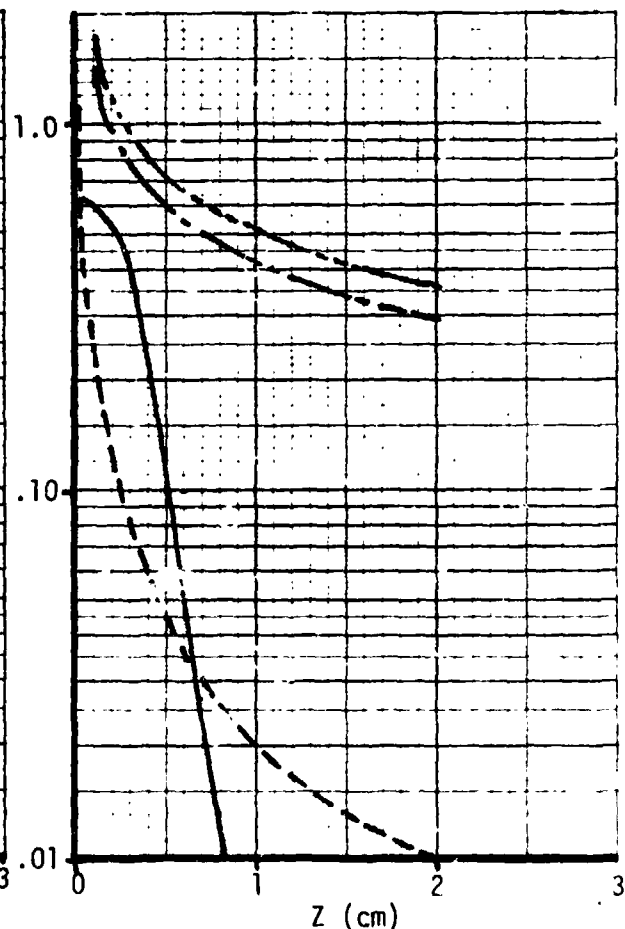


Figure 104

COMPARISON OF LAMINAR THEORIES WITH 10 MW ARC TUNNEL DATA

——— DATA FAIRING
 - - - BURGGRAF
 - - - HODGSON q/q_S
 - - - HODGSON q/q_{ECK}

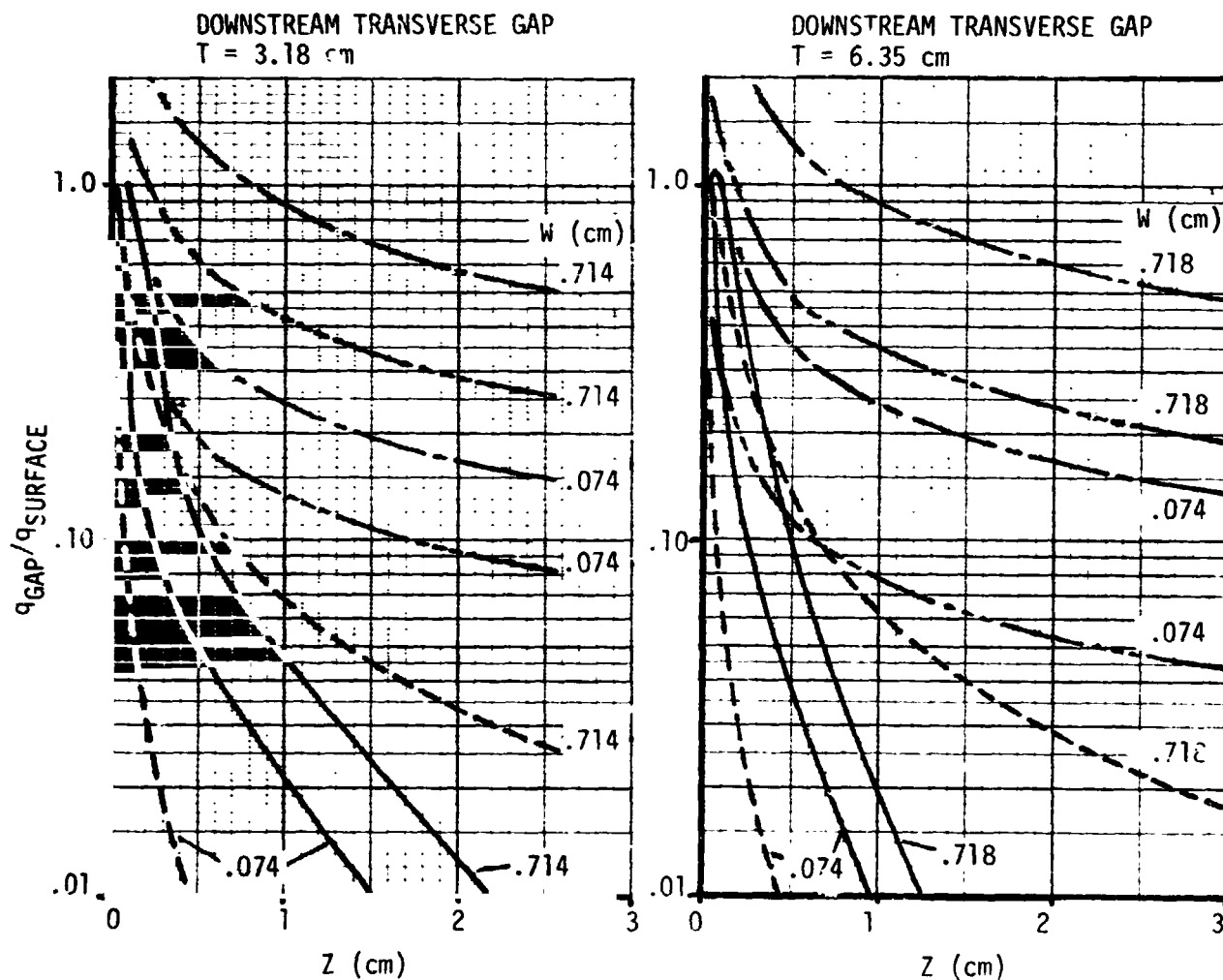
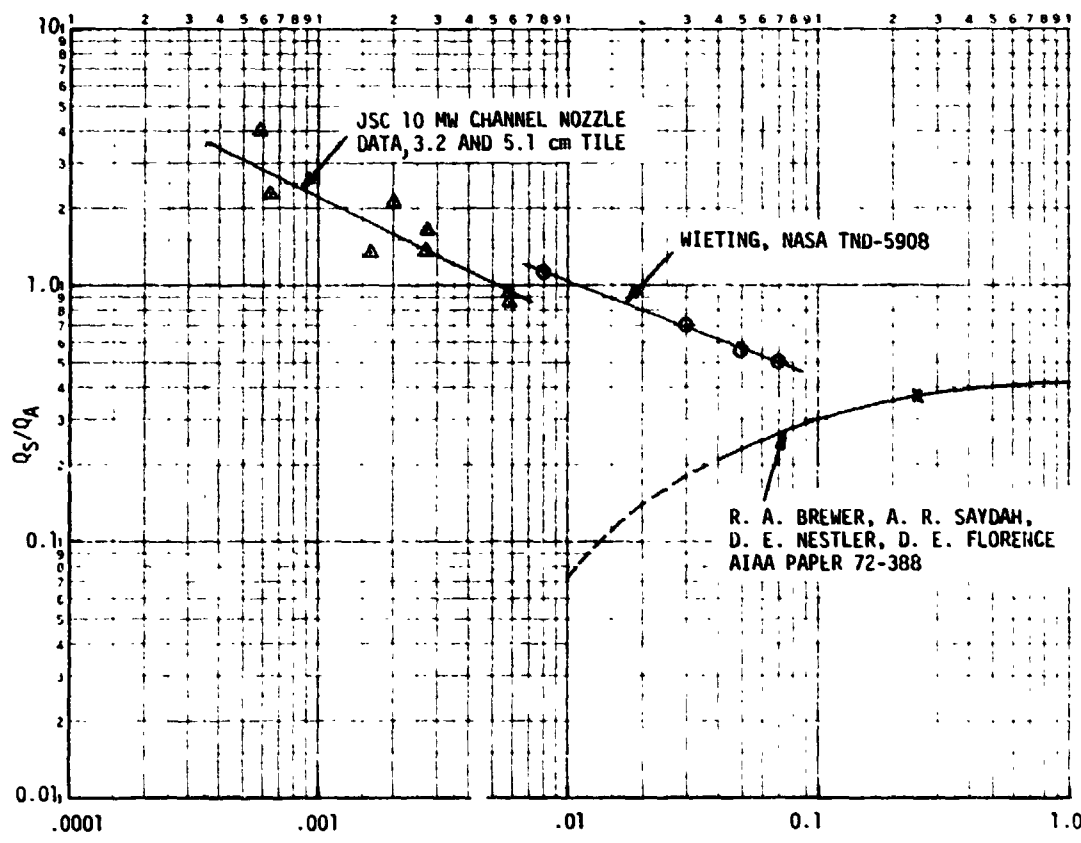


Figure 105

RATIO OF AVERAGE SEPARATED TO ATTACHED HEAT FLUX FOR LAMINAR FLOW



Q_s = ENERGY FLUX CROSSING
 SHEAR LAYER OVER GAP "W"
 Q_a = ENERGY FLUX TO AREA "W"
 IF ATTACHED FLOW EXISTED

W/L



Figure 106



**RSI GAP HEATING
ANALYSIS**

**FINAL REPORT
VOLUME I**

**REPORT MDC E1003
29 JANUARY 1974**

The laminar theories that were investigated did not agree with the measured heating in the gaps. Hodgson's theory consistently overpredicts wind tunnel and Arc tunnel results. Burggraf's theory agrees somewhat better with wind tunnel data.

Burggraf's method shows a greater sensitivity to gap width than observed in the Arc tunnel data, appearing to under predict heating for narrow gaps and over predict for the wide gaps. Additional effort is therefore warranted in developing theoretical models of flow and convective heating in gaps.



FINAL REPORT
VOLUME I

REPORT MDC E1003
29 JANUARY 1974

5.0 DATA CORRELATION

The gap heating data which were analyzed were also correlated in terms of gap dimensions, location of gap, location in the gap and boundary layer parameters. A general data management system was set up so a common approach could be applied to correlate data from available sources. Test results were ordered, and combined with physical dimensions, instrumentation coordinates and boundary layer parameters to form a data bank. Over 17000 individual heat transfer measurements were assimilated into the data bank which is functional on the McDonnell Douglas computer. This data management system permits quick access of data sets with similar attributes including direct input to a MRA (Multiple Regression Analysis) computer program. The MRA program assisted in correlating test data from the JSC 10 MW channel nozzle facility, the LaRC CFHT and the LaRC $M = 8$ V.D.T. Correlations were obtained for transverse gaps, in-line gaps, effects of flow angularity, and effects of steps in the presence of both laminar and turbulent boundary layers.

5.1 Data Correlation Procedure - Test information supplied by each test facility was received on magnetic data tapes, computer tabs, work sheets, and facility test reports. Format and methods of transmitting data were suggested to each facility and where possible these recommendations were incorporated consistent with what was most convenient for that facility. Data from each facility were processed into the data bank and representative data listings for the JSC 10 MW, CFHT, $M = 8$ V.D.T. and the Ames 3.5 foot HWT are contained in Figures 107 thru 110. Volume II contains a complete listing of the data and associated descriptive information.

A procedure was set up for ordering data and combining of data with flow field parameters. In a following section the mechanics of the correlation procedure are described with the aid of a data handling flow chart. Also included in the procedure are discriminators used to select data for correlation using the Multiple Regression Analysis program.

5.1.1 Data Ordering and Marriage with Flow Field Parameters - Each piece of gap heating data incorporated in the data bank was assigned 24 attributes which provide traceable information about its origin, instrumentation location in the joint, heat transfer parameters and boundary layer parameters. The assigned 24 attributes are listed in Figure 111. Traceable information about test program origin, run number and instrumentation designation constitutes the first attribute word. The system is formulated so that information from other tests can be added to the data bank. Information about the boundary layer flow over the RSI joints,



BUTT JOINT HEATING RATE DISTRIBUTION PARAMETERS JSC 10 MW CHANNEL NOZZLE TEST TRANSVERSE CAP

FINAL REPORT

VOLUME I

**REPORT MDC E1003
29 JANUARY 1974**

TYPICAL

HEAT FLUX DISTRIBUTION (q_{GAP}/q_{SUP}) OBTAINED FROM INVERSE SOLUTION



**FINAL REPORT
VOLUME I**

**REPORT MDC E1003
29 JANUARY 1974**

TYPICAL

1960 1961 1962 1963 1964 1965 1966 1967 1968 1969 1970 1971 1972 1973 1974 1975

**RSI GAP HEATING
ANALYSIS**

**FINAL REPORT
VOLUME I**

**REPORT MDC E1003
29 JANUARY 1974**

TYPICAL

PAGE 1

MACH 6 V.O. TEST 6221, C. S. JOHNSON RSI TILE GAPS, RUN 1 1972
 TSTAG(1) = 6.7972E+02
 PSTAG(NM2) = 3.9043E+05
 O CODE = 1
 DEG OF FIT = 1
 RC/METER = 1.0181E+06
 MACH = 7.500
 XMSTRF = .005
 XAW/TT = SNQ1(PRI) FOR ML+MR
 TAW/TT = IP111.333 FOR MT
 PARALLEL TILE CONF.
 TUNNEL WALL POSITION
 M1 IS FOR TC-19 = 1.9638E+00

T/C	X	Y	Z	ML (CM)	ML (W/M2-K)	ML (W/M2-K)	HT (W/M2-K)	HT/HR ML/ML	HT/HR ML/H1	HT/H1	SFL	STT	STREL	TILE	GAP			
1	21.600	10.250	.976	1.50E+02	5.292E+01	6.70E+01	1.59E+01	.2036	.2036	1.29E+01	1.16E+01	6.47E+02	LUPS	1587PE	.2452			
2	21.600	11.250	.953	4.05E+01	1.634E+01	1.29E+01	0.432	.0390	.0035	.0730	.0658	3.0E+05	1.15E+02	LUPS	.0064			
3	21.600	13.250	1.087	3.60E+01	1.27E+02	1.14E+02	0.432	.035	.0035	.0065	.0059	3.0E+05	1.56E+03	1587PE	.0059			
4	26.700	13.250	.676	3.70E+01	6.05E+02	6.05E+02	20.33	.1831	.3087	.2781	.146E+04	1.35E+04	8.23E+02	LUPS	1587PE	.2078		
5	26.700	10.250	.953	0.10E+01	2.66E+01	2.53E+01	0.982	.0006	.0006	.1460	.1316	7.01E+05	6.31E+05	LUPS	1587PE	.167		
6	26.700	10.250	.1507	4.24E+00	1.405E+02	1.44E+02	0.054	.0049	.0049	.0082	.0071	3.02E+06	3.53E+06	2.19E+03	LUPS	1587PE	.0071	
7	34.300	10.250	.676	1.52E+02	2.339E+01	4.05E+01	2.04E+01	.1645	.2745	.2473	.122F+04	1.15E+04	6.30E+02	LUPS	1587PE	.2255		
8	34.300	10.250	.953	3.40E+01	1.053E+01	9.577E+02	0.41	.0164	.0164	.0088	.260F+03	2.34E+05	1.64E+03	LUPS	1587PE	.0445		
9	34.300	10.250	.1507	6.09E+00	2.150E+02	1.937E+02	0.074	.00140	.00140	.0140	.0099	5.04E+04	4.73E+04	3.31E+03	LUPS	1587PE	.0090	
10	21.600	.230	.476	1.20E+02	4.22E+01	3.82E+01	0.216	.01174	.01174	.2163	.1999	1.04E+04	9.38E+05	5.19E+02	LUPS	1587PE	.1960	
11	21.600	.230	.953	4.32E+01	1.529E+01	1.377E+01	0.461	.0110	.0110	.0779	.0702	3.74E+05	3.37E+05	LUPS	1587PE	.0700		
12	21.600	.230	1.507	3.58E+01	1.268E+01	1.14E+01	0.383	.01345	.01345	.0646	.0502	3.0E+05	2.75E+05	1.55E+02	LUPS	1587PE	.0550	
13	26.700	.230	.476	1.55E+02	2.466E+01	6.92E+01	1.936	.1654	.2781	.2589	.124E+04	1.20E+04	7.43E+02	LUPS	1587PE	.2146		
14	26.700	.230	.953	6.22E+01	1.998E+01	1.998E+01	0.661	.0655	.0655	.1126	.1061	3.64E+05	3.19E+05	1.97E+02	LUPS	1587PE	.0972	
15	26.700	.230	1.507	1.15E+01	1.469E+01	1.30E+01	0.066	.0636	.0636	.0738	.0661	3.64E+05	3.19E+05	1.97E+02	LUPS	1587PE	.0860	
16	34.300	.230	.476	4.76E+01	1.44E+01	5.44E+01	2.229	.2071	.3077	.2772	.164E+04	1.33E+04	9.30E+02	LUPS	1587PE	.2250		
17	34.300	.230	.953	1.71E+02	6.04E+01	5.44E+01	2.229	.2071	.2071	.0077	.2772	1.64E+04	1.33E+04	9.30E+02	LUPS	1587PE	.2250	
18	34.300	.230	1.507	2.07E+01	6.04E+01	5.44E+01	2.229	.0003	.0003	.0005	.208E+07	2.08E+07	1.45E+04	LUPS	1587PE	.0004		
19	22.900	.510	0.000	6.16E+02	2.179E+00	1.95E+03	0.673	.6102	.11101	.0001	.0001	5.31E+04	4.88E+04	2.74E+01	LUPS	1587PE	.0004	
20	25.400	.513	0.000	9.29E+02	2.222E+00	2.032E+00	.7279	.6559	.1321	.0200	.0200	5.43E+04	4.89E+04	2.95E+01	LUPS	1587PE	.0004	
21	27.900	.510	0.000	6.31E+02	2.337E+00	2.076E+00	.7890	.7110	.1110	.00550	.0550	5.6E+04	5.1E+04	3.19E+01	LUPS	1587PE	.0053	
22	31.100	5.110	3.00	6.67E+02	2.317E+00	2.120E+00	.8581	.7696	.2006	.01810	.01810	5.76E+04	5.10E+04	3.46E+01	LUPS	1587PE	.0053	
23	34.300	.510	0.000	6.76E+02	2.393E+00	2.15E+00	.9005	.8186	.2173	.01366	.01366	5.4E+04	5.21E+04	3.66E+01	LUPS	1587PE	.0053	
24	37.500	.513	0.000	6.02E+02	2.417E+00	2.04E+00	.9500	.8637	.2229	.10195	.10195	5.3E+04	5.33E+04	3.69E+01	LUPS	1587PE	.0053	
25	42.100	1.250	.676	4.92E+02	6.04E+02	6.04E+02	0.975	.4427	.1623	.2268	.121E+04	1.21E+04	2.09E+02	20MN	1587PE	.2838		
26	42.100	1.250	.953	1.05E+02	4.92E+01	4.43E+01	2.079	.0165	.0165	.0500	.0472	.0605	3.22E+05	2.95E+05	2.52E+02	20MN	1587PE	.0444
27	42.100	1.250	.476	1.25E+02	4.92E+01	4.43E+01	2.079	.0165	.0165	.0500	.0472	.0605	3.22E+05	2.95E+05	2.52E+02	20MN	1587PE	.0444
28	47.100	1.250	.676	1.32E+02	4.658E+01	4.195E+01	2.073	.1867	.2373	.2137	.114E+04	1.01E+04	6.41E+02	20MN	1587PE	.1953		
29	47.100	1.250	.953	2.06E+01	7.292E+02	6.558E+02	0.324	.0292	.0292	.0019	.0371	.0336	1.0E+05	1.31E+02	20MN	1587PE	.0053	
30	47.100	1.250	1.507	1.34E+00	4.730E+03	4.261E+03	0.021	.0019	.0019	.0024	.0022	.116E+06	8.5E+04	2.0E+02	20MN	1587PE	.0020	
31	50.600	3.025	.476	1.64E+02	5.092E+01	4.592E+01	.2466	.2204	.2204	.2594	.2337	1.24E+04	1.12E+04	9.91E+02	20MN	1587PE	.167	
32	54.000	1.250	.953	3.00E+01	1.202E+01	1.031E+01	.0510	.0520	.0520	.0612	.0532	.204E+05	2.61E+05	2.04E+02	20MN	1587PE	.0460	
33	54.000	1.250	1.507	1.17E+01	1.17E+02	3.72E+02	.0199	.0179	.0179	.0211	.0190	1.01E+05	9.10E+05	8.05E+01	20MN	1587PE	.0460	
34	42.100	.230	.476	1.25E+02	4.636E+01	3.936E+01	1.049	.1603	.1603	.2260	.2096	1.0E+04	9.7E+03	7.57E+02	20MN	1587PE	.1630	
35	42.100	.230	.953	4.08E+01	1.728E+01	1.523E+01	.0720	.0756	.0756	.0880	.0793	1.22E+05	3.01E+05	2.95E+02	20MN	1587PE	.0713	
36	42.100	.230	1.507	2.05E+01	9.379E+02	6.46E+02	.0395	.0355	.0355	.0479	.0460	2.29E+05	2.04E+05	1.68E+02	20MN	1587PE	.0387	
37	47.100	.230	.476	1.52E+02	5.393E+01	4.635E+01	.2403	.2164	.2164	.2747	.2675	3.02E+04	1.91E+04	9.73E+02	20MN	1587PE	.2262	
38	47.100	.230	.953	5.37E+01	1.997E+01	1.709E+01	.0666	.0762	.0762	.0967	.0971	6.64E+05	4.18E+05	3.42E+02	20MN	1587PE	.0796	



**FINAL REPORT
VOLUME I**

**REPORT MDC E1003
29 JANUARY 1974**

TYPICAL

Figure 110



FINAL REPORT
VOLUME I

REPORT MDC E1003
29 JANUARY 1974

24 ATTRIBUTES WORDS ASSIGNED
TO EACH GAP HEATING DATA POINTS

WORD	TYPE	
1	REAL	XX OYYY . ZZZ T/C OR CHANNEL NUMBER RUN NUMBER TEST NUMBER
2	INTEGER	GAP CONFIGURATION 1 = BUTT, 2 = CONTOURED, 3 = OVERLAP, 4 = INCLINED
3	INTEGER	INSTRUMENTATION LOCATION 1 = UPSTREAM SIDE OF GAP, 2 = DOWNSTREAM SIDE OF GAP, 3 = IN-LINE 4 = STAGNATION, 5 = TILE TOP, UPSTREAM SIDE OF GAP, 6 = TILE TOP DOWN SIDE OF GAP
4	REAL	x COORDINATES OF AN INSTRUMENTATION POINT, z = 0
	REAL	y AT TOP SURFACE OF THE TILE, x = DISTANCE DOWNSTREAM
6	REAL	z FROM CENTER OF TILE, y (RIGHHAND RULE), (cm)
7	REAL	\bar{x} , DISTANCE FROM LEADING EDGE OF EACH TILE (cm)
8	REAL	NOT USED
9	REAL	FLOW ORIENTATION (RADIAN)
10	REAL	GAP WIDTH (Δ)
11	REAL	STEP HEIGHT (Δ)
12	REAL	GAP FLOW LENGTH (cm)
13	REAL	TILE THICKNESS (cm)
14	INTEGER	TILE PATTERN, 0 = STAGGERED, 1 = IN-LINE
15	REAL	LOCAL MACH NUMBER
16	REAL	REYNOLDS NUMBER/METER
17	REAL	MOMENTUM THICKNESS (cm)
18	REAL	DISPLACEMENT THICKNESS (cm)
19	REAL	SUB-LAYER THICKNESS (cm)
20	REAL	HEAT TRANSFER COEFFICIENT (h), (KG/M ² SEC)
21	REAL	h/h_{ref}
22	REAL	STANTON NUMBER
23	REAL	T_{wall}/T_e , TEMPERATURE RATIO ACROSS BOUNDARY LAYER
24	INTEGER	BOUNDARY LAYER STATE, 1 = LAMINAR, 2 = TRANSITIONAL, 3 = TURBULENT

Figure 111



FINAL REPORT
VOLUME I

REPORT MDC E1003
29 JANUARY 1974

as discussed in Section 4.6, was married with the instrumentation location and the gap heating data to complete the data bank. The 24 attributes are also used to select a particular set of data for correlation. The 24 attribute information is stored on magnetic data tape.

5.1.2 Data Handling Flow Chart - The functioning of the data management system is illustrated in Figure 112. For example, results from the CFHT tests stored on a data tape are combined with test matrix information, T/C coordinates and boundary layer flow field parameters in the "RSI C" program to generate a 24 word attribute tape. Companion tapes from the other tests are prepared in a similar manner. These tapes are then processed by another program which selects data according to a list of discriminators specified for a particular type of gap to be analyzed. Information from the JSC tests contained on data cards can be read by either the "Select" program or by the Multiple Regression Analysis (MRA) program. The MRA program processes the selected data and determines the best fit for candidate correlation equations.

DATA HANDLING FOR GAP HEATING CORRELATION

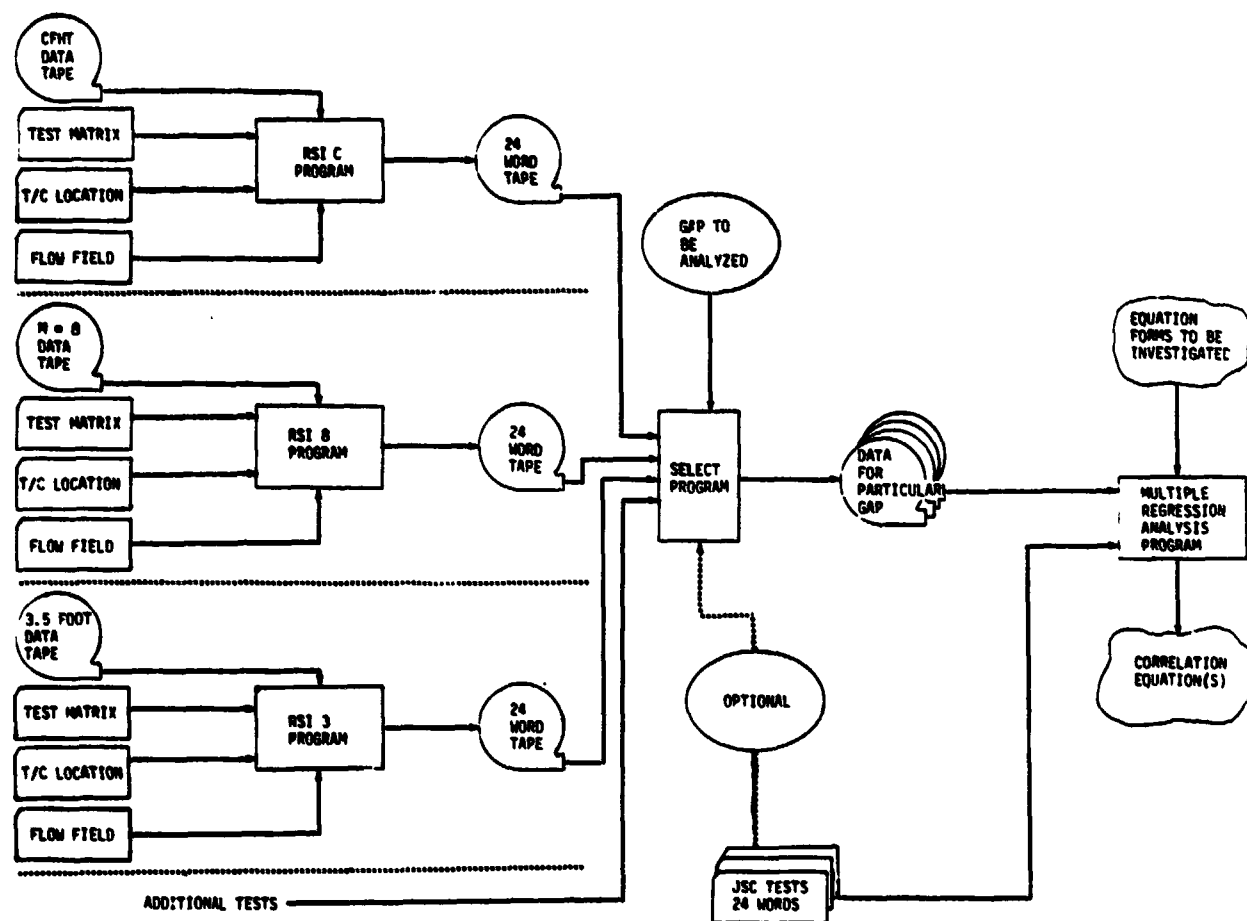


Figure 112



FINAL REPORT
VOLUME I

REPORT MDC E1003
29 JANUARY 1974

5.1.3 Selecting Data for Correlation - A list of 29 discriminators was prepared for selecting data from the 24 attribute tapes for correlation. Figure 113 shows an input form for the "SELECT" program. Upper and lower limit discriminators were used to facilitate the selection process. Tabulations as well as tapes were generated containing the selected data. The tabulated information was valuable for identifying trends, anomalies and for checking data.

5.1.4 Multiple Regression Analysis - Because of the large amount of heating data available for correlation, an automated multiple regression technique was used to obtain consistent-nonbiased correlation equations. Multiple regression relieves the analyst of many tedious calculations involved in obtaining sound correlations. The step-wise Multiple Regression Analysis (MRA) computer program (Reference 19) provided information as to the adequacy of candidate correlation function and the equation coefficients. A modified version of the MRA computer program which accepts information stored in the data bank was used for this study. The principal modifications included accepting information stored in the data and auxiliary statistical analyses. The MRA computes a series of multiple linear regression equations in a stepwise manner. At each step, one parameter is added to the equation. The variable added is the one which makes the greatest reduction in the variance about the mean. Equivalently, it is the parameter which, if it were added, has the highest "F" ratio. Figure 114 lists the form of the correlating equation(s) and the statistical parameters used by the MRA to obtain the most appropriate correlation.

Local heating at the gap ratioed to undisturbed flat plate heating was designated as the dependent variable for all correlations. Correlations were obtained in terms of natural logarithms of the dependent variable because gap heating experiences a decrease of several orders of magnitude with distance into the gap. For the JSC 10 MW data the ratio was formed using measured convective heating rates. For all other tests the ratio utilized measured convective heat transfer coefficients. The heating rate ratio and heat transfer coefficient ratio become identical for high enthalpy flow produced by the JSC 10 MW facility. The independent variables considered in the MRA included boundary layer parameters, gap dimensions, locations in the gap and ratios formed from these quantities. Local flow properties (e.g. Mach number and Reynolds number) were considered as correlation parameter because they affect embedded shock strength, flow expansion angle, boundary layer growth, boundary layer structure, etc. Other independent parameters considered cavity geometry and properties of the mass "captured" by the cavity relative to the structure and energy level of the recirculating flow in the cavity. No individual test program had sufficient



**FINAL REPORT
VOLUME I**

**REPORT MDC E1003
29 JANUARY 1974**

VARIABLES AVAILABLE FOR SELECTING DATA

COMPUTER SCIENCES SELECT INPUT FORM		REQUESTOR <u> </u>	DEPT. <u> </u>
PROBLEM RSI GAP HEATING SCREENING		DATE <u> </u>	PAGE 1 OF <u> </u>
2	DESCRIPTION (DO NOT KEY PUNCH)	DIMENSION	
\$LIST1			
CASE =	CASE NUMBER		
NEFILES =	NUMBER OF FILES TO BE SKIPPED ON TAPE 30 FOR PLACEMENT OF CURRENT CASE		
XLOW =	X-LOWER LIMIT (cm)		
XHIGH =	X-UPPER LIMIT (cm)		
YLLOW =	Y-LOWER LIMIT(cm)		
YHIGH =	Y-UPPER LIMIT (cm)		
ZLOW =	Z-LOWER LIMIT (cm)		
ZHIGH =	Z-UPPER LIMIT (cm)		
XBLLOW =	X-LOWER LIMIT (cm)		
XBHIGH =	X-UPPER LIMIT (cm)		
YBLLOW =	Y-LOWER LIMIT (cm)		
YBHIGH =	Y-UPPER LIMIT (cm)		
ALPHAL =	FLOW ORIENTATION - LOWER LIMIT (RADIAN)		
ALPHAH =	FLOW ORIENTATION - UPPER LIMIT (RADIAN)		
GAPWL =	GAP WIDTH - LOWER LIMIT (cm)		
GAPWH =	GAP WIDTH - UPPER LIMIT (cm)		
STEPL =	STEP HEIGHT - LOWER LIMIT (cm)		
STEPH =	STEP HEIGHT - UPPER LIMIT (cm)		
GAPFL =	GAP FLOW LENGTH LOWER LIMIT (cm)		
GAPPH =	GAP FLOW LENGTH - UPPER LIMIT (cm)		
THKL =	TILE THICKNESS - LOWER LIMIT (cm)		
THKH =	TILE THICKNESS - UPPER LIMIT (cm)		
IPATN(1) =	TILE PATTERN: 0-STAGGERED, 1-IN-LINE	IPATN(9)	
IBL(1) =	BOUNDARY LAYER STATE: 1=LAMINAR, 2=TRANSITIONAL, 3=TURBULENT,	IBL(9)	
IGAPC(1) =	GAP CONFIGURATION: 1=BUTT, 2=CONTOURED, 3=OVERLAP, 4=INCLINED	IGAPC(9)	
IGLOC(1)	GAP LOCATION: 1=UPSTREAM SIDE OF GAP, 2=DOWNTSTREAM SIDE OF GAP, 3=PARALLEL, 4=STAGNATION, 5=TILE TOP, UPSTREAM SIDE OF GAP, 6=TILE TOP, DOWNTSTREAM SIDE OF GAP	IGLOC(9)	
NTDL(1) =	TOTAL NUMBER OF DESIRED DATA POINTS ON EACH TAPE TO BE READ: 0 READS ENTIRE FILE	NTDL(9)	
IW =	INTERMEDIATE DIAGNOSTIC PRINT-OUT OF FIRST IW DATA POINTS		
HRLAW =	LOWEST ACCEPTABLE HEATING RATE RATIO		
HRHIGH =	HIGHEST ACCEPTABLE HEATING RATE RATIO		
SEND			

Figure 113



FINAL REPORT
VOLUME I

REPORT MDC E1003
29 JANUARY 1974

MULTIPLE REGRESSION ANALYSIS

N = SAMPLE SIZE

Y = DEPENDENT VARIABLE

X_i = INDEPENDENT VARIABLE

df = DEGREES OF FREEDOM

o STANDARD DEVIATION OF ALL "Y" VALUES. $\sigma = \sqrt{\frac{\sum (Y - \bar{Y})^2}{N-1}}$

o CORRELATION EQUATION: $Y = C_0 + C_1 X_1 + C_2 X_2 + C_3 X_3 + \dots$

o RESIDUAL = Y_{MEASURED} - Y_{CALCULATED}

o STANDARD ERROR OF ESTIMATE: $S = \sqrt{\frac{1}{N-df} \sum (Y_{MES} - Y_{CAL})^2}$

o CORRELATION COEFFICIENT: $R = \sqrt{1 - \frac{S^2}{\sigma^2}}$ "R $\rightarrow 1$ DENOTES GOOD FIT"

o TOTAL VARIANCE ABOUT MEAN: $S_T^2 = S_{X_1}^2 + S_{X_2}^2 + S_{X_3}^2 + \dots + S_{UNEXPLAINED}^2$

o F TEST: $F = \frac{S_{EXPLAINED}^2}{S_{UNEXPLAINED}^2}$

o TERMS ARE INCLUDED INTO CORRELATION EQUATION STARTING WITH LARGEST "F"

o COEFFICIENTS "C_i", DETERMINED BY LEAST SQUARES

Figure 114



FINAL REPORT
VOLUME I

REPORT MDC E1003
29 JANUARY 1974

variation in free stream conditions to completely evaluate all candidate parameters. Additional experimental data are needed to completely determine the impact of these parameters on gap heating.

In addition to the final function (or equations), intermediate regression equations are obtained after each step in the MRA, giving an indication of which variables are most important. Also, some parameters in the candidate correlation function were rejected because they had no significant effect on the dependent variable (heating ratio).

Statistical information is produced regarding goodness of fit, multiple correlation coefficient (R) and significance of interaction among independent variables. Of particular importance is the standard error of estimate (S) for each step which represents the MTS error of prediction (or confidence band around the regression line). In following selections values of " S " and " R " are used to evaluate candidate function adequacy.



FINAL REPORT
VOLUME I

REPORT MDC E1003
29 JANUARY 1974

5.2 Correlation of 10 MW Channel Nozzle Data - Candidate correlation equations were obtained for the transverse and in-line gap models tested in the Channel Nozzle of the 10 MW Arc Tunnel at NASA-JSC. Correlations were obtained in terms of gap width, gap depth and distance into the gap.

5.2.1 Transverse Gap Heating Correlation for 10 MW Channel Nozzle Tests - Transverse gap heating data described in Section 4.2 were correlated using the MRA program. A series of fifty candidate equations was investigated. Both dimensional and non-dimensional parameters were examined. Some of these parameters were based on terms appearing in boundary layer equations or in available gap heating equations. The nine candidate equation forms which had the highest correlation coefficients are listed in Figure 115. Also contained in the figure are the standard errors of estimate. Each of the candidate functions was also plotted against the gap heating data to screen out abnormalities. The terms in each equation are listed (Figure 115) from left to right in the order of their contribution in correlating the data. It should be noted that terms were omitted from the correlation equation because they did not contribute significantly to the correlation. Equation 9 produced the best fit with a high correlation coefficient (0.9822) and a low standard error of estimate. Distance into the gap contributed most to the correlation, the gap width, and then the interaction between distance into the gap and gap depth. Figure 116 gives a visual comparison of the correlation (Equation 9) with measured data on the gap face for four gap widths and three gap depths. The effect of gap depth (tile thickness) is quite obvious and the heating at the top of the gap increases with gap width. Increasing gap depth decreases gap heating. At the widest gap width (0.716 cm), the heating ratio at the top of the gap was "1.1".

In Figure 117 and 118 the candidate functions are compared against one another and against the data for the widest gap (0.716 cm). Several of the candidate functions shown in Figure 117 do not correlate the data and Equation 5 which is in terms of (Z/W) underpredicts gap heating near the top of the gap and over-predicts gap heating at lower regions into the gap. Equation 1 has the best fit for all equations in Figure 117. Figure 118 compares Equation 1 and Equation 9 with the measured data. Equation 1 does not have a gap depth effect and hence passes through the center of the data. The correlation equation for convective heating in the transverse butt joint exposed to the environments produced by the



FINAL REPORT
VOLUME I

REPORT MDC E1003
29 JANUARY 1974

10 MW channel nozzle is;

$$\frac{q_{GAP}}{q_{SURFACE}} = e^{(-.3716 - 5.0249Z + 2.5604Z^2 + 1.0733W - .03797ZT^2 - .03654(Z/W) - 6.0719(Z/T)^2)}$$

(Equation 9)

5.2.2 In-Line Gap Heating Correlation for 10 MW Channel Nozzle Tests -

In-line gap heating data described in Section 4.2 were correlated using the MRA program. Data measured upstream as well as downstream of the transverse gap were included in the analysis. This was necessary because instrumentation malfunctioned during the test. As a result the gap heating data do not show a consistent trend with gap depth. Nevertheless parameters involving gap depth were inserted into the candidate function. It was shown statistically that gap depth could not be used to correlate the data.

Figure 119 lists the more competitive correlation forms, their correlation coefficients and their standard errors of estimate. Equation 25 was selected as the most descriptive. Distance into the gap, distance into the gap ratioed to gap width and gap width were the important quantities. The correlation equation for convective heating in the in-line butt joint exposed to environments produced by the 10 MW channel nozzle is;

$$\frac{q_{GAP}}{q_{SURFACE}} = e^{(-0.3319 - 4.3979Z + 1.5630Z^2 - 0.2295(Z/W) + 1.0148W)} \quad (Equation 25)$$

Figure 120 shows the comparison of the correlation with data from the in-line gap used for the correlation.



**CORRELATION FUNCTIONS INVESTIGATED FOR
TRANSVERSE GAP -- JSC TESTS**

$$\ln q/q_s = C_0 + \sum C_i A_i$$

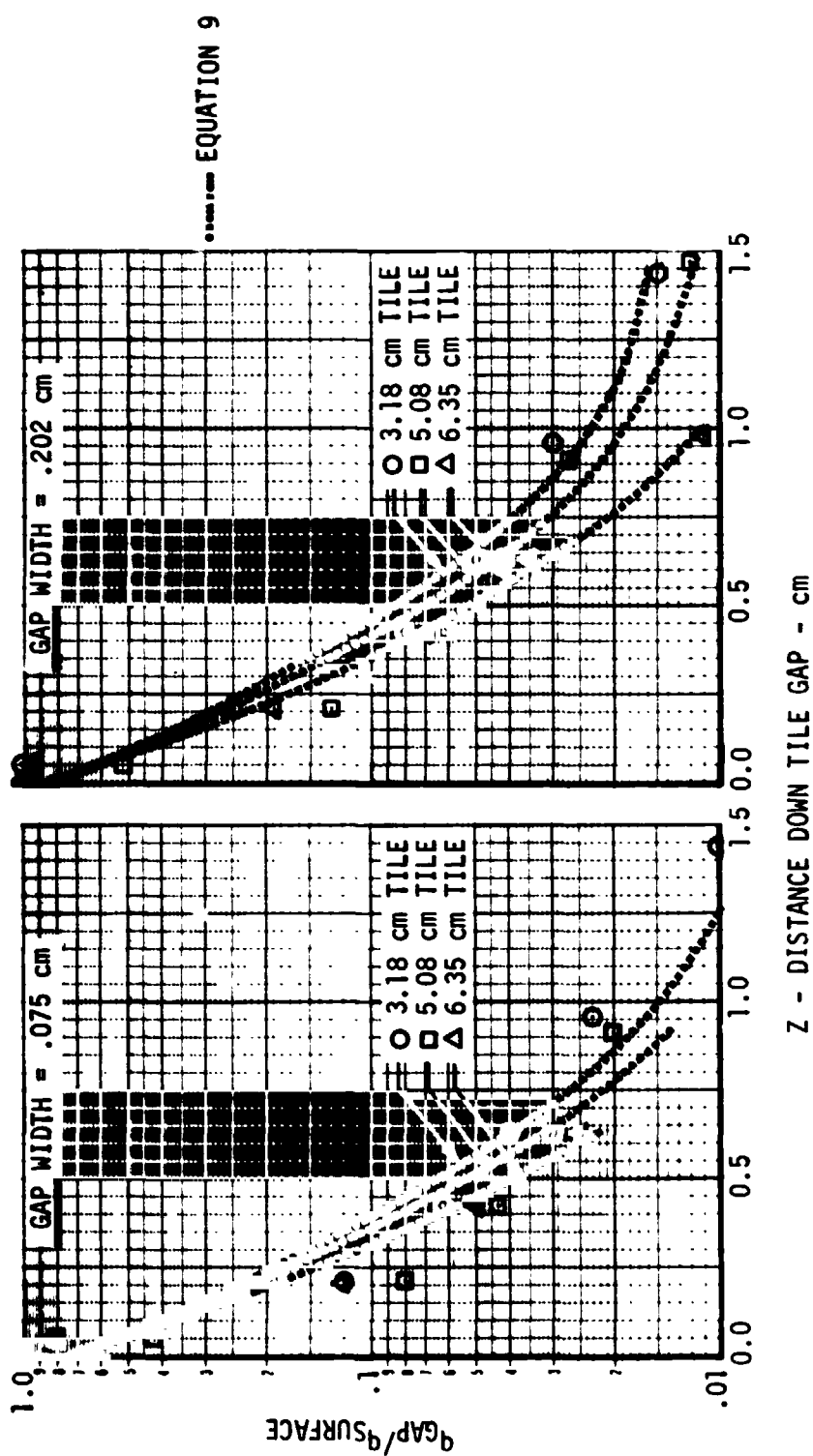
EQUATION	A _i	R	S
1	Z, Z ² , W,	.9761	.3392
2	ln(Z/W),	.8409	.8331
3	(Z+C), 1/(Z+C), (Z+W), W ² /(Z+C),	.9623	.4274
4	Z, Z ² ,	.9550	.4596
5	(Z/W), (Z/W) ² ,	.8278	.8693
6	(Z/W ⁵), (Z/W ⁵) ² ,	.9584	.4423
7	Z, Z ² , W, (Z/T), (Z/W),	.9799	.3158
8	Z, Z ² , W, (Z/T),	.9783	.3252
9*	Z, Z ² , W, ZT ² , (Z/W), (Z/T) ² ,	.9822	.2989

R = CORRELATION COEFFICIENT (BASED ON \ln)
 S = STANDARD ERROR OF ESTIMATE (BASED ON \ln)
 Z = DISTANCE INTO GAP
 W = GAP WIDTH
 T = GAP DEPTH

TERMS OMITTED BY F-TEST (95% CONFIDENCE
LEVEL)

* SELECTED EQUATION

COMPARISON OF CORRELATION WITH JSC 10 MW TESTS BUTT JOINT,
TRANSVERSE GAP



COMPARISON OF CORRELATION WITH JSC 10 MW TEST BUTT JOINT,
TRANSVERSE GAP

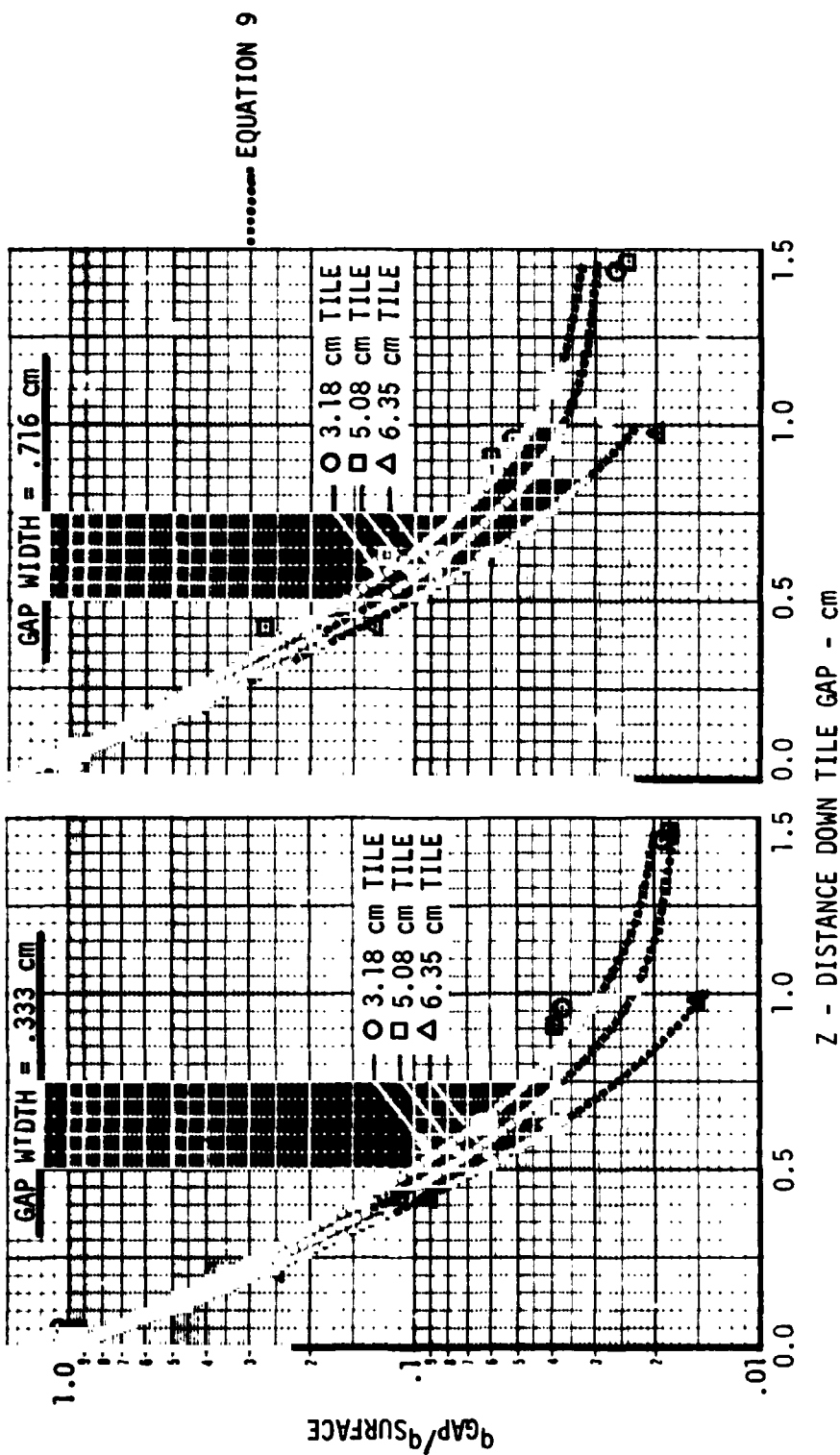


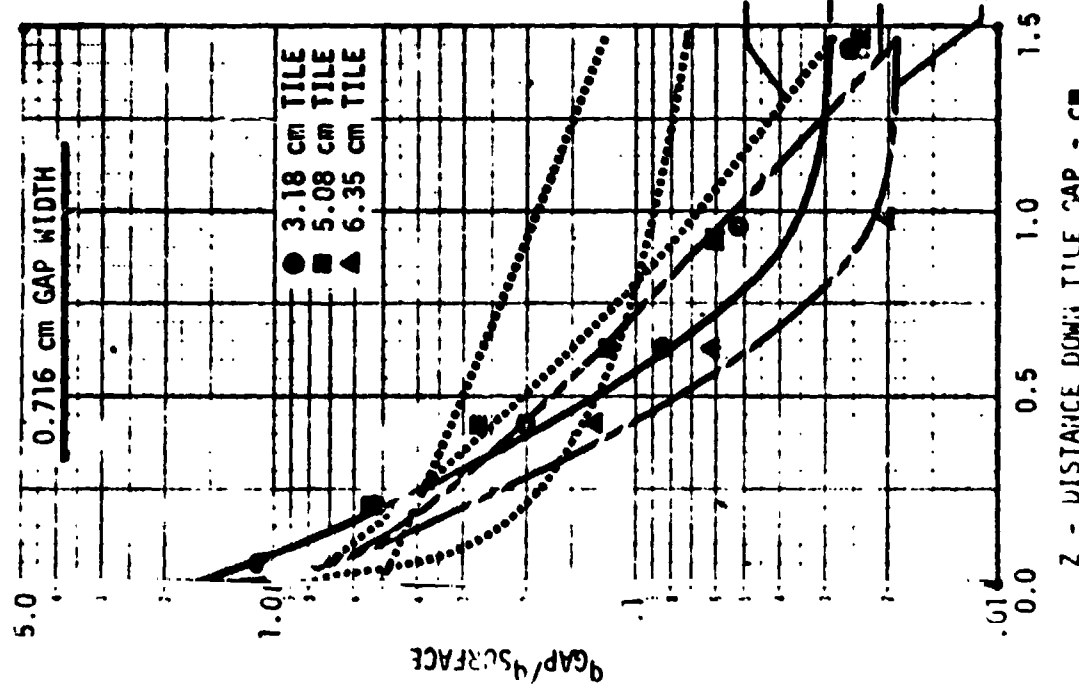
Figure 116 Concluded

**RSI GAP HEATING
ANALYSIS**

**COMPARISON OF CORRELATIONS WITH JSC 10 MW TEST BUTT JOINT,
TRANSVERSE GAP**

**FINAL REPORT
VOLUME I**

**REPORT MDC E1003
29 JANUARY 1974**

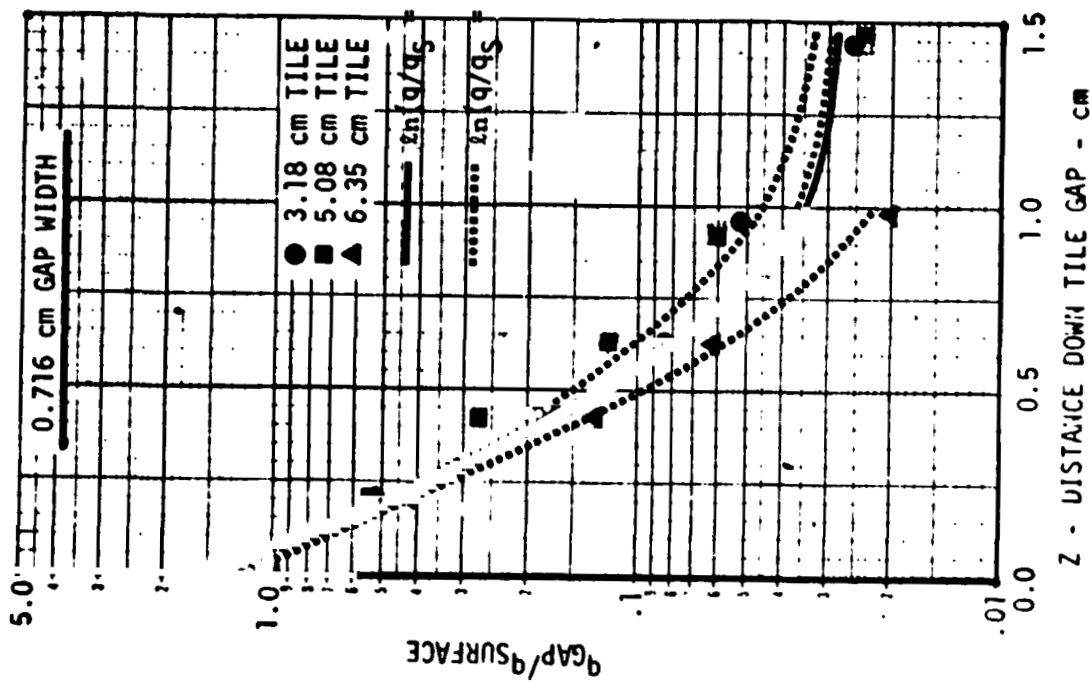


**COMPARISON OF CORRELATIONS WITH JSC 10 MW TEST BUTT JOINT,
TRANSVERSE GAP**



**FINAL REPORT
VOLUME I**

**REPORT MDC E1003
29 JANUARY 1974**





CORRELATION FUNCTIONS INVESTIGATED FOR IN-LINE GAP -- JSC TESTS

$$\ln q/q_S = C_0 + \sum c_i A_i$$

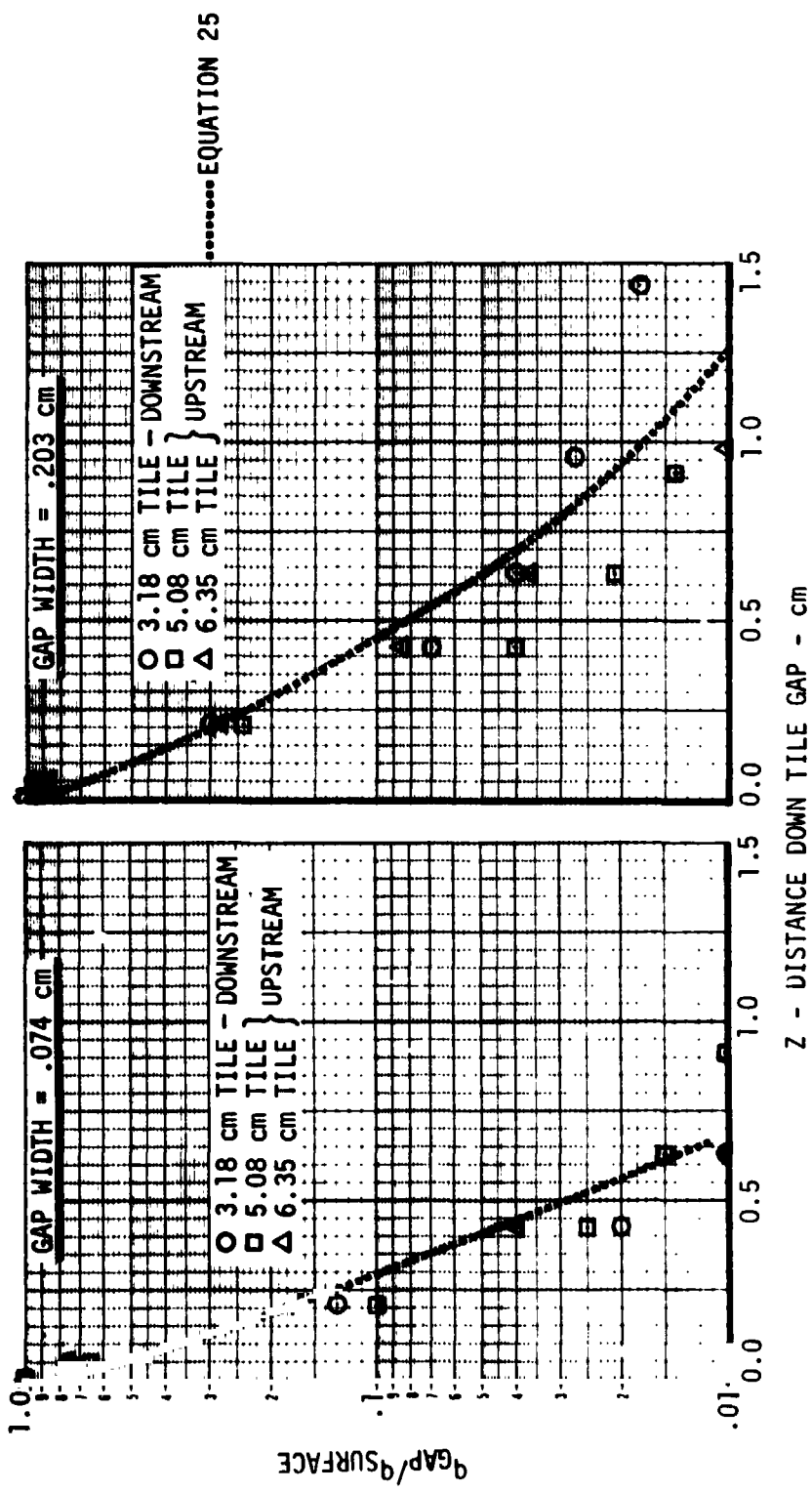
R = CORRELATION COEFFICIENT (BASED ON λ_n)
 S = STANDARD ERROR OF ESTIMATE (BASED ON λ_n)
 TERMS OMITTED BY F-TEST (95% CONFIDENCE LEVEL)

* SELECTED EQUATION

$$\text{EQUATION 25: } \ln(q/q_S) = - .3319 - 4.3979 Z + 1.5630 Z^2 - .2295 (Z/W) + 1.0148 W$$

**REPORT MDC E1003
29 JANUARY 1974**

COMPARISON OF CORRELATION WITH JSC 10 MW TESTS BUTT JOINT,
IN-LINE GAP



COMPARISON OF CORRELATION WITH JSC 10 MW TEST BUTT JOINT,
IN-LINE GAP

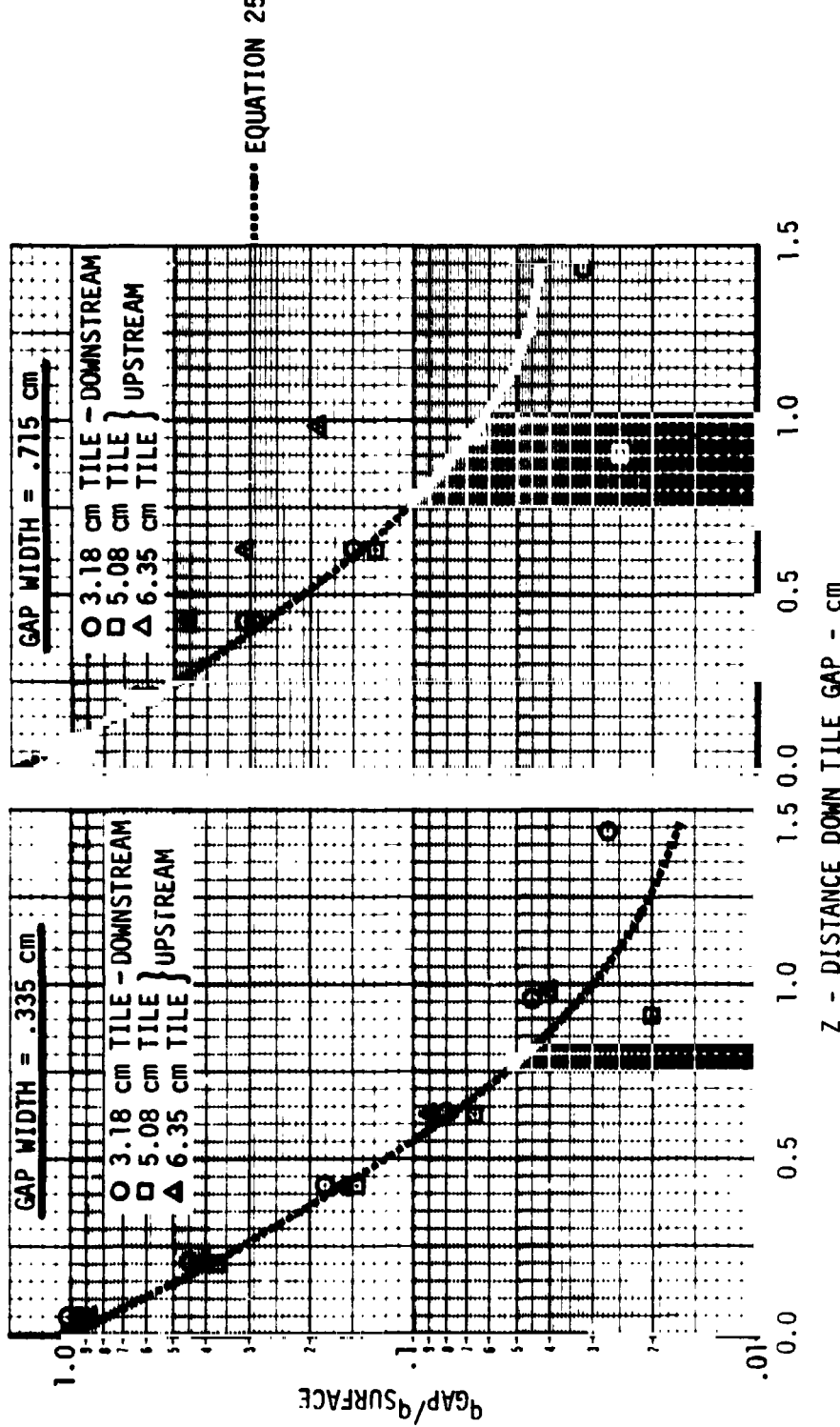


Figure 120 Concluded



FINAL REPORT
VOLUME I

REPORT MDC E1003
29 JANUARY 1974

5.3 Correlation of Heating in Transverse Gaps for Turbulent Boundary Layers in CFHT and M=8 Tests - Individual sets of data for transverse gaps submerged in turbulent boundary layer flow were examined to establish trends with boundary layer and gap geometry parameters. CFHT heating data (Figure 121) shows a linear decrease with distance (Z) into the gap when plotted on log-log graph paper. The correlation lines in the Figure change systematically with gap width (W) which suggests a dependency of the lines' intercepts and slope on gap width. Values of the intercepts (a) and slope (b) are dependent on (W), as also shown in the Figure. The resulting form for candidate correlation terms were combined with other terms in a MRA analysis to determine the most appropriate equation. Figure 122 summarizes the MRA analysis. Correlation coefficients (R) and standard error of estimate (S) for both the natural logarithm correlation and for an auxiliary calculation using cartesian coordinates are listed in the Figure. The curve fitting is accomplished in logarithmic coordinates and is the most appropriate for judging goodness of fit. As can be seen a correlation coefficient of 0.9837 was obtained out of a possible 1.0. The resulting correlation equation (CFHT, transverse gap) is:

$$\ln \frac{h}{h_{FP}} = \left\{ -1.73903 - 1.74049 W^{-2/7} \ln Z + 1.20206 \ln W + 0.08495 \left[\ln \frac{Z}{W} \right]^3 \right\}$$

Figure 123 is a plot of the residual (difference between measured and calculated dependent variable) versus the value of $\ln(h/h_{FP})$ measured and calculated. It should be noted that the plots use natural logarithms. The integers on the plots represent data points and their uniform spacing indicates a non-biased correlation equation. The same information is shown in Figure 124 for cartesian coordinates. The maximum difference between the measured and calculated heat transfer coefficient ratio (h/h_{FP}) is less than 0.07. The predicted parameter (h/h_{FP}) has values ranging from 0.007 deep within the gap to 0.821 near the gap top.

Data from the tests conducted on the wall of the LaRC M=8 tunnel were also examined for trends. The evolution of a candidate equation is shown in Figure 125 and shows a trend with distance into the gap and unit Reynolds number. The data examined were for a single gap width, hence a sensitivity with gap width could not be obtained. The MRA analysis of these data resulted in the following equation:

$$\ln \frac{h}{h_{FP}} = -3.13609 - 2.322 \ln Z - 0.38806 \ln(Re/10^6 \text{ meter})$$

which reduces to:



FINAL REPORT
VOLUME I

REPORT MDC E1003
29 JANUARY 1974

$$\frac{h}{h_{FP}} = .04345(z^{-2.322}) \left(\frac{Re}{10^6 \text{ meter}} \right)^{-0.38806}$$

The correlation coefficient (based on natural logarithms) was 0.9115 with a standard error of estimate of 0.4531. In this case the exponent of Z was a constant value of -2.322 independent of unit Reynolds number.

Next, information from the CFHT and M=8 turbulent boundary layer tests was combined in a MRA analysis using candidate terms derived from the tests preceding analyses. Figure 126 summarizes the step wise development of the correlating equation. The resulting equation (#18) is:

$$\frac{h}{h_{REF}} = 0.01384 \left[z^{(-1.46402W^{-2/7})} \left(\frac{T_w}{T_e} \right)^{-2.549} \left(\frac{Re}{10^6 \text{ meter}} \right)^{-0.5362} \left(W^{.7806} \right) \right]$$

The independent variables used in this equation had ranges as follows

$$0.36 \leq Z \leq 5.74 \text{ cm}$$

$$0.127 \leq W \leq 0.711 \text{ cm}$$

$$0.29 \leq \frac{T_w}{T_e} \leq 0.44$$

$$1.158 \times 10^6 \leq Re \text{ (Unit Reynolds number } m^{-1}) \leq 19.37 \times 10^6$$

The residuals (\ln) for Equation 18 are plotted in Figure 127 versus measured and calculated heat transfer coefficients. The residuals have a more or less even distribution which indicates a non-biased correlation and that all important independent variables have been used. Figure 128 contains the same information plotted in cartesian coordinates. The measured heat transfer coefficient ratio had a range of 0.008 to 0.784 whereas the computed ratio had a range from 0.005 to 0.629. Again it should be noted that the log-log plots reflect the goodness of fit rather than the cartesian plots.

The M=8 V.D.T. gap heating data were also investigated to establish trends in terms of lateral location in a transverse gap. Data for a set of tunnel runs at the same unit Reynolds number were correlated. Figure 129 contains the development of the correlation. MRA analysis was not performed because only two gap settings were used during the test. As can be seen from the figure, heating is a strong function of distance into the gap (Z). The heating for the narrower gap (0.159cm) is lower and has a different power coefficient than the wider gap (0.317 cm). The heating in the gap does not change in the lateral direction (Y) for the



FINAL REPORT
VOLUME I

REPORT MDC E1003
29 JANUARY 1974

narrow gap whereas a definite increase in heating is present in the wider near the intersection with an in-line gap. The correlation developed in Figure 129 can be used to determine the effect of lateral location in the transverse gap. Additional investigations are warranted in this area.



**DEVELOPMENT OF CORRELATION FOR HEATING IN TRANSVERSE GAP
FOR TURBULENT BOUNDARY LAYERS IN CFHT ("Z AND W")**

FINAL REPORT
VOLUME I

REPORT MDC E1003
29 JANUARY 1974

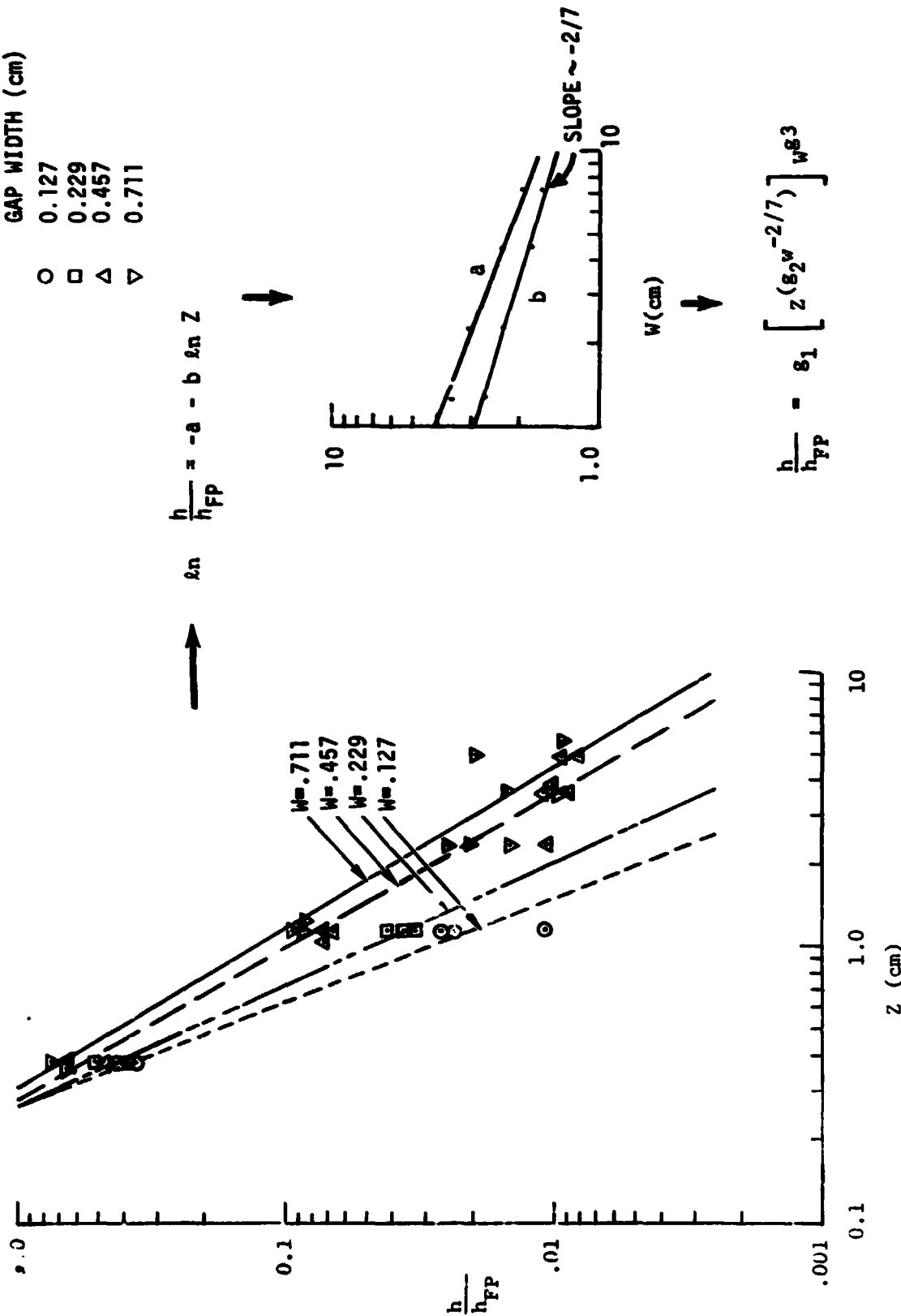


Figure 121



**CORRELATION EQUATIONS FOR TRANSVERSE GAP
IN TURBULENT BOUNDARY LAYER
(CFHT TESTS)**

TESTS CONSIDERED	EQ. NO.	DEP. VAR.	EQUATION	NATURAL LOG			CARTESIAN			COMMENTS
				R	S	R	S	R	S	
CFHT	16	$\frac{h}{\ln h_{FP}}$	$-2.61730 - 1.23208 W^{-2/7} \ln Z$	0.93750	0.5392	0.8172	1.1330	33 POINTS		
			$-1.87517 - 1.41057 W^{-2/7} \ln Z + 0.75177 \ln W$	0.97650	0.3401	0.8789	1.1119		0.0512=S'	
			$-1.73903 - 1.74049 W^{-2/7} \ln Z + 1.20206 \ln W$	0.98370	0.2888	0.9629	0.0643		0.0211=S'	
SELECTED →			$+ .08495 [t, \frac{Z}{W}]^3$							
			$+ W^2 \ln Z$							
			AD-1, PROP. EQUATIONS NOT INCLUDED BY F-TEST							

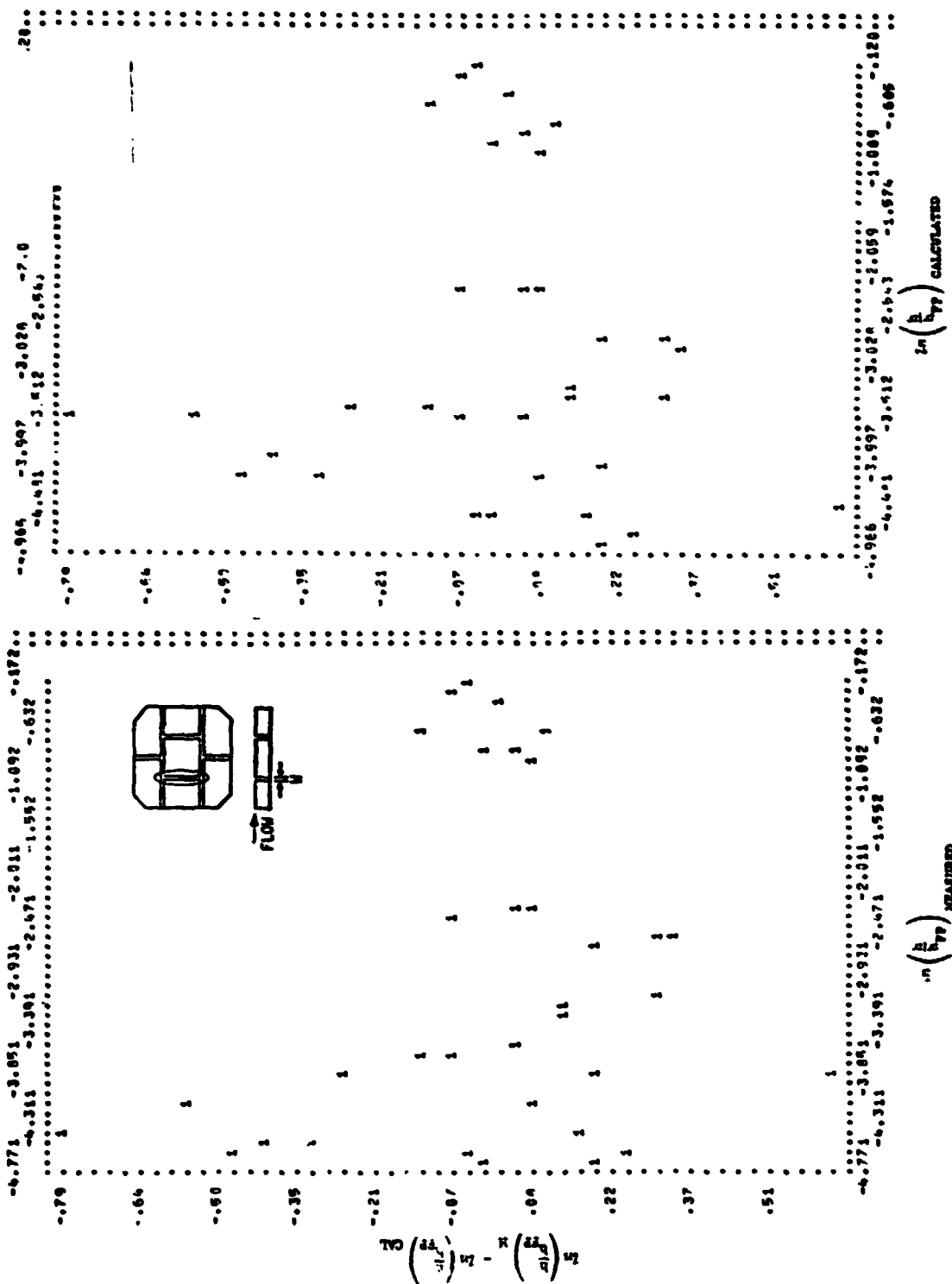
REPORT MDC E1003
29 JANUARY 1974

$Z = \text{DISTANCE FROM TILE SURFACE (cm)}$
 $W = \text{GAP WIDTH (cm)}$
 $t = \text{DISPLACEMENT THICKNESS, STARRED (cm)}$
 $L = \text{FLOW LENGTH (cm)}$
 $Re_L = \text{LOCAL REYNOLDS NUMBER}/10^6 \text{METERS}$

$R = \text{MULTIPLE REGRESSION COEFFICIENT}$
 $S = \text{STANDARD ERROR OF ESTIMATE}$

Figure 122

RESIDUALS ($\ln h$) FOR TRANSVERSE HEATING (CFHT TESTS),
EQUATION 16



**RSI GAP HEATING
ANALYSIS**

**RESIDUALS (CARTESIAN) FOR TRANSVERSE GAP HEATING
(CFHT TESTS), EQUATION 16**

**FINAL REPORT
VOLUME I**

**REPORT MDC E1003
29 JANUARY 1974**

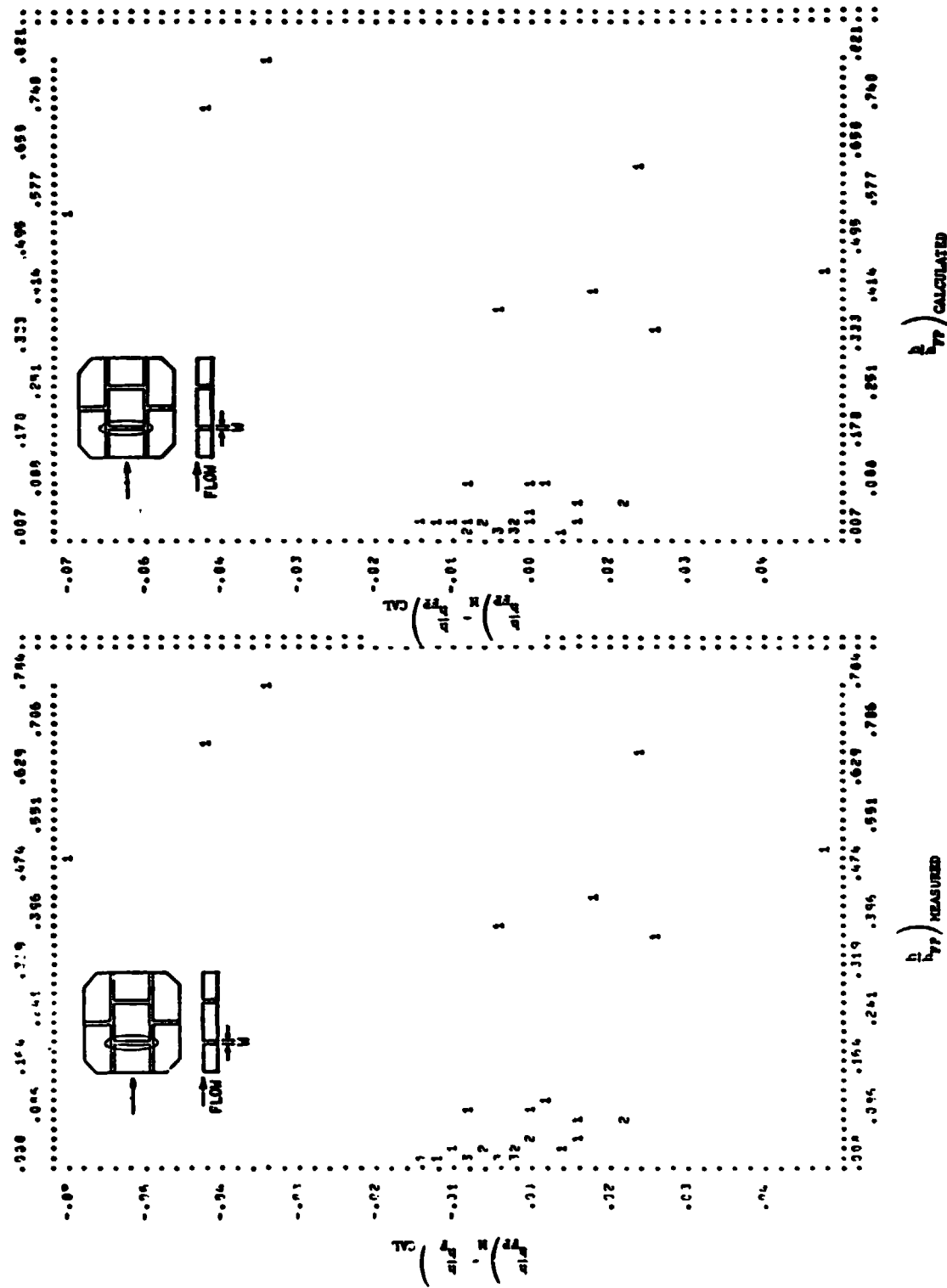
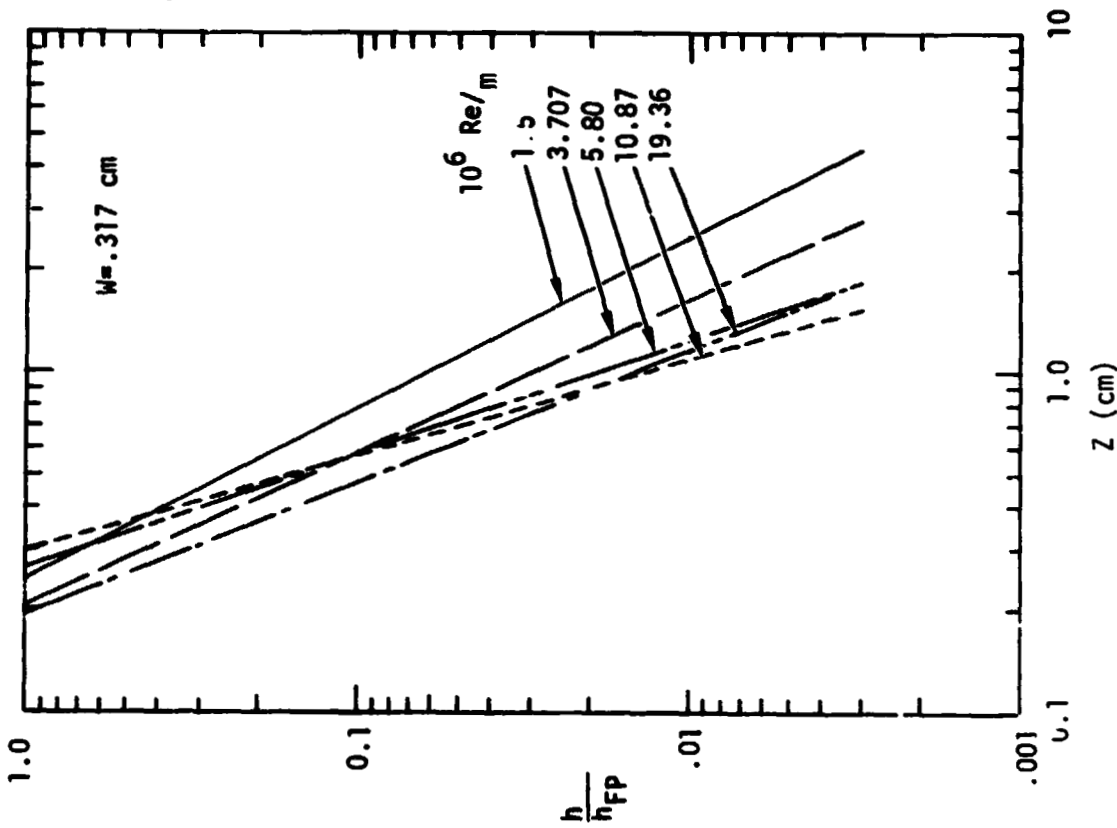


Figure 124

 RSI GAP HEATING
ANALYSIS

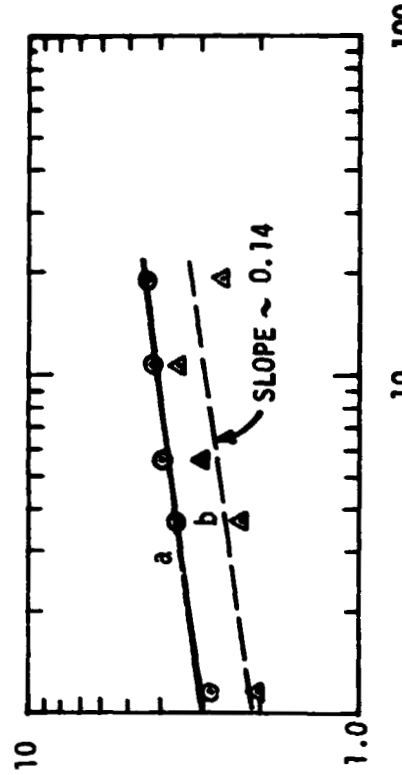
DEVELOPMENT OF CORRELATION FOR HEATING IN TRANSVERSE GAP FOR
TURBULENT BOUNDARY LAYERS IN M - 8 V.D.T. ("Z AND Re/METER ")



$$\ln \frac{h}{h_{FP}} = -a - b \ln z$$

FINAL REPORT
VOLUME I

REPORT MDC E1003
29 JANUARY 1974



$$\frac{h}{h_{FP}} = g_4 \left[z^{(g_5 Re)^{14}} \right] \left[\frac{Re}{10^6 \text{ METER}} \right]^{g_6}$$



**CORRELATION EQUATIONS FOR TRANSVERSE GAP IN TURBULENT
BOUNDARY LAYERS (CFHT AND $M_\infty = 8$, CENTERLINE OF TILES)**

**FINAL REPORT
VOLUME I**

REPORT MDC E1003
29 JANUARY 1974

TESTS CONSIDERED	EQ. NO.	DEP. VAR.	EQUATION	NATURAL LOG			CARTESIAN			COMMENTS
				R	S	R	S	R	S	
$M = 8$, CFHT	18	$\ln \frac{h}{h_{REF}}$	$-3.04954 - 1.13556 W^{-2/7} \ln Z$ $-5.92101 - 1.25543 W^{-2/7} \ln Z - 2.68084 \ln \frac{T_w}{T_e}$ $\left(-5.47019 - 1.30869 W^{-2/7} \ln Z - 2.90719 \ln \frac{T_w}{T_e} \right)$ $-.53548 \ln Re_L$.8377	.7392	.6809	.1336	60 DATA POINTS		
SELECTED →										
$-4.28021 - 1.46402 W^{-2/7} \ln Z - 2.5490 \ln \frac{T_w}{T_e}$ $-.53620 \ln Re_L + .7806 \ln W$ $\ln Z + \ln Z / W + \ln Z + W^2 \ln Z + Re_L \cdot 14 \ln Z$										
Additional terms omitted by F-Test										

Z = DISTANCE FROM TILE SURFACE (cm)
 W = GAP WIDTH (cm)
 Re_L = LOCAL REYNOLDS NUMBER/ 10^6 METERS
 T_w = WALL TEMPERATURE (OK)
 T_e = TOTAL TEMPERATURE (OK) AT EDGE OF BOUNDARY LAYER

R = MULTIPLE REGRESSION COEFFICIENT
 S = STANDARD ERROR OF ESTIMATE
 T_w = WALL TEMPERATURE (OK)

Figure 126



FINAL REPORT
VOLUME I

REPORT MDC E1003
29 JANUARY 1974

RESIDUALS (\ln) FOR CORRELATION TRANSVERSE GAP
IN TURBULENT BOUNDARY LAYER
($M_\infty = 8$ AND CFHT), EQUATION 18

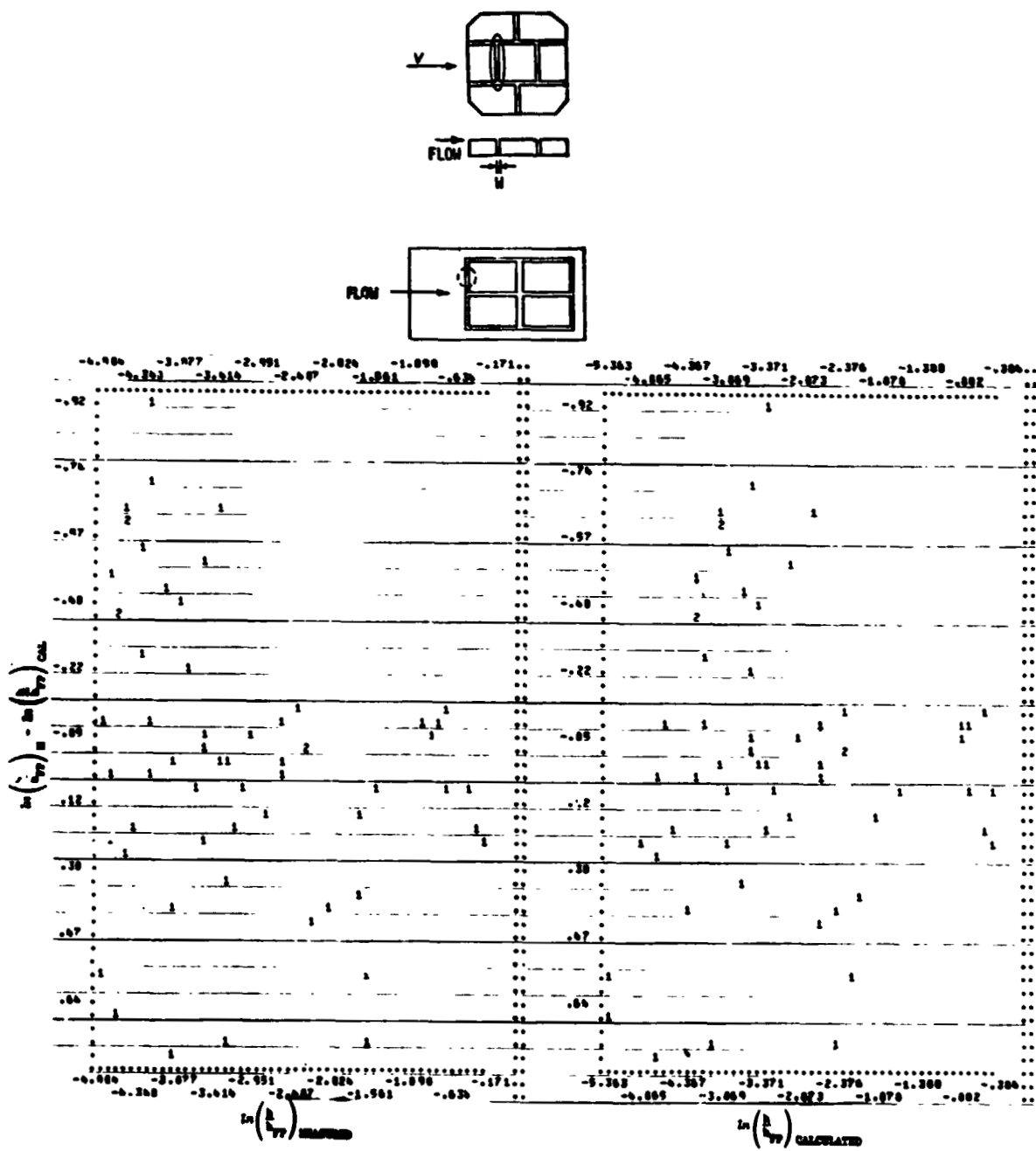


Figure 127



FINAL REPORT
VOLUME I

REPORT MDC E1003
29 JANUARY 1974

RESIDUALS (CARTESIAN) FOR CORRELATION OF TRANSVERSE
GAP IN TURBULENT BOUNDARY LAYER
($M_\infty = 8$ AND CFHT TESTS), EQUATION 18

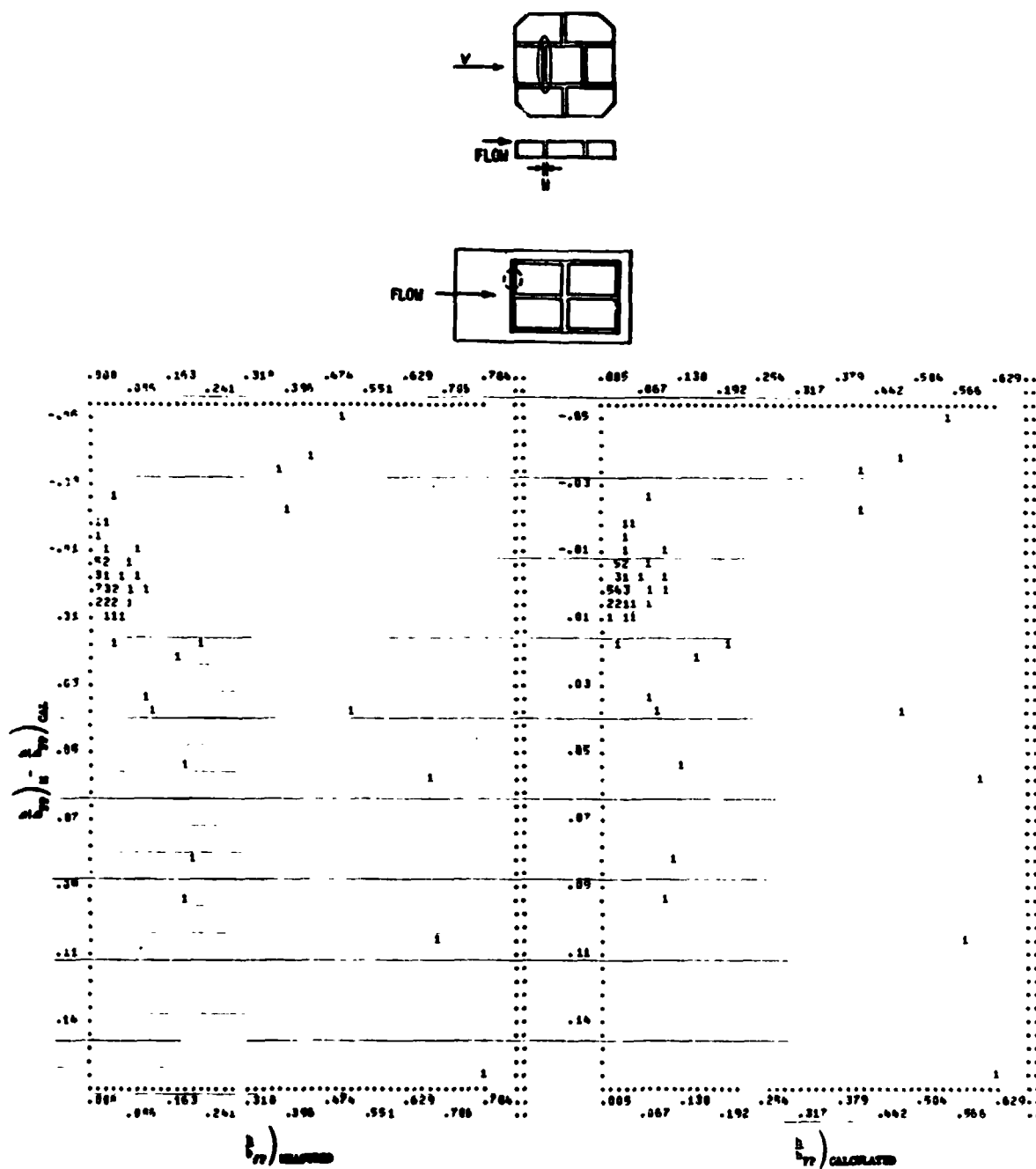
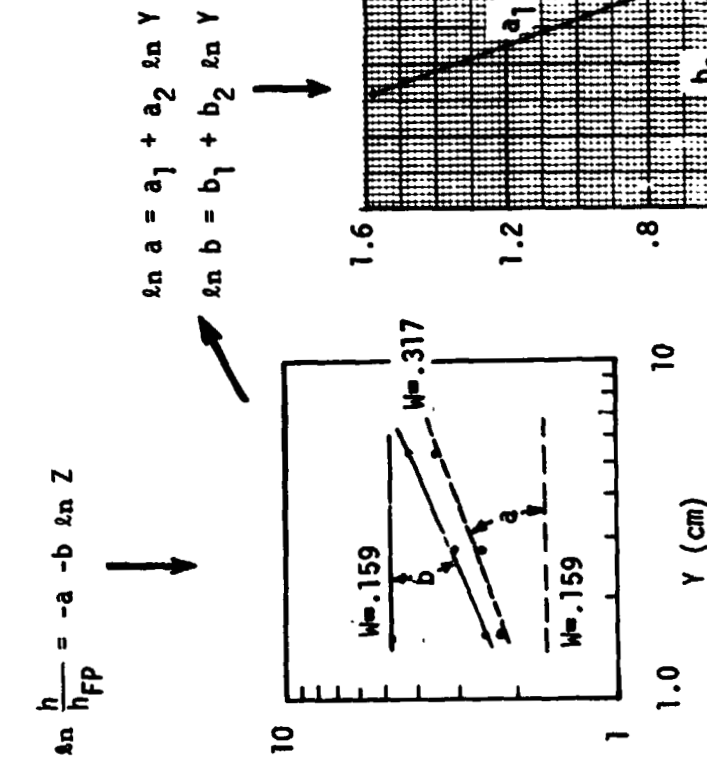
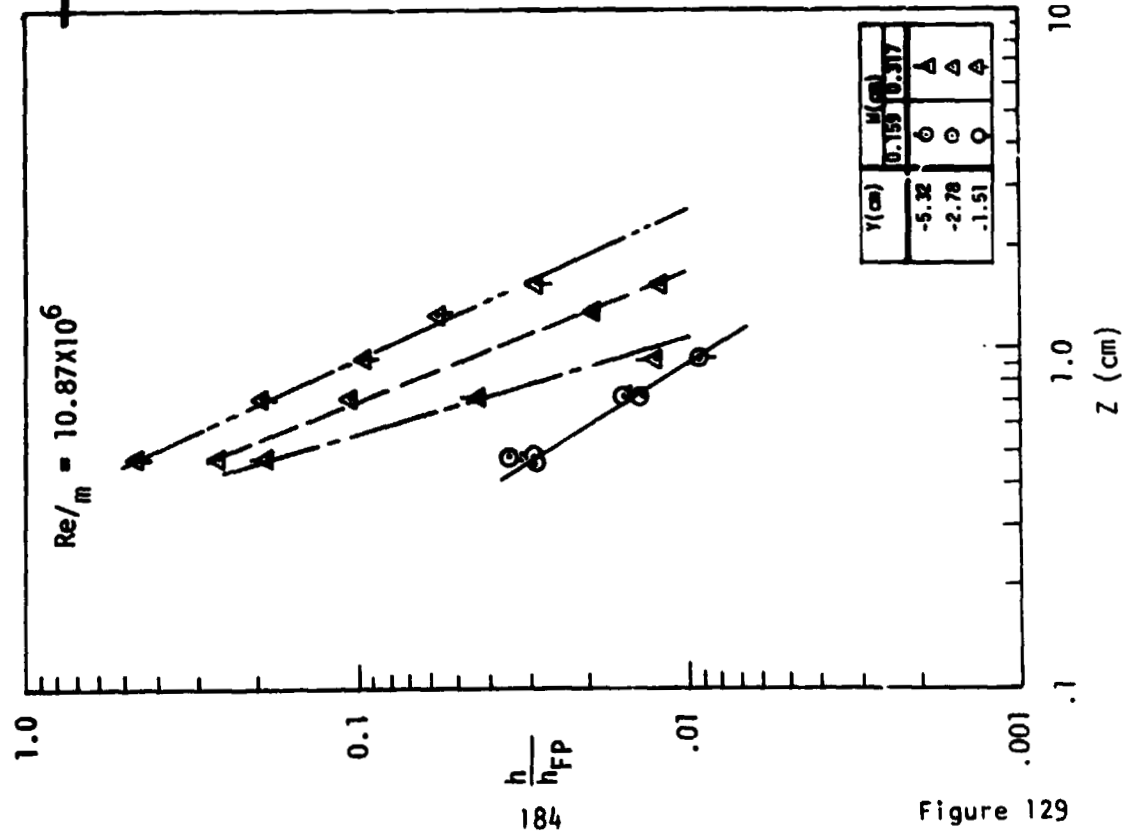


Figure 128



DEVELOPMENT OF A CORRELATION FOR HEATING IN TRANSVERSE GAP FOR TURBULENT BOUNDARY LAYERS IN $M = 8$ V.D.T. -- (Z, Y, AND W)



FINAL REPORT
VOLUME I

REPORT MDC E1003
29 JANUARY 1974



FINAL REPORT
VOLUME I

REPORT MDC E1003
29 JANUARY 1974

5.4 Correlation of CFHT Data, Effects of Flow Angle and Steps - Two types of correlation were performed on the CFHT data in the study of flow angle on gap heating. In one approach, maximum and average heating ratios were examined for the tile top and the walls of the gap. In the other approach, data were correlated using Multiple Regression Techniques.

5.4.1 Correlation of Maximum and Average Heating, CFHT - The CFHT tests provided data on the top and four sides of a thin skin tile as a function of gap width, flow angle, and step height. Average heating rates for the top of the tile and on each of the four sides at 0.3 cm into the gap were computed and are presented as functions of the test parameters. The average heating on top of the tile is shown in Figure 130. Step height has a greater effect on average heating than either gap width or flow angle for the range of parameters tested. For flush tiles, increasing gap width increases the average surface heating. For tiles with a positive 0.25 cm step height, the average heating reached a maximum at a gap width of 0.46 cm or approximately twice the step height. The sensitivity of average surface heating to flow angle increases as step height is increased. The average heating is not affected by flow angle when the tile is recessed (negative 0.17 cm step height). Data were taken for a gap width of 0.23 cm only at this step height. For flush tiles the heating is insensitive to flow angle between 0 and 30 degrees. The average surface heating increases when the flow angle increases above 30 degrees. For the positive step tiles, any flow angle greater than 0 degrees resulted in higher average heating to the top of the tile. The maximum heating that was measured on the top of the tile is shown in Figure 131. A positive step height (+0.25 cm) resulted in a significant increase in maximum surface heating. For some gap width/flow angle conditions the maximum surface heating on the positive step tile was twice that measured on a flush tile. For flush tiles, increasing gap width increases the maximum surface heating. For tiles with a positive step, the maximum heating increases as the gap width increases up to 0.46 cm. The effect of increasing the gap width above 0.46 cm on maximum surface heating varies with flow angle, but generally the maximum heating does not increase. For tiles with negative step heights, there is little effect of flow angle at the gap width tested ($W = 0.23$ cm). The flush tiles experienced an increase in maximum surface heating with increasing flow angle up to approximately 30 degrees. Further increases in flow angle had little effect on maximum surface heating. The tiles with a positive step show great sensitivity to flow angle at all gap widths. The maximum heating to the top of the tile occurs at a flow angle of 45 degree.

AVERAGE HEATING ON TOP OF THE TILE CFHT TEST

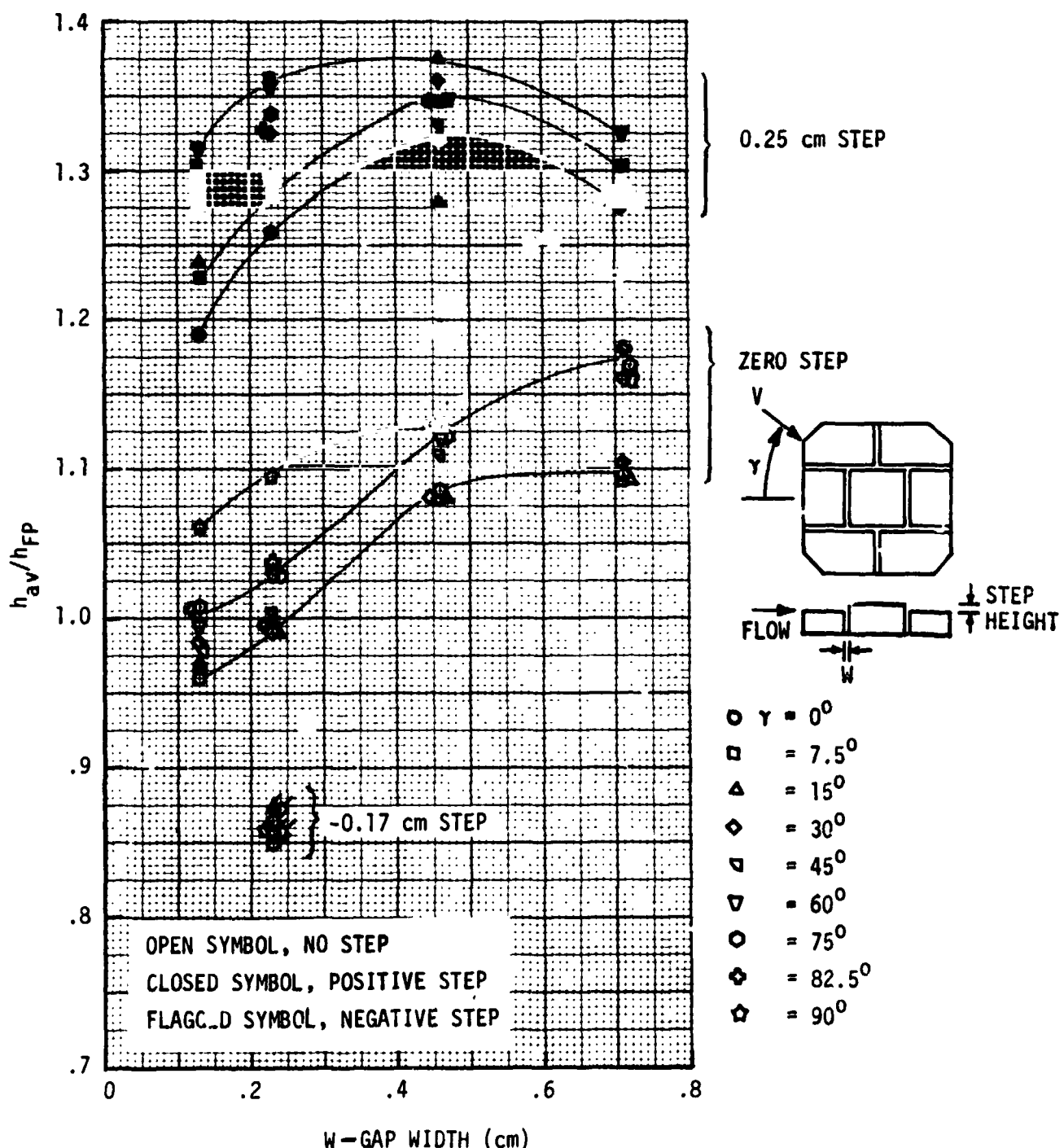


Figure 130

MAXIMUM HEATING ON TOP OF TILE CFHT TESTS

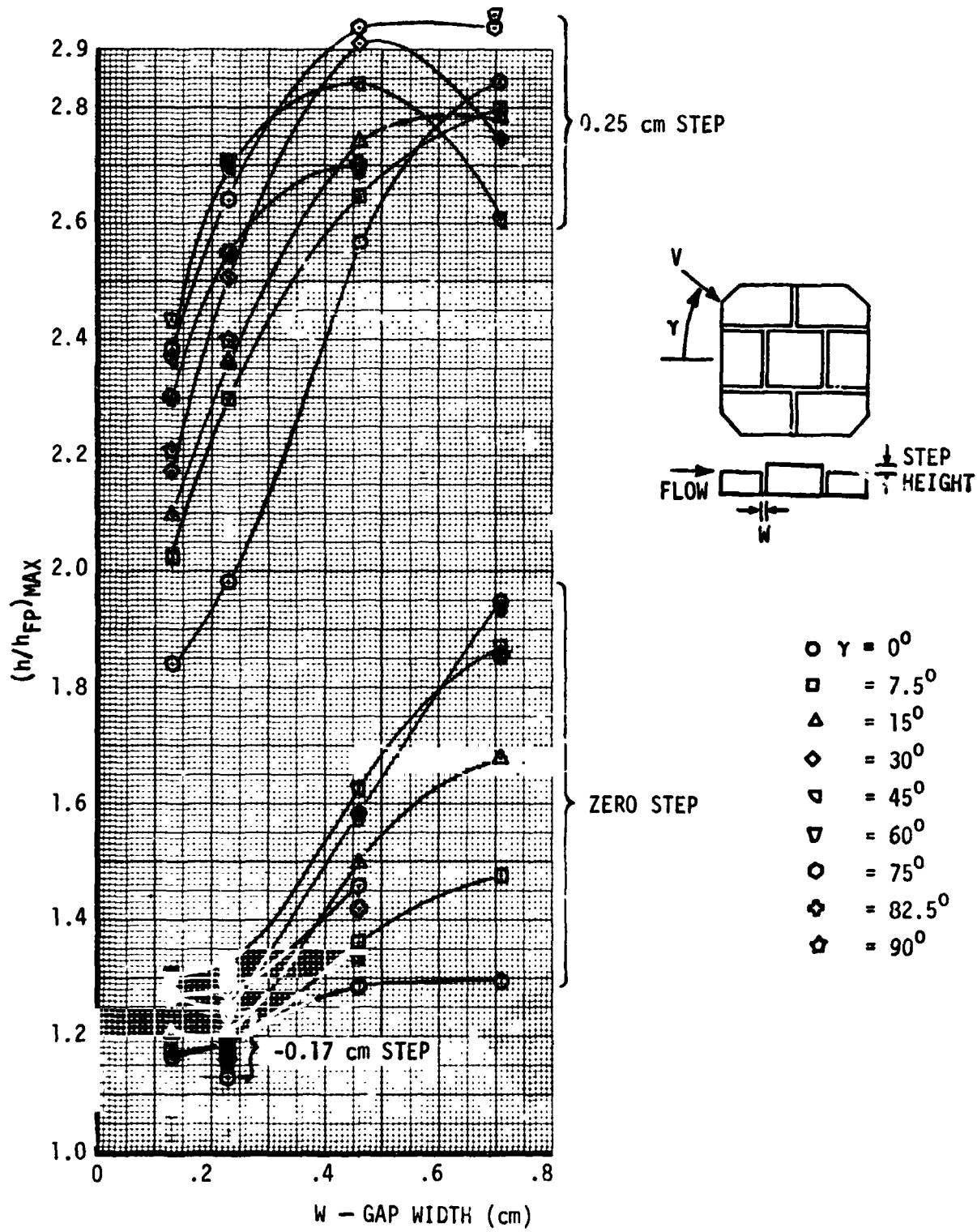


Figure 131



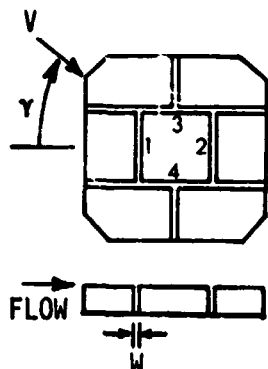
FINAL REPORT
VOLUME I

REPORT MDC E1003
29 JANUARY 1974

The average heating on the four sides of flush tiles at 0.3 cm into the gap summarized in Figure 132. Data are presented for all flow angles as a function of gap width. The average heating on the downstream sides of the gap (1 and 3) is consistently higher than the average heating on the upstream sides of the gap (2 and 4) as γ varies from 0° to 90° . The effect of gap width on average heating is more pronounced on the downstream sides (1 and 3) than on the upstream sides (2 and 4). The general effect was for average gap heating to increase with increasing gap width. The effect of gap width and flow angle on average gap heating was examined more closely in Figures 133 and 134. Figure 133 shows the average heating for sides 1 and 2 as a function of flow angle f - all gap widths tested. The downstream side of the gap (1) is significantly affected by gap width while the upstream side (2) is fairly insensitive to gap width for flow angles between 0° and 70° . As the flow approached 90° sides 1 and 2 become inline gap faces and are both affected by changes in gap width. Figure 134 presents average heating for sides 3 and 4. Similar conclusions can be shown from this figure as were drawn from Figure 133.

The sensitivity of the average gap heating at 0.3 cm down the gap to step height is presented in Figures 135 thru 138 for sides 1, 2, 3 and 4, respectively. Average heating for side 1 (Figure 135) is presented as a function of flow orientation for the step heights and gap widths tested. The shaded areas represents the flush tile data that was previously presented in Figure 133. The positive step height data shows significantly higher side 1 average heating than the flush tile data. The sensitivity of side 1 average heating to gap width and flow orientation is enhanced when the tile has a positive step. The negative step data indicate lower average heating than for flush tiles at all flow orientations. The average heating 0.3 cm down the gap for side 2 is shown in Figure 136. The effect of step height on side 2 average heating is minimal for the lower flow angles. As the flow angle approaches 90° , side 2 becomes part of an inline gap and the effect of step height becomes more pronounced. Also the effect of gap width on average heating to side 2 becomes greater as the flow angle approaches 90° . The average heating to side 3 at 0.3 cm down the gap is presented in Figure 137. Side 3 average heating trends are much the same as those discussed for side 1. Similarly, the average heating to side 4 at 0.3 cm down the gap (Figure 138) indicates the same trends as side 2 average heating.

AVERAGE HEATING ON SIDES OF TIL'S AT 0.3 CM INTO GAP (ZERO STEP) CFHT TESTS



DATA FOR FLOW ANGLES OF:
 $\gamma = 0, 7.5, 15, 30, 45,$
 $60, 82.5 \text{ & } 90 \text{ DEGREES}$

SIDES 1 AND 3 HAVE CLOSED SYMBOLS
 SIDES 2 AND 4 HAVE OPEN SYMBOLS
 SIDE 2 DOES NOT HAVE 90° DATA

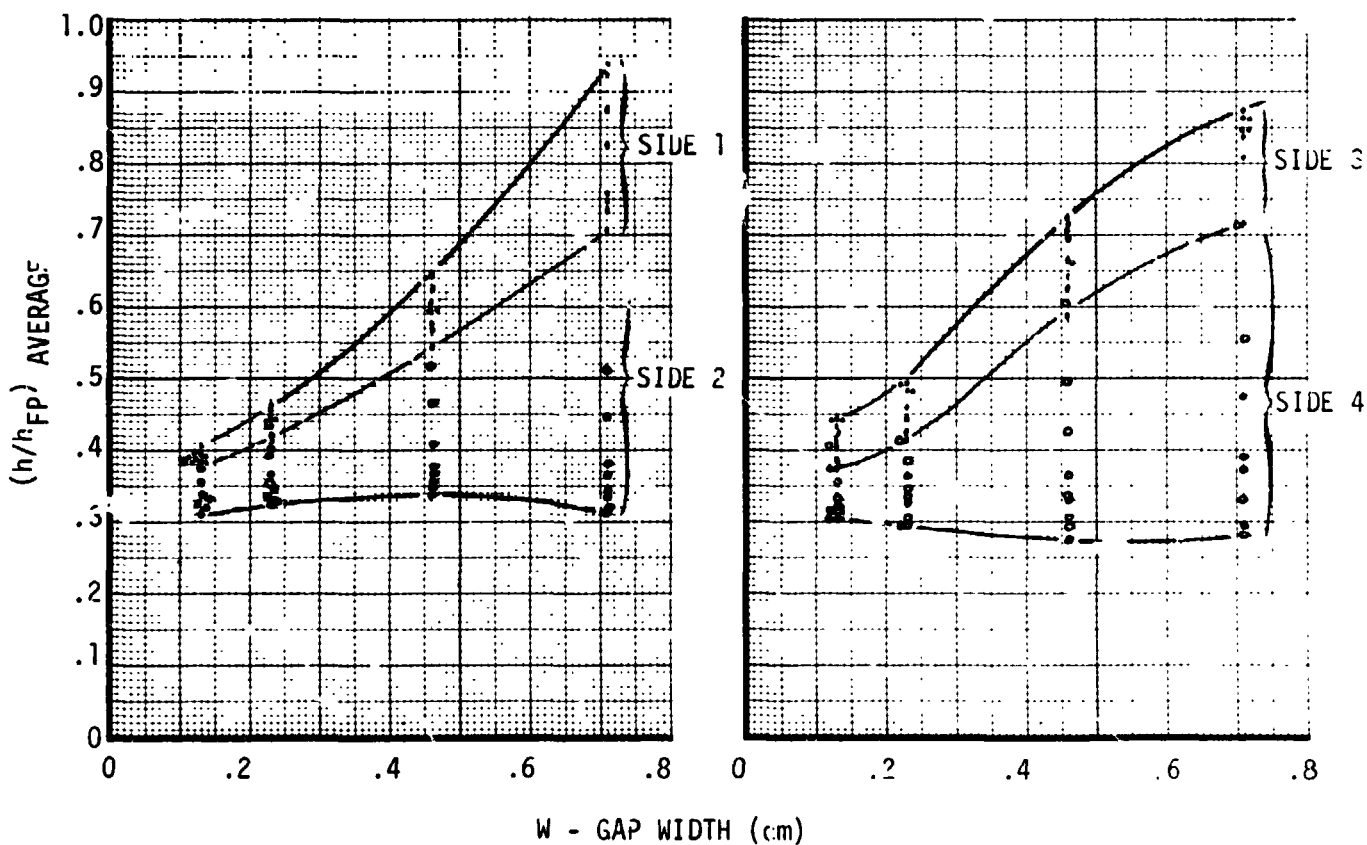


Figure 132

AVERAGE HEATING ON SIDES OF TILES AT 0.3 CM
INTO GAP (ZERO STEP) CFHT TESTS

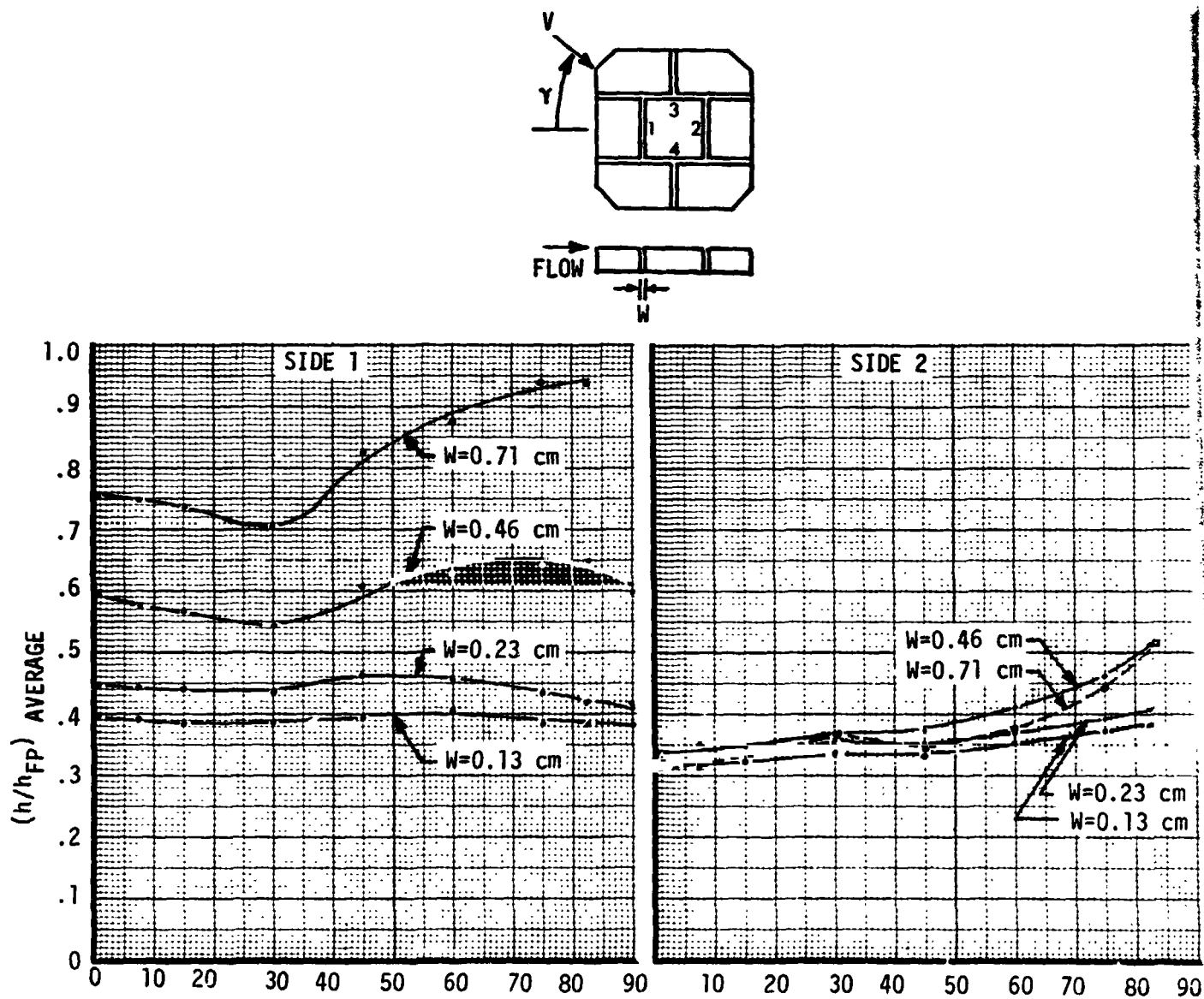
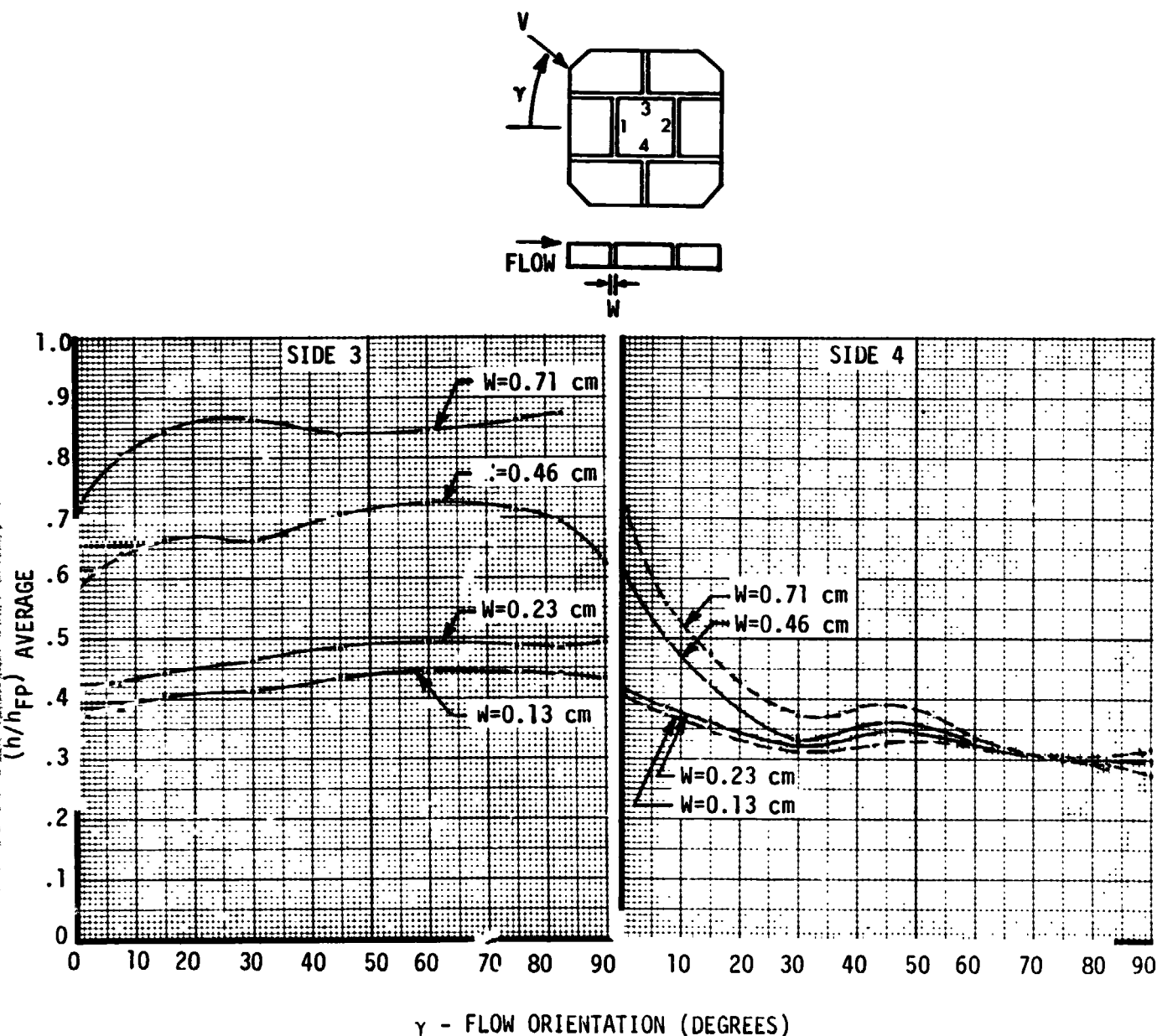


Figure 133

γ - FLOW ORIENTATION (DEGREES)

**AVERAGE HEATING ON SIDES OF TILES AT 0.3 CM
INTO GAP (ZERO STEP) CFHT TESTS**

Figure 134

SENSITIVITY OF AVERAGE GAP HEATING TO STEP HEIGHT
AND FLOW ORIENTATION AT 0.3 CM DOWN SIDE 1 OF
CENTER TILE CFHT TEST

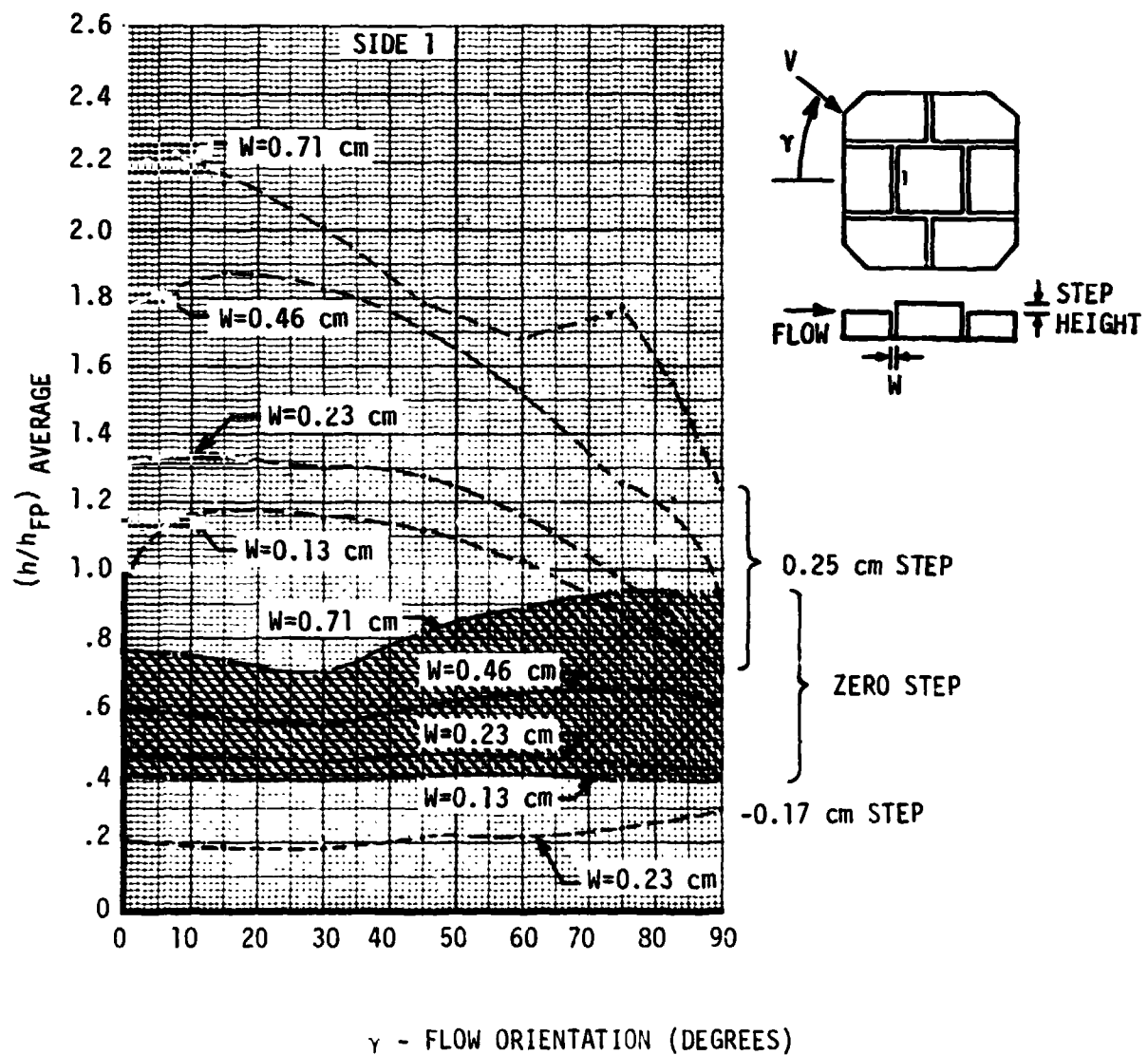


Figure 135

**SENSITIVITY OF AVERAGE GAP HEATING TO STEP HEIGHT
AND FLOW ORIENTATION AT 0.3 CM DOWN SIDE 2 OF
CENTER TILE CFHT TEST**

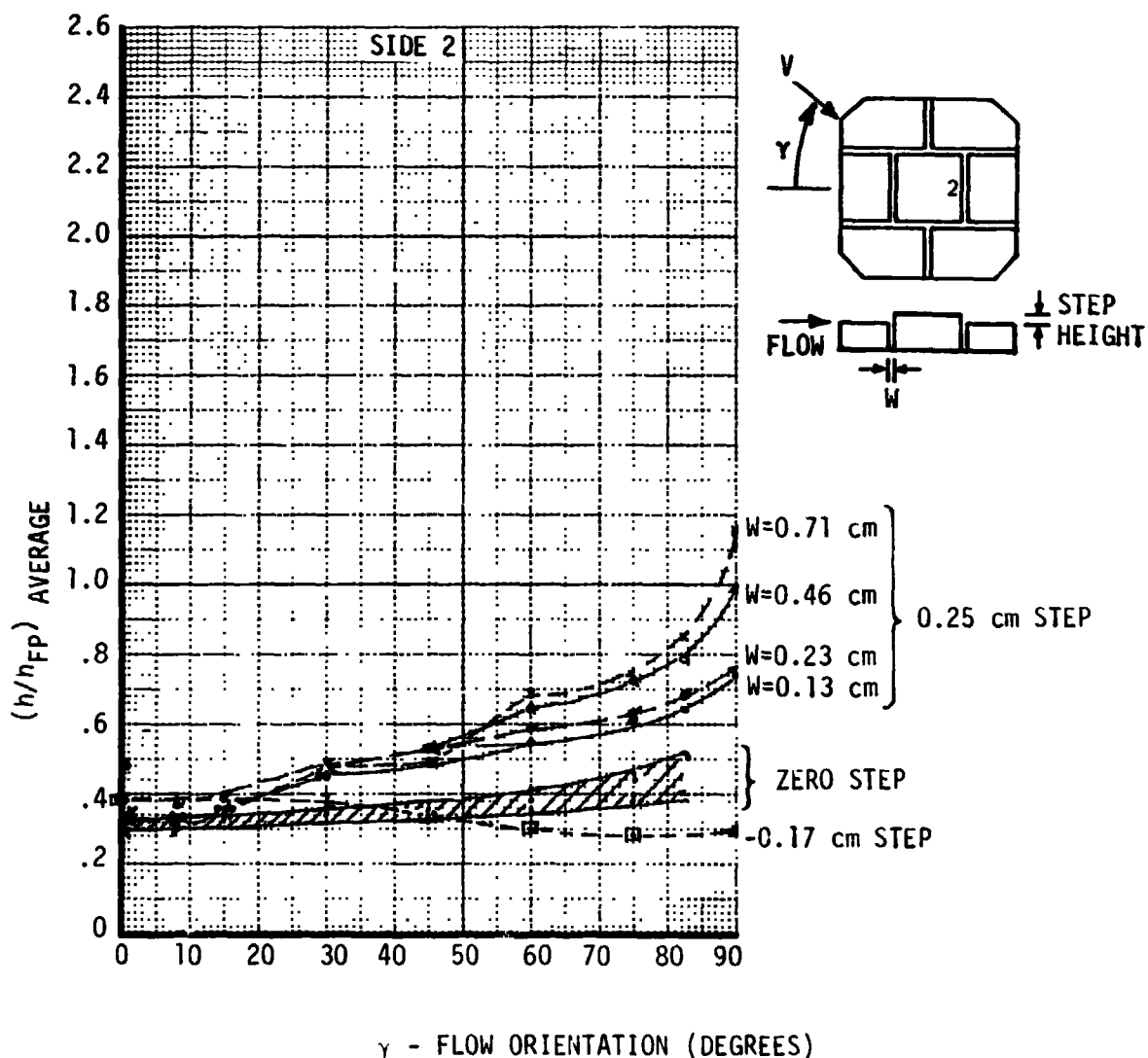


Figure 136

SENSITIVITY OF AVERAGE GAP HEATING TO STEP HEIGHT
AND FLOW ORIENTATION AT 0.3 CM DOWN SIDE 3
OF CENTER TILE CFHT TEST

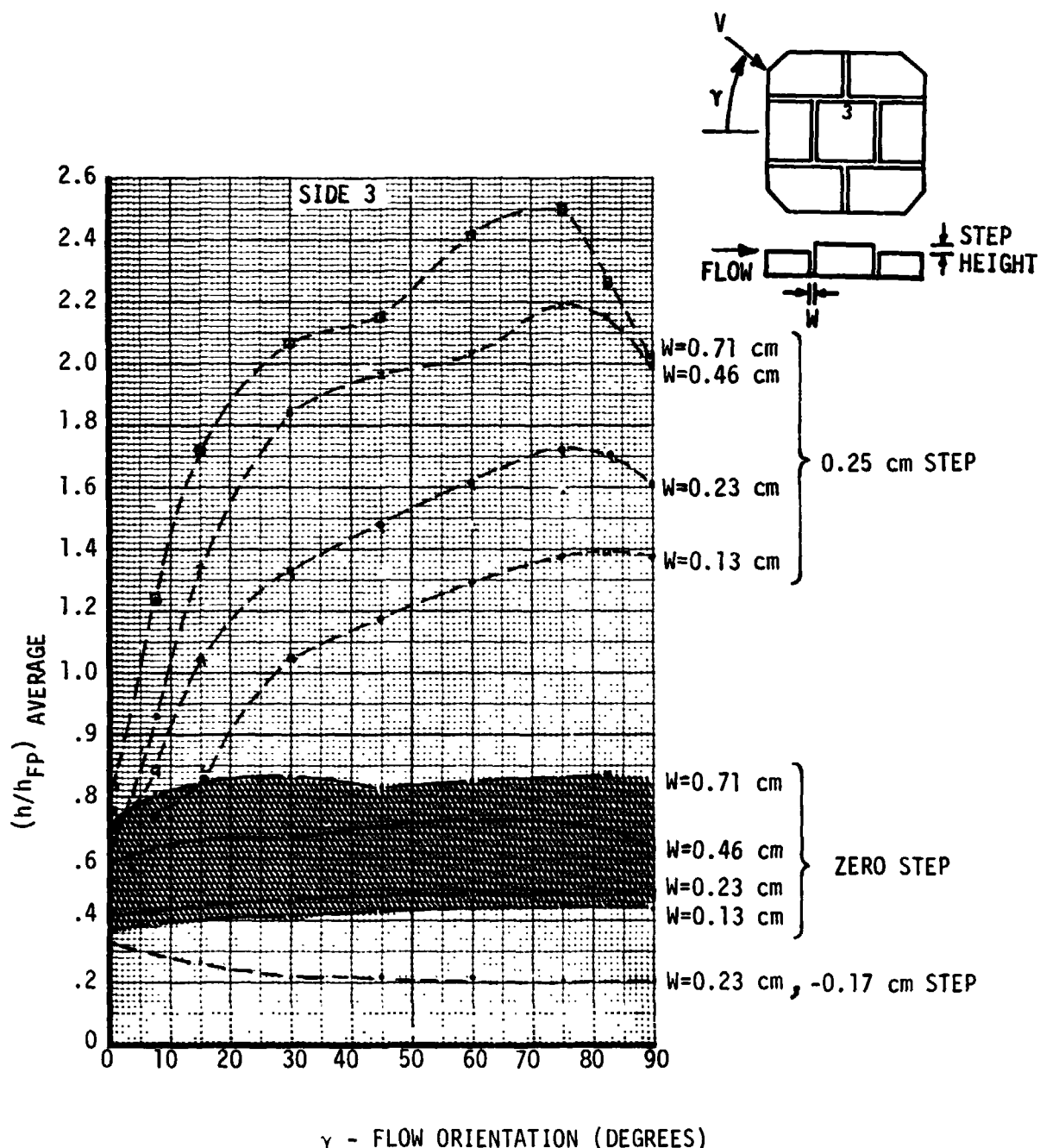


Figure 137

**SENSITIVITY OF AVERAGE GAP HEATING TO STEP HEIGHT
AND FLOW ORIENTATION AT 0.3 CM DOWN SIDE 4
OF CENTER TILE CFHT TEST**

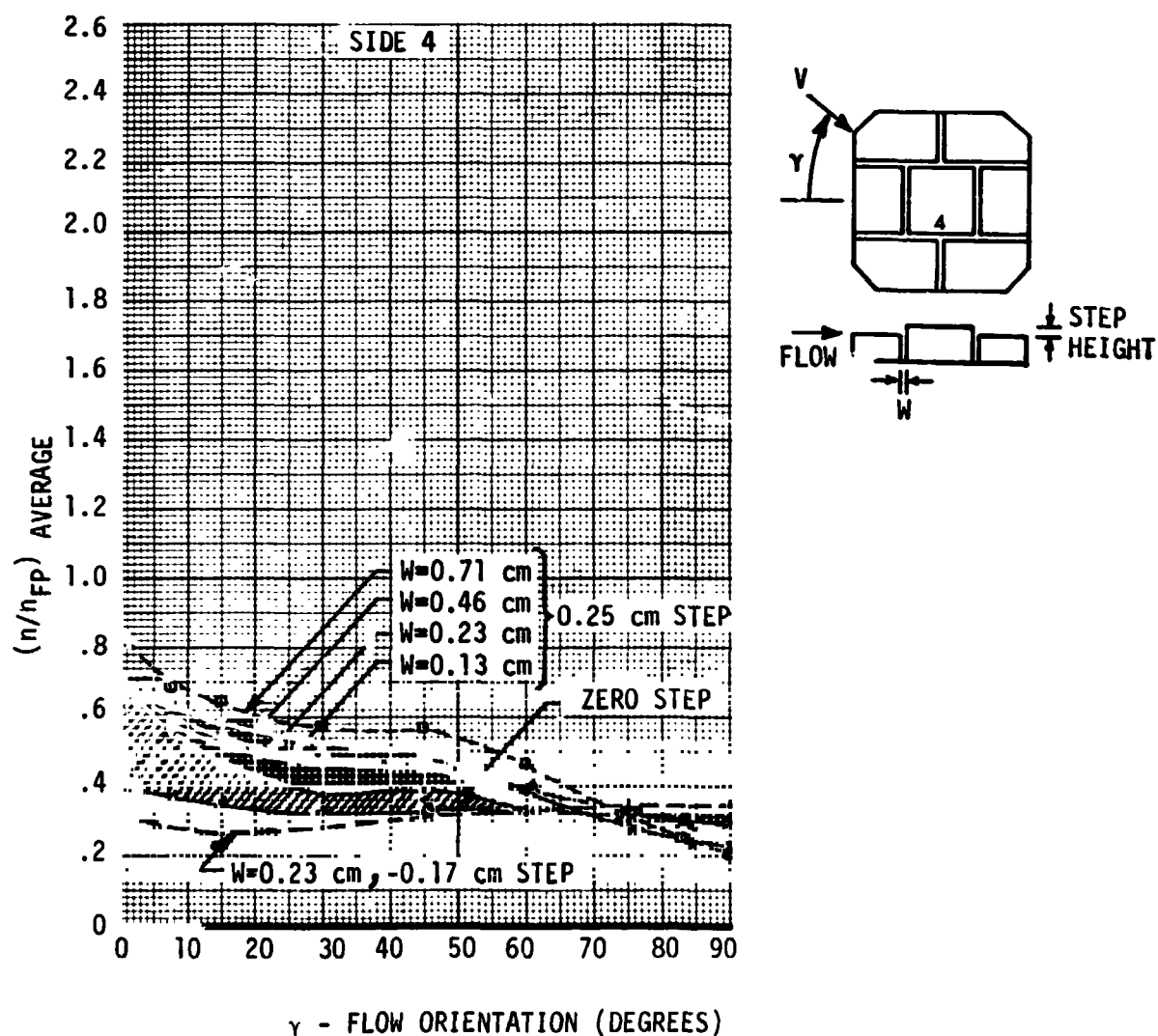


Figure 138



FINAL REPORT
VOLUME I

REPORT MDC E1003
29 JANUARY 1974

5.4.2 Correlation of CFHT Gap Heating Distribution with Flow Angle - Data from the CFHT were investigated to determine the influence of distance into the gap (Z), gap width (W), distance along the gap (Y) and flow orientation (γ) on gap heating. Figure 139 lists the variables considered and the equation forms investigated. Correlations for the top row of thermocouples as well as for all thermocouples were studied. The correlation for all instrumentation is contained in subsequent figures. Using the top row of instrumentation did not improve the correlations. The polynomial function (I) was superior to the trig function II. Hence only results using the polynomial function are presented. Figure 140 summarizes the development of the correlating function (12A) and Figure 141 and 142 are the residual plots. Some 458 data points were used and a high correlation coefficient (0.977) was obtained but the standard error of estimate was also undesirably large (0.3266). Additional correlation activities are warranted for these data. The form of the correlation equation should be investigated further as indicated in Figures 143 and 144. The heating in the gap at 30° and 60° exhibit similar exponential functions of distance into the gap.

5.5 Correlation Conclusions for Turbulent Boundary Layer Tests - Several conclusions can be drawn from the correlation of heating data for transverse gaps for turbulent boundary layers. The correlation equations show the influence of gap geometry and boundary layer parameters on gap heating. Data from CFHT and M=8 tunnels were correlated.

- o CFHT (Equation 16)

$$\frac{h}{h_{FP}} = 0.1757 \left(Z^{-1.74W^{-2/7}} \right) \left(W^{1.2} \right) \left(e^{0.0849 \left[\ln Z/W \right]^3} \right)$$

- o CFHT and M=8 (Equation 18)

$$\frac{h}{h_{FP}} = 0.01384 \left(Z^{-1.464W^{-2/7}} \right) \left(\frac{T_w}{T_e} \right)^{-2.549} \left(\frac{Re}{10^6 \text{ meter}} \right)^{-0.5362} \left(W^{0.7806} \right)$$

- o For flush tiles, the average heating on top of the tile increases with gap width and increase when flow orientation (γ) is greater than 30° .
- o Protruding tiles experience higher average heating than flush tiles while recessed tiles have a lower average heating rate.
- o Maximum heating on top of tiles increases with gap width and increases more significantly at (γ) between 45° and 60° .



**RSI GAP HEATING
ANALYSIS**

**FINAL REPORT
VOLUME I**

**REPORT MDC E1003
29 JANUARY 1974**

- o Average heating in gaps around four sides of a tile
 - oo Average heating on upstream side of gap is insensitive to " γ " and "W"
 - oo Average heating on downstream side of gap is fairly insensitive to " γ " and is a strong function of gap width
 - oo Average heating on downstream side of gap is much higher at all " γ " when tile is protruding. Effect is less for upstream side of gap
 - oo Recessing the tile, generally decreases average heating on tile sides
 - oo Heating distributions on side of tile are affected by " γ "

CORRELATIONS INVESTIGATED FOR EFFECT OF "Y" ON HEATING IN TRANSVERSE GAP

OO VARIABLES CONSIDERED:

DISTANCE INTO GAP - - - - - Z

GAP WIDTH - - - - - W

DISTANCE ALONG GAP - - - - Y

"Y" FLOW ORIENTATION - - - A

OO DATA INVESTIGATED (CFHT TESTS)

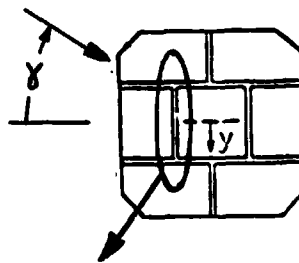
ALL INSTRUMENTATION ($0 < z < 4$ cm)

TOP ROW OF INSTRUMENTATION ($z \approx 0.3$ cm)

OO CANDIDATE FUNCTIONS

I

$$\frac{H}{H_{FP}} = e^{\left\{ (C_0 + C_1 A + C_2 A^2) (C_3 + C_4 W + C_5 W^2) (C_9 + C_{10} Y + C_{11} Y^2) (C_{12} + C_{13} Z + C_{14} Z^2) \right\}}$$



II

$$\frac{H}{H_{FP}} = e^{\left[1 + (a + bY + cY^2) \sin 2A \right] \left[d + eZ + fZ^2 \right] \left[h + iW \right]}$$

Figure 139



**CORRELATION EQUATIONS FOR TRANSVERSE GAP
ROTATED THROUGH $\pi/2$ RADIANS**

**FINAL REPORT
VOLUME I**

**REPORT MDC E1003
29 JANUARY 1974**

TESTS CONSIDERED	EQ. NO.	DEP. VAR.	EQUATION	NATURAL LOG			CARTESIAN			COMMENTS
				R	S	R	S	R	S	
CFHT { TOP 3 T/C IN GAP	12A	$\frac{H}{H_{FP}}$	$-1.07817 - 1.11615Z$ $0.27211 - 3.44061Z + 0.59668Z^2$ $-0.36298 - 3.56164Z + .58664Z^2 + 1.91514W$ $-0.35296 - 3.57726Z + .58853Z^2 + 1.91204W + .06633YW$ $(-0.1054 - 3.71478Z + .60432Z^2 + 1.92179W - .00692Y^2 + 0.04315YW + .01768YG + .00235YZ)$.8142	.8829	.6288	.2029	458 DATA POINTS		



Z = DISTANCE FROM TILE SURFACE
W = GAP WIDTH
Y = DISTANCE ALONG GAP
G = FLOW ORIENTATION

Figure 140

 RSI GAP HEATING
ANALYSIS

FINAL REPORT
VOLUME I

REPORT MDC E1003
29 JANUARY 1974

RESIDUALS (\ln) FOR TRANSVERSE GAP
ROTATED 0 TO $\pi/2$ (CFHT TESTS, $0 < z < 4$ CM),
EQUATION 12A (POLYNOMIAL)

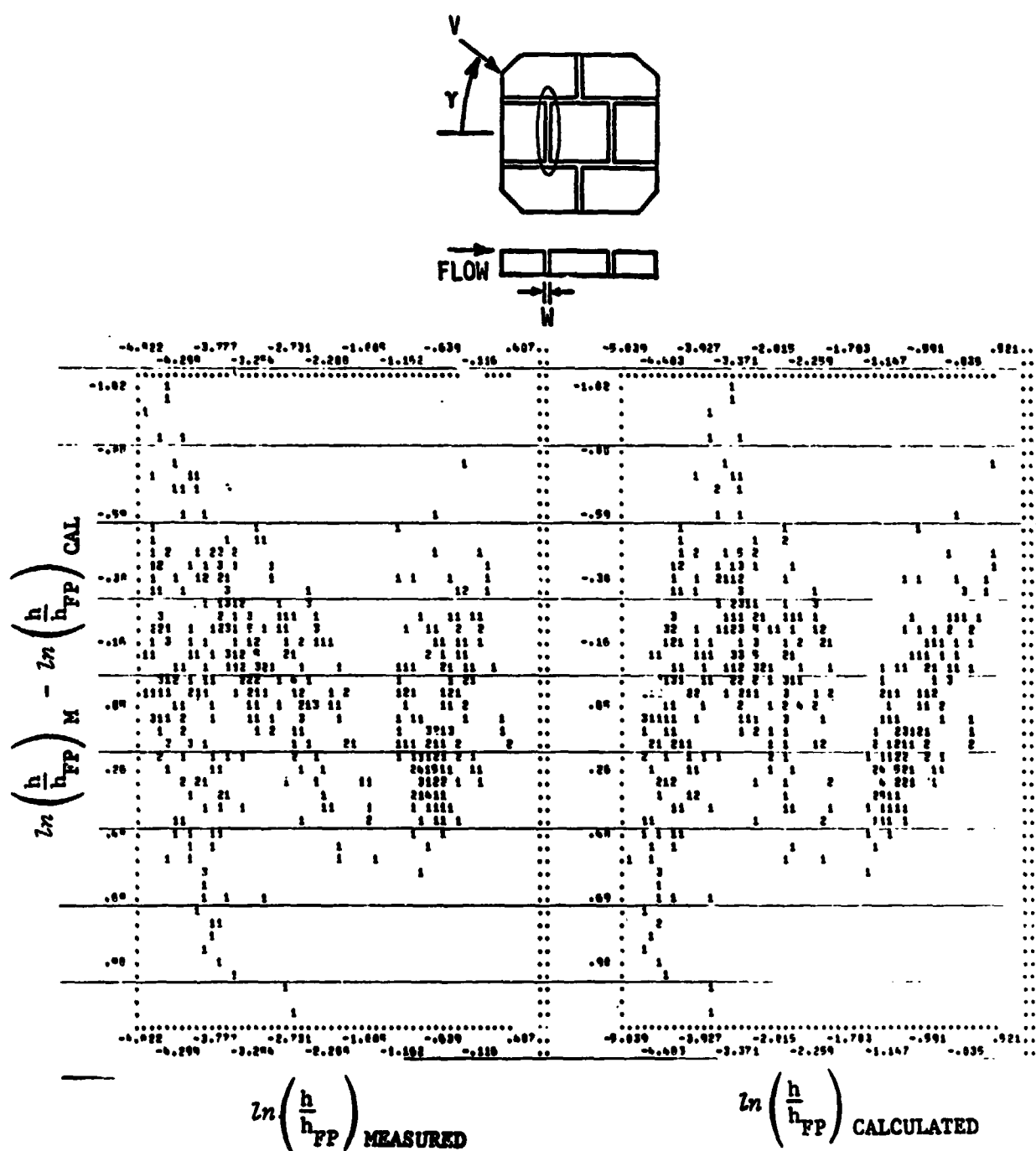


Figure 141

 RSI GAP HEATING
ANALYSIS

FINAL REPORT
VOLUME I

REPORT MDC E1003
29 JANUARY 1974

RESIDUALS (CARTESIAN) FOR TRANSVERSE GAP
ROTATED 0 TO $\pi/2$
(CFHT TESTS, $0 < Z < 4$ CM), EQUATION 12A

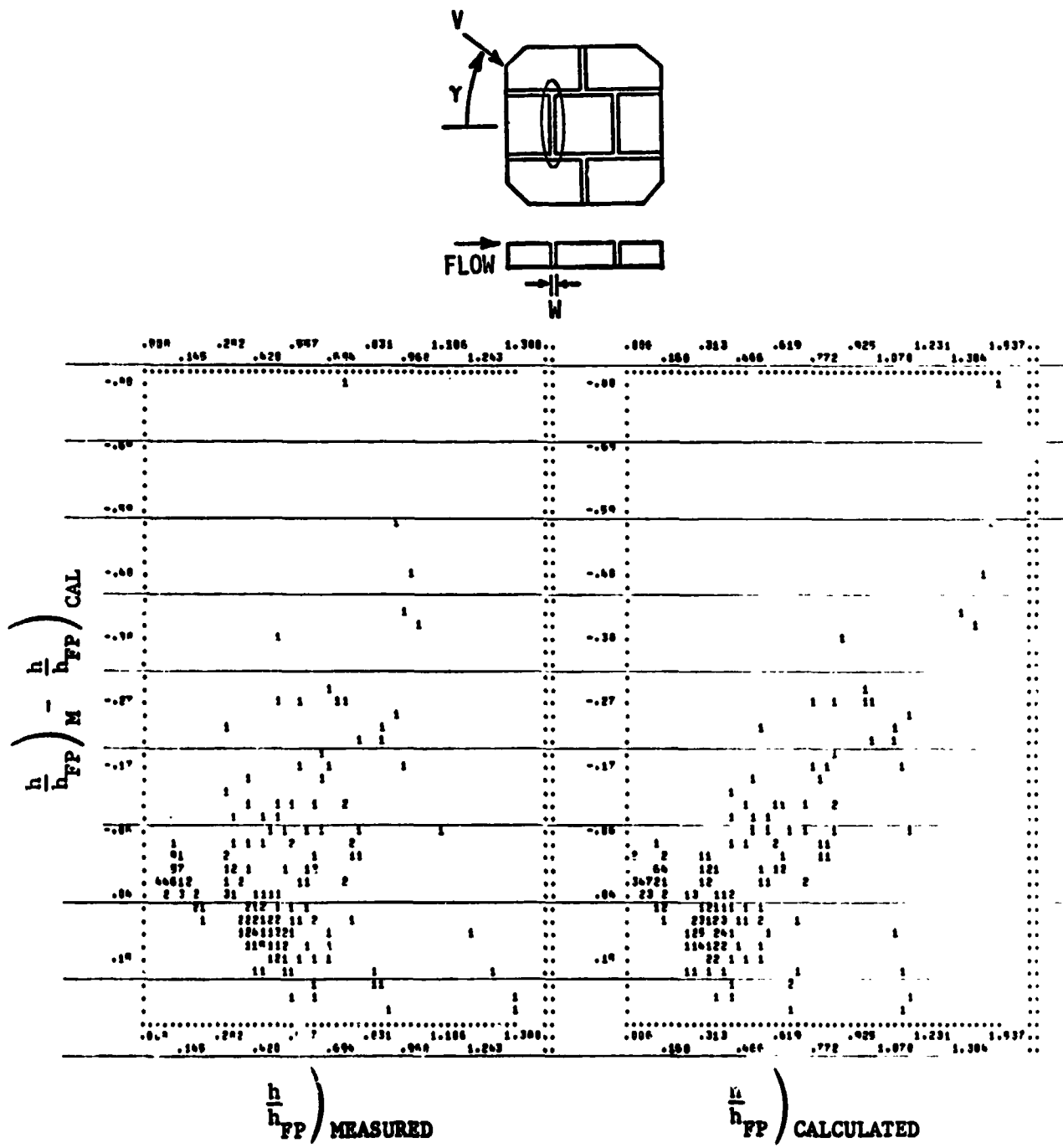


Figure 142

**HEATING IN TRANSVERSE GAP, FLOW ORIENTED AT
.52 RADIANS (30°), FOR A TURBULENT BOUNDARY LAYER**

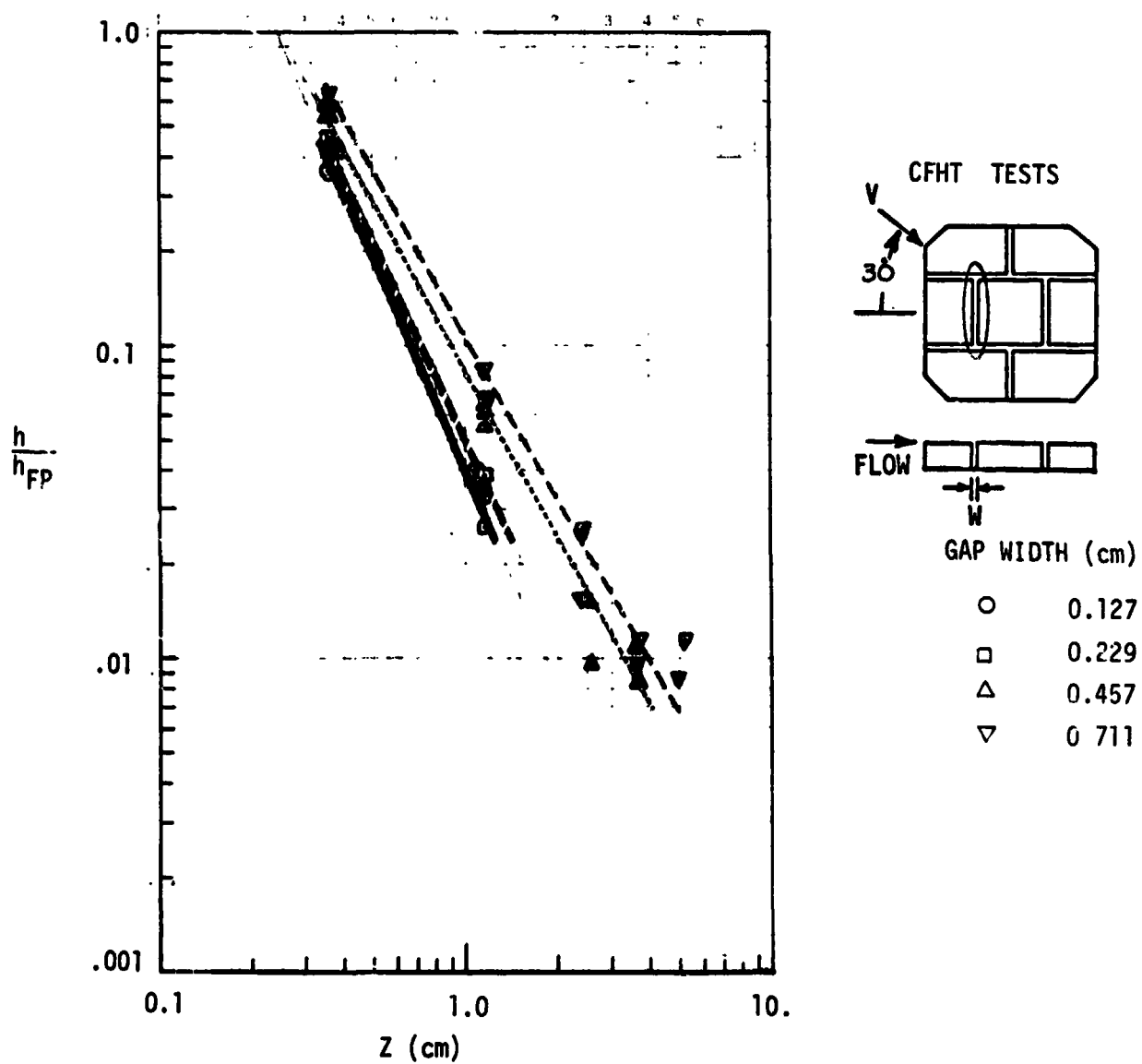


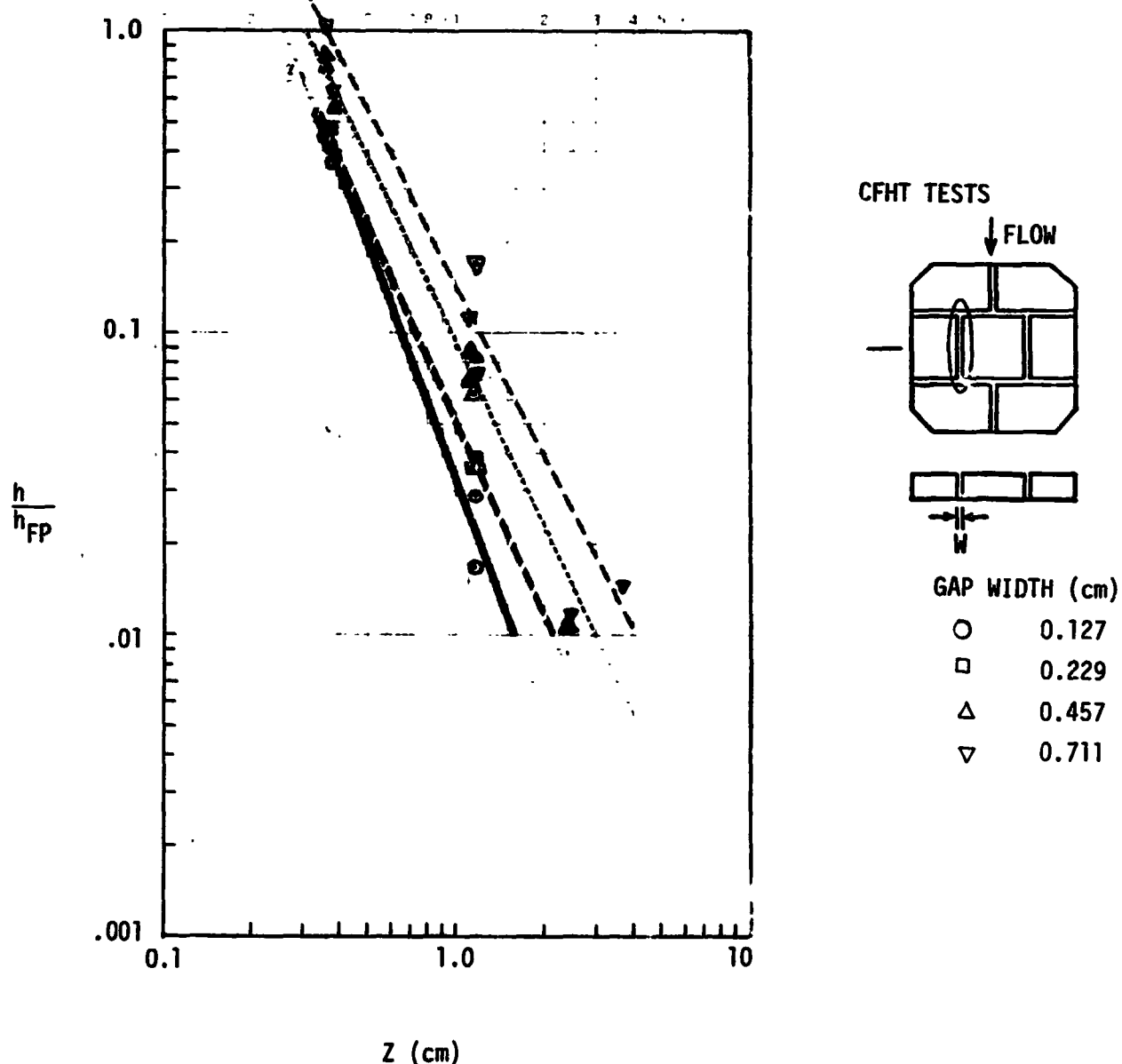
Figure 143

 RSI GAP HEATING
ANALYSIS

FINAL REPORT
VOLUME I

REPORT MDC E1003
29 JANUARY 1974

HEATING TRANSVERSE GAP, FLOW ORIENTED AT
 $\pi/2$ RADIANS, FOR A TURBULENT BOUNDARY LAYER





FINAL REPORT
VOLUME I

REPORT MDC E1003
29 JANUARY 1974

6.0 FORMULATION OF GAP HEATING CALCULATION PROCEDURE

A general calculation procedure has been designed so that the derived correlations can be used in sizing TPS and determining system performance and structural temperatures. The sets of correlation equations and control logic are setup in a subroutine format so that the package is selfcontained with well defined interfaces and easily identified input and output. The subroutine is designed to be compatable with general heat transfer computer programs such as the MDAC-E HEATRAN and SINDA. The input list consists of the location within the gap where convective heating is to be computed, gap geometry descriptors and boundary layer descriptors. Figure 145 describes the interfaces of the subroutine. The argument list is sized so that the subroutine can be expanded as more correlations are added. The parameters in the argument list will have preset default values to insure proper functioning of the subroutine in the case that parameters are not supplied by the calling program.



FINAL REPORT
VOLUME I

REPORT MDC E1003
29 JANUARY 1974

GAP HEATING SUBROUTINE "GAPH"

- o FORMULATION IS SETUP SO "GAPH" CAN ACCEPT MANY CORRELATIONS
- o SUBROUTINE WORKS WITH HEATRAN AND SINDA

SUBROUTINE GAPH (J, NTAB, ZTAB, QTAB, ARGL)

J = -1 SETS UP SUBROUTINE NAME (HEATRAN, ONLY)
= 0 READS SUBROUTINE INPUT CARDS (HEATRAN, ONLY)
= 1 COMPUTES GAP HEATING

NTAB = NUMBER OF POINTS IN ZTAB (15 MAX)

ZTAB = TABLE OF GAP Z-CORDINATES WHERE HEATING RATES ARE TO BE COMPUTED (15 MAX)

QTAB = TABLE OF COMPUTED HEATING RATES CORRESPONDING TO ZTAB (15 MAX)

ARGL, ARGUMENT LIST (DIMENSIONED TO 25)

ARGL (1) = IBL = BOUNDARY LAYER STATE: 1 = LAMINAR, 2 = TRANSITIONAL,
3 = TURBULENT

ARGL (2) = IGLOC = GAP LOCATION: 1 = UPSTREAM SIDE OF GAP, 2 = DOWNSTREAM
SIDE OF GAP

3 = IN-LINE GAP, 4 = STAGNATION POINT,
5 = TILE TOP

ARGL (3) = ICOR = CORRELATION NUMBER TO BE USED: IF ZERO IBL AND IGLOC
DETERMINE CORRELATION TO BE USED

ARGL (4) = IGAPC = JOINT CONFIGURATION: 1 = BUTT, 2 = COUNToured, 3 = OVERLAP,
4 = INCLINED

ARGL (5) = FOR FUTURE EXPANSION

ARGL (6) = ALPHA = FLOW ORIENTATION (RADIANs)

ARGL (7) = GAPW = GAP WIDTH (cm)

ARGL (8) = GAPD = GAP DEPTH (cm)

ARGL (9) = STEP = STEP HEIGHT (cm)

ARGL (10) = GAPFL = GAP FLOW LENGTH (cm)

ARGL (11) = H0HLOW = LOWER LIMIT ON HEATING RATIO

ARGL (12) = H0HHI = UPPER LIMIT ON HEATING RATIO

ARGL (13) = AMACH = LOCAL MACH NUMBER

ARGL (14) = REPM = REYNOLDS NUMBER/METER

ARGL (15) = DTHK = MOMENTUM THICKNESS (cm)

ARGL (16) = DTHK = DISPLACEMENT THICKNESS (cm)

ARGL (17) = SLYR = SUBLAYER THICKNESS (cm)

ARGL (18) = HFP = HEATING RATE OR HEAT TRANSFER COEFFICIENT FOR LOCAL
CONDITIONS ON A SMOOTH VEHICLE

ARGL (19) = TWOTE = T_{WALL}/T_e , TEMPERATURE RATIO ACROSS BOUNDARY LAYER

ARGL (20) To (25) = FOR FUTURE EXPANSION

Figure 145



FINAL REPORT
VOLUME I

REPORT MDC E1003
29 JANUARY 1974

7.0 INFLUENCE OF GAP HEATING ON TPS REQUIREMENTS

A major study activity was to examine the effect of gap heating on thermal protection system (TPS) requirements. Bondline temperature penalties are expected to be associated with fabrication to loose tolerances (i.e. large gap widths and tile mismatches), joint configuration and gap orientation. The effects of heating in transverse and in-line gaps of a simple butt joint were determined. A 40% tile thickness increase resulted when the convective heating in the gaps was considered.

The thermal model used in this analysis is basically the same as described in Section 4.2.1 except for the removal of the channel wall and associated radiosity nodes and material properties. Convective heating of a typical Shuttle trajectory was imposed on the model surface with the gap heating correlation applied to the gap walls. The heating distribution correlation curves from the arc jet data of Section 5.2, Figures 116 and 120, were used for the transverse and in-line gaps to get the gap heating effects on TPS requirements. As seen on these figures, the curves do not extend to the bondline. Referring to Section 4.2 and Figure 25 a discussion of two extrapolation extremes to the bottom of the gap is considered. A third extrapolation, somewhere between the two, was also suggested. For this study the third extrapolation was used. This was accomplished by assuming that the heating at the bondline for a 6.35 centimeter thick tile was equal to zero. For the other tile thicknesses, this same extrapolation slope was assumed. It is believed that some heating does exist at the bondline for the thinner tiles.

Figure 146 summarizes the maximum bondline temperature, amount of LI-900 tile insulation so bondline temperature does not exceed 177°C, and weight increase based on zero gap width. Three tile thicknesses and three gap widths were considered for the transverse and in-line gaps. The transverse and in-line gaps for the 0.2 centimeter width required the same amount of insulation for the conditions considered. The intermediate gap width (0.07 cm) for the in-line tile requires approximately 40% of the transverse gap requirements.



FINAL REPORT
VOLUME I

REPORT MDC E1003
29 JANUARY 1974

EFFECT OF TRANSVERSE GAP HEATING ON TPS REQUIREMENTS

GAP WIDTH \ THICKNESS OF TILE	3.18 cm	5.08 cm	6.35 cm	INSULATION REQUIRED FOR BONDLINE NOT TO EXCEED 177°C	WEIGHT INCREASE BASED ON 177°C BONDLINE TEMPERATURE
	MAX. BONDLINE TEMP. - °C			177°C REQUIREMENTS	
NO GAP	210	143	120	3.937 cm	0.000 Kgs/m ²
0.075 cm	249	178	139	5.105 cm	1.685 Kgs/m ²
0.202 cm	268	196	148	5.588 cm	2.380 Kgs/m ²

ABOVE RESULTS BASED ON EQUATION 9

EFFECT OF IN-LINE GAP HEATING ON TPS REQUIREMENTS

GAP WIDTH \ THICKNESS OF TILE	3.18 cm	5.08 cm	6.35 cm	INSULATION REQUIRED FOR BONDLINE NOT TO EXCEED 177°C	WEIGHT INCREASE BASED ON 177°C BONDLINE TEMPERATURE
	MAX. BONDLINE TEMP. - °C			177°C REQUIREMENTS	
NO GAP	210	143	120	3.937 cm	0.000 Kgs/m ²
0.074 cm	228	157	133	4.394 cm	0.659 kgs/m ²
0.203 cm	255	187	165	5.588 cm	2.380 Kgs/m ²

ABOVE RESULTS BASED ON EQUATION 25
(CORRELATION OF JSC 10 MW CHANNEL NOZZLE TESTS)

TRAJECTORY

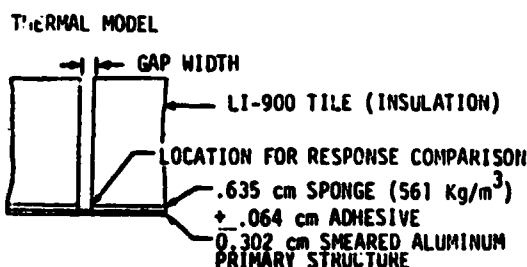
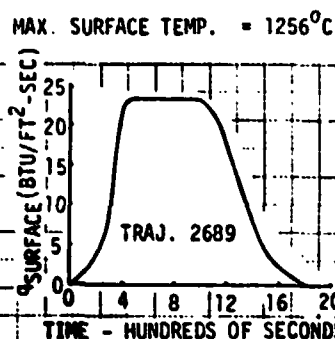


Figure 146



FINAL REPORT
VOLUME I

REPORT MDC E1003
29 JANUARY 1974

8.0 CONCLUSIONS

The nature of convective heating on the surface and in the gaps between RSI tiles on the Shuttle has been studied by an indepth program wherein data from NASA tests facilities were assimilated, analyzed and correlated. The major conclusions from the program follow.

Gap heating data and test environments from NASA facilities across the country were assimilated into a computerized data bank using a common data format. Information describing model configuration and instrumentation and boundary layer flow parameters were merged into the data bank.

This permitted the access, analysis and correlation of all available data for a particular gap configuration in an expeditious manner.

Heat Protection Ability of Candidate Joints - The series of RSI gap models tested in the JSC 10 MW Channel nozzle provided insight about the heat protection characteristics of candidate joints.

- o The rate of bondline heat up varies directly as gap width
- o Thin tiles experience higher gap heating than thick tiles
- o Deep narrow gaps inhibit penetration of hot external flow
- o Gaps wider than 0.127 cm experience significant convective heating which may result in bondline overheating
- o 3-D recirculation evident in gaps and out-flow in the transverse gap emanates at tile intersection
- o For wide gaps, contoured joints provide significantly greater heat protection than butt joints
- o Reducing emittance on gap wall lowers gap temperature near top of gap, but does not significantly lower bondline heat up rate
- o For some models, the in-line gap experienced a higher bondline heat up rate than the transverse gap
- o Inclined joint experienced higher heating in the in-line gap than the butt joint
- o The RSI filler block within the overlap block joined experienced high heating
- o Forward facing steps cause increased bondline heat-up for wide gaps whereas an aft facing step results in low bondline heatup even for large gaps.



FINAL REPORT
VOLUME I

REPORT MDC E1003
29 JANUARY 1974

The inverse solution technique was applied to results from nine RSI gap models each tested at four gap width setting. Consistent heating distributions were obtained by this technique. The heating distributions corroborated the conclusions drawn from the "heat protection ability" investigation and quantified the effects.

The conclusions are:

- o The level of convective heating drops off rapidly into the gap
- o Gap heating increases with gap width
- o Heating in the in-line gap is higher than in the transverse gap
- o Heating in the in-line gap is more sensitive to gap width than in the transverse gap
- o Significant heating penetrates deeper into wide gaps
- o For wide gaps ($W = 0.7$ cm), q/q_s near the top of the gap can be higher than unity
- o For most conditions, increasing gap depth, lowers gap heating distribution
- o Forward facing steps distort gap heating distribution causing significant increase in heating. The increase which results from boundary layer gas recirculation may be an order of magnitude especially at wide gaps.

The tests performed in the wall of the CFHT provided valuable insight about the effects of a thick turbulent boundary layer on gap heating.

- o Enhanced convective heating observed on the top of tiles
- o Tiles arranged in staggered patterns experience higher ($1.32/1.18 = 1.12$) heating on top surface than in-line tiles
- o Heating pattern on top of tile is two dimensional and lowest near gap
- o Heating on top of tile drops off drastically near trailing edge of tile indicating local distortion of boundary layer flow
- o Heating pattern on tile top changes with gap width
- o Study of flow orientation indicates higher heating occurs at gap orientations other than 0° and 90°
- o Position of maximum gap heating shifts to tile corners as flow is rotated
- o Maximum heating in the gap is in the general location of maximum heating on top of tile
- o Heating on tile with (0.254 cm) forward facing step increases to 1.82 over calibration plate; for staggered tiles heating rates increase to 2.0 over the calibration plate.



FINAL REPORT
VOLUME I

REPORT MDC E1003
29 JANUARY 1974

- o Sensitivity study concluded that including thermal conduction in calculating heating affects results. Near top of gap a 5% difference was obtained.
- o Deep in the gap the accuracy of absolute temperature perturbed results. The tests performed in the wall of the M = 8 V.D.T. provided insight about the influence of Reynolds number and turbulent boundary layer heating on gap heating.
- o Uniform heating on the top of the tiles occurred for both in-line and staggered tile patterns
- o High heating ($h/h_B = 3.65$) was measured on the faces of staggered tile and a hot spot ($h/h_B = 0.5$) was observed which had a radius of 1.5 cm. The magnitude of heating is affected by unit Reynolds number
- o For a transverse gap (in-line tiles) the upstream side of the gap experienced equal or higher heating than downstream side of gap. This same type heating was observed for free stream tests.

Free stream tests in the M = 8 V.D.T. provided information about effects of laminar and transitional flow on gap heating. Increasing unit Reynolds number caused the boundary layer to become transitional.

- o Extremely high heating measured in stagnation region of staggered tile during free stream tests. The magnitude is affected by unit Reynolds number.

Free stream tests in the Ames 3.5 foot H.W.T. provided additional insight about effects of Reynolds number, heating near the gap and effects of gap orientation.

- o Increasing unit Reynolds number caused the boundary layer to become transitional
- o Heating on top of tile experienced perturbation near gap
- o Heating near top of downstream side of gap was higher than upstream side of gap
- o For gaps with 30° and 60° flow orientation, heating ratio near gap surface increases as boundary layer becomes thinner. Boundary layer becomes thinner as unit Reynolds number increases. Heating distribution near gap was similar in shape to that measured in CFHT
- o Heating on top of tile near gap increased along in-line gap similar to that observed in CFHT tests.

Boundary layer parameters were examined and several conclusions were derived.

- o Exact boundary layer analysis gave excellent agreement with measured flat plate heat transfer data
- o Calibration data from LaRC M = 8 V.D.T. and Ames 3.5 foot H.W.T. are valid



FINAL REPORT
VOLUME I

REPORT MDC E1003
29 JANUARY 1974

- o Boundary layer parameters were accurately determined
 - o Flat plate calibration data (heat transfer, pressure and temperature profiles through boundary layer) are an important part of any gap heating test. Heating distributions measured in arc and wind tunnels were compared.
 - o Laminar wind tunnel data agrees reasonably well with laminar arc tunnel data
 - o Turbulent wind tunnel data indicates turbulent boundary layers result in higher heating in gaps than laminar boundary layers.
- Available gap heating theories were examined and it was concluded that simple laminar theories are inaccurate and that turbulent theories do not exist.

From the correlation activities, relationships were obtained from 10 MW, CFHT and M = 8 data.

- o Correlation equations were obtained in terms of dimensional and non-dimensional parameters (All Facilities)
- o The independent variables used in the correlations were:
 - oo Z (distance into the gap)
 - oo W (gap width)
 - oo T (gap depth)
 - oo Z/W , Z^2 , T^2 , $(Z/T)^2$, W to a power
 - oo Z to a power of W
 - oo Re (unit Reynolds number)
 - oo T_w/T_e (temperature ratio across the boundary layer)
- o For flush tiles, the average heating on top of the tile increases with gap width and increases when flow orientation (γ) is greater than 30° . (CFHT)
- o Protruding tiles experience higher average heating than flush tiles while recessed tiles have a lower average heating rate. (CFHT)
- o Maximum heating on top of tile increases with gap width and increases more significantly at (γ) between 45° and 60° . (CFHT)
- o Average heating in gaps around four sides of a tile (CFHT)
 - oo Average heating upstream side (2) of gap is insensitive to " γ " and "W"
 - oo Average heating on downstream side of gap is fairly insensitive to " γ " and is a strong function of gap width.



FINAL REPORT
VOLUME I

REPORT MDC E1003
29 JANUARY 1974

- oo Average heating on downstream side of gap is much higher at all "Y" when tile is protruding. Effect is less for upstream side of gap.
- oo Recessing the tile, generally decreases average heating on tile sides
- oo Heating distributions on side of tile are affected by "Y".



FINAL REPORT
VOLUME I

REPORT MDC E1003
29 JANUARY 1974

9.0 RECOMMENDATIONS

Although assimilation, analysis and correlation of available gap heating data has been accomplished, many questions about gap heating as influenced by boundary layer flow parameters and gap geometry need to be resolved. Following is a list of some of the more important activities which need to be accomplished.

- o Assessment of 2 and 3 dimensional effects of flow within gaps by adding flow dams to test panels which employ fields of tiles
- o Evaluate heating data obtained from models with zero gaps.
- o Evaluate the effects of wall temperature on gap heating.
- o Evaluate the effect of tile edge radius on gap heating.
- o Determine the effect of tile orientation, especially near 45° and in laminar boundary layers
- o Develop theoretical method for predicting gap heating for a turbulent boundary layer.
- o Incorporate results from 8 foot HTST, JSC 10 MW Laminar Duct, AMES 20 MW Turbulent Duct, AMES 3.5 foot 1974 tests, AFFDL 50 MW Arc Tunnel, and other gap heating data into data bank and correlate results.
- o Continue evaluation of candidate correlations to improve fits and to correlate larger data bank.
- o Expand calculation procedure to include refined correlations and other correlations subsequently developed.



FINAL REPORT
VOLUME I

REPORT MDC E1003
29 JANUARY 1974

10.0 REFERENCES

1. Throckmorton, D. A. "DATA MAN Report on the CFHT Tests," NASA TMX 71945 "Heat Transfer to Surface in Gaps of RSI Tile Arrays in Turbulent Flow at $M = 10.3$," April 1974.
2. Johnson, C. B. "Heat Transfer Data to Cavities Between Simulated RSI Tiles at Mach 8," DMS-DR-2043, NASA CR-128,770, June 1973.
3. DATA MAN DMS-DR 2035 NAS CR 134,007, "Thermal Protection System Gap Heating Rates of the Rockwell International Flat Plate Heat Transfer Model (OH2A and OH2B), by Thomas F. Foster (RI), William K. Lockman (NASA AMES) and William J. Grifall (RI).
4. "Reusable Surface Insulation (RSI) Thermal Protection Development for Shuttle, Volume II, Design Methodology," MDC Rpt. E0557, 21 March 1972, page 3-72.
5. Haugen, R. L., and Dhanak, A. M., "Momentum Transfer in Turbulent Separated Flow Past a Rectangular Cavity," Journal of Applied Mechanics, Sept. 1966.
6. Rhudy, J. P., and Magnan, J. D., Jr., "Investigation of Heat Transfer Distribution in Several Cavity & Step Configurations at Mach 10," AEDC TDR-64-220, Oct. 1964.
7. "Development and Design Application of Rigidized Reusable Surface Insulation (RSI) Thermal Protection System (TPS)," MDC Report No. E0725, page 7-21, 31 December 1972.
8. Feller, W. V., "Effects of Upstream Wall Temperatures on Hypersonic Tunnel Wall Boundary Layer Profile Measurements," AIAA Journal, Vol. II, No. 4, April 1973.
9. Private Communication with J. C. Dunavant, Langley Research Center, 24 January 1974.
10. Beckwith, I. E., Harvey, W. D., Clark, F. L., "Comparison of Turbulent Boundary-Layer Measurements at Mach Number 19.5 with Theory and an Assessment of Probe Errors," NASA TN D-6192, June 1971.
11. Keller, H. B. and Cebeci, T., "Accurate Numerical Methods for Boundary Flows," AIAA Paper 71-164, January 1971.
12. Cebeci, T., "Calculation of Compressible Turbulent Boundary Layers with Heat and Mass Transfer," AIAA Journal, Vol. 9, No. 6, June 1971.
13. Chen, K. K. and Thyson, N. A., "Extension of Emmons' Spot Theory to Flows on Blunt Bodies," AIAA Journal, Vol. 9., No. 5, May 1971.
14. Fivel, H. J., Masek, R. V., and Mockapetris, I., "Analytical Comparison of Hypersonic Flight and Wind Tunnel Viscous/Inviscid Flow Fields--Study Results," Final Report to NASA Contract NAS1-11728 to be published.



FINAL REPORT
VOLUME I

REPORT MDC E1003
29 JANUARY 1974

15. Telecon with Mark Hartun/Rockwell International, 28 January 1974
16. Burggraf, Odus R., "A Model of Steady Separated Flow in Rectangular Cavities at High Reynolds Number," Proceedings of the 1965 Heat Transfer and Fluid Mechanics Institute. Andrew F. Charwatt ed Stanford University Press, 1963, pp. 190-229.
17. Hodgson, J. W., "Heat Transfer in Separated Laminar Hypersonic Flow," AIAA Journal, Vol. 8, No. 12, December 1970.
18. Brewer, R. A., Saydah, A. R., Nestler, D.E., and Florence, D E., "Thermal Performance Evaluation of REI Panel Steps and Gaps for Space Shuttle Thermal Protection System," AIAA Paper No. 72-388, 10 April
19. Dixon, W. J., Editor, BMD; Biomedical Computer Program, University of California Press, Berkely, 1970.



FINAL REPORT
VOLUME I

REPORT MDC E1003
29 JANUARY 1974

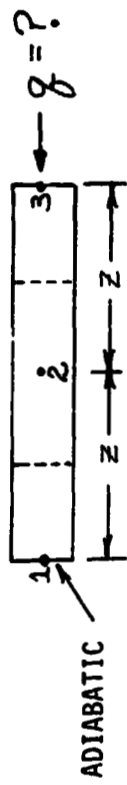
APPENDIX A
INVERSE SOLUTION

Convective heat in the gap between RSI tiles is computed using an "inverse solution" technique which is automated on the General Heat Transfer Computer program. In a standard transient solution, the heat fluxes are supplied as boundary conditions and the nodal temperature computed. In the inverse solution, the measured temperature histories recorded by the thermocouples are boundary conditions and the required heat fluxes are computed. To illustrate the functioning of the inverse solution technique, a simple one dimensional heat conduction problem is setup in Figure A-1. The bar is divided into three nodes with node 1 located at an adiabatic boundary and node 3 located at the boundary where the temperature history is known. The required heat flux is to be computed at the node 3 boundary. Thermal conduction and heat storage terms are defined for the energy balance at each node. "A" defines cross sectional area and " $\Delta\theta$ " describes the time step. The primed temperatures (T_1^1) are at the end of the time step. In the example, (T_3^1) is known and (T_1^1 , T_2^1 and q) are the unknown quantities obtained by solving the matrix.

Figure A-2 illustrates how the inverse solution works.



**EXAMPLE OF HOW INVERSE SOLUTION FUNCTIONS
(CONDUCTION, HEAT STORAGE AND A KNOWN TEMPERATURE HISTORY)**



HEAT BALANCE EQ.

$$\begin{aligned} \frac{\partial}{\partial z}(T_2' - T_1') &= \frac{\rho C_p A}{\Delta \theta} \frac{z}{2} (T_1' - T_1) \\ -T_2' + \frac{\rho A}{z} (T_3' - T_2') &= \frac{\rho C_p A z}{\Delta \theta} (T_2' - T_2) \\ f &+ \frac{\rho A}{z} (T_2' - T_3') = \frac{\rho C_p A z}{2} (T_3' - T_3) \end{aligned}$$

MATRIX SOLUTION

$$\begin{bmatrix} \frac{\rho A}{z} - \frac{\rho C_p A z}{2 \Delta \theta} & 0 & 0 \\ 0 & \frac{\rho A}{z} - \frac{\rho A}{2} - \frac{\rho C_p A z}{2 \Delta \theta} & 0 \\ 0 & 0 & \frac{\rho A}{z} \end{bmatrix} \begin{bmatrix} T_1' \\ T_2' \\ T_3' \end{bmatrix} = \begin{bmatrix} 0 \\ g \\ 1 \end{bmatrix}$$

**FINAL REPORT
VOLUME I**

**REPORT MDC E1003
29 JANUARY 1974**

- IMPLICIT FORMULATION
- T_3' IS KNOWN
- HEAT FLUX OBTAINED AT SAME TIME AS TEMPERATURE



FINAL REPORT
VOLUME I

REPORT MDC E1003
29 JANUARY 1974

HOW THE INVERSE SOLUTION WORKS

- 1 MATRIX IS FORMULATED DESCRIBING ENERGY TRANSPORT FOR EACH NODE.

$$\begin{bmatrix} \text{COEFFICIENTS} \\ "C" \end{bmatrix} \times \begin{bmatrix} \text{UNKNOWN} \\ "T" \end{bmatrix} = \begin{bmatrix} \text{CONSTANTS} \end{bmatrix}$$

- 2
- 3 WHEN A NODES TEMPERATURE HISTORY IS KNOWN, IT IS MULTIPLIED BY ITS COEFFICIENT AND TRANPOSED INTO THE CONSTANT ARRAY. THIS THEN FREES A ROW AND A COLUMN IN "C" AND A TERM IN "T". THE UNKNOWN HEAT FLUX IS THEN SUBSTITUTED INTO THE MATRIX.

Figure A-2



FINAL REPORT
VOLUME I

REPORT MDC E1003
29 JANUARY 1974

APPENDIX B

The units used in this volume are SI Units, except Section 2 where the raw data presented was in English Units. Conversion factors required for units used herein are given in the following table:

Physical quantity	U.S. Customary Unit	Conversion factor (*)	SI Unit
Convective Heating Rate	Btu/ft ² -sec	1.134×10^4	Watts/m ²
Convective Heat Transfer Coefficient Based on $T_{aw}/T_t = 0.895$	lbm/ft ² -sec	4.88	Kg/m ² -S
Enthalpy	Btu/lbm	2.324×10^3	J/Kg
Heat Transfer Coefficient	Btu/ft ² -sec-°F	2.042×10^4	Watts/m ² -°C
Length	in.	2.54×10^{-2}	m
Length	ft.	0.305	m
Pressure	lbf/ft ²	47.88	N/m ²
Pressure	lbf/ft ²	47.88×10^3	KN/m ²
Pressure	lbf/ft ²	47.88×10^6	MN/m ²
Reynolds Number	Re/ft	3.28	Re/m
(RHO V)l Freestream Density - Velocity Product	lbm/ft ² -sec	4.88	Kg/m ² -S
Temperature	°F	$5/9(°F-32)$	°C
Temperature	°F	$5/9(°F+460)$	°K

*Multiply value in U.S. Customary Unit by conversion factor to obtain equivalent value in SI Unit.